THE ROLE OF MITOCHONDRIA IN *DROSOPHILA* WOUND HEALING

SUSANA ISABEL PEREIRA DA PONTE

Tese para obtenção do grau de Doutor em Envelhecimento e Doenças Crónicas

Doutoramento em associação entre:

Universidade NOVA de Lisboa (Faculdade de Ciências Médicas | NOVA Medical School - FCM|NMS/UNL)

Universidade de Coimbra (Faculdade de Medicina - FM/UC)

Universidade do Minho (Escola de Medicina - EMed/UM)

setembro, 2019

THE ROLE OF MITOCHONDRIA IN *DROSOPHILA* WOUND HEALING

Susana Isabel Pereira da Ponte

Orientadores:

António Jacinto, Investigador Principal e Professor da Faculdade de Ciências Médicas | NOVA Medical School, Universidade NOVA de Lisboa

Paulo J. Oliveira, Investigador Principal do Centro de Neurociências e Biologia Celular (CNC) e Professor assistente convidado da Universidade de Coimbra

Tese para obtenção do grau de Doutor em Envelhecimento e Doenças Crónicas

VERSÃO PROVISÓRIA

Doutoramento em associação entre:

Universidade NOVA de Lisboa (Faculdade de Ciências Médicas | NOVA Medical School - FCM|NMS/UNL)

Universidade de Coimbra (Faculdade de Medicina - FM/UC)

Universidade do Minho (Escola de Medicina - EMed/UM)

PROGRAMAS DE DOUTORAMENTO FCT

setembro, 2019

The research described here was performed at the Chronic Diseases Research Center (CEDOC), NOVA Medical School - Faculdade de Ciências Médicas, between 2015 and 2019. Its execution was supported by a PhD fellowship from the Portuguese Foundation for Science and Technology (PD/BD/106058/2015).

Este trabalho de investigação foi realizado no Centro de Estudos de Doenças Crónicas (CEDOC) da NOVA Medical School - Faculdade de Ciências Médicas, entre 2015 e 2019, ao abrigo de uma bolsa de Doutoramento, financiada pela Fundação para a Ciência e a Tecnologia (PD/BD/106058/2015).

Trabalho realizado ao abrigo da Bolsa (Ref. PD/00291/2012), com o apoio da FCT (Fundação para a Ciência e a Tecnologia), do FSE (Fundo Social Europeu) e do POCH (Programa Operacional Capital Humano)

“One, remember to look up at the stars and not down at your feet.

Two, never give up work. Work gives you meaning and purpose and life is empty without it.

Three, if you are lucky enough to find love, remember it is there and don't throw it away.”

— Stephen Hawking

Para o meu avô

TABLE OF CONTENTS

THESIS PUBLICATIONS

Part of the work shown in this thesis is included in the following publication:

Susana Ponte, Lara Carvalho, Maria Gagliardi, Isabel Campos, Paulo J. Oliveira, António Jacinto. Drp1-mediated mitochondrial fission regulates calcium and F-actin dynamics during wound healing.
In submission

The work performed during one of the lab rotations of this PhD is included in the following publication:

Susana Ponte, António Jacinto, Lara Carvalho. The occluding junction protein Neurexin-IV is required for tissue integrity in the Drosophila wing disc epithelium. Matters (ISSN: 2297-8240) 2019. DOI: 10.19185/matters.201903000014

During the course of this PhD the author has contributed to the following publications:

Lara Carvalho, Pedro Patricio, Susana Ponte, Carl-Philipp Heisenberg, Luis Almeida, André S. Nunes, Nuno A.M. Araújo, Antonio Jacinto. Occluding junctions as novel regulators of tissue mechanics during wound repair. J Cell Biol. 2018 Dec 3;217(12):4267-4283. doi: 10.1083/jcb.201804048.

Inês Cristo, Lara Carvalho, Susana Ponte, António Jacinto, Novel role for Grainy head in the regulation of cytoskeletal and junctional dynamics during epithelial repair. J Cell Sci. 2018 Sep 3;131(17). pii: jcs213595. doi: 10.1242/jcs.213595.

THESIS CONTRIBUTIONS

The author designed and performed the great majority of experimental procedures, analysis of the results and assembly of the figures in this thesis. The author wrote all the Chapters of this thesis.

Lara Carvalho designed, performed the experiments, analysed the results shown in Figure 28. Lara Carvalho also helped to perform the experiments shown in Figure 27.

Telmo Pereira and Carolina Crespo helped with feedback on image analysis and quantifications in Figures 14, 15, 29 and 30.

ACKNOWLEDGEMENTS

"You cannot teach a man anything; you can only help him discover it in himself."

- Galileo

I would like to thank the people who helped me accomplish this PhD.

To my supervisor, António Jacinto, for giving me the opportunity to work in his lab for the past 8 years. Thank you for making me and independent scientist and always trusting my ideas. Thank you for recruiting the best lab mates one could wish for. Thank you for all the parties and lab retreats, it sure is fun to work in your lab.

To my co-supervisor, Paulo J. Oliveira, for always being available to discuss my work and for reviewing this thesis.

To the PHDOC Board, for giving me the opportunity to do a PhD. It was not always pleasant, but it was definitely lifechanging and I will never regret it.

To my favourite post-doc of all times, Lara Carvalho, for letting me grow as a scientist whilst supporting me all the way through this PhD. I once told you that 99% of what I know about being a good scientist I have learnt from you. This is still true. Thank you for all your help during this PhD and for reviewing this thesis. Thank you for the yoga classes. Namaste!

To Telmo, for all his help with image acquisition, image analysis and quantifications. Sorry for all the times I complained about the Spinning Disk!

To Carolina Crespo, for always trying to help me get the best images and the best graphs. Thank you for all your motivational speeches and for reviewing this thesis.

To Ana Sofia Brandão, for being a role model of what a good PhD student should be, for all the times you changed the laying pots, for reviewing this thesis, for always being there for me.

To all my lab colleagues, past and present, for all the laughs, for all the fun, for always supporting me. It is definitely easier to a PhD with your company. All of you helped me somehow along this way and I will be forever grateful to have met you.

To Inês Cristo, for all the motivation from far far away.

To Maria Gagliardi and Isabel Campos, for providing the preliminary results that led to this project and for always encouraging me.

To Marta Santos and Teresa Gomes for making life easier for me and for the flies.

To the CEDOC fly community, for all the insightful discussion about my work.

To Rita Teodoro, for providing the anti-HA antibody and for all the feedback regarding my work.

To the IGC, specially to Nuno Pimpão Martins and Gabriel Martins from the imaging facility and to Élio Sucena for hosting me for a couple of months to do the calcium experiments.

To Petra Pintado and Fábio Valério for helping me with the microinjection and to the Catarina Craveiro (from the CCU) for the microinjection needles.

To Ana Roberto, Fernanda Baptista, Ângela Dias and Ana Sofia Almeida, for making my life easier when it comes to bureaucracy.

To Cláudia Pereira and Ana Soares, for sharing this journey with me and helping me endure the difficult times and celebrate the good ones.

To all my fellow PHDOC colleagues, for all the fun and good food in Braga and Coimbra (and a bit of science as well).

To my friends and family, for always supporting me even though they have no idea what I do for a living.

To Eduardo, for all your help and understanding, for believing in me and always motivate me to do better. Love is not in grand gestures; love is in the little things.

ABSTRACT

Epithelia form the barrier that protects our body against the external environment. An injury represents a challenge to barrier homeostasis and must be repaired efficiently to maintain epithelial integrity and function. Wound healing in different types of epithelia varies in complexity but encompasses a series of conserved responses. The wound triggers the release of molecules that signal to the surviving tissue, leading to a cascade of events that include an immune response, and coordinated changes in the cellular cytoskeleton and adhesion machineries to close the wound and restore epithelial integrity. Understanding the molecular mechanisms involved in these different steps is highly relevant from the biological and biomedical perspective. Embryonic tissues have a remarkable ability to deal with injury by closing the wounds in a quick and scarless manner. The lessons learned from this model system should be useful to improve the current therapeutics for wound healing complications in humans, such as chronic wounds. Embryonic wound healing relies on the formation of a contractile cable at the wound leading edge, formed by the actin and myosin cytoskeleton, that coordinates the collective tissue movement that brings the wound edges together and closes the gap. This process is coordinated with cell crawling, cellular rearrangements and shape changes, in order to close the wound without the involvement of cell proliferation.

Mitochondria are pivotal organelles for cell survival. Known as the powerhouse of the cell due to their energy production capability, they also perform other critical cellular functions, such as the regulation of calcium and redox homeostasis and apoptosis. Mitochondria are dynamic organelles, being able to change their shape, number and localization to adapt to the cellular needs. These events are collectively termed mitochondrial dynamics and play an important role in modulating mitochondrial functions. Mitochondrial dynamics includes fusion and fission events, which modulate morphology; mitochondrial biogenesis and mitophagy, which regulate mitochondrial number and quality control; and mitochondrial trafficking, which controls the subcellular distribution of mitochondria in response to the cellular needs. Dysfunction in the molecular machinery that governs mitochondrial dynamics is associated with a plethora of human pathologies, such as cancer, and neurodegenerative and metabolic diseases. However, the role of mitochondria and mitochondrial dynamics in epithelial repair *in vivo* has so far not been investigated.

In this work, we took advantage of genetically-encoded fluorescent markers, high-resolution imaging and advanced laser ablation techniques to understand the contribution of mitochondrial dynamics to epithelial repair in vivo, in the *Drosophila* embryonic epidermis. Using a genetic screen assay, we identified proteins involved in mitochondrial fission, fusion and trafficking as novel wound healing regulators. *In vivo* live imaging of the wound closure process revealed that Dynamin related protein 1 (Drp1) and Optic Atrophy 1 (Opa1) proteins, that are central players in mitochondrial fission and fusion, respectively, regulate calcium

and actin cytoskeleton dynamics during wound healing. Moreover, we showed that wounding induces changes in mitochondrial morphology in the cells facing the wound, suggesting that the injury induces mitochondrial fission. We found that Drp1 loss of function leads to defects in both cytosolic and mitochondrial calcium dynamics upon wounding. Calcium ions are important second messengers in a myriad of signalling pathways and key players in the most important wound healing events. Wounding induces a quick and striking increase in intracellular calcium in the cells closer to the wound, which triggers a cascade of events that leads to the formation of the contractile cable and consequent wound closure. We showed that, besides this rise in cytosolic calcium, wounding also prompts an increase in mitochondrial calcium upon wounding. The uptake of calcium by mitochondria is known as an essential mechanism in controlling cytosolic calcium levels. Given the pleiotropic effects of calcium ions in the cell, its concentration needs to be tightly regulated in a spatial and temporal manner. Based on our results, we propose that Drp1 regulates the mitochondrial calcium buffering capacity, which then controls cytosolic calcium levels. Consistent with the described role of calcium in coordinating F-actin dynamics during wound healing, we also show that *Drp1* mutants display significant defects in F-actin accumulation at the wound edge and in wound closure kinetics. Altogether, our results lead us to propose a model where mitochondrial fission is induced upon injury; this leads to a controlled increase in intracellular calcium, which then activates the main cytoskeleton changes needed to promote efficient wound healing. This work places Drp1 and mitochondrial fission as upstream players in the cascade leading to the main events of wound healing. As calcium and F-actin are crucial elements of the wound healing response across different types of epithelia, our work has relevant implications in the understanding of epithelial repair in other systems. Finally, our results also expand the knowledge about mitochondria biology and their relevance for different cellular processes.

RESUMO

Os epitélios formam uma barreira que protege o nosso corpo do ambiente externo. Uma lesão constitui um desafio a esta função de barreira e deve ser resolvida de forma eficiente para manter a integridade e função dos epitélios. A cicatrização de feridas varia no grau de complexidade depedendo do tipo de epitélio, mas envolve uma série de respostas conservadas. A ferida promove a libertação de moléculas que servem como sinais para o tecido circundante coordenar uma cascata de eventos, que inclui uma resposta imunitária e alterações coordenadas no citoesqueleto e adesões celulares, de forma a fechar a ferida e restaurar a integridade epitelial. Compreender os mecanismos moleculares envolvidos nestes diferentes passos é extremamente relevante do ponto de vista biológico e biomédico. Os tecidos embrionários têm uma capacidade notável de resolver lesões, fechando as feridas de forma rápida e sem deixar cicatriz. O conhecimento adquirido através destes modelos poderá ser útil para melhorar as terapêuticas atuais para complicações inerentes à cicatrização de feridas em humanos, como é o caso das feridas crónicas. A cicatrização de feridas no estádio embrionário envolve a formação de um cabo contrátil de actina e miosina na margem da ferida que coordena o movimento coletivo do tecido de forma a aproximar os limites da ferida e fechar a brecha. Este processo acontece em paralelo com migração celular e rearranjos na forma e posição das células, de forma a fechar a ferida sem o envolvimento de proliferação celular.

As mitocôndrias são organelos cruciais para a sobrevivência das células. São organelos conhecidos principalmente pela sua capacidade de produção de energia, mas desempenham outras funções críticas nas células, tais como a regulação do cálcio e do estado redox, e da morte celular. As mitocôndrias são organelos dinâmicos, com a capacidade de mudar a sua forma, número e localização como forma de adaptação às necessidades celulares. Estes processos são denominados de dinâmica mitocondrial e possuem um papel importante no controlo das funções mitocondriais. A dinâmica mitocondrial inclui eventos de fusão e fissão que modulam a morfologia das mitocôndrias, processos de biogénese e mitofagia que regulam o número de mitocôndrias e o seu controlo de qualidade, e mecanismos de tráfego mitocondrial que controlam a localização subcelular das mitocôndrias em resposta às necessidades da célula. A disfunção na maquinaria molecular que controla a dinâmica mitocondrial está associada a várias patologias humanas, tais como cancro e doenças neurodegenerativas e metabólicas. Contudo, o papel das mitocôndrias e dinâmica mitocondrial na reparação de tecidos *in* vivo não foi até agora investigado.

Neste trabalho tirámos partido de marcadores fluorescentes geneticamente codificados, imagiologia de alta resolução e técnicas de ablação avançadas para compreender a contribuição da dinâmica mitocondrial na reparação epitelial *in vivo,* usando a epiderme do embrião da mosca-da-fruta (*Drosophila melanogaster*) como modelo. Este estudo permitiu-nos identificar proteínas envolvidas na fissão, fusão e tráfego mitocondrial como novos reguladores da cicatrização de feridas. A observação do processo de fecho de ferida *in vivo* e em tempo real revelou que as proteínas Drp1 e Opa1, envolvidas na fissão e fusão mitocondrial,

respetivamente, regulam o cálcio e o citoesqueleto de actina durante a cicatrização da ferida. Adicionalmente, descobrimos que a ferida promove alterações na morfologia mitocondrial que sugerem uma indução de fissão mitocondrial. A perda de função de Drp1 conduz a defeitos na dinâmica do cálcio citosólico e mitocondrial em resposta à ferida. Os iões de cálcio são importantes segundos-mensageiros em várias vias de sinalização e são reguladores fundamentais no processo de cicatrização de feridas. A ferida induz um aumento rápido e dramático no aumento dos níveis intracelulares de cálcio, que despoleta a cascata de eventos que culmina na formação do cabo de actina e miosina e consequente fecho da ferida. Neste trabalho mostrámos que, para além do aumento de cálcio no citosol, a ferida também induz um aumento no cálcio mitocondrial. Sabe-se que o influxo de cálcio para o interior das mitocôndrias é um mecanismo essencial para a regulação dos níveis de cálcio no citosol. Dado a variedade de funções desempenhadas pelo cálcio, a sua concentração celular deve ser regulada no tempo e no espaço. Com base nos nossos resultados, propomos que Drp1 regula a capacidade de captação de cálcio pelas mitocôndrias, o que por sua vez controla os níveis de cálcio no citosol. Em concordância com o papel descrito do cálcio na regulação do citoesqueleto de actina durante a cicatrização de feridas, mostrámos ainda que mutantes para Drp1 possuem defeitos significativos na acumulação de actina nas margens da ferida e na dinâmica de fecho da ferida. Em suma, os nossos resultados levam-nos a propor um modelo onde a fissão mitocondrial é induzida pela ferida, levando a um aumento controlado dos níveis intracelulares de cálcio, o que então regula as alterações no citoesqueleto necessárias para promover a cicatrização de forma eficiente. Este trabalho coloca a proteína Drp1 e a fissão mitocondrial no topo da cascata de sinalização que leva aos principais eventos na cicatrização de feridas. Dado que o cálcio e a actina são elementos cruciais na resposta à ferida em diferentes tipos de tecidos epiteliais, o nosso trabalho tem implicações relevantes na compreensão da reparação de tecidos noutros sistemas. Por fim, os nossos resultados aumentam o conhecimento da biologia mitocondrial e da sua relevância para diferentes processos celulares.

LIST OF ABBREVIATIONS

Abbreviations – Full form

% - percent, percentage

(-) – minus

(+) – plus

[O2]•– - superoxide

’ – minutes

µg - microgram

µL – microliter

µm – micrometer

µM – micromolar

1O2 - singlet oxygen

ADP - Adenosine diphosphate

AJs - Adherens Junctions

AMP - Adenosine monophosphate

AMPK - AMP-activated protein kinase

Arp2/3 - actin-related proteins 2/3

Atg - autophagy-related protein

ATP - Adenosine triphosphate

Bcl-2 - B-cell lymphoma 2

Bnip3 - Bcl2/adenovirus E1B 19-kDa interacting protein 3

BSA - Bovine Serum Albumin

bw – before wounding

C. elegans - Caernorhabditis elegans

Ca2+ - calcium ions

Caf4 – CCR4-associated factor 4

CaMKIV - calcium/calmodulin-dependent protein kinase IV

CaMKIα - calcium/calmodulin-dependent protein kinase Iα

cAMP – cyclic adenosine monophosphate

caspase - cysteine protease cleaving after Asp

CCR4 - C-C chemokine receptor type 4

Cdc42 - Cell division control protein 42 homolog

ChFP- Cherry fluorescent protein

CoA - coenzyme A

CREB - cAMP-response-element-binding protein

Cu - copper

cyt c - cytochrome c

DABCO - 1,4-diazabicyclo[2.2.2]octane

DAPI - 4', 6-diamidino-2-phenylindole

Dia – Diaphanous

DIABLO - direct IAP-binding protein with low pI

DMSO - Dimethyl sulfoxide

DN - dominant-negative

DNA - deoxyribonucleic acid

Dnm1 – Dynamin-related protein 1

Drosophila – Drosophila melanogaster

Drp1 - Dynamin-related protein 1

dUTP - Deoxyuridine Triphosphate

EAT-3 – C. elegans homolog of Opa1

E-cad – E-cadherin

ECM – extracellular matrix

EM – electron microscopy

EMRE - essential MCU regulatory element

ER – endoplasmic reticulum

ETC - electron transport chain

EYFP – enhanced yellow fluorescent protein

F-actin – filamentous actin

FAs – Focal adhesions

Fis1 - Mitochondrial fission 1 protein

FUNDC1 - FUN14 Domain Containing 1

Fzo – fuzzy onions

g – gram

G-actin – globular actin

Gdap1 - ganglioside-induced differentiation-associated protein 1

GDP - Guanosine diphosphate

GED - GTPase effector domain

GFP – greeh fluorescent protein

GSH – reduced Glutathione

GSSG – oxidized Glutathione

GTP – Guanosine triphosphate

GTPase – GTP hydrolase

h – hour

H+ - proton

H2O – water

H2O2 – hydrogen peroxide

HCX - Na+ independent (H+/Ca2+) exchanger

HOCl - hypochlorous acid

HTRA2 - high temperature requirement protein A2

IAP - inhibitor of apoptosis protein

IBM - inner boundary membrane

IFN2 - Inverted Formin 2

IMM – inner mitochondrial membrane

IMS - intermembrane space

IP3R - inositol triphosphate receptor

L – liter

LC3 - Microtubule-associated protein 1A/1B-light chain 3

LC3-II - lipidated form of LC3

LETM1 - leucine zipper EF-hand- containing transmembrane protein 1

LIR - LC3 interacting region

L-Opa1 – large isoform of Opa1

M – molar

MAMs - mitochondria-associated ER membranes

Marf - Mitochondrial assembly regulatory factor

mCherry – mCherry fluorescent protein

MCU – mitochondrial calcium uniporter

MCUb - mitochondrial calcium uniporter b

MDCK - Madin-Darby Canine Kidney

Mdm36 – Mitochondrial distribution and morphology protein 36

Mdv1 – Mitochondrial division protein 1

MELC – myosin essential light chain

Mff - mitochondrial fission factor

Mfn1 – Mitofusin 1

Mfn2 – Mitofusin 2

Mgm1 – mitochondrial genome maintenance 1

MHC – myosin heavy chain

MICU1 - mitochondrial calcium uptake 1

MICU2 - mitochondrial calcium uptake 2

MiD49 - mitochondrial dynamics proteins of 49 kDa

MiD51 - mitochondrial dynamics proteins of 51 kDa

Min – minutes

MiNA - Mitochondrial Network Analysis

Miro - Mitochondrial Rho

mL – milliliter

mm – millimeter

mM – millimolar

MOMP - mitochondrial outer membrane permeabilization

MPT - mitochondrial permeability transition

mpw - minutes post-wounding

MRLC – myosin regulatory light chain

mRYR - mitochondrial ryanodine receptor

mtDNA – mitochondrial DNA

MTP18 - mitochondrial protein of 18 kDa

Mtpα - Mitochondrial trifunctional protein α subunit

Myo19 - Myosin XIX

NA – numerical aperture

NAD+ – Nicotinamide adenine dinucleotide

NADH – reduced form of NAD+

NCX - Na+ dependent (Na+/Ca2+) exchanger

nm – nanometers

nM – nanomolar

NO - nitric oxide

NRF-1 - nuclear respiratory factor 1

NRF-2 - nuclear respiratory factor 2

NSF - N-ethylmaleimide-sensitive factor

Num1 – Nuclear migration protein 1

ºC – degrees Celsius

OJs – Occluding Junctions

OMA1 – named after its overlapping activity with m-AAA protease

OMM – outer mitochondrial membrane

Opa1 - Optic atrophy 1

Orp1 - oxidant receptor peroxidase 1

OXPHOS - oxidative phosphorylation

PBS - phosphate-buffered saline

PGC-1α - PPAR-γ coactivator-1α

PH - pleckstrin homology

PI3K - phosphatidylinositol (3)-phosphate kinase

PINK1 - PTEN-induced kinase 1

Pkn – Protein kinase N

PLCγ - Phospholipases Cγ

PPAR - peroxisome proliferator-activated receptor

PTEN - Phosphatase and Tensin Homolog deleted on Chromosome 10

Rho – Ras homologous

RhoGAPs - Rho GTPase-activating proteins

RhoGEFs – Rho guanine nucleotide exchange factors

RNA - ribonucleic acid

Rok – Rho kinase

ROS - reactive oxygen species

RT – room temperature

SAM - sorting and assembly machinery

SJs – Septate Junctions

SNARE - soluble NSF attachment receptor

Sod1 - superoxide dismutase 1

S-Opa1 – small isoform of Opa1

Spire1C - Protein spire homolog 1

spw - seconds post-wounding

Sqh - spaghetti squash

Src – pronounced sarc, as it comes from the word “sarcoma”

SUMO - small ubiquitin-like modifier

TCA - Tricarboxylic Acid

TdT - terminal deoxynucleotidyl transferase

Tfam - mitochondrial transcription factor A

TJs – Tight Junctions

TMRM - Tetramethylrhodamine Methyl Ester

TNTs - intercellular tunneling nanotubes

TOM - translocator of the outer mitochondrial membrane

TORC - transducer of regulated CREB-binding protein

TRPC3 - short transient receptor potential channel 3

TRPM - transient receptor potential channel, melastatin family

TUNEL - TdT-mediated dUTP-X nick end labelling

UCP1 - mitochondrial uncoupling protein 1

UCP2 - mitochondrial uncoupling protein 2

VDAC - voltage-dependent anion channel

WASp - Wiskott–Aldrich syndrome protein

WAVE - WASp-family verprolin homologous protein

X. laevis – Xenopus laevis

Zip – Zipper

Zn – zinc

LIST OF FIGURES

LIST OF TABLES

CHAPTER 1. INTRODUCTION

"What we know is a drop, what we don't know is an ocean."

- Isaac Newton

1. EPITHELIAL WOUND HEALING

For Metazoans, the maintenance of epithelial integrity is critical to sustain life. Epithelial tissues cover all the exposed surfaces of our body, inside and out, and form the functional units of secretory glands. Epithelia are cohesive sheets of specialized cells for absorption, secretion and to act as a barrier against abrasion, radiation, chemical stress and invasion by pathogens. Epithelia are classified in terms of the number of cell layers and the shape of the epithelial cells. They can be simple, when composed of just one cell layer, or stratified, containing several layers of epithelial cells. Epithelia are classified as squamous (flat cells), cuboidal (similar cellular width and height) or columnar (tall cells). The cellular shape and the tissue stratification are related to the epithelial function. For example, the stratified nature of our skin is ideal for its barrier function. In contrast, the squamous shape of the alveolar cells from our lungs facilitates gas exchanges (Lowe and Anderson, 2015). Given all the critical functions of epithelial tissues, it is of the upmost importance to deal with injury in a quick, efficient way. Epithelial cells have developed mechanisms to cope with wounds, either at the single cell level, or at the tissue scale.

This thesis has focused on wound healing of the *Drosophila melanogaster* (hereafter *Drosophila*) embryonic epidermis, a simple epithelium. A detailed review of embryonic and other simple epithelia repair mechanisms will be provided in this section, along with brief mentions to single cell repair and wound healing of more complex epithelia.

1.1. Embryonic and simple epithelia

Embryonic tissues have been used as models to understand epithelial repair because of their remarkable ability to efficiently deal with injury (Garcia-Fernandez et al., 2009). Early studies, relying on electron microscopy, have highlighted that the embryonic wound closure process is very fast, ranging from minutes to less than a day (Smedley and Stanisstreet, 1984; Stanisstreet et al., 1980). The current view of the phases of this process are depicted in Figure 1. Damage signals released by the wounded tissue trigger a response by the surviving cells. This response leads to the accumulation of cytoskeleton components, namely actin filaments and non-muscle myosin II (hereafter called myosin) molecular motors at the wound edge, forming a ring-like contractile structure called the actomyosin cable (Rothenberg and Fernandez-Gonzalez, 2019). As the actomyosin structures form, immune cells from the leukocytic lineage, such as macrophages and neutrophils, are recruited to the wound in order to clear cell debris and fight the entry of pathogens. Sliding of myosin motors along actin filaments at the front-edge of wound-facing cells leads to tissue movement, contraction and concomitant reduction of the wound area over time. In addition, and possibly as

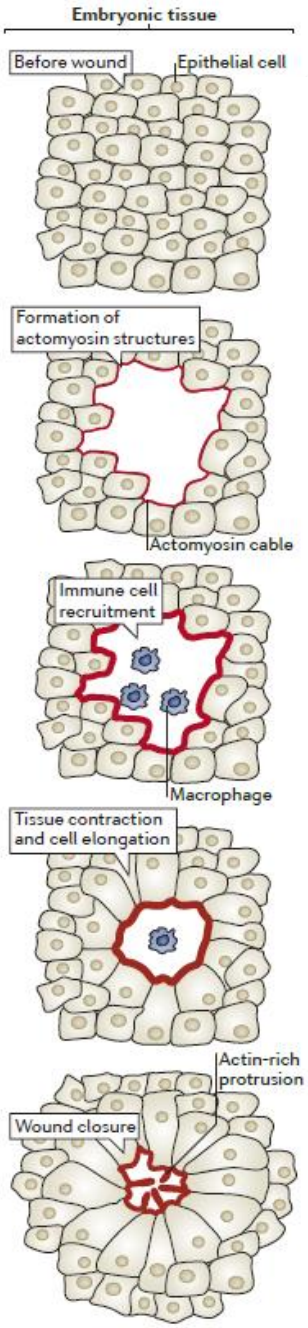

Figure 1. Wound healing in embryonic tissues.
The wound healing process includes the formation of actomyosin structures that promote tissue contraction and cell elongation to bring the wound edge cells together. Immune cells are recruited to the wounded region to clear cell debris and prevent infection. Actin protrusions mediate the final adhesion of the wound edge cells. Adapted from (Cordeiro and Jacinto, 2013).

a consequence, wound edge cells elongate to further reduce the wound size. In addition to the actomyosin cable, leading edge cells form actin-rich protrusions that promote cell crawling and mediate contacts between opposing sides of the wound (Cordeiro and Jacinto, 2013).

We will now address these steps in more detail, highlighting the known and unknown molecular mechanisms involved in the repair of embryonic and other simple epithelia.

1.1.1. Actomyosin cable

Wound healing of embryonic epithelia is characterized by accumulation of F-actin and Myosin at the cell membranes that face the wound, forming an actomyosin cable. Actin is the most abundant intracellular protein and exists in two conformations: as a globular monomer called G-actin and as a filamentous polymer called F-actin. Actin filaments are formed by polymerization of G-actin subunits, with consequent expenditure of adenosine triphosphate (ATP). F-actin organization in complex networks forms a cytoskeleton that modulates cellular shape. The polymerization, depolymerization and organization of F-actin into different types of networks are regulated by actin-binding proteins. Actin is also involved in the formation of cellular protrusions, like microvilli, which increase the apical membrane surface area, or filopodia and lamellipodia, which establish contacts with the underlying cell substrate and are involved in cell migration (Lodish et al., 2000). Myosins are molecular motors that move along actin filaments by conformational changes induced by hydrolysis of ATP. Myosin is a multimeric protein, composed of two heavy chains (MHC), two essential light chains (MELC) and two regulatory light chains (MRLC) (Betapudi, 2014). The movement of myosin across F-actin networks generates contractile forces. The actin-myosin contractile machinery spans the apical cell surface of the epithelial cells and is anchored to cell-cell junctions, namely the Adherens

Junctions (AJs). This localization allows contraction that lead to changes in cell shape and are coupled with tissue movements (Kasza and Zallen, 2011).

In the early 90s, Martin and Lewis characterized the closure of the chick embryo epidermis and observed that the epidermal tissue moves inwards over time. The fact that lamellipodia were not detected in the leading-edge cells suggested that this movement was independent of cell migration. Combined with the observation that the tissue was under tension, it led them to propose that closure must rely on circumferential contractile forces at the wound margin, that bring the wound edges together, closing the hole in a purse string manner. Consistent with this hypothesis, they observed accumulation of F-actin at the wound edge minutes after wounding and remaining there until the wound was closed (Martin and Lewis, 1992). The purse string hypothesis (Martin and Lewis, 1992) was compatible with previous observations that the shape of the epidermal cells changes upon wounding, suggesting that the tissue is under tension, and that the leading-edge cells elongate during wound closure, indicating that they are being pulled by contractile forces (Smedley and Stanisstreet, 1984; Stanisstreet et al., 1980). A few years later, the same purse string wound closure mechanism was observed in the mouse embryo and disruption of the actin cable by cytochalasin D treatment impaired re-epithelialization, confirming its requirement for proper wound closure (McCluskey and Martin, 1995). It was also found that myosin was part of the cable, accumulating at the wound edge together with F-actin, further highlighting the contractile nature of this ring-like structure (Bement et al., 1993; Brock, 1996).

Over the past years, many efforts have been made to understand how epithelia sense the wound and form the actomyosin cable. Actomyosin cables are not exclusive of wound healing. They have been observed during morphogenesis in embryonic development (Jacinto et al., 2002; Wood et al., 2002; Young et al., 1993), in extrusion of apoptotic cells (Ninov et al., 2007; Rosenblatt et al., 2001), and during the separation of dividing cells in the process of cytokinesis (Pollard, 2010). Studies on these processes have also helped to understand how actomyosin cables work in wound healing. Advances in microscopy techniques, allowing the live imaging of the wound closure process have improved our understanding of how the actomyosin cable is formed and how it drives wound closure.

1.1.2. Cell migration

Studies in epithelial monolayers *in vitro* have shown that wounds can close either by actomyosin cable-mediated contraction or by cell migration/crawling to cover the wound or a combination of the two processes (Altan and Fenteany, 2004; Begnaud et al., 2016; Bement et al., 1993; Fenteany et al., 2000; Tamada et al.,

2007). Cell migration is not exclusive of wound healing *in vitro*. Wounds in the *Drosophila* abdomen epidermis also close through cell shape changes and lamellipodia formation (Rämet et al., 2002) and in embryonic wound healing the actin protrusions work together with the actomyosin cable to drive the collective movement of the epithelial tissue.

Cell migration-mediated wound closure involves actomyosin cytoskeleton remodelling to form protrusive structures and to create the intracellular forces required for cell movement. Cells adjacent to the wound repolarize and become migratory and lead the other epithelial cells, in a process referred to as collective cell migration (Begnaud et al., 2016). Polarized leader cells extend protrusions in the direction of movement. Cell migration is associated with two types of F-actin protrusions: lamellipodia, which look like large sheets, and contain highly branched and cross-linked actin filaments (Ballestrem et al., 2000); and filopodia, thin finger-like structures, with parallel bundles of F-actin, that often project beyond the edge of the lamellipodium (Mattila and Lappalainen, 2008). The generation of the intracellular forces occurs through attachment sites, called focal adhesions (FAs). FAs link the intracellular actin cytoskeleton with the extracellular matrix (ECM) and this interaction is mediated by integrins. New FAs form behind the leading edge of the cell and pull the cell forward. Release of attachment sites at the rear of the cell allows the rear end to move in the direction of movement (Lambrechts et al., 2004). The regulators of the actomyosin cable and F-actin protrusions are conserved and are discussed below (1.1.3 Rho GTPases and their effectors and 1.1.4 Calcium).

1.1.3. Rho GTPases and effectors

The regulation of actomyosin contractile structures relies on the action of Ras homologous (Rho) GTPase protein family. Rho GTPases are cytoskeletal regulators that alternate between an inactive (GDP-bound) and an active (GTP-bound) form. This switch is regulated by Rho guanine nucleotide exchange factors (RhoGEFs), which catalyse the phosphorylation of GDP to GTP, and by Rho GTPase-activating proteins (RhoGAPs), which hydrolyse the GTP to GDP. When active, Rho GTPases are able to activate effector proteins that regulate F-actin polymerization and myosin contraction. In mammals, this protein family is composed of 20 proteins, but the most well studied and conserved members are Rho, Rac and the Cell division control protein 42 homolog (Cdc42) (Heasman and Ridley, 2008; Sit and Manser, 2011). Rho GTPases are known regulators of the actin cytoskeleton in mammalian cultured cells (Hall, 1994) and are also important during wound healing *in vivo* (Abreu-Blanco et al., 2012a; Brock, 1996)

In the wound healing of the chick wing bud during development, treatment with C3 transferase, a bacterial enzyme that inactivates Rho, prevents the assembly of the actomyosin cable, leading to failure of wound closure. The Rho protein was found to be indispensable for actomyosin cable formation (Brock, 1996). In *Drosophila*, *Rho1* mutants or embryos expressing dominant-negative (DN) versions of Rho1 fail to form the actomyosin cable during dorsal closure, a morphogenetic movement during *Drosophila* embryonic development that resembles wound closure (Lu and Settleman, 1999; Magie et al., 1999). The family of Rho GTPases cooperates during wound healing: Rho1 regulates the formation of the actomyosin cable and Cdc42 mediates filopodia and lamellipodia formation. F-actin protrusions are important to mediate cell crawling during the contraction phase and to mediate the final approximation and adhesion of the wound-edge cells in the final stages of wound closure (Abreu-Blanco et al., 2012b; Verboon and Parkhurst, 2015; Wood et al., 2002). *In vitro*, Rac is the Rho GTPase responsible for lamellipodia formation (Das et al., 2015; Fenteany et al., 2000; Yamaguchi et al., 2015). The role of Rac in wound closure in vivo is less clear. Expression of DN-Rac in both the chick wing bud (Brock, 1996) and mutations in Rac genes in the *Drosophila* embryo (Wood et al., 2002) do not lead to detectable wound healing defects. However, a more recent study has identified a significant wound healing delay in Rac mutants, although no visible impairment in either the actomyosin cable or the actin protrusions was detected (Verboon and Parkhurst, 2015).

Active Rho GTPases exert their function by activating effector proteins that regulate F-actin and myosin. Rho1 effectors include the formin Diaphanous (Dia) and the Rho kinase (Rok). Dia promotes the polymerization of unbranched F-actin (Narumiya et al., 1997). Rok acts on myosin by activating MRLC, either directly, by phosphorylation, or indirectly, by inactivation of myosin phosphatases, leading to actomyosin contractility (Amano et al., 1996; Kimura et al., 1996; Ueda et al., 2002). Knockdown of both Rok and Dia impairs actomyosin dynamics in the *Drosophila* pupa wound healing (Antunes et al., 2013). Rok^{2} mutant embryos show delayed wound healing (Verboon and Parkhurst, 2015) and dia^{5} mutants have defects in the formation of the actomyosin cable and actin protrusions (Matsubayashi et al., 2015). The Cdc42 effector protein Wiskott-Aldrich Syndrome protein (WASp) and the Rac effector WASp-family verprolin homologous protein (WAVE), both implicated in the nucleation of branched actin filaments (Miki and Takenawa, 2003), have also been linked to *Drosophila* embryonic wound healing, but their roles are still not well understood (Matsubayashi et al., 2015).

The actomyosin cable and the actin protrusions collaborate to drive wound closure (Abreu-Blanco et al., 2012b; Ducuing and Vincent, 2016). Disruption of either of the actin-based structures leads to delayed wound healing, but the wounds eventually close. *Rho1* and zip^{1} (*zipper*, the *Drosophila* MHC gene) mutants, in which the actomyosin cable does not fully form, are able close their wounds by increased formation of actin protrusions. Conversely, the wounds in *cdc42* mutants, are able to contract through the action of the

actomyosin cable and defects are only observed in the final adhesion stage (Abreu-Blanco et al., 2012b; Wood et al., 2002). The absence of either mechanism of wound closure seems to be compensated by the other. Only the simultaneous disruption of the actomyosin cable and actin protrusions leads to fully impairment of wound healing (Abreu-Blanco et al., 2012b).

1.1.4. Remodelling of cell junctions

The AJs mediate adhesion between neighbouring cells, thus being essential to maintain tissue architecture. AJs are composed of:

- calcium-dependent transmembrane proteins called cadherins. About 20 different cadherins have been described but E-cadherin is characteristic of epithelial tissues (Takeichi, 1988). Binding of calcium controls the conformation of the cadherin extracellular domain, leading to homophilic interactions between cadherins of neighbouring cells (Pokutta et al., 1994).
- cytosolic proteins called catenins, which include p120-catenin, α-catenin and β-catenin. These catenins in turn bind a variety of other molecules.

AJs are connected to the actin cytoskeleton via α-catenin, that binds both β-catenin and actin cytoskeleton regulators such as vinculin. In polarized epithelial cells, AJs are localized apically on the cell lateral membrane and an adhesion belt, called the circumferential actin belt, as they completely encircle the cells along with the F-actin lining on the cytosolic side (Hartsock and Nelson, 2008; Meng and Takeichi, 2009).

During wound healing, at the same time of actomyosin cable formation, E-cadherin has been found to localize in clusters at the wound margin, presumably representing the sites that link the actomyosin cable in adjacent cells (Brock, 1996). The AJ components E-cadherin (Abreu-Blanco et al., 2012b; Brock, 1996), α-catenin (Wood et al., 2002) and β-catenin (Zulueta-Coarasa et al., 2014) are removed from the cell cortex that face the wound and remain only at the cell-cell junctions linking adjacent cells. E-cadherin exclusion from the wound edge is mediated through remodelling by endocytosis (Hunter et al., 2015; Matsubayashi et al., 2015) and by transcriptional regulation by the NFκB-pathway (Carvalho et al., 2014). The dynamics of E-cadherin localization is critical for the formation of the actomyosin cable, as both E-cadherin mutations and overexpression impair the formation of the actomyosin cable (Abreu-Blanco et al., 2012b; Hunter et al., 2015; Matsubayashi et al., 2015).

Besides AJs, other types of cell junctions have been implicated in wound healing. Occluding Junctions (OJs) localize close to the AJs. OJs are known for their permeability barrier function, controlling the transepithelial passage of molecules, and for maintenance of cell polarity, constituting a “fence” that

separates the apical and basolateral membrane compartments. OJs are termed Tight Junctions (TJs) in vertebrates and Septate Junctions (SJs) in invertebrates (Jonusaite et al., 2016; Shen, 2012). Recently it was reported that several mutants for SJ components fail to close epithelial wounds. A functional analysis of the mutant *kune-kune* (*kune*), a transmembrane SJ component of the Claudin family, revealed that SJ loss of function severely impairs the wound closure process and actomyosin cable formation. As seen for AJs, SJ proteins are also removed from the wound edge, but the mechanisms are still unknown. Interestingly, SJ loss of function affects the mechanical properties of the epithelial tissue and the cell shape changes and rearrangements that occur during wound healing (Carvalho et al., 2018). However, the molecular mechanisms involved remain completely unknown.

1.1.5. Calcium

An increase in cytoplasmic calcium in cells adjacent to the wound is the first response signal to be detected upon injury. This has been observed both in *in vitro* (Hinman et al., 1997; Leiper et al., 2006; Shabir and Southgate, 2008; Sung et al., 2003), and in *in vivo* models (Antunes et al., 2013; Razzell et al., 2013; Xu and Chisholm, 2011).

It is still unclear which are the calcium sources contributing to the increase of cytoplasmic calcium in the different wound healing models. In fact, there is evidence supporting both calcium influx from the extracellular environment and calcium release from internal stores. In the epidermis of the nematode *Caenorhabditis elegans* (*C. elegans)*, the rise in intracellular calcium is mediated by the transient receptor potential calcium channels of the melastatin subfamily (TRPM) at the plasma membrane. Additionally, there is calcium release from the endoplasmic reticulum (ER) via the Inositol 1,4,5-trisphosphate (IP3) receptor (IP3R), that seems to be mediated by G-protein coupled receptor (GPCR) signalling (Xu and Chisholm, 2011). Knockdown of TRPM also reduces the wound-induced intracellular calcium levels in the *Drosophila* pupal epithelium (Antunes et al., 2013). In both *C. elegans* and *Drosophila* models, impairment of the intracellular calcium rise leads to actomyosin cable defects (Antunes et al., 2013; Hunter et al., 2018a; Xu and Chisholm, 2011; Xu and Chisholm, 2014). Depletion of ER calcium stores or extracellular calcium also promote a reduction in Reactive Oxygen Species (ROS) production (Hunter et al., 2018a; Razzell et al., 2013; Xu and Chisholm, 2014) and immune cell recruitment (Razzell et al., 2013).

High-speed imaging of the wound-induced calcium rise has shown that calcium increases in the leading cells and then spreads a few cell rows away from the wound, propagating in an intercellular wave manner. After this initial dispersion, the calcium levels decrease from the periphery towards the wound edge (Antunes

et al., 2013; Narciso et al., 2015; Razzell et al., 2013; Restrepo and Basler, 2016; Shannon et al., 2017). The propagation of the intercellular calcium wave depends on IP3-mediated calcium release from internal stores and calcium transport across cells via Gap Junctions (Narciso et al., 2015; Razzell et al., 2013; Restrepo and Basler, 2016).

The exact mechanisms through which calcium mediates the wound healing response are still not fully understood. Data suggests that calcium regulates the actomyosin cable by activating actomyosin regulators. Knockdown of the calcium-dependent actin filament–severing protein Gelsolin (Sun et al., 1999) in the *Drosophila* pupa impairs the actomyosin flow towards the wound and consequent cable formation (Antunes et al., 2013). There is also evidence that the activation of Rho and Cdc42 GTPases upon wounding is calcium-dependent (Benink and Bement, 2005). Recent work has also shown that the regulation of the actomyosin cable occurs through the calcium-mediated production of ROS (Hunter et al., 2018a; Xu and Chisholm, 2014). ROS can regulate Rho GTPases and Rok by acting on redox-sensitive motifs in these proteins (Muliyil and Narasimha, 2014; Xu and Chisholm, 2014) and control E-cadherin remodelling by oxidizing the Src kinase Src42A (Hunter et al., 2018a).

1.1.6. Immune cell recruitment

Although the immune system differs between embryos and adults, wounding of embryonic tissues also triggers an inflammatory response, that involves the recruitment of immune cells to the wound site (Babcock et al., 2008; Moreira et al., 2010; Niethammer et al., 2009b; Razzell et al., 2013; Stramer et al., 2005; Wood et al., 2006). Upon wounding, immune cells such as macrophages and neutrophils are attracted to and migrate towards the wound site, to phagocytose pathogens and cellular debris resulting from the death of wounded cells (Babcock et al., 2008; Stramer et al., 2005). Wound-induced hydrogen peroxide production, which is downstream of calcium signalling triggered by the injury (Razzell et al., 2013), seems to contribute to immune cell recruitment (Moreira et al., 2010; Niethammer et al., 2009b; Razzell et al., 2013). Interestingly, it was shown that hemocytes, the *Drosophila* equivalent to macrophages, are not required for reepithelialisation (Stramer et al., 2005). This suggests that wound closure is not mediated by signals coming from these immune cells, neither the cell debris removal is critical to achieve wound healing. Nevertheless, although they do not affect the wound healing process, it is possible that hemocytes are important to prevent infection and ensure embryo survival, but this is yet to be addressed.

1.2. Repair in complex and adult epithelia

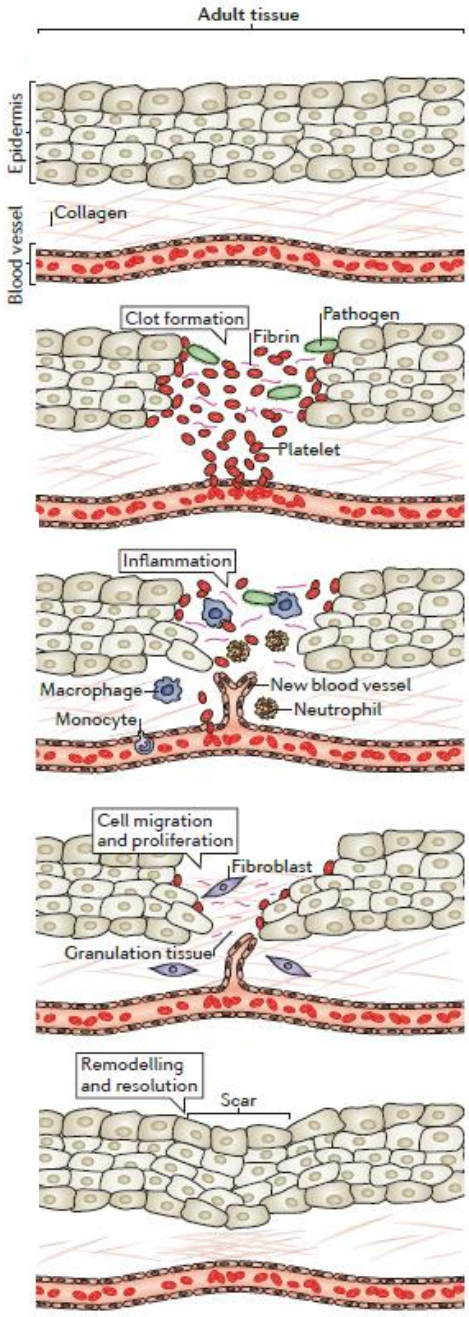

Unlike embryonic wound healing, the repair of more complex adult epithelia is a slow process, taking days or months to fully restore the epidermal tissue, and leaves a scar (Cordeiro and Jacinto, 2013; Gurtner et al., 2008; Sonnemann and Bement, 2011). Both inefficient and excessive wound healing are associated with pathological conditions. Wound healing delay and defects are associated with chronic wounds (Frykberg and Banks, 2015), whereas an exacerbated response leads to hypertrophic and keloid scars (Rabello et al., 2014). In contrast to embryonic wound healing, the repair of adult epithelia involves a coordinated and tightly regulated interaction between epithelial cells and other cell types, such as fibroblasts, immune cells and platelets. This process occurs in four distinct phases that are sequential but are also overlapping: 1) hemostasis, 2) inflammation, 3) proliferation and migration, and 4) remodelling and resolution (Fig. 2).

Figure 2. Wound healing of complex epithelia.
The wound healing of complex epithelia, such as the adult skin, occurs in 4 phases: hemostasis (clot formation), inflammation (accumulation of leukocytes and angiogenesis), cell migration and proliferation (to replace the lost tissue) and resolution (remodeling). Adapted from (Cordeiro and Jacinto, 2013).

1.2.1. Hemostasis

This initial phase is characterized by the formation of a clot that serves as a shield against the physical and chemical extracellular environment, preventing tissue/fluid leakage and pathogen entry. During this phase, blood vessels constrict, mediated by the vascular smooth muscle cells, to limit blood loss. Platelets leak from damaged blood vessels and aggregate to form a plug at the lesioned area (Palta et al., 2014). The subsequent release of platelet-secreted factors such as platelet-derived growth factor (PDGF), epidermal growth factor (EGF) and transforming growth factor-β (TGF-β) lead to the formation of a fibrin clot that plugs the wound hole. The factors released by the platelets also serve as

chemoattractants to the immune cells that are recruited to mediate the next phase of wound healing (Pakyari et al., 2013; Pierce et al., 1991; Schultz et al., 1991).

1.2.2. Inflammation

Immune cells infiltrate the wound. The first cells to arrive are neutrophils, whose main function is to kill pathogens, through the release of proteases and ROS (Wilgus et al., 2013). Later on, monocytes arrive at the wound site, where they differentiate into macrophages and remove debris and apoptotic neutrophils by phagocytosis (Zaja-Milatovic and Richmond, 2008). Macrophages also secrete cytokines and growth factors to recruit other immune cells, such as lymphocytes, fibroblasts and endothelial cells (Park and Barbul, 2004). T-lymphocyte infiltration is also observed. $CD4^+$ cells (T-helper cells) play a positive role in wound healing, whereas $CD8^+$ cells (T-suppressor-cytotoxic cells) have an inhibitory effect in wound healing (Park and Barbul, 2004). There are also skin -resident T cells (γδ-T cells) that have roles in epidermal keratinocyte proliferation and survival (Havran and Jameson, 2010). Angiogenesis, the formation of new blood vessels, is also triggered at this stage. Vessels close to the wound produce branches that reach the lesioned area facilitating the migration of immune cells and providing oxygen and nutrients to the wound site (Rosenkilde and Schwartz, 2004).

1.2.3. Proliferation and migration

Re-epithelialization is achieved by proliferation of epithelial cells, specifically keratinocytes, and tissue contraction. Keratinocytes undergo a transient dedifferentiation process: they change shape to a more flattened and elongated phenotype and remodel the contacts with the ECM and the F-actin cytoskeleton to form lamellipodia. These changes allow keratinocytes to migrate into the wound area as a cohesive sheet, referred as the migrating tongue. Keratinocytes behind the migrating tongue proliferate to provide sufficient number of cells to reconstitute the lost tissue (Pastar et al., 2014).

Fibroblasts also proliferate and migrate to the wound. They secrete a large amount of ECM proteins, such as collagen, into the wound area. Some fibroblasts also differentiate into myofibroblasts, which are contractile cells. The newly formed ECM, together with the fibroblasts, myofibroblasts, and the new blood vessels form the so-called granulation tissue. Contraction of the myofibroblasts pulls the cells associated with the granulation tissue, leading to tissue contraction and alignment of the ECM collagen fibres, and contributing to the re-epithelialization (Li et al., 2007).

1.2.4. Remodelling and resolution

After re-epithelialization, the structures formed in the previous stages are removed or remodelled. Epidermal cell migration and proliferation stops and the remaining leukocytes either leave the wound site or undergo apoptosis. The blood vessel network is reorganized and the granulation tissue is removed by metalloproteinases secreted by the remaining immune cells. At the end of this phase, only the aligned ECM filaments are maintained, forming the scar tissue (Gurtner et al., 2008; Li et al., 2007).

1.3. Repair of single cell wounds

Damage to the plasma membrane poses a threat to cell survival. The cell must avoid leakage of internal contents and the entry of foreign unwanted material, and needs to maintain the electrical and chemical gradients required for normal cellular functions (Nakamura et al., 2018). How cells sense a plasma membrane breach is still not clearly understood. The first signal to be detected upon membrane injury is the influx of extracellular calcium. This rise in intracellular calcium has been detected in different cellular models and is required for the wound response (Bement et al., 1999; Bi et al., 1995; Heilbrunn, 1930; Miyake and McNeil, 1995; Steinhardt et al., 1994; Terasaki et al., 1997; Yumura et al., 2014). Calcium triggers the initiation of wound repair by regulating membrane (Bi et al., 1995; Luxardi et al., 2014; Steinhardt et al., 1994) and cytoskeleton changes (Bement et al., 1999). Alternative signals that trigger wound healing include the entry of ROS (Cai et al., 2009), plasma membrane depolarization (Luxardi et al., 2014) and the decrease in membrane tension (Togo et al., 2000). Single cell wound healing occurs at two levels: plasma membrane resealing and cortical cytoskeleton remodelling.

Cell repair occurs through the successive fusion of cytosolic vesicles with each other and with the plasma membrane to form an impermeant and transient patch at the site of the membrane lesion (Fig. 3) (Cooper and McNeil, 2015; Davenport and Bement, 2016; McNeil et al., 2000; Terasaki et al., 1997). Proteins necessary for vesicle exocytosis have been shown to be required for this process. These proteins include the calcium/calmodulin kinase, kinesin and soluble N-ethylmaleimide-sensitive factor (NSF) attachment receptor (SNARE) proteins (Steinhardt et al., 1994). Based on increasing evidence, the current model proposes that calcium-dependent exocytosis of lysosomal-derived vesicles is immediately followed by endocytosis, which leads to lesion internalization and restoration of plasma membrane integrity (Corrotte et al., 2013; Idone et al., 2008; Tam et al., 2010).

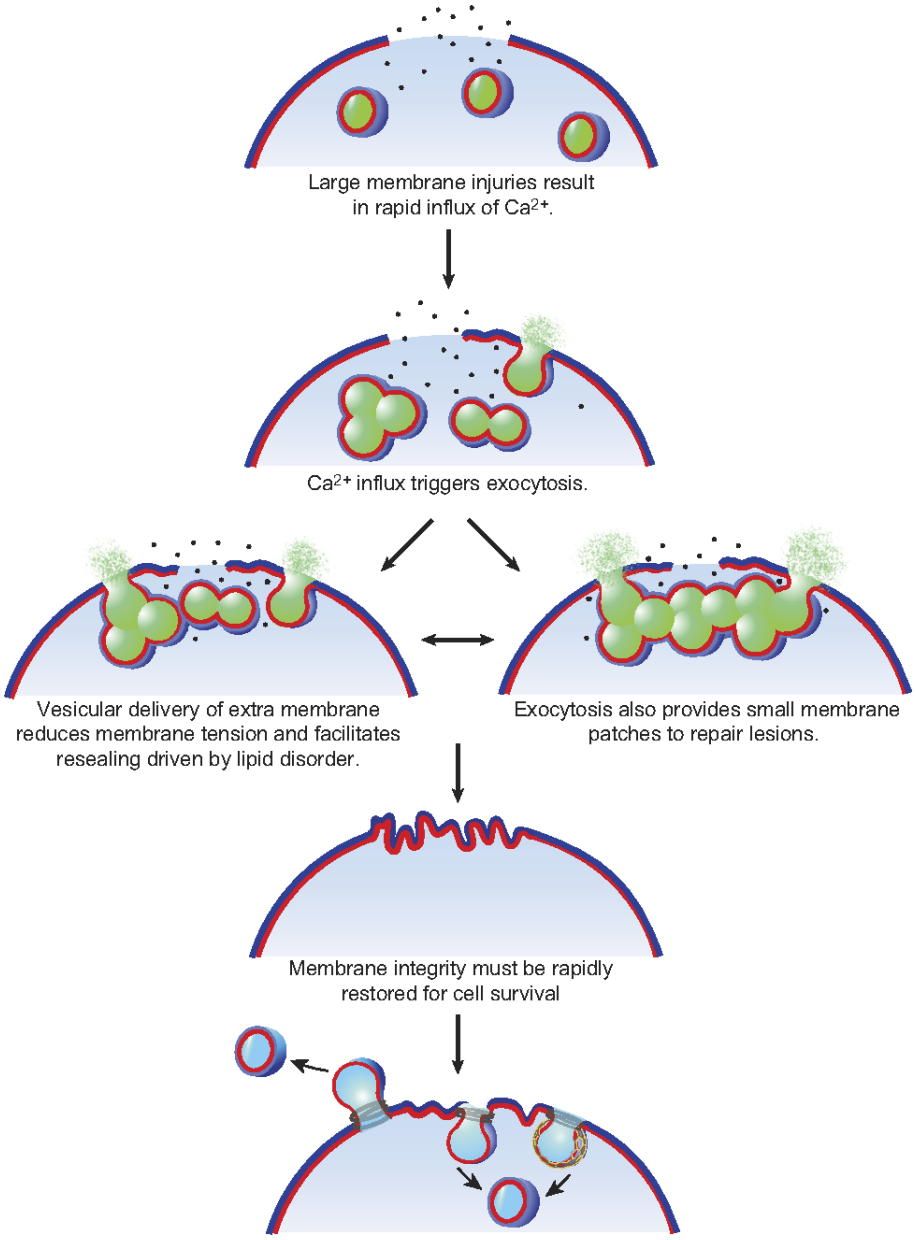

Figure 3. Cell wound repair.
Plasma membrane disruptions result in calcium influx that activates vesicular exocytosis and fusion of cytoplasmic vesicles. Exocytic fusion reduces membrane tension, and vesicle-vesicle fusion events form a transient patch to replace the membrane barrier missing at the lesion site. The membrane patch is subsequently remodelled and removed via exocytic and/or endocytic machinery. Adapted from (Cooper and McNeil, 2015).

Regarding cortical cytoskeleton remodelling, an enrichment in cortical F-actin close to the lesion has been observed in different single cell repair models and is required for wound closure (Nakamura et al., 2018). Different mechanisms seem to control this localized F-actin accumulation. In *Drosophila* and *Xenopus laevis* (*X. laevis*) models, the membrane lesion triggers the formation of F-actin and myosin rings, that contract and reduce the wound area progressively until it closes. The contraction of the cortical cytoskeleton ring is accompanied by concomitant movement of the overlying membrane to fully repair the wound (Abreu-Blanco et al., 2011; Bement et al., 1999; Mandato and Bement, 2001). The assembly and contraction of the

actomyosin cortical ring is mediated by members of the Rho GTPase family and their effectors, which also localize at the vicinity of the wound (Abreu-Blanco et al., 2014; Benink and Bement, 2005; Nakamura et al., 2017). When active, Rho GTPases are able to activate effector proteins that regulate F-actin polymerization and myosin contraction (Benink and Bement, 2005). In other models, in which F-actin rings are absent (Henson et al., 2002; Yumura et al., 2014), cortical F-actin polymerization is mediated by the actin-related proteins 2/3 (Arp2/3) complex (Henson et al., 2002).

Both cortical cytoskeleton changes and membrane resealing mechanisms contribute to single cell wound closure, but it is still unknown how they are coordinated. In some cell types, the cortical F-actin constitutes a barrier for the vesicle-plasma membrane fusion events. Destabilization of actin favours the membrane resealing process (Miyake et al., 2001; Togo et al., 1999; Xie and Barrett, 1991), whereas treatments to stabilize F-actin have the opposite effect (Miyake et al., 2001). An initial transient disassembly of the cortical cytoskeleton may be needed to allow the vesicle-plasma membrane fusion (Miyake et al., 2001). The fact that the cortical cytoskeleton contraction is accompanied by the plasma membrane suggests that they must be connected (Mandato and Bement, 2001). One possible link appears to be the AJ protein E-cad, that co-localizes with the F-actin ring. Mutants for E-cadherin shown wound overexpansion and F-actin ring defects. However, wounds still manage to close in these mutants, suggesting that other cellular components are needed to mediate cytoskeleton-plasma membrane tethering (Abreu-Blanco et al., 2011).

1.4. Comparison between wound healing mechanisms

To summarize this section about wound healing, there are obvious differences and similarities between wound repair in single cells, simple epithelia and complex epithelia.

Single cell wound repair involves resealing of the plasma membrane and cytoskeletal rearrangements (Nakamura et al., 2018). When we go from a single cell to an epithelial tissue, the actomyosin cable still seems to be the most accepted main driving force for wound healing, and the actomyosin regulators, Rho GTPases and their effectors, are conserved. However, there is another layer of complexity: epithelial cells in a tissue are closely linked to each other and the integrity of the tissue must be maintained during the wound repair. For this purpose, epithelial cells rely on cellular junctions, which are also required for wound healing (Rothenberg and Fernandez-Gonzalez, 2019).

In complex epithelia, different cell types have to mount a coordinated wound healing response, so the process takes longer. Although with different degrees of complexity, an immune response is common to embryonic and adult (complex epithelia) wound healing. The mechanisms involved in cell migration in both simple and complex epithelia share similarities. Unlike most embryonic wound healing models, healing of adult complex epithelia also requires cell proliferation (Thiruvoth et al., 2015).

Despite all the mentioned differences, understanding how wound healing occurs in different cells and tissues is a fascinating subject from the cell biology perspective. Importantly, the fundamental knowledge gathered in simple epithelia wound closure models may be useful to improve current therapeutics for wound healing-related disease in humans.

2. MITOCHONDRIAL BIOLOGY

2.1. Origin

The origin and evolution of mitochondria has long fascinated biologists. Mitochondria seem to be as old as the first Eukaryote, since all known eukaryotic lineages possess mitochondria or mitochondrion-related organelles (Van Der Giezen, 2009) or at least have contained them at some point (Karnkowska et al., 2016). The endosymbiont hypothesis (Sagan, 1967) is the most widely accepted theory of mitochondrial origin. Although many questions in the evolution of mitochondria and eukaryotes remain unanswered, mitochondria are thought to be derived from an α-proteobacterial endosymbiont that integrated into an archaebacteria host (Cox et al., 2008; Gray, 2012; Gray, 2017; Lane and Martin, 2010).

2.2. Structure

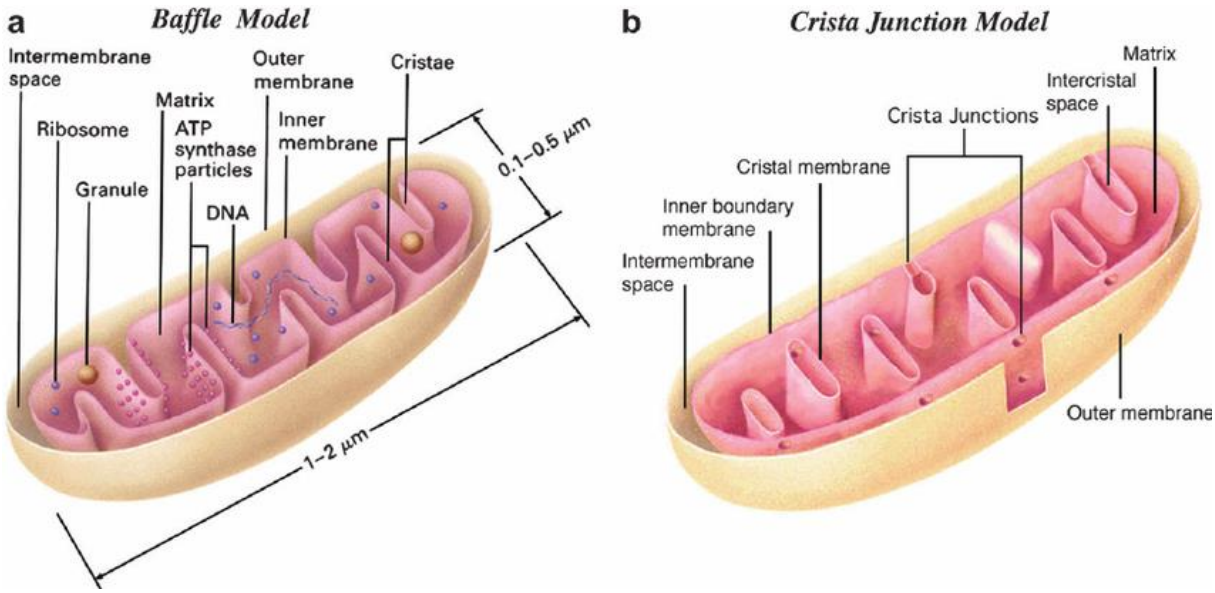

Figure 4. Models of mitochondrial membrane structure.
(a) Infolding or Baffle Model. (b) Crista Junction Model. Opposed to the Baffle Model, which shows large openings connecting the intercristal space to the intermembrane space, the Crista Junction Model shows that these connections are narrow tubular openings (crista junctions). Cristae can have more than one crista junction, on the same side of the mitochondrial periphery, or on opposite sides. Adapted from (Logan, 2006).

Mitochondria are double-membrane organelles, composed of an outer mitochondrial membrane (OMM), an inner mitochondrial membrane (IMM) and two aqueous compartments, the intermembrane

space (IMS) and the matrix. Early studies of mitochondrial structure, based on electron microscopy (EM), highlighted that the IMM extends all across the mitochondrial diameter, forming compartments that divide the matrix (Palade, 1952; Sjöstrand, 1956). Palade's observations (Palade, 1952) were the basis of the "Baffle Model" that states that these compartments, called *cristae mitochondriales*, are plate-like infoldings of the IMM. This corresponds to the typical textbook representation of mitochondria (Fig. 4 a). Later studies reported that this model was not entirely accurate and that, instead, cristae look like flat sacs, with multiple narrow tubules that connect to the peripheral surface of the IMM (called the inner boundary membrane, IBM) and to each other (Mannella et al., 1994). These tubular connections were called *pediculi crista* by Daems and Wisse (Daems and Wisse, 1966) or crista junctions by Perkins and colleagues (Perkins et al., 1998), leading to a new model of mitochondrial structure, called the "Crista Junction Model". In this model, the IMM is subdivided in IBM, cristae membrane and crista junctions (Fig. 4 b).

Crista junctions are important for the establishment of mitochondrial contact sites (Hackenbrock, 1966) between the OMM and the IBM. The contact sites facilitate the communication between the cytoplasm and mitochondrial matrix and have been assigned several different functions, such as lipid transfer (Hoppins et al., 2011; Scharwey et al., 2013), import and sorting of nuclear encoded proteins (Dekker et al., 1997; von der Malsburg et al., 2011), exchange of ions and metabolites (Brdiczka, 1991), IMM stability (von der Malsburg et al., 2011) and even inheritance of mitochondrial deoxyribonucleic acid (mtDNA) (Li et al., 2016).

The OMM and IMM diverge not only in shape but also in composition. Unlike the IMM, the OMM is very permeable, due to the presence of channels that allow transport of ions and small molecules between the cytosol and the IMS. These channels include, to name a few:

- the voltage-dependent anion channel (VDAC), the most abundant protein in the OMM, which regulates the entry of ions, nucleotides and other metabolites (Colombini, 1980; Shoshan-Barmatz et al., 2010);
- the translocator of the outer mitochondrial membrane (TOM) complex, which acts as the principal entry point for almost all nuclear-encoded mitochondrial proteins (Rapaport, 2002);
- the sorting and assembly machinery (SAM) complex, which inserts protein precursors into the outer membrane (Pfanner et al., 2004).

The IMM is characterized by the presence of the mitochondria-specific phospholipid cardiolipin (Horvath and Daum, 2013) and a high amount of membrane-associated proteins, that include the oxidative phosphorylation (OXPHOS) system components (Schenkel and Bakovic, 2014). The IMM is dynamic and cristae morphology changes in response to alterations in osmotic and metabolic conditions. For instance, in response to low adenosine diphosphate (ADP) concentrations, the IMM changes from a 'condensed' state,

with a dense matrix and wide cristae, to an 'orthodox' state, with an expanded, matrix and more compact cristae compartment (Hackenbrock, 1966). Another example is the widening of crista junctions that occurs during programmed cell death (Scorrano et al., 2002). The IMS is subdivided into the peripheral IMS, which is adjacent to the OMM and IBM, and the cristae space, which is formed by invaginations of the IMM. The IMS is an important link in the transport of ions, metabolites and proteins across the two mitochondrial membranes (Backes and Herrmann, 2017).

The mitochondrial matrix is packed with multiple copies of mitochondrial DNA, ribonucleic acids (RNAs) and ribosomes needed for its translation, metabolic enzymes and pools of metabolites including nicotinamide adenine dinucleotide NAD^+, NADH (reduced form of NAD^+), ATP, and ADP (Friedman and Nunnari, 2014; Logan, 2006).

2.3. Mitochondrial DNA

The mtDNA of most Metazoans is a small (approximately 16 kb in size) circular DNA molecule, present in multiple copies and composed of 37 genes, encoding 13 protein subunits required for OXPHOS, 2 ribosomal RNAs (one for each of the two mitochondrial ribosome subunits) and 22 transport RNAs (Clary and Wolstenholme, 1985; Jansen, 2000). Inside mitochondria, mtDNA forms a complex with proteins involved in mtDNA replication, repair, and transcription, forming the so-called nucleoids (Spelbrink, 2010; Zinovkina, 2019).

mtDNA is histone-free nature and has a limited repair ability. Exons are tightly packed, with no spacing introns, so mutations have higher chances of affecting the function of the encoded proteins (Jansen, 2000). These mtDNA features lead to a higher mutation-fixation rate than the nuclear genome in most vertebrate species (Allio et al., 2017; Wallace et al., 1987),

2.4. Inheritance

Mitochondria are not created *de novo*, they arise from the growth and division of pre-existing mitochondria, so they must be inherited. In the majority of eukaryotes, the inheritance of mitochondria is uniparental, coming from the mother (Allen, 1996; Pyle et al., 2015). In mammals, this is achieved by ubiquitination of sperm mitochondria that leads to degradation upon fusion with the oocyte (Sutovsky et al., 1996; Sutovsky et al., 1999; Thompson et al., 2003). In other organisms, such as angiosperms, maternal

inheritance occurs by exclusion of the paternal mitochondrial genomes from the male reproductive cells before fertilization (Nagata et al., 1999; Sodmergen et al., 2002).

During the cell cycle, mitochondria undergo a period of massive mitochondrial elongation, followed by a phase of mitochondrial division and uniform segregation of the mitochondria within the cell (Salazar-Roa and Malumbres, 2017). During mitosis, mitochondria are distributed in proportion to the volume of cytoplasm received by each daughter cell (Jajoo et al., 2016).

2.5. Functions

Mitochondria perform a myriad of functions in the cell, ranging from energy production, regulation of calcium and redox homeostasis, apoptosis, among others. We will present a general overview of these mitochondrial functions and focus on the most relevant ones for the work of this thesis.

2.5.1. Cellular Metabolism

The cellular metabolism comprises the biochemical reactions that take place within the cell. These reactions can be subdivided into catabolic reactions, that convert nutrients into to energy in the form ATP, and anabolic reactions that lead to the synthesis of larger biomolecules. The reactants, intermediates and products of these reactions are called metabolites (Yang, 2016). Cellular metabolism is vital for the cells to perform their functions and adapt to different environments (Metallo and Vander Heiden, 2013). Mitochondria are a central organelle for energy production within the cell: in the IMM cristae they harbour the respiratory complexes and the F_1F_o-ATP synthase; on both mitochondrial membranes there are transporters for metabolites; and the IMS is the site where many metabolic pathways take place (Spinelli and Haigis, 2018). The aim of this section is to provide a general overview of the metabolic pathways controlled by mitochondria, focusing on a few examples.

2.5.1.1. Metabolic pathways in the mitochondrial matrix

Many metabolic pathways take place, at least partially, in the mitochondrial matrix. We selected a few important examples: Tricarboxylic Acid (TCA) cycle and fatty acid β-oxidation.

The TCA cycle, also called the Krebs cycle or the citric acid cycle (Fig. 5 A), is the major energy-producing metabolic pathway in cells. Its functions include the production of intermediate compounds for the

biosynthesis of substances such as amino and fatty acids., and the formation of large quantities of ATP, which is used as energy for various cellular processes (Bender, 2003; Kumari, 2018). The TCA is a series of eight enzymatic reactions that consumes and regenerates citrate and uses acetyl-coenzyme A (acetyl-CoA), coming from the metabolism of carbohydrates and lipids. The oxidation of acetyl-CoA produces, among other things, the reducing agents NADH and succinate (via $FADH_2$, the reduced form of flavin adenine dinucleotide FAD) (Fernie et al., 2004). These two molecules are the electron donors that transfer electrons to the mitochondrial respiratory chain to begin the process of OXPHOS (Fig. 5 B).

Fatty acid β-oxidation is responsible for the catabolism of fatty acids. It is an important pathway in energy metabolism, particularly when the glucose supply is limited. Plasma free fatty acids or lipoprotein-associated triglycerides are converted to acyl-coenzyme A (acyl-CoA) in the cytosol and imported into mitochondria. Inside mitochondria, acyl-CoAs are degraded into acetyl-CoA by a series of four reactions called β-oxidation. Acetyl-CoA, as mentioned previously, can feed into the Krebs cycle (Fig. 5 A) (Houten and Wanders, 2010; Spinelli and Haigis, 2018).

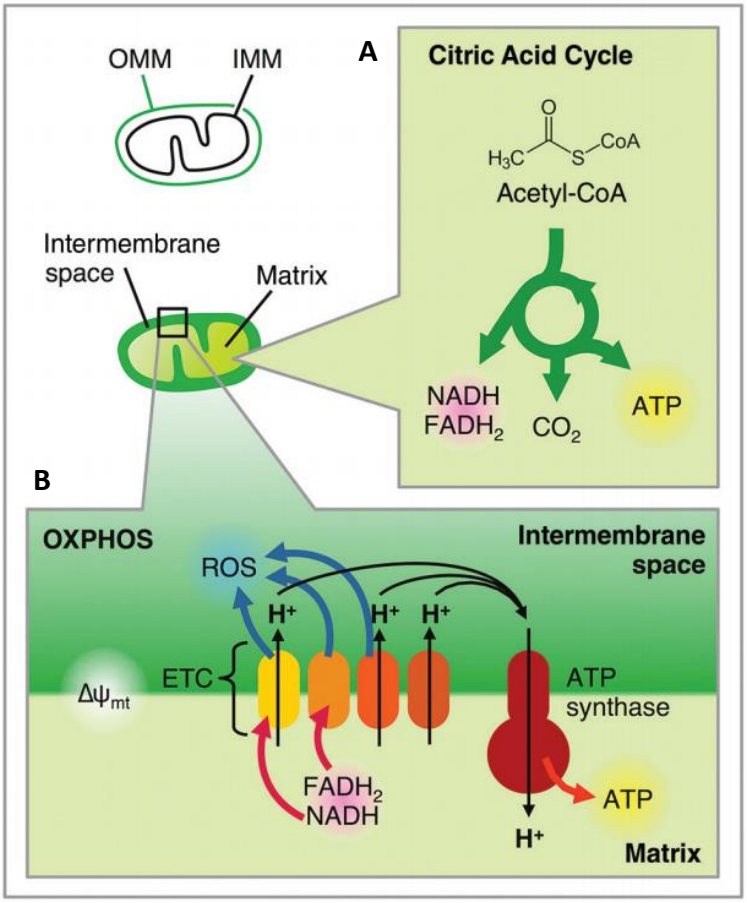

Figure 5. Mitochondrial bioenergetics.
(A) The citric acid cycle takes place in the matrix and involves the oxidation of acetyl-CoA to yield carbon dioxide (CO_2), ATP, and reducing equivalents - NADH and $FADH_2$. (B) These reducing equivalents fuel the electron transport chain (ETC) located in the IMM. The chain of redox reactions across the ETC leads to proton (H^+) pumping from the matrix to the intermembrane space (IMS), thus generating an electrochemical gradient that creates the mitochondrial transmembrane potential (ΔΨmt). The ETC generates ROS as a by-product of its redox activity. Accumulated H^+ in the IMS are pumped back to the matrix through the ATP synthase, which uses H^+ translocation as a driving force for ATP production. Adapted from (Bravo-Sagua et al., 2017).

2.5.1.2. Oxidative phosphorylation

Mitochondria's canonical role is to serve as the powerhouses of the cell, by producing ATP through OXPHOS (Fig. 5 B). Oxidation of metabolites produces electrons that are transferred by NADH to the mitochondrial electron transport chain (ETC), composed of large protein complexes: NADH-ubiquinone oxidoreductase (complex I), succinate dehydrogenase (complex II), ubiquinone-cytochrome c oxidoreductase (complex III), and cytochrome c oxidase (complex IV). Complexes I–IV shuttle electrons to their final acceptor, oxygen, to form water. This electron flow generates an electro-chemical gradient – ΔΨmt - by the pumping of protons (H^+) from the mitochondrial matrix to the IMS (Mitchell, 1966; Sousa et al., 2018). The flow of H^+ back into the mitochondrial matrix, via the H^+ transport subunits of F_1Fo ATP synthase complex, leads to conformational changes that promote the conversion of ADP and phosphate to ATP (Senior et al., 2002).

2.5.2. Heat production

Mitochondrial OXPHOS is not perfectly coupled to ATP synthesis. Approximately a quarter of the H^+ pumped by the ETC leak back across the IMM and are not coupled to ATP production, thus this energy is lost as heat (Brand, 2000; Murphy, 1989). Cells can take advantage of this phenomenon to purposely augment thermogenesis, by expressing uncoupling proteins that promote mitochondrial heat production, as reported in brown fat thermogenesis in mammals (Busiello et al., 2015). It is even argued that the heat generating ability of mitochondria provided selective advantage for proto-mitochondrion maintenance during the evolution of eukaryotes (Dunn, 2017).

2.5.3. Apoptosis

Apoptosis is essential for embryonic development and maintenance of the adult tissue homeostasis. Apoptosis can be classified as extrinsic or intrinsic. Extrinsic apoptosis is triggered by external signals that are recognized by plasma membrane death receptors. On the other hand, intrinsic apoptosis is triggered by different stimuli, such as DNA damage, nutrient deficiency, oxidative stress, developmental cues, among others (Danial and Korsmeyer, 2004; Galluzzi et al., 2012; Vakifahmetoglu-Norberg et al., 2017). Mitochondria participate in the intrinsic pathway of apoptosis, the most common pathway of vertebrate cell death. Irrespective of the initial apoptosis trigger, mitochondria are central players in this pathway, as the stimulation of mitochondrial outer membrane permeabilization (MOMP) is always involved (Kroemer et al., 2007).

MOMP leads to the dissipation of the ΔΨmt with consequent impairment of ATP production and ΔΨmt-dependent transport to the mitochondria. Additionally, there is release of proteins from the IMS, including cytochrome c (cyt c). cyt c triggers the formation of a multimeric protein complex - the apoptosome - which in turn activates a class of proteins called caspases (cysteine protease cleaving after Asp). The apoptosome activates initiator caspases, such as caspase-9, that will then cleave and activate the executioner caspases 3, 6 and 7. The action of the executioner caspases results in cell shrinkage, chromatin condensation, DNA damage, nuclear fragmentation, blebbing, and phosphatidylserine exposure on the surface of the plasma membrane (Elmore, 2007). MOMP triggers the release of other proteins from mitochondria besides cyt c: direct inhibitor of apoptosis protein (IAP)-binding protein with low pI (DIABLO) and high temperature requirement protein A2 (HTRA2), which sequester and/or degrade several members of the IAP family, thus facilitating caspase activation (Chai et al., 2000; Srinivasula et al., 2003; Yang et al., 2003).

2.5.4. Calcium homeostasis

Calcium ions (Ca^{2+}) are important second messengers in a plethora of signalling pathways involved in cell proliferation (Pinto et al., 2015), differentiation (Tonelli et al., 2012), migration (Tsai et al., 2015) and death (Zhivotovsky and Orrenius, 2011), as well as in muscle contraction (Kuo and Ehrlich, 2015) and neurotransmission (Südhof, 2012), among others. Mitochondria and the ER are crucial organelles in the regulation of calcium homeostasis. The ability of mitochondria to uptake calcium is recognized since the 60s (DeLuca and Engstrom, 1961; Vasington and Murphy, 1962). Mitochondria accumulate high concentrations of calcium inside the matrix. Under resting conditions, the concentration of calcium inside mitochondria is not much different from the cytosolic calcium levels (100–200 nM). However, under stimulating conditions, mitochondria can accumulate 10 to 20 times more calcium than the cytosol. Mitochondrial calcium uptake is stimulated by an increase in cytosolic calcium, that can come from the extracellular environment or other calcium internal stores, such as the ER. Calcium accumulation inside mitochondria is followed by rapid extrusion into the cytoplasm by calcium antiporters, restoring the basal state (Belosludtsev et al., 2019; Bravo-Sagua et al., 2017; De Stefani et al., 2016).

2.5.4.1. Calcium influx

The ΔΨmt generated by the mitochondrial respiratory chain constitutes the electrochemical force required for positively charged ions, such as Ca^{2+}, to enter the matrix. The OMM is rich in VDAC, forming pores through which calcium can cross (Gincel et al., 2001; Messina et al., 2012). VDAC is not limiting for calcium flow across the OMM (Colombini, 2012; Tan and Colombini, 2007), so the challenge for calcium is to

cross the IMM (Belosludtsev et al., 2019). Calcium can enter through several different channels: the mitochondrial ryanodine receptor (mRyR) (Altschafl et al., 2007; Ryu et al., 2010), the short transient receptor potential channel 3 (TRPC3) (Feng et al., 2013), the mitochondrial uncoupling protein 2 and 3 (UCP2/3) (Trenker et al., 2007), and the leucine zipper EF-hand-containing transmembrane protein 1 (LETM1) (Jiang et al., 2009). However, the main route of calcium uptake across the IMM is the Mitochondrial Calcium Uniporter (MCU) channel (Baughman et al., 2011; De Stefani et al., 2011).

The MCU channel is formed by oligomerization of four subunits of MCU. Vertebrates possess another MCU related protein, MCUb, with 50% homology to MCU, that acts as a dominant-negative version of MCU. This protein can be integrated in the MCU complex, fine-tuning its regulation in different cell types (De Stefani et al., 2016; Raffaello et al., 2013). MCU lacks the classic EF-hand domain (Calcium-binding domain) (Baughman et al., 2011; De Stefani et al., 2011). Therefore, its calcium-dependent activity is controlled by regulatory proteins: essential MCU regulatory element (EMRE) and mitochondrial calcium uptake 1 (MICU1). MICU1 and its paralog MICU2 are found in the IMS and control the activity of MCU. At low intracellular calcium concentrations, MICU1/2 inhibit calcium entry. As the cytosolic calcium concentration increases, calcium binding to the EF-hand domains of MICU1/MICU2 leads to conformational changes, opening the channel and allowing calcium entry into the matrix (Csordás et al., 2013; Paillard et al., 2017; Perocchi et al., 2010; Plovanich et al., 2013). EMRE is a transmembrane protein required for MCU function, as EMRE knockout abrogates calcium influx, even upon MCU overexpression, and is necessary for the interaction between MCU and MICU1/2 (Sancak et al., 2013; Vais et al., 2016).

2.5.4.2. Calcium efflux

Calcium release from the mitochondria is mediated by Na^+ dependent (Na^+/Ca^{2+}) exchangers (NCX) in excitable tissues (e.g. brain, heart) (Carafoli et al., 1974; Palty et al., 2010); and by Na^+ independent (H^+/Ca^{2+}) exchangers (HCX) in non-excitable tissues (e.g. liver) (Lin and Stathopulos, 2019; Pozzan et al., 1977; Tsai et al., 2014), located at the IMM. In both systems, the rate of calcium transport is significantly slower than the rate of calcium uptake through the MCU (Marinelli et al., 2014; Wingrove and Gunter, 1986). Other non-specific modes of calcium efflux exist, such as the mitochondrial permeability transition (MPT) pore, that forms at the IMM in calcium-loaded mitochondria and leads to increased mitochondrial permeability (Haworth and Hunter, 1979).

2.5.4.3. Calcium microdomain signalling

One puzzling property of the mitochondrial calcium uptake is the MCU's very low affinity for calcium (Marchi and Pinton, 2014). This fact implies that the rise in cytosolic calcium necessary to induce

mitochondrial calcium uptake should be much higher than those observed in living cells. How can mitochondria so rapidly uptake calcium in these conditions? This is achieved by the close proximity between mitochondria and hotspots of calcium increase. These so-called microdomains of high cytosolic calcium occur at sites of calcium influx at the plasma membrane or of calcium release from intracellular stores. At these locations, calcium transiently reaches higher levels than in the overall cytoplasm. Calcium signalling occurs preferentially at contact sites between mitochondria and the ER, termed mitochondria-associated ER membranes (MAMs). MAMs are enriched in ER-calcium channels, such as IP3R, that release calcium which then is transferred into the mitochondrial matrix (Fujimoto and Hayashi, 2011; Lee and Min, 2018; Rizzuto et al., 1993; Rizzuto et al., 1998).

2.5.5. Redox homeostasis

Mitochondria are known sources of ROS. ROS are radical and non-radical oxygen species derived from oxygen. The reduction of oxygen by the addition of electrons leads to the formation of different types of ROS including: Superoxide ($[O_2]^{\bullet-}$), hydrogen peroxide (H_2O_2), hypochlorous acid (HOCl) and singlet oxygen ($^1O_2$). Most ROS are generated as by-products of the mitochondrial ETC reactions. Occasionally during the flow of electrons, oxygen molecules undergo one- or two-electron reduction reactions to form ROS, being $[O_2]^{\bullet-}$ and H_2O_2 the most commonly produced (Dickinson and Chang, 2011; Murphy, 2009).

ROS are widely known for their detrimental effects and thought to be the main contributors to the aging process. This free radical theory of aging proposes that aging is a consequence of the accumulation of oxidative damage, caused by ROS (Harman, 1956). ROS mediate redox modifications on biomolecules, the most commonly described being the oxidation of the thiol side chains of cysteine residues. If the redox homeostasis is not controlled, ROS will lead to oxidative stress, characterized by damage of nucleic acids, proteins and lipids (Dickinson and Chang, 2011).

The cell developed ways to control redox homeostasis, such as ROS buffers and antioxidant enzymes (Dickinson and Chang, 2011; Munro and Treberg, 2017; Zorov et al., 2014). Glutathione (GSH), a tripeptide of glutamic acid, cysteine and glycine, is one of the most prevalent and important thiol buffers in the cell. The ratio of GSH (reduced) and its disulfide, GSSG (oxidized), reflects the redox capacity of the cell. The ratio is controlled by oxidation/reduction reactions involving GSH peroxidase and GSH reductase. Oxidative stress leads to a dramatic depletion of GSH, thereby promoting cell death (Franco and Cidlowski, 2009; Xiong et al., 2011). Antioxidant enzymes act by neutralizing ROS. The Cu/Zn superoxide dismutase 1 (Sod1) dismutates $[O_2]^{\bullet-}$ to H_2O_2, that is further reduced to H_2O by catalase, glutathione peroxidases or peroxiredoxins. All of these proteins are examples of antioxidant enzymes and are localized either in the cytosol or in the mitochondria (Rhee et al., 2005).

Despite their potentially harmful effects, ROS have important functions in physiological cellular processes (Ray et al., 2012; Zorov et al., 2014). As an example, ROS have been implicated in the control of cell migration. H_2O_2 can act by regulating the actin cytoskeleton. H_2O_2-mediated oxidation of a cofilin regulatory phosphatase leads to cofilin activation. This actin regulatory protein then induces membrane ruffling and cell motility (Kim et al., 2009). At the whole-organism level, tissue-scale fluxes of H_2O_2 have been observed in *Danio rerio* (zebrafish) *Drosophila* embryos after injury, that contribute to the recruitment of leukocytes (Niethammer et al., 2009a; Razzell et al., 2013).

Mitochondria are thus critical mediators of redox homeostasis, either by the production or by the detoxification of ROS.

2.6. Mitochondrial dynamics

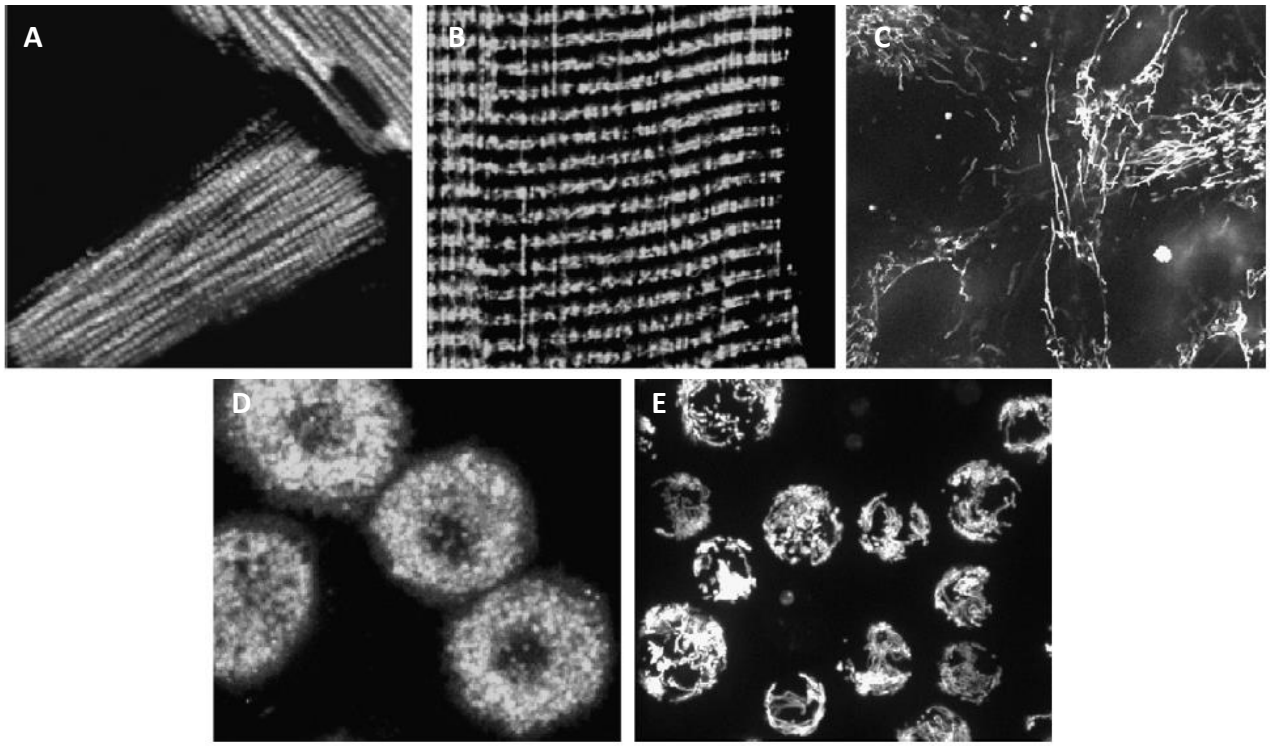

Figure 6. Mitochondrial morphology in different cell types.
(A) rat cardiomyocytes, (B) rat skeletal muscles, (C) human pancreatic cells, (D) rat hepatocytes, (F) promyeloid cells. Mitochondria were imaged by confocal fluorescent live microscopy using mitochondria-specific fluorescent probes TMRM or MitoTracker (A, B, C, and E) or autofluorescence

Mitochondrial morphology, number and position can vary depending on the cell type or developmental stage (Bereiter-Hahn and Vöth, 1994; Collins et al., 2002; Kuznetsov et al., 2009; Rastogi et al., 2019). Just to give a few examples, in cardiac or skeletal muscle cells (Fig. 6 A, B, respectively), mitochondria display a very regular arrangement, mostly confined to the spaces between myofibrils. Pancreatic cells (Fig. 6C) have a dense network of elongated mitochondrial surrounding the nuclei, while in other cells, such as hepatocytes or promyeloid cells (Fig. 6 D, E), mitochondria are distributed rather uniformly across the cell (Kuznetsov et al., 2009).

The observation of living cells defied the textbook definition of mitochondrial morphology. Instead of being static bean-shaped organelles, as depicted in many textbooks, mitochondria can change their size, number, shape and localization. This dynamic behaviour of mitochondria was first described more than a century ago by Lewis and Lewis (Lewis and Lewis, 1914) in cultured cells and has been observed in many other cell types ever since (Bereiter-Hahn, 1990; Westermann, 2010). The concept of mitochondrial dynamics was created to include all these aspects of mitochondrial behaviour. Some authors have a broader mitochondrial dynamics definition, including the events that control mitochondrial morphology changes,

trafficking, biogenesis and quality control (Eisner et al., 2018), while others just refer to the antagonizing fusion and fission events that determine mitochondrial shape and number (Dorn, 2018; Friedman and Nunnari, 2014).

2.6.1. Fission

Mitochondrial fission is the process through which one mitochondrion divides into two mitochondria. It facilitates mitochondrial calcium transport, elimination of damaged mitochondria and equal segregation of mitochondria during cell division, among other functions (Lee and Yoon, 2016). Mitochondrial fission is accomplished by Dynamin-related protein 1 (Drp1) (Lee and Yoon, 2016; Scott and Youle, 2010). The implication of Drp1 in the control of mitochondrial morphology was first described in budding yeast (Otsuga et al., 1998) and cultured human cells (Smirnova et al., 2001). Drp1 is a large GTPase and, as other members of the dynamin superfamily of proteins, contains an amino terminal GTPase domain, a middle domain, and a GTPase effector domain (GED) (Bliek, 1999). When inactive, Drp1 is found mostly in the cytosol; when activated, it is recruited to the mitochondria and oligomerizes in a ring-like manner around these organelles (Bleazard et al., 1999; Labrousse et al., 1999; Smirnova et al., 2001; Yoon et al., 2001). GTP hydrolysis is the driving force to change conformation and constrict the mitochondria (Ingerman et al., 2005; Mears et al., 2011). Some studies suggest that Drp1-mediated constriction alone is not sufficient to divide the mitochondria (Yoon et al., 2001) and that additional dynamin proteins aid in the final steps of constriction and scission (Lee et al., 2016).

Drp1 oligomers dynamically and randomly assemble and disassemble on the OMM, independently of fission or constriction events (Ji et al., 2015; Legesse-Miller et al., 2003). So, what leads to a fission event? Fission sites are marked by contacts with the ER that wraps around mitochondria even before recruitment of Drp1 (Friedman et al., 2011). The ER-resident actin regulator Inverted Formin 2 (INF2) and the mitochondria resident actin-nucleating Spire protein (Spire1C) cooperate and coordinate polymerization of actin filaments, followed by recruitment of the myosin IIa motor, whose movement on F-actin leads to constriction of mitochondria (Korobova et al., 2013; Korobova et al., 2014; Manor et al., 2015). These events culminate in oligomerization and accumulation of Drp1 at the OMM (Hatch et al., 2014; Ji et al., 2015; Prudent and McBride, 2016) (Fig. 7).

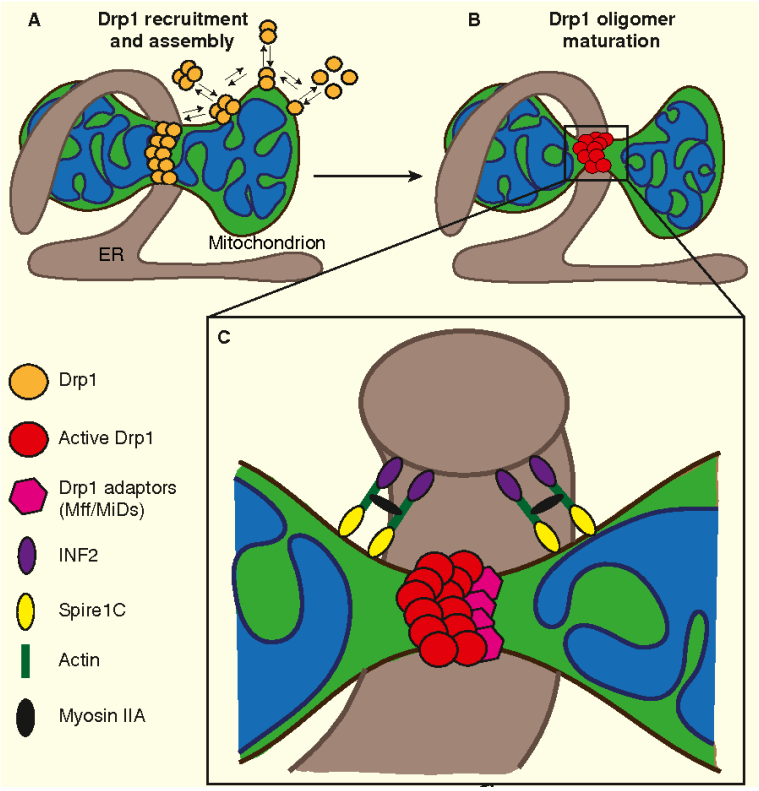

Figure 7. Mitochondrial fission.
(A) Drp1 dimers shift between the cytosol and the OMM. Oligomeric Drp1 accumulates at sites of ER-driven constriction. (B) Drp1 assembly into a ring structure further constricts the mitochondria. (C) Mature Drp1 oligomers hydrolyse GTP, resulting in fission. The zoomed area shows the factors regulating mitochondrial division. ER-localized INF2 and mitochondrial Spire1C drive F-actin polymerization. Myosin IIa motor possibly acts as the force generator required for mitochondrial constriction. The accumulation of F-actin at the ER–mitochondrial contact sites promotes Drp1 recruitment, which is also aided by Drp1 adaptors. Adapted from (Prudent and McBride, 2016).

In addition to ER-mediated mitochondrial constriction, Drp1 is recruited to mitochondria by pro-fission factors. Drp1 has an intrinsic ability for membrane binding (Yoon et al., 2001), but, depending on the organism, different adaptor proteins can recruit Drp1 to the OMM. Dynamin-related protein 1 (Dnm1, Drp1 yeast homolog) recruitment and distribution at the OMM is controlled by the OMM protein Mitochondrial fission 1 protein (Fis1) (Mozdy et al., 2000) and the adaptor proteins C-C chemokine receptor type 4 (CCR4)-associated factor 4 (Caf4) and Mitochondrial division protein 1 (Mdv1) (Griffin et al., 2005; Guo et al., 2012; Tieu and Nunnari, 2000). Caf4 and Mdv1 bind both Dnm1 and Fis1, forming a link between Fis1 and Dnm1, thus bringing Dnm1 to the OMM (Naylor et al., 2006). An alternative fission complex in yeast involves the accessory proteins Mitochondrial distribution and morphology protein 36 (Mdm36) and Nuclear migration protein 1 (Num1), which seem to anchor mitochondria at the cell cortex and aid mitochondrial scission through membrane tension (Cerveny et al., 2007; Hammermeister et al., 2010).

In mammals, fission is promoted by association of Drp1 to mitochondria via OMM receptors such as Fis1 (James et al., 2003; Stojanovski et al., 2004; Yoon et al., 2003), the mitochondrial fission factor (Mff) (Gandre-Babbe and van der Bliek, 2008; Otera et al., 2010) and the mitochondrial dynamics proteins of 49 and 51 kDa MiD49/51 (Losón et al., 2013; Palmer et al., 2011; Palmer et al., 2013; Zhao et al., 2011a). Other proteins have been suggested to participate in the regulation of fission, but their role and interaction with Drp1 is still not clearly understood. Those include the mitochondrial protein of 18 kDa (MTP18) (Tondera et al., 2005),

the ganglioside-induced differentiation-associated protein 1 (Gdap1) (Niemann et al., 2005; Pedrola et al., 2005) and Endophilin B1 (Karbowski et al., 2004).

To add another layer of complexity to this process, Drp1 is regulated post-translationally by a myriad of different modifications, including phosphorylation, S-nitrosylation, SUMOylation, ubiquitination, and O-GlcNAcylation (Chang and Blackstone, 2010). Just to give an example, phosphorylation of Drp1 is the most widely studied post-translational modification, and has opposing effects on its activity, depending on the phosphorylated residue. At Ser 616, it leads to Drp1 activation and consequently to mitochondrial fission (Kashatus et al., 2011; Taguchi et al., 2007), while phosphorylation at Ser 367 is inhibitory of Drp1 GTPase activity (Chang and Blackstone, 2007; Cribbs and Strack, 2007).

It is also worth mentioning that, in addition to mitochondria fission, the fission machinery components Drp1, Mff, Gdap1 and Fis1 are also involved in peroxisomal division (Honsho et al., 2016; Huber et al., 2013).

2.6.2. Fusion

Fusion describes the process of tethering and union of apposed mitochondria. Fusion of mitochondria requires the successful union of both the OMM and the IMM (Fig 6), resulting in mitochondria elongation. A fused network of mitochondria is usually observed in high energy demanding cells (Westermann, 2012). Similar to mitochondrial fission, fusion is mediated by Dynamin related proteins (Dorn, 2018; Lee and Yoon, 2016). The fusion of both membranes requires GTP hydrolysis. Additionally, IMM fusion is dependent on the maintenance of the ΔΨmt (Meeusen et al., 2004) (Fig. 8).

The first member of the Dynamin family required for OMM fusion was found in *Drosophila*. In a study about spermatogenesis, Hales and Fuller reported that *fuzzy onions* (*fzo*) mutant males have defects in mitochondrial fusion and are sterile. By mutating its predicted GTPase domain, they found that the Fzo GTPase activity was required for its function in mitochondrial fusion (Hales and Fuller, 1997). Fzo mammalian homologs, Mitofusin 1 (Mfn1) and Mitofusin 2 (Mfn2), are tethered to the OMM by two transmembrane domains. The cytosolic portion contains the GTPase domain and two coiled-coil protein-interaction domains that mediate homotypic or heterotypic binding of Mfn proteins (Koshiba et al., 2004; Rojo et al., 2002). Binding of Mfn isoforms from neighbouring mitochondria promotes mitochondrial tethering and Mfn GTPase activity mediates OMM fusion (Detmer and Chan, 2007; Koshiba et al., 2004).

Mfn1/2 proteins are regulated post-transcriptionally by ubiquitination, which leads to their degradation and inhibition of OMM fusion (Durr et al., 2006; Tanaka et al., 2010; Youle and Narendra, 2011).

The protein mediator of IMM fusion is called mitochondrial genome maintenance 1 (Mgm1) in yeast, EAT-3 in *C. elegans* (Kanazawa et al., 2008), and Optic atrophy 1 (Opa1) in mammals and *Drosophila* (Alexander et al., 2000; Delettre et al., 2000; Misaka et al., 2002; Yarosh et al., 2008). Mgm1 name derives from the defects in mitochondrial genome maintenance caused by mutation of the corresponding gene (Jones and Fangman, 1992). Later on, this phenotype was found to be a consequence of impaired IMM fusion (Wong et al., 2000). Opa1 designation comes from the optic atrophy defects associated with *OPA1* mutation in humans (Alexander et al., 2000; Delettre et al., 2000). Opa1 undergoes post-translational cleavage downstream of its transmembrane domain by IMM-associated metalloproteases: OMA1 and YME1L (Anand et al., 2013; Consolato et al., 2018; Ehses et al., 2009). Therefore, two forms of Opa1 coexist: an IMM-anchored long Opa1 (L-Opa1) and a transmembrane region-free short Opa1 (S-Opa1) in the IMS. This balance of L-Opa1 and S-Opa1 forms is required for the maintenance of both normal mitochondrial morphology and mitochondrial DNA (Herlan et al., 2003). Induction of Opa1 cleavage prevents IMM fusion and facilitates fission, while L-Opa1 is required for fusion (Ishihara et al., 2006; MacVicar and Langer, 2016).

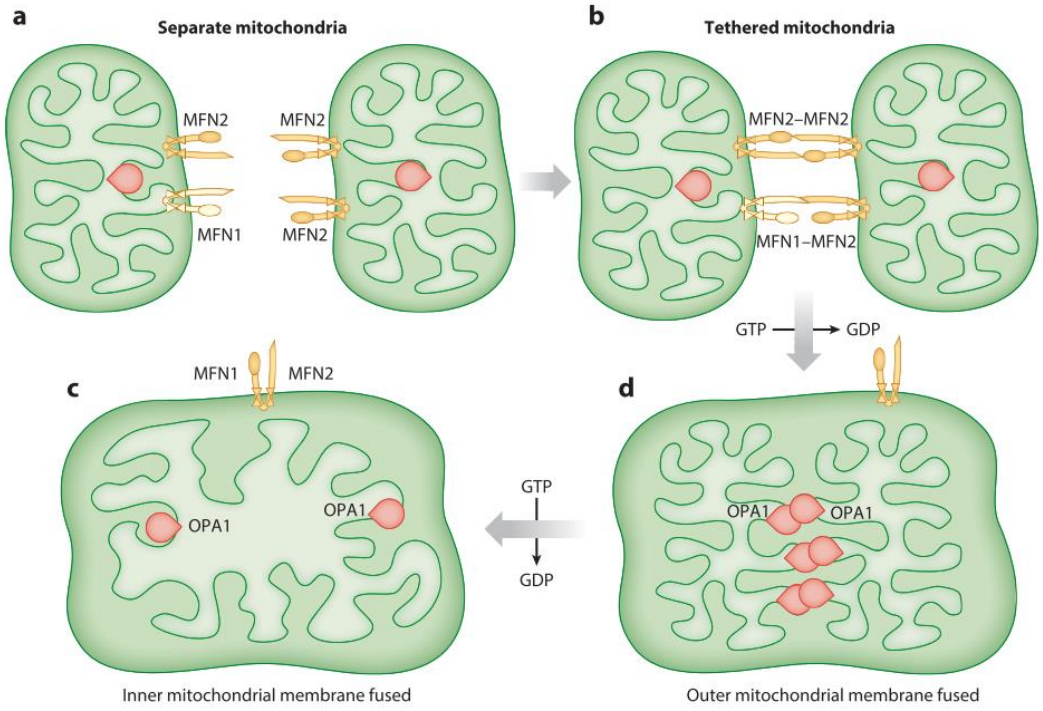

Figure 8. Mechanism of mitochondrial fusion.
(a) Separate mitochondria with MFN1 and MFN2 localized at the OMM and OPA1 localized at the IMM. (b) Tethering by MFN homo- or heterodimers. (c) After GTP-dependent MFN-mediated OMM fusion. (d) After GTP-dependent OPA1-mediated IMM fusion. Adapted from (Dorn, 2018).

Opa1 is essential not only for IMM fusion, but also for maintaining mitochondria cristae structure (Frezza et al., 2006; Meeusen et al., 2006; Olichon et al., 2003) and anchoring nucleoids to the IMM (Elachouri et al., 2011). Mfn2 also localizes to the ER membrane and, by interacting with Mfn1 or Mfn2 of the mitochondria,

it controls the establishment of ER-mitochondria contacts (De Brito and Scorrano, 2008; Filadi et al., 2015; Leal et al., 2016; Wang et al., 2015). Additionally, Mfn2 is involved in mitophagy (see section 2.7.4) (Chen and Dorn, 2013) and in tethering mitochondria to microtubules (Misko et al., 2010).

2.6.3. Trafficking

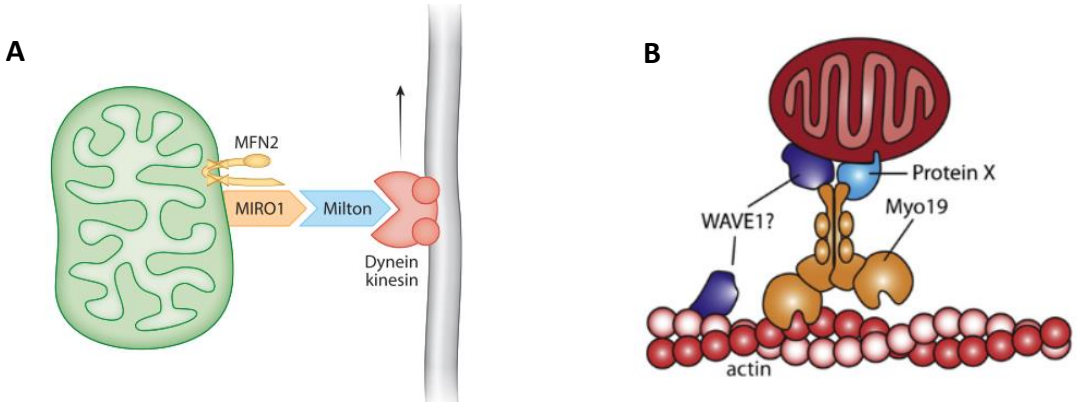

Figure 9. Mitochondrial trafficking.
(A) Microtubule-based mitochondrial transport: Miro binds mitochondria via Mfn2 and interacts with Milton, coupling mitochondria with dynein and kinesin molecular motors that move along microtubules. (B) Actin-based mitochondrial transport: Myo19 motor mediates transport along actin filaments. The adaptor proteins are still not well characterized but might involve WAVE1. Protein X – unknown adaptor protein. Adapted from (Dorn, 2018; Lovas and Wang, 2013).

Mitochondria must be able to position themselves at the right place to perform their functions efficiently. In migrating cells, mitochondria localize at the leading edge of the cell, where most energy is needed (Schuler et al., 2017). In sperm cells, mitochondria are located at the proximal part of the flagellum to supply the flagellar motor proteins with energy to sustain the movements of the sperm cell (Fawcett, 1975). In neurons, some mitochondria reside far away (sometimes up to a meter) from the cell body, to fuel the synapses (Schwarz, 2013). Trafficking of mitochondria is accomplished by attachment of mitochondria to the cellular cytoskeletal tracks. Both actin- and microtubule-based transport have been reported (Lovas and Wang, 2013; Morris and Hollenbeck, 1995).

Mitochondrial movement occurs predominantly along microtubules by kinesin and dynein motors. Microtubules are polarized polymers with a plus (+) end, usually facing the cell periphery, and a minus (-) end, anchored at the centrosome near the nucleus. Anterograde movement toward the (+) ends of microtubules is mediated by kinesin motors, while retrograde movement toward the (-) ends is mediated by dynein motors (Barlan and Gelfand, 2017). The tethering of mitochondria to microtubules is achieved via the Miro-Milton-Molecular motor complex. Although alternative adaptor complexes have been reported, the Miro-Milton-Kinesin complex (Fig. 9 A), that acts in anterograde movement, is the most well established

(Lovas and Wang, 2013). The small GTPase Mitochondrial Rho (Miro) integrates the OMM through a C-terminal hydrophobic domain and binds to the adaptor protein Milton (Milt), which in turn binds to kinesin. Retrograde movement of mitochondria is not so well studied, but evidence from *Drosophila* suggests that it is mediated by Miro as well (Russo et al., 2009).

Short-distance trafficking of mitochondria occurs through actin filaments (Fig. 9 B). The actin-based motor Myosin XIX (Myo19) regulates mitochondrial morphology and transport along actin filaments. However, the link between mitochondria, Myo19 and F-actin is still not well understood. Myo19 has a unique 30-45 amino acids motif in its C-terminal domain that is necessary and sufficient for mitochondrial localization (Quintero et al., 2009; Rohn et al., 2014; Shneyer et al., 2016). WAVE1, a known regulator of F-actin polymerization (Kim et al., 2006), has been implicated in depolarization-induced mitochondrial movement in neurons (Sung et al., 2008), but it is still not clear if or where it fits in the Myo19-based transport mechanism (Fig. 9 B). A recent study suggested that Miro1/2 are mitochondrial receptors of Myo19 (López-Doménech et al., 2018; Oeding et al., 2018), suggesting that these adaptor proteins coordinate both microtubule- and actin-based mitochondrial movement.

Not only can mitochondria travel within the cell, but they can also be transferred to neighbouring cells (Plotnikov et al., 2015). The transfer of mitochondria via intercellular tunnelling nanotubes (TNTs) can rescue OXPHOS or prevent cell death in cells with dysfunctional mitochondria (Guo et al., 2018; Spees et al., 2006). TNTs are F-actin-based structures, which have been observed both *in vitro* and *in vivo*, mediate the transfer of molecules and organelles between cells (Austefjord et al., 2014; Marzo et al., 2012). Notably, Miro has also been implicated in this mode of mitochondrial transport (Ahmad et al., 2014).

2.6.4. Mitophagy

Given all the important functions performed by mitochondria (reviewed in 2.5), it is of the upmost importance to maintain a functional population of mitochondria. Damaged mitochondria are usually a source of ROS and thus toxic for the cell. Therefore, dysfunctional mitochondria must be recognized, separated from the healthy ones and eliminated. The cell accomplishes this by the process of mitochondrial autophagy or mitophagy. This selective catabolic pathway is regulated by several autophagy-related (Atg) proteins and involves the sequestration of mitochondria in a double-membrane organelle termed autophagosome (Moyzis et al., 2015).

A general overview of mitophagy is shown in Figure 10 A, which involves the following steps:

1) Nucleation: a small group of molecules, called the class III phosphatidylinositol (3)-phosphate kinase (PI3K) complex, are mobilized to the site of autophagosome formation (phagophore) (Suzuki et al., 2001);

2) Elongation: two ubiquitin-like conjugation systems, Atg12-AtgG5 and Atg8/light chain 3 (LC3), contribute to the elongation of the phagophore. Once it is completed, the mature lipidated form of LC3 (LC3-II) remains at the autophagosome membrane;

3) Sequestration: LC3-II interacts with proteins that label dysfunctional mitochondria (Lamark et al., 2009), that are then engulfed by the autophagosome;

4) Maturation and fusion: the autophagosome docks and fuses with the lysosome;

5) Degradation: mitochondria are digested by lysosomal enzymes.

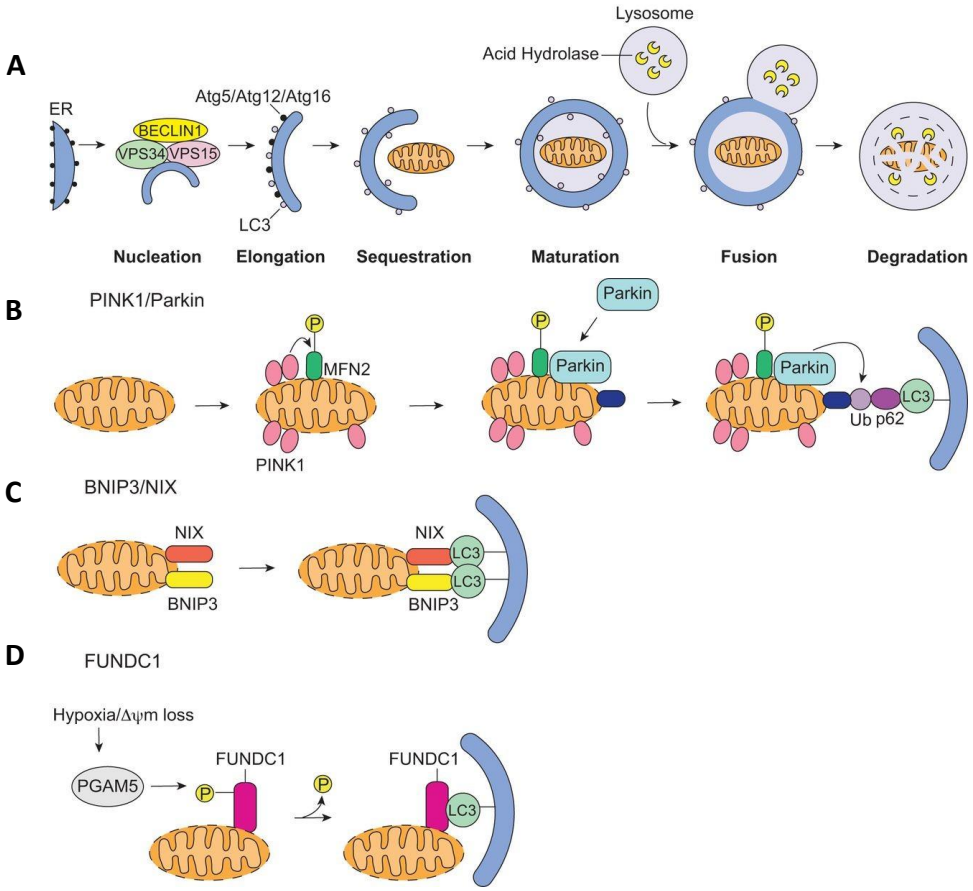

Figure 10. Mitophagy.

(A) Mitochondrial autophagy initiates with nucleation by BECLIN 1/VPS34/VPS15, leading to the formation of the autophagosome. Next, ATG5/ATG12/ATG16 and light chain 3 (LC3) elongate the membrane. The autophagosome fuses around a mitochondrion. Finally, the autophagosome fuses with a lysosome and the mitochondrion is degraded by lysosomal hydrolases. ER, endoplasmic reticulum. (B-D) Mitophagy pathways. (B) PINK1/Parkin-mediated mitophagy starts with accumulation of PINK1 at the OMM of depolarized mitochondria. PINK1 then phosphorylates Mitofusin 2 (MFN2), which leads to recruitment of Parkin. The p62 adaptor protein binds to Parkin-ubiquitinated proteins and LC3 on the autophagosome. (C) BNIP3 and NIX act as mitochondrial receptors and directly bind to LC3 to induce mitophagy. (D) Dephosphorylation of FUNDC1 by PGAM5 allows FUNDC1 to directly interact with LC3 to induce mitophagy. Adapted from (Moyzis et al., 2015)

Different selective mitophagy pathways have been described, that differ in the way mitochondria are targeted for destruction (Fig. 10 B-D). In the PINK1/Parkin-mediated mitophagy (Fig. 10 B), loss of ΔΨmt promotes the accumulation of the serine/threonine kinase Phosphatase and Tensin Homolog deleted on Chromosome 10 (PTEN)-induced kinase 1 (PINK1) at the OMM. PINK1 phosphorylates Mfn2, which acts as a receptor for the E3 ubiquitin ligase Parkin (Chen and Dorn, 2013). Activated Parkin ubiquitinates mitochondrial proteins that are recognized by the p62 adaptor protein, linking targeted mitochondria to LC3-II on the autophagosome. In mitochondrial receptor-mediated mitophagy (Fig. 10 C-D), the B-cell lymphoma 2 (Bcl-2)-related proteins Nix and Bcl2/adenovirus E1B 19-kDa interacting protein 3 (Bnip3) (Hanna et al., 2012; Novak et al., 2010) or FUN14 Domain Containing 1 (FUNDC1) (Liu et al., 2012) act as receptors that interact with LC3-II via their LIR (LC3 interacting region) motif (Moyzis et al., 2015).

2.6.5. Biogenesis

Mitochondrial biogenesis is the regulated growth and division of pre-existing mitochondria and involves coordinated and increased production of nuclear and mitochondrial-encoded proteins. High energy demands, cold exposure, caloric restriction, oxidative stress, cell division and renewal, or the need to restore the number of functional mitochondria after mitophagy, are triggers of this pathway. After the incorporation of lipids and import of proteins to the existing mitochondrial pool, there are fission and fusion events to modulate the mitochondrial network, according to the cellular needs (Dorn et al., 2015; Jornayvaz and Shulman, 2010; Ventura-Clapier et al., 2008).

The main regulator of mitochondrial biogenesis is PPAR (peroxisome proliferator-activated receptor)-γ coactivator-1α (PGC-1α) (Puigserver et al., 1998). PGC-1α is a co-transcription factor that activates different transcription factors, such as nuclear respiratory factors (NFRs) 1 and 2 (Baar et al., 2002; Wu et al., 1999). This leads to the increased expression of the genes encoding mitochondrial proteins (e.g. components of the ETC complexes) (Ventura-Clapier et al., 2008) and of the mitochondrial transcription factor A (Tfam), which controls the transcription and the replication of mtDNA (Virbasius and Scarpulla, 1994).

The mitochondrial biogenesis cascade is triggered by many factors including exercise, diet, hormones, and stressors. For example, AMP-activated protein kinase (AMPK), an important regulator of the energy metabolism, triggers mitochondrial biogenesis in times of energy crisis (Hardie, 2007; Zong et al., 2002). Other activators of the biogenesis pathway include calcium/calmodulin-dependent protein kinase IV (CaMKIV) (Wu et al., 2002), nitric oxide (NO) (Nisoli et al., 2003) and transducer of regulated CREB (cAMP-

response-element-binding protein)-binding protein (TORC) (Wu et al., 2006), among others (Jornayvaz and Shulman, 2010).

2.6.6. Mitochondrial dynamics in health and disease

Mitochondrial dynamics enable mitochondria to quickly adapt to the cell energetic demands. Mitochondrial fusion favours higher OXPHOS rates (Westermann, 2012; Yao et al., 2019). The impairment of fusion results in mitochondrial dysfunction and loss of mitochondrial respiratory capacity (Chen et al., 2005). Fusion promotes the exchange of intramitochondrial material, which can rescue mild mitochondrial dysfunction as it dilutes the damaged components (Nakada et al., 2009), and is important for mtDNA maintenance, as it preserves a balanced proteome, including the mtDNA synthesis enzymes (El-Hattab et al., 2017; Jones and Fangman, 1992). If fusion is not enough, then mitochondrial quality control relies on fission to selectively separate healthy from dysfunctional mitochondrial parts, followed by mitophagy (Twig et al., 2008). Mao and colleagues have shown that interfering with the interaction between the autophagy protein Atg11 and Drp1 severely blocks mitophagy (Mao et al., 2013). Activation of Drp1 has been observed in Bnip3-mediated mitophagy (Lee et al., 2011) and is also implicated in PINK1-Parkin mitophagy pathway (Buhlman et al., 2014). Fission is also required to regulate programmed cell death (Frank et al., 2001; Goyal et al., 2007). Inhibition of Drp1 can prevent several apoptosis hallmarks, such as ΔΨmt dissipation, MOMP and release of cyt c (Frank et al., 2001). In addition, mitochondrial fission also facilitates mitochondrial transport (Fukumitsu et al., 2016) and ensures equal mitochondrial segregation between the two daughter cells during cell division (Fukumitsu et al., 2016; Taguchi et al., 2007).

Given the crucial contribution of mitochondria to normal cellular functions or to the apoptosis of dysfunctional cells, and the interplay between mitochondrial dynamics and function, it is not surprising that mitochondrial dynamics are implicated in disease. Proper regulation of mitochondrial dynamics is essential for development, hence mutations in the mitochondrial fission and fusion machinery components lead to developmental defects and lethality (Chen et al., 2003; Ishihara et al., 2009; Waterham et al., 2007). Moreover, mutations in mitochondrial dynamics genes are implicated in the development of human diseases. Mutations in the *MFN2* human genes lead to development of Type 2 Charcot-Marie-Tooth disease, characterized by abnormalities in the axons of peripheral nerve cells, leading to physical weakness, atrophy, sensory loss, among other symptoms (Kijima et al., 2005; Züchner et al., 2004). OPA1 is mutated in Autosomal Dominant Optic Atrophy, a hereditary disorder that leads to progressive loss of visual acuity, colour vision deficits and central visual field defects (Alexander et al., 2000; Delettre et al., 2000).

Additionally, dysregulation of mitochondrial dynamics is implicated in a wide range of human pathologies, such as neurodegenerative diseases (Johri and Beal, 2012), like Alzheimer's (Zhu et al., 2012), Parkinson's (Van Laar and Berman, 2009), and Huntington's (Chaturvedi et al., 2009; Reddy, 2014) diseases, but also in type II diabetes (Rovira-Llopis et al., 2017) and cancer (Anderson et al., 2018; Trotta and Chipuk, 2017; Wallace, 2012). Just to give a few examples, the proposed link between mitochondrial dynamics and neurodegeneration involves age-dependent increased production and abnormal accumulation of proteins in mitochondria (Amyloid-β in Alzheimer's Disease, Huntingtin in Huntington's disease, PINK/Parkin in Parkinson's disease) that promote ROS production and activate the fission machinery. The excessive fragmentation of mitochondria impairs energy production and supply at the nerve terminals, leading to synaptic neurodegeneration (Reddy et al., 2011). In cardiac tissues, the distribution of mitochondria is highly limited by the myofibrils and thus fusion and fission events are rare. Nevertheless, the mitochondrial dynamics machinery performs other functions and has been implicated in the development of cardiomyopathies. Impairment of the function of Mfn1/2 leads to increased mitochondrial fragmentation, dissipation of the ΔΨmt, increased ROS production and apoptosis (Marín-García and Akhmedov, 2016). Moreover, disruption of Drp1 function impairs mitophagy, leading to accumulation of dysfunctional mitochondria and consequent cardiac dysfunction (Ikeda et al., 2015)

In conclusion, the mitochondrial dynamics machinery is a critical regulator of mitochondrial function and research on this topic will help to understand the cellular and molecular mechanisms involved in several biological processes and how their failure leads to development of diseases.

3. THE ROLE OF MITOCHONDRIA AND EPITHELIAL WOUND HEALING

The contribution of mitochondria to the development of human diseases is a hot topic of research. As previously mentioned, mitochondrial dysfunction has been linked to the aetiology or the aggravation of metabolic diseases (Bhatti et al., 2017), neurodegeneration (Cabezas-Opazo et al., 2015; Chaturvedi and Flint Beal, 2013; Chen and Chan, 2009; Reddy et al., 2011; Zorzano and Claret, 2015), muscle disorders (Zulian et al., 2016), cardiovascular diseases (Forini et al., 2015; Marín-García, 2013) and cancer (Wallace, 2012). However, the contribution of mitochondria and mitochondrial dynamics to epithelial repair has not been so deeply investigated.

It is known that ROS regulate many aspects of wound healing. Low levels of ROS are required for the inflammatory response to fight invading pathogens and for cell survival. However, excessive ROS production or inefficient ROS detoxification leads to oxidative damage, which is the main cause of non-healing chronic wounds (Sanchez et al., 2018). The amelioration of oxidative stress by manipulation of mitochondrial ROS production or detoxification, treatment with antioxidants, or transfer of healthy mitochondria to dysfunctional cells, improves wound healing in mammals and represents a potential therapeutic to treat wound healing complications in humans (Demyanenko et al., 2015; Demyanenko et al., 2017; Dunnill et al., 2017; Janda et al., 2016; Sanchez et al., 2018; Zhou et al., 2019). In contrast, in models of simple epithelia wound healing, ROS production is beneficial to the wound closure. Injury-induced calcium increase triggers the production of mitochondrial ROS, which have been shown to regulate several aspects of the wound healing response: immune cell recruitment (Razzell et al., 2013), cell junction remodelling (Hunter et al., 2018a) and actomyosin dynamics (Hunter et al., 2018a; Xu and Chisholm, 2014).

Increasing evidence supports a role for mitochondrial calcium in cell migration. Knockdown of MCU during zebrafish (*Danio rerio*) development leads to reduced mitochondrial calcium levels and impairment of cell migration (Prudent et al., 2013). MCU knockdown in the epidermis of *C. elegans* leads to wound healing impairment (Xu and Chisholm, 2014). In human cancer cell lines, depletion of MCU also leads to a drastic reduction of cell migration (Prudent et al., 2016; Tang et al., 2015; Tosatto et al., 2016).

A recent report compared normal skin fibroblasts with keloid fibroblasts, found in keloid scars which represent an abnormal response to cutaneous wound healing. Li and colleagues found that keloid fibroblasts present mitochondrial dysfunction, as they showed reduced ATP production and increased proton leakage. Interestingly, they observed an increase in mitochondrial mass and in the expression of fission, fusion and biogenesis genes, in addition to abnormal mitochondrial morphology. This work suggests that the dysregulation of mitochondrial dynamics might be involved in abnormal tissue repair (Li et al., 2019). Another study has found that Drp1 mediated-mitochondrial fission induces an increase in mitochondrial ROS that activate Rho GTPases, inducing F-actin formation in human mesenchymal stem cells (hMSCs). Furthermore,

treatment of skin excision wounds with hMSCs enhanced wound closure, vascularization and re-epithelialization, suggesting a role for Drp1 in tissue repair (Ko et al., 2017). Moreover, evidence from cancer models shows that an imbalance in mitochondrial dynamics towards mitochondrial fission favours cancer cell migration, and inhibiting fission or promoting fusion can impair cancer invasion (Ferreira-da-Silva et al., 2015; Peiris-Pagès et al., 2018; Zhao et al., 2013). Drp1 is also implicated in the regulation of T cell activation and migration (Simula et al., 2018).

Although these data suggest that mitochondrial dynamics have the ability to regulate the cellular processes and the different cell types involved in wound healing, further research is required to get the big picture and understand how mitochondrial dynamics influences epithelial repair.

4. AIMS

The work described in this thesis aims to understand the contribution of mitochondria to epithelial repair. As mitochondrial function and dynamics are intimately connected, we aim to investigate how mitochondrial dynamics impacts on mitochondrial function during wound healing, using the *Drosophila* embryonic epidermis as a model system. To achieve this goal, this work has three specific aims:

1) To identify the mitochondrial dynamics machinery components that are required for wound healing;
2) To characterize mitochondrial dynamics during wound healing;
3) To analyse the wound closure phenotype of the loss of function of the mitochondrial dynamics mediators.

CHAPTER 2. MATERIALS & METHODS

“Everything is theoretically impossible, until it is done.”

– Robert A. Heinlein

1. *Drosophila* strains and handling

Flies were maintained at 18ºC, except for crosses which were kept at 25ºC, on standard *Drosophila* medium. Detailed information about the fly lines used in this work is listed on Table 1. The detailed composition of the *Drosophila* medium is listed on Table 2.

ubi-PLCγPH::ChFP and *UAS-mito::GCaMP3* were a gift from Y. Bellaïche and F. Kawasaki, respectively. *UAS-mito-roGFP2-Grx1*, *UAS-cyto-roGFP2-Grx1*, *UAS-mito-roGFP2-Orp1* and *UAS-cyto-roGFP2-Orp1* were kindly provided by Tobias P.Dick. *Zip* $^{CPTI\text{-}100036}$*::GFP* and *ubi-E-cad::GFP* were obtained from the Kyoto *Drosophila* Genomics and Genetic Resources Stock Center, Kyoto Institute of Technology, Kyoto, Japan. All the remaining fly lines were obtained from the Bloomington *Drosophila* Stock Center, Indiana University, Bloomington, USA.

For live imaging, the *Drp1*^{KG03815} and *Opa1*^{EY09863} mutant alleles were recombined with live reporter lines. Mutant alleles, transgenic and recombinant lines were crossed to balancer stocks that express GFP driven by a *Twist-Gal4* driver (Halfon et al., 2002).

Fly lines were crossed in laying pots and embryos were collected at 25°C overnight in apple juice agar plates. Embryos were dechorionated in 50% bleach and washed extensively with distilled water. Homozygous mutant embryos were identified by the absence of GFP fluorescence. Stage 15-16 embryos were selected by the shape of the yolk (Campos-Ortega and Hartenstein, 1997).

2. Generation of recombinant fly lines

Generation of recombinant flies was done as previously described (Roote and Prokop, 2013).

Mutant flies [*Dynamic-related protein* (*Drp1*)^{KG03815} or *Optic atrophy* (*Opa1*)^{EY09863}] were crossed with flies carrying the transgenic construct of interest (fluorescent marker for live imaging). As meiotic recombination only happens in females, trans-heterozygous females from the first filial generation (F1) were crossed with males carrying a balancer chromosome. Each individual in F2 is the result of an individual recombination event in its mother's germline. Therefore, it was necessary to screen single animals for the presence of the mutation/transgenic construct. F2 males were individually crossed with females carrying a balancer chromosome. F3 males and females were incrossed to establish all potential recombinant lines that were then screened for the presence of the transgenic construct and the mutation.

The presence of the fluorescent marker was assessed by live imaging of embryos from each incross. The presence of the mutation was screened by a complementation test. Potential recombinant flies were crossed with parental mutant flies. *Drp1*^{KG03815} and *Opa1*^{EY09863} homozygosity is embryonic lethal, so the absence of homozygous flies confirms the existence of the mutation in the potential recombinant fly line.

3. Reagents

The reagents used in this work are listed in Table 2.

4. Wounding assay

The wounding assay was performed as previously described (Campos et al., 2010). Selected mutant and control embryos were mounted on double-sided tape affixed to a slide, covered with halocarbon oil 700 and a 32x32mm coverslip, and sealed with nail polish. A 24x24mm coverslip bridge was used between the slide and the top coverslip to avoid embryo squashing.

The embryos were wounded at 25 ºC by using a nitrogen laser-pumped dye laser (435 nm; Micropoint Photonic Instruments) connected to a Nikon/Andor Revolution XD spinning-disk confocal microscope with an electron-multiplying charge-coupled device (EMCCD) camera (iXon 897) using the iQ software (Andor Technology) and using a 60× Plan Apochromat VC Perfect Focus System (PFS) 1.4 NA oil-immersion objective. After wounding, the top coverslip was carefully removed and the embryos were left to recover in a humid chamber at 20 ºC. About 16h later, the wounded embryos were scored under a stereomicroscope for closed, intermediate and open wounds.

The percentage of open wounds was calculated as the ratio of nearly hatching embryos with open wounds over the total number of wounded embryos (dead animals and intermediate wound phenotypes were excluded).

Images of representative embryos depicting open, intermediate and closed wounds were acquired using a Zeiss Axio Imager Z2 widefield system equipped with an Axiocam 506 monochromatic CCD camera, a 10x EC Plan-Neofluar 0.3 NA objective and the Zen Pro 2012 software. Individual Z slices with a step size of 10 µm were acquired. Stacks were processed using the Extended Depth of Field plugin based on the complex wavelet method on Fiji (Forster et al., 2004; Schindelin et al., 2012).

5. Embryo permeabilization

Different embryo permeabilization methods were performed. Dechorionated stage 15 embryos were incubated in either:

- 1:1 heptane:dye solution for 10-30 minutes (min). Drug/dye solutions consisted of Mitotracker 300 nM in PBS 1X at room temperature (RT) (Razzell et al., 2013);

- 1:10 limonene/Citrasolv in MilliQ water, phosphate-buffered saline (PBS) 1X or 5% Tween 20 in PBS 1X (agitated at 37ºC) for 1.5-5 min at RT, followed by 5-15 min incubation in Mitotracker 300 nM in PBS 1X (Rand et al., 2010);
- 1 µM Mitotracker diluted in a 1:1 or 1:2 limonene:heptane solution for 20-30 min at RT (Schulman et al., 2013).

After incubation, the embryos were thoroughly washed with PBS 1X, mounted in glass-bottomed culture dishes (MatTek) coated with embryo glue (double-sided tape dissolved in heptane) and imaged (see 2.8 Live imaging section for details).

6. Embryo microinjection

Dechorionated stage 13-15 embryos were mounted on their ventral side on glass-bottomed culture dishes (MatTek) coated with embryo glue and covered with a 1:1 halocarbon oil 27:700 mixture. Dishes were cut on one side to allow the entrance of the microinjection needle.

Microinjection needles were made using glass capillaries (Harvard Apparatus, ref. 30-0020) and a P-97 Flaming/Brown Micropipette Puller (Sutter Instrument). Injections were done using a PV820 Pneumatic PicoPump (World Precision Instruments) microinjector.

Compounds (0.5 nL) were injected inside the embryo or into the perivitelline space and are predicted to be diluted 50-fold in the embryo (Foe and Alberts, 1983). Dimethyl sulfoxide (DMSO) was added to desiccated compounds to establish stock solutions. Working solutions were made using MilliQ water or PBS 1X. Injected compounds were: 1 µg/ml Fluorescein, 1-10 µM Mitotracker, 25 µM - 25 mM Tetramethylrhodamine methyl ester, perchlorate (TMRM), 23mM Diamide and 5mM Amplex UltraRed.

7. Immunohistochemistry and imaging of fixed samples

7.1. HA-Drp1

Dechorionated embryos were fixed for 20 min in a glass vial containing a mix of 1:1 heptane and 4% formaldehyde in PBS 1X at RT, manually devitellinized and washed in PBSTT (PBS 1X + 0.1% Triton X-100 + 0.1% Tween 20). Embryos were incubated in blocking solution [1% Bovine Serum Albumin (BSA) + PBSTT] overnight (ON) at 4ºC, followed by an ON incubation at 4°C with primary antibody (anti-HA, 1:500). Embryos were washed with PBSTT, incubated with secondary antibodies for 2 hours (h) at RT. Phalloidin staining was performed to label actin. Alexa Fluor® 568 Phalloidin 1:100 was added to the secondary antibody incubation.

4', 6-diamidino-2-phenylindole (DAPI) 1:500 in PBST was added in the last 15 min of secondary antibody incubation. Embryos were washed with PBSTT before adding anti-fading mounting medium [2% 1,4-diazabicyclo[2.2.2]octane (DABCO) + PBS 1X(1:4) + glycerol]. Stained embryos were kept at 4ºC in the dark until mounting.

7.2. TUNEL assay

The TUNEL assay was adapted from a previously described protocol (Arama and Steller, 2006). Dechorionated embryos were fixed for 20 min in a glass vial containing a mix of 1:1 heptane and 8% formaldehyde in PBS at RT. Embryos were devitellinized in a solution of 1:1 heptane:methanol, with vigorous shaking for 1 min. Devitellinized embryos were washed with 100% methanol, rehydrated by sequential incubation in 70%, 50% and 30% methanol solutions in PBS and washed with PBSTT. Embryos were permeabilized in 10 µg/ml proteinase K in PBSTT for 5 min at RT, washed with PBSTT, re-fixed in 8% formaldehyde in PBS at RT for 20 min and washed with PBSTT. Embryos were then incubated in blocking solution (1% BSA in PBSTT) for 30 min at RT and then with primary antibody (anti-Cora C615.16 1:500) ON at 4ºC. For positive controls, embryos were treated with DNaseI (1 µL DNaseI + 4 µL DNase I buffer + 35 µL MilliQ water) during 15 min at 37ºC to induce DNA damage and washed with PBSTT. Embryos were incubated in TUNEL reaction mixture (TUNEL label solution + TUNEL enzyme) ON at 4ºC, followed by DAPI treatment for 15 min at RT. Secondary antibody was diluted in the TUNEL reaction mixture. For negative controls, embryos were incubated in TUNEL label solution (without the TUNEL enzyme). After rinsing in PBSTT, embryos were kept in the dark in anti-fading mounting medium at 4ºC until mounting.

7.3. Mounting and imaging

Stained embryos were mounted between two 24x60 mm coverslips in a drop of mounting medium. The coverslips were separated by one-coverslip-high bridge to avoid embryo squishing and sealed using nail polish. Imaging was performed on an LSM 710 confocal microscope (Zeiss) with a 63× Plan Apochromat 1.4 NA oil-immersion objective (Zeiss). Stacks were acquired using the Zen software (Zeiss) and a step size of 0.5 µm.

8. Live imaging

Live imaging was performed as described previously (Carvalho et al., 2018). Dechorionated stage 15 embryos were mounted on their ventral side on glass-bottomed culture dishes (MatTek) coated with embryo glue and covered with halocarbon oil 27. Embryos were wounded as described above for the wounding assay except that the laser power was lower in order to inflict smaller wounds that are able to close during the imaging procedure.

Time-lapse microscopy of transgenic embryos was performed at 25°C on a Nikon/Andor Revolution XD spinning-disk confocal microscope with a 512 EMCCD camera (iXon 897) with a 60× Plan Apochromat VC PFS 1.4 NA oil-immersion objective or a 60× Plan Apochromat VC PFS 1.2 NA water-immersion objective (Nikon) and using the iQ software (Andor Technology). In Figures 14, 15, 17, 27 and 28 we used an 1.5x auxiliary Optovar magnification. Individual Z slices with a step size of 0.28-0.5 µm were acquired (see Figure legends for detailed number of Z slices).

For roGFP imaging, roGFP fluorescence was excited by the 405 nm and 488 nm lasers and emission was detected at 500–570 nm (Albrecht et al., 2011). For all other imaging experiments, we used the 405 nm laser to excite GFP and the 561 nm laser to excite mCherry/ChFP.

9. Image analysis and quantifications

All images were processed and analyzed using Fiji (ImageJ 1.52p; National Institutes of Health [NIH]; (Schindelin et al., 2012), unless stated otherwise. Z-stacks were processed to obtain maximum Z-projections.

9.1. Mitochondrial morphology

EYFP::mito Z-stacks were deconvolved with the Huygens Remote Manager (Scientific Volume Imaging, The Netherlands, http://svi.nl), using the Classic Maximum Likelihood Estimation (CMLE) algorithm, with Signal to Noise Ratio (SNR) of 15 and 30 iterations. Individual cells were manually outlined and cropped from maximum Z projections of deconvolved *sqh-mito-YFP* (mitochondrial maker) merged with *PLCγPH::ChFP* (membrane marker) Z-stacks. Mitochondrial morphology from the selected cells was quantified using MiNA (Mitochondrial Network Analysis) 2.0.0 macro for Image J (Valente et al., 2017) (https://github.com/StuartLab/MiNA), selecting a Maximum Entropy Threshold Method and Ridge Detection. The branch length mean and network branches mean output parameters for each cell were plotted. The branch length mean, which was called mitochondrial length for simplicity, is the mean length of

all the lines used to represent the mitochondrial structures. The network branches mean is the mean number of attached lines used to represent each structure.

9.2. Wound area

sqh-GFP::Moesin maximum Z projections were used. An ellipse was drawn along the wound edge over time, and the area was obtained using the Measure tool. For each embryo, the area was normalized relative to the initial wound area. For statistical comparisons, only the first 30 min after wounding were considered, as shortly after that wounds start to close in control embryos.

9.3. Fluorescence intensity measurements

To measure F-actin and myosin intensities at the wound edge, maximum Z projections of *sqh-GFP::Moesin mCherry::Moesin* (F-actin), and *Zip::GFP* (myosin) stacks were used after Rolling Ball Background Subtraction (15 pixel). The wound edge and the cortical region of epithelial cells (10 cells per embryo) before wounding were outlined using a 3-pixel-wide segmented line, and the mean grey value was obtained using the Measure tool. For F-actin quantifications, cells containing actin-rich denticle precursor structures were excluded as they mask the actin present at the cable and cell cortex.

To measure E-cadherin (E-cad) intensities, maximum Z projections of *ubi-E-cad::GFP* stacks were used. Background fluorescence was subtracted from each image. The *mCherry::Moesin* channel was used to confirm the location of the wound edge. Junctions were outlined using a 4-pixel-wide segmented line and the average intensity obtained using the Measure tool. To calculate the intensity decrease (fold-change) at the wound edge, the intensity value for each wound edge junction after wounding (10 and 30 minutes post-wounding, mpw) was divided by the intensity value obtained for the same junction before wounding.

To measure Rok intensities, maximum Z projections of *sqh-GFP::Rok* stacks were used after Rolling Ball Background Subtraction (5 pixel). The *mCherry::Moesin* channel was used to confirm the location of the wound edge. The wound edge and the cortical region of epithelial cells (10 cells per embryo) before wounding were outlined using a 3-pixel-wide segmented line, and the mean grey value was obtained using the Measure tool.

To measure mitochondrial and intracellular Ca^{2+} dynamics, *mito::GCaMP3* and *GCaMP-6f* maximum Z projections were used after applying a median filter (0.5 pixel). The wound area, measured from *mCherry::Moesin* maximum Z projections from respective embryos, was deleted from *mito::GCaMP3* and *GCaMP-6f* maximum Z projections to exclude the signal coming from cellular debris and wound-recruited hemocytes. The region of Ca^{2+} increase upon wounding was selected by applying an Intensity Threshold

[Otsu's method (Otsu, 1979)]. The Mean Grey Value, Area and Integrated Density (the product of Area and Mean Grey Value) were obtained using the Measure Tool, before and during wound closure. The Integrated density normalized to pre wound values and the area of Ca^{2+} increase normalized to the initial wound area were plotted.

9.4. Statistics

Statistical analysis was performed using GraphPad Prism 6.01 (GraphPad Software, La Jolla California, USA). Statistical tests, P values, sample sizes, and error bars are indicated in the respective figure legends.

Table 1. Fly lines used in this study

Fly stock	Information	Origin
Control and mutant alleles used in the wounding assay Information on the nature of the mutant alleles can be found on Flybase (Thurmond et al., 2019)		
w^{1118}	Control for wounding assay experiments	BDSC # 3605
Marf ^{B}	*Marf* mutant allele (amorphic)	BDSC # 67154
Marf ^{E}	*Marf* mutant allele	BDSC # 67155
Marf ^{I}	*Marf* mutant allele	BDSC # 57097
Marf ^{J}	*Marf* mutant allele	BDSC # 57096
Opa1^{s3475}	*Opa1* mutant allele (hypomorphic)	BDSC # 12188
Opa1^{EY09863}	*Opa1* mutant allele	BDSC # 20054
Fis1^{MI10520}	*Fis1* mutant allele	BDSC # 55496
Gdap1^{MB07860}	*Gdap1* mutant allele	BDSC # 25575
Tango11 ^{1}	*Tango 11* mutant allele	BDSC # 36320
Drp1^{KG03815}	*Drp1* mutant allele	BDSC # 13510
Df(2L)^{D20}*, Drp1*^{D20} *nrd*^{D20}	*Drp1* mutant allele	BDSC # 3911
Drp1^{T26}	*Drp1* mutant allele	BDSC # 8662
milt^{EY01559}	*milt* mutant allele	BDSC # 15518
milt^{k04704}	*milt* mutant allele	BDSC # 10553
Miro^{B682}	*Miro* mutant allele	BDSC # 52003
Balancer stocks		
gla/CyO, Twi-Gal4, UAS-GFP	2nd chromosome balancer	BDSC # 6662 (Halfon et al., 2002)
w^{1118}*/Dp(1;Y)y*$^{+}$*; CyO/nub*^{1} *b*^{1} *sna*^{Sco} *lt*^{1} *stw*^{3}*; MKRS/TM6B, Tb*^{1}	2nd and 3rd chromosome balancer	BDSC # 3703
w**; Kr* $^{If-1}$*/CyO; D*^{1}*/TM3, Ser*^{1}	3rd chromosome balancer	BDSC # 7198
Transgenic constructs		
sqh-EYFP::mito	Ubiquitously expressed mitochondrial marker	BDSC # 7194; (Lajeunesse et al., 2004)
ubi-PLCγPH::ChFP	Ubiquitously expressed membrane marker	(Herszterg et al., 2013) (kindly provided by Yohanns Bellaïche)
sqh-GFP::Moesin	Ubiquitously expressed F-actin marker	BDSC # 59023 (Kiehart et al., 2000)
Zip $^{CPTI-100036}$*::GFP*	Myosin II heavy chain marker (fluorescent protein-trap)	Kyoto DGGR # 115082 (Lye et al., 2014)
ubi-E-cad::GFP	Ubiquitously expressed E-cadherin fused with GFP	Kyoto DGGR # 109007 (Oda and Tsukita, 1999)
UAS-mCherry::Moesin	UAS-dependent F-actin marker	(Millard and Martin, 2008)
e22c-Gal4	GAL4 driver (drives expression of UAS transgenes mainly in the epidermis)	BDSC # 1973

UAS-GCaMP6f	UAS-dependent intracellular calcium sensor	BDSC # 52869 (Chen et al., 2013)
UAS-mito::GCaMP3	UAS-dependent mitochondrial calcium sensor	(Lutas et al., 2012)
UAS-Atg8::GFP	Expresses GFP-tagged Atg8a protein under UAS control	BDSC # 52005
HA-Drp1	Expresses HA-tagged Drp1 protein from the native *Drp1* promoter	BDSC # 42208
UAS-GFP::mito	Expresses GFP with a mitochondrial import signal under UAS control	BDSC # 8442 (Rizzuto et al., 1995)
sqh-GFP::Rok	Ubiquitously expressed Rok fused to GFP	BDSC # 52289 (Abreu-Blanco et al., 2014)
UAS-mito::roGFP2-Orp1	Mitochondrial hydrogen peroxide sensor	(Albrecht et al., 2011) (kindly provided by Tobias P. Dick)
Recombinant lines		
e22c-Gal4, UAS-mCherry::Moesin		
Drp1^{KG03815}, *e22c-Gal4, UAS-mCherry::Moesin*		
Opa1^{EY09863}, *e22c-Gal4, UAS-mCherry::Moesin*		
Drp1^{KG03815}, *Zip* $^{CPTI\text{-}100036}$*::GFP*		
Opa1^{EY09863}, *Zip* $^{CPTI\text{-}100036}$*::GFP*		
Drp1^{KG03815}, *ubi-E-cad::GFP*		
Opa1^{EY09863}, *ubi-E-cad::GFP*		
Drp1^{KG03815}, *ubi-PLCγPH::ChFP*		
Opa1^{EY09863}, *ubi-PLCγPH::ChFP*		
Drp1^{KG03815}, *UAS-GFP::mito*		
Opa1^{EY09863}, *UAS-GFP::mito*		

BDSC – Bloomington Drosophila Stock Center (funded by NIH P40OD018537), Dept Biology, Indiana University, Bloomington, USA
Kyoto DGGR – Kyoto Drosophila Genomics and Genetic Resources Stock Center, Center for Advanced Insect Research Promotion, Kyoto Institute of Technology, Kyoto, Japan

Table 2. Reagents used in this study

Reagent	Reference	Supplier
Heptane	34873	Sigma-Aldrich
Formaldehyde	F8775	Sigma-Aldrich
Methanol	M/4056/17	Fisher Chemical
Triton X-100	AC215680010	ACROS Organics™
TWEEN® 20	P9416	Sigma-Aldrich
Halocarbon oil 700	H8898	Sigma-Aldrich
Halocarbon oil 27	H8773	Sigma-Aldrich
Bovine Serum Albumin	A3294	Sigma-Aldrich
DABCO (1,4-Diazabicyclo[2.2.2]octane)	D27802	Sigma-Aldrich
Glycerol	MB16101	NZYTech
DMSO (Dimethyl sulfoxide)	D5879	Sigma-Aldrich
D-Limonene	155234	MP Biomedicals
Citra Solv		Citra Solv
Drosophila Standard medium		
Barley Malt Syrup, 45 g/L		Provida
Agar, 10 g/L		NZYtech
Biological Corn Flour, 70 g/L		Provida
Yeast Extract, 20 g/L		Provida
Sugar, 75 g/L		Sidul
10% Niapagin in 96% ethanol, 25 mL/L		Tegosept, Dutscher UK
Distilled water		
Drosophila Ringers Solution, pH 7.1		
2 mM KCl	104936	Merck
128mM NaCl	S/3120/65	Fisher Chemical
35.5 mM sucrose	S9378	Sigma-Aldrich
5 mM HEPES (2-[4-(2-hydroxyethyl)-1-piperazinyl]ethanesulphonic acid)	441485H	VWR
4 mM $MgCl_2$	M8266	Sigma-Aldrich
Phosphate Buffer Saline (PBS), pH 7.4		
1.4 M NaCl	S/3120/65	Fisher Chemical
27 mM KCl	104936	Merck
Na2HPO4, 102.1 mM	319540250	Biochem Chemopharma
17.6 mM KH_2PO_4	60229	Sigma-Aldrich
Enzymes		
Proteinase K	3115836001	Roche
DNaseI	004716728001	Roche
Antibodies, dyes and probes		
Anti-HA-Tag (C29F4), rabbit, 1:500	#3724	Cell Signaling Technology
Anti-Cora, mouse, 1:500	C615.16	Developmental Studies Hybridoma Bank

Alexa Fluor® 568 Phalloidin, 1:100	A12380	Invitrogen™
DAPI (4', 6-diamidino-2-phenylindole), 1:500		Sigma-Aldrich
TUNEL - In Situ Cell Death Detection Kit, Fluorescein	11684795910	Roche
Fluorescein dextran	D1821	Invitrogen™
TMRM (Tetramethylrhodamine methyl ester, perchlorate)	#70017	Biotium
MitoTracker® Red CMXRos	M7512	Invitrogen™

CHAPTER 3. RESULTS

“I seem to have been only like a boy playing on the seashore, and diverting myself in now and then finding a smoother pebble or a prettier shell than ordinary, whilst the great ocean of truth lay all undiscovered before me.”

- Isaac Newton

1. Mitochondrial dynamics proteins are required for wound healing

As a first approach to test whether the mitochondrial dynamics machinery (Fig. 11 A) is required for epithelial repair, we performed a genetic screen based on a previously described wounding assay in the *Drosophila* embryonic epidermis (Campos et al., 2010). We laser-wounded late-stage embryos bearing wild-type and mutant alleles of proteins related to mitochondrial dynamics and assessed the wound healing phenotype by the percentage of embryos with non-healing wounds (Fig. 11 B). This assay is a crude way of finding potential genes required for wound healing. If mutants for a certain gene present increased number of open wounds compared to controls, it suggests that this gene is required for wound healing.

Mitochondrial dynamics comprises the changes in mitochondrial morphology, through fission and fusion events; in their localization, controlled by mitochondrial trafficking; and in mitochondrial number and quality control, mediated by mitophagy and biogenesis (Dorn, 2018; Sebastián et al., 2017). We tested mutants for the proteins involved in mitochondrial fusion, fission and trafficking. Figure 11 A shows a scheme of mitochondrial dynamics with all the tested proteins represented.

Mitochondrial fusion is mediated by large GTPases of the dynamin family: Mitofusins 1 and 2 (Mfn1/2) fuse the outer mitochondrial membrane (OMM), whereas Optic Atrophy 1 (Opa1) fuses the inner mitochondrial membrane (IMM) (Lee and Yoon, 2016; van der Bliek et al., 2013). *Drosophila* has two Mfn1/2 homologs: Fuzzy Onions (Fzo) and Mitochondrial assembly regulatory factor (Marf). Fzo was the first OMM fusion protein to be described and was named after the fuzzy and onion-like appearance of unfused mitochondria in electron micrographs of mutants for this protein (Hales and Fuller, 1997). *fzo* is only expressed in the male germ line whereas *Marf* is widely expressed in the embryo (Hwa et al., 2002), so we tested four *Marf* alleles, each carrying a different point mutation (Haelterman et al., 2014; Sandoval et al., 2014): $Marf^{B}$, $Marf^{E}$, $Marf^{I}$ and $Marf^{J}$. Concerning fusion of the IMM, we tested two *Opa1* alleles: $Opa1^{s3475}$ (hypomorphic) (Yarosh et al., 2008) and $Opa1^{EY09863}$ (McQuibban et al., 2006).

Mitochondrial fission relies on the activity of Dynamin-related protein (Drp1) (Aldridge et al., 2007; Lee and Yoon, 2016), so we tested three loss-of-function *Drp1* alleles [$Drp1^{KG03815}$ (Verstreken et al., 2005), $Drp1^{D20,}$ $Drp1^{T26}$ (Littleton and Bellen, 1994)] and a heteroallelic combination ($Drp1^{KG03815/T26}$). Unlike fusion proteins, Drp1 is largely cytosolic and needs to be recruited to mitochondria upon certain stimuli. Several proteins have been shown to recruit Drp1 to mitochondria (Lee et al., 2016; Roy et al., 2015). The ones with known *Drosophila* homologs are Mitochondrial Fission Factor (Mff) (Gandre-Babbe and van der Bliek, 2008) and Mitochondrial fission protein 1 (Fis1) (Yang et al., 2008). Ganglioside-induced differentiation associated protein 1 (Gdap1) also contributes to mitochondrial fission but its function is not well understood (Huber et al., 2013; López del Amo et al., 2017; Pedrola et al., 2005). Mutants for *Tango 11*, the *Drosophila Mff* homolog (Gandre-Babbe and van der Bliek, 2008), have severe developmental defects and we could not obtain healthy

stage 15 embryos to perform the wounding assay. Therefore, we only tested *Fis1*^{MI10520} (Venken et al., 2011) and *Gdap1*^{MB07860} mutant embryos (Metaxakis et al., 2005).

Mitochondria move by interacting with different cytoskeleton components, such as microtubules and actin filaments (Lovas and Wang, 2013; Morris and Hollenbeck, 1995). In animal cells, the most studied interaction has been between mitochondria and microtubules (Anesti and Scorrano, 2006). Mitochondrial Rho (Miro), a calcium-sensing member of the Ras homologous (Rho)-GTPase family that localizes at the OMM, interacts with Milton (Milt), linking mitochondria to kinesin motors (Saotome et al., 2008). To test their loss of function, we used the following alleles: *Miro*^{B682} (Guo et al., 2005), *milt*^{k04704} (Spradling et al., 1999) and *milt*^{EY01559} (Bellen et al., 2004). Most *milt*^{k04704} embryos died before reaching stage 15, so we only tested *milt*^{EY01559} embryos.

We observed three types of wound closure phenotypes: open, intermediate and closed wounds (Fig. 11 C). Closed wounds are identified by a small melanized spot. Open wounds show a continuous well-defined melanized ring around the hole. In the intermediate phenotype, melanization occurs in a large circular area but a clear hole is absent, making it uncertain whether the wound is open or closed. As it is unclear whether the intermediate wounds represent a closure impairment or just a melanization defect, we excluded these wounds from the statistical analysis of the wound healing phenotype (Fig. 11 E).

As previously shown (Carvalho et al., 2018), control embryos (w^{1118}) have an outstanding capacity for epithelial repair, as 94.7% of the wounds closed (Fig. 11 D). Mutations in either mitochondrial fission or fusion genes increased the frequency of open and intermediate wounds (Fig. 11 D), indicating they are required for wound closure. For all mitochondrial fission genes, the percentage of open wounds was significantly higher than in controls. Regarding mitochondrial fusion, from the four tested *Marf* alleles, *Marf* ^{J} showed increased percentage of open wounds compared to controls, while both *Opa1* alleles showed a significant wound closure phenotype. Considering the mitochondrial trafficking proteins, *milt*^{EY01559}, but not *Miro*^{B682} embryos, showed a mild increase in the percentage of open wounds compared to controls (Fig. 11 E).

This assay led to the identification of novel wound healing regulators. As we observed wound closure defects for mutated versions of mitochondrial fusion, fission and trafficking proteins, these data strongly suggest that the regulation of mitochondrial dynamics is essential for proper wound healing.

We chose the two most significant hits from the wounding assay screen, *Drp1*^{KG03815} and *Opa1*^{EY09863} (52% and 50% of open wounds, respectively), to further investigate the role of mitochondrial dynamics in the *Drosophila* epidermis wound healing. Although Drp1 and Opa1 are well-described proteins involved in mitochondrial fission and fusion, respectively, their role in embryonic wound healing has so far never been investigated.

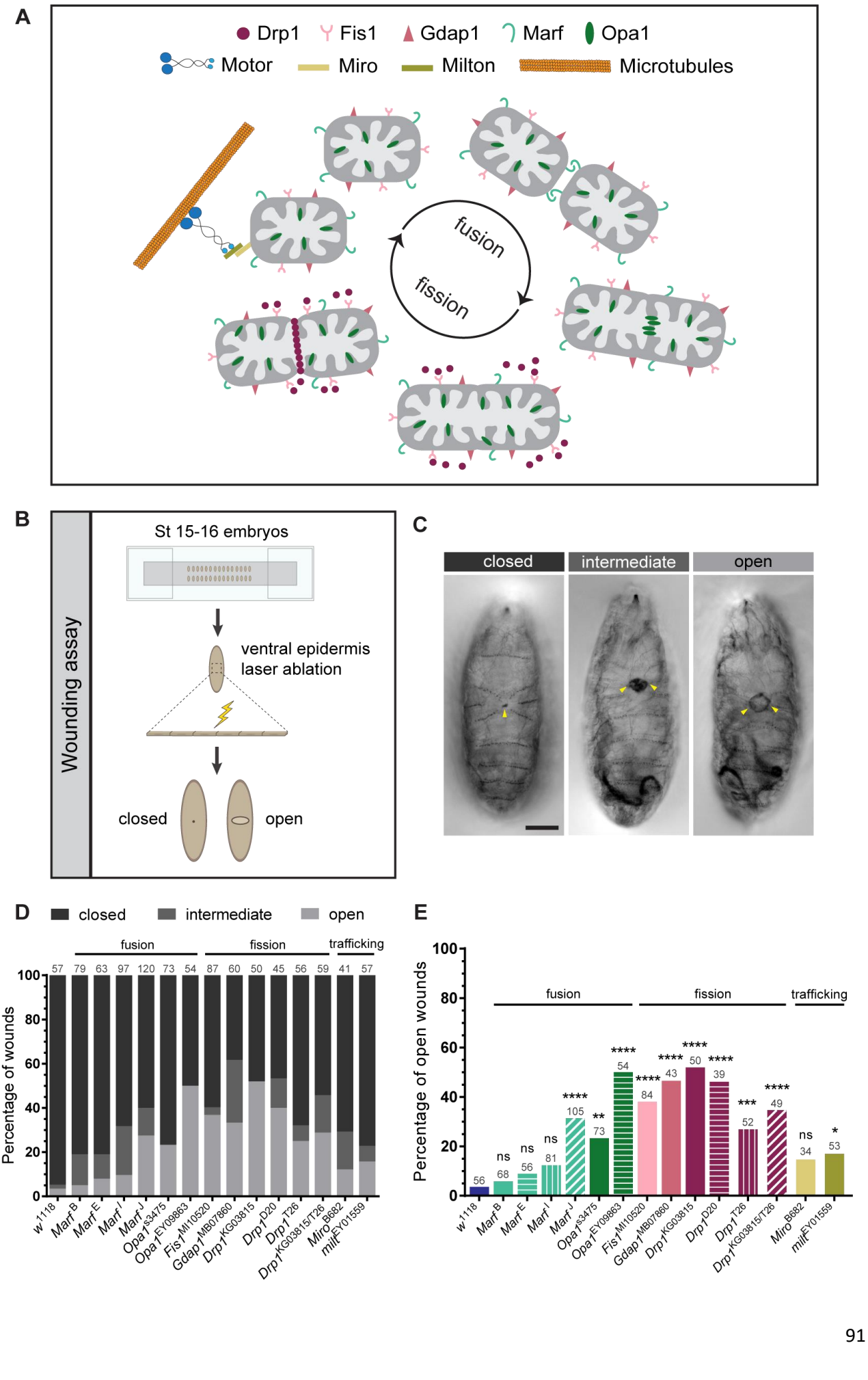
A
Drp1
Fis1
Gdap1
Marf
Opa1
Motor
Miro
Milton
Microtubules
fusion
fission
B
Wounding assay
St 15-16 embryos
ventral epidermis
laser ablation
closed
open
C
closed
intermediate
open
D
closed
intermediate
open
fusion
fission
trafficking
Percentage of wounds
E
Percentage of open wounds
fusion
fission
trafficking

Figure 16. Mitochondrial dynamics proteins are required for wound healing.
(A) Schematic representation of mitochondrial dynamics, illustrating the proteins used in the wounding assay screen. We tested proteins involved in mitochondrial fission (Drp1, Fis1 and Gdap1), fusion (Marf and Opa1) and trafficking (Miro and Milt). (B) Wounding assay protocol: the ventral epidermis of stage 15-16 mutant embryos was laser-ablated. 16 h after wounding the number of open, intermediate (not represented) and closed wounds was scored. (C) Representative images of hatching larvae, showing the three observed wound phenotypes: closed, intermediate and open. Closed wounds present a small scab, while open wounds show a ring of melanization around the hole. Intermediate wounds have more melanization than closed and open wounds but not a clear hole. Arrowheads point to the wound region. Scale bar = 200 µm. (D) Graph of percentage of closed, intermediate and open wounds in controls (w^{1118}) and mutant alleles for mitochondrial dynamics proteins. (E) Graph showing the percentage of open wounds in controls and mutant alleles for mitochondrial dynamics proteins. Regarding fusion, both *Opa1* alleles showed increased percentage of open wounds compared to controls; for Marf, only the $Marf^{J}$ mutation shows significantly increased percentage of open wounds compared to controls. All the tested fission genes showed higher percentage of open wounds compared to controls. Regarding mitochondrial trafficking mutants, only $milt^{EY01559}$ but not $Miro^{B682}$ embryos presented an increased percentage of open wounds in comparison to controls. Fisher's exact test was used to test for significant differences between groups. ns – not significant ($P > 0.05$), * $P = 0.0261$, ** $P = 0.0020$, *** $P = 0.0008$, **** $P < 0.0001$. The number of embryos per condition is indicated above the respective bar in D and E.

2. Drp1 is present in the embryonic epidermis

The expression and localization of Drp1 in the *Drosophila* embryonic epidermis has never been assessed. We took advantage of a fly transgenic line expressing an HA-tagged version of Drp1 under the control of its endogenous promotor and used an antibody directed at HA to detect Drp1 (Fig. 12) by immunofluorescence.

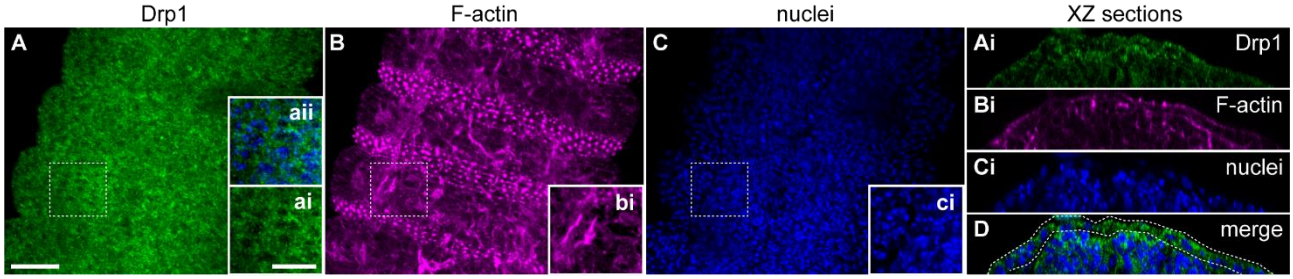

Figure 17. Drp1 localization in the embryonic epidermis.
Representative confocal images of embryos expressing HA-Drp1 stained with an HA antibody (A, green), phalloidin to label F-actin (B, magenta) and DAPI to label nuclei (C, blue). Images are maximum Z projections of 48 slices (24-µm-thick stack) Scale bar = 20 µm. Insets (ai-ci, aii) show a zoom of the region outlined by the dashed square. Inset scale bar = 10 µm. (Ai-Ci) XZ sections of A-C, respectively. (D) XZ merge from Ai and Ci, showing Drp1 (green) and nuclei (blue). Dashed lines delimit the epidermis. Drp1 is present all over the embryo, including in the epidermis. At the subcellular level, it is localized all over the cell, except in the nucleus (aii, D).

Drp1 was found to be localized throughout the embryo (Fig. 12 A), including in the epidermis (Fig. 12 D, the epidermis is outlined by dashed lines). At the subcellular level, Drp1 was distributed in the whole cell, except in the nucleus (Fig. 12 A, ai, aii, Ai, D), which corroborates previous studies in human cell lines (Smirnova et al., 1998). A fly transgenic line expressing HA-Opa1 has been recently published (Tsuyama et

al., 2017) and there is also an antibody that recognizes the *Drosophila* Opa1 (Yarosh et al., 2008) but, due to time constraints, we were not able to investigate the Opa1 expression and localization in the embryonic epidermis.

Our results reveal that Drp1 is expressed in the *Drosophila* embryonic epidermis.

3. *Drp1* and *Opa1* mutations do not compromise cell viability in Drosophila embryos

Our wounding assay screen revealed that mutations in the mitochondrial dynamics machinery impair wound healing, suggesting that mitochondrial dynamics is involved in the repair process. Another possibility is that this phenotype is related to unspecific effects of these mutations in other tissues, that would compromise embryo development and survival. With the exception of *Fis1*^{MI10520}, *Gdap1*^{MB07860} and *milt*^{EY01559} mutants, which are viable, the remaining tested mitochondrial dynamics mutants are either lethal (*Drp1*^{KG03815}, *Drp1*^{D20,} *Drp1*^{T26}, *Opa1*^{EY09863}, *Marf* ^{B}, *Marf* ^{E}, *Marf* ^{I} and *Marf* ^{J}) or partially lethal, meaning that the majority dies before eclosion (*Miro*^{B682} and *Opa1*^{s3475}).

Therefore, we tested whether *Drp1*^{KG03815} and *Opa1*^{EY09863} mutants have an increase in cell death that might affect embryo or epidermis viability. For this purpose, we performed a TUNEL (TdT-mediated dUTP-X nick end labelling) assay that detects dying cells, based on the presence of DNA fragmentation, a hallmark of apoptosis (Zhang and Xu, 2000). DNA breaks (nicks) are detected by labelling the free 3'-OH termini with modified nucleotides (in this case we used fluorescein-dUTP) in an enzymatic reaction catalysed by a terminal deoxynucleotidyl transferase (TdT). The fluorescein-dUTP positive cells were visualized by confocal microscopy of fixed embryos. As a negative control, we used control (w^{1118}) embryos incubated without the TdT (Fig. 13 A-Aii); as a positive control, we incubated control embryos with DNase I to induce DNA breaks (Fig. 13 B-Bii).

As expected, no TUNEL positive cells were observed in the negative control (Fig. 13 A), whereas all cells were labelled in the positive control (Fig. 13 B), confirming the accuracy and specificity of the assay. In addition to TUNEL labelling, we stained the embryo with DAPI (Fig. 13, Ai-Ei) to label the cell nuclei and with an antibody for Coracle, a component of the Occluding Junctions, to outline the cells (Fig. 13, Aii-Eii). As reported in other studies (Bardet et al., 2008; Muro et al., 2006), dying cells are present throughout the embryo in the wild type (Fig. 13, C). We also observed TUNEL positive cells in *Drp1* and *Opa1* mutant embryos but did not detect any major differences in their number when compared to controls. Although these are

preliminary results, since they lack quantitative analysis, they suggest that the wound closure defects of Drp1 and Opa1 loss of function are not due to increased cell death in the embryonic epidermis.

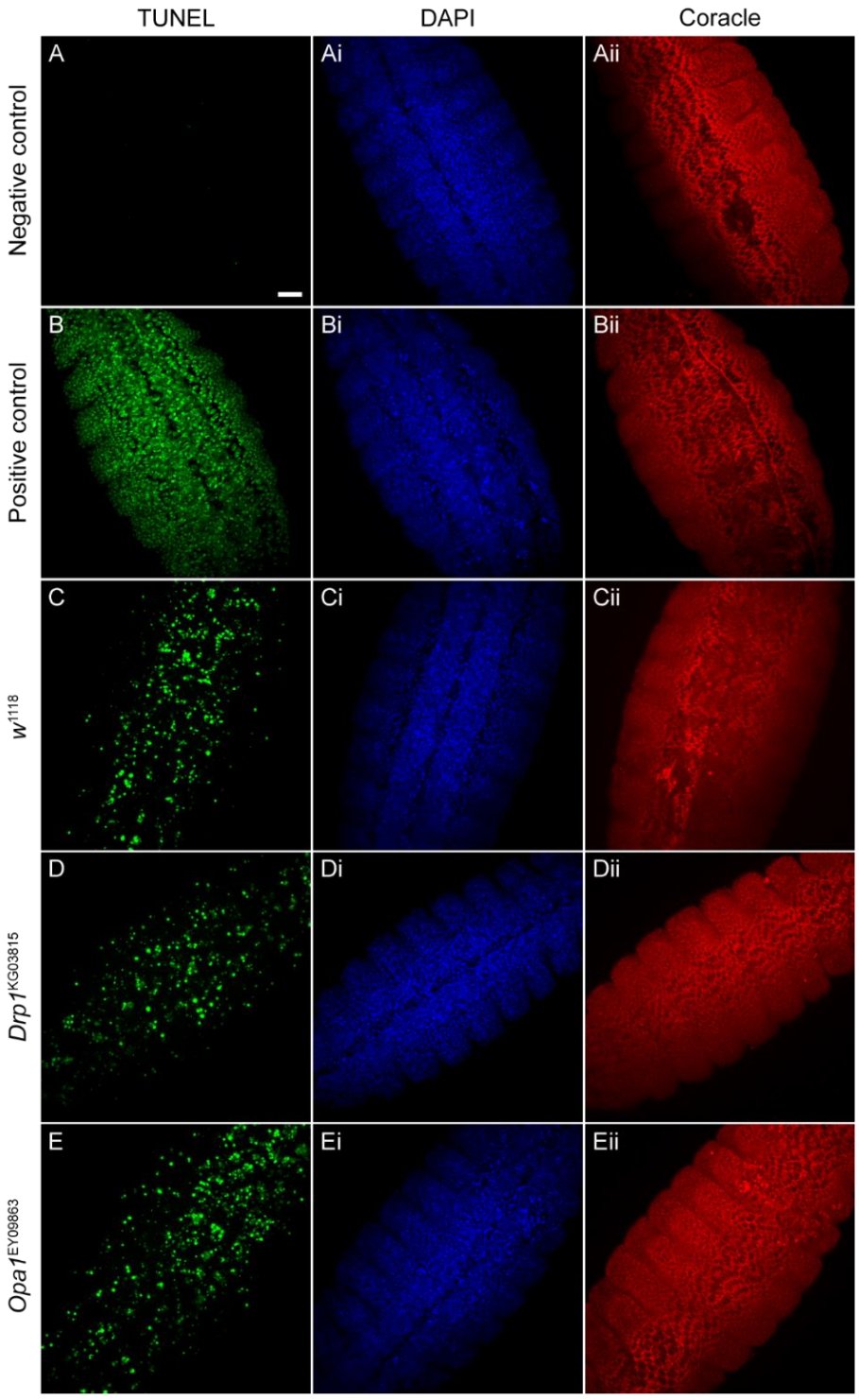

Figure 18. *Drp1* and *Opa1* mutations do not seem to affect apoptosis.
Confocal images of negative control (A), positive control (B), control (w^{1118}, C), $Drp1^{KG03815}$ (D) and $Opa1^{EY09863}$ (E) embryos labelled with TUNEL (in green) to detect apoptotic cells. Embryos were stained with DAPI (blue, Ai-Ei) to label nuclei and Coracle (red, Aii-Eii) to mark the cell outline. Images are maximum Z projections of approximately 85 slices (42.5-µm-thick stack). We observed no major differences in the number of apoptotic cells in control and mutant embryos. Scale bar = 20 µm. n=3 per condition

4. Analysis of mitochondrial morphology and localization in the embryonic epidermis

4.2. *Drp1* mutants have altered mitochondrial morphology

By controlling mitochondrial fission and fusion events, Drp1 and Opa1 are known modulators of mitochondrial morphology (Lee and Yoon, 2016). To characterize the mitochondrial morphology in the embryonic epidermis and assess whether it is affected by mutations in *Drp1* and *Opa1*, we used embryos expressing mitochondria (*EYFP::mito*) and membrane (*PLCγPH::ChFP*) markers. The *EYFP::mito* transgenic flies express EYFP tagged with a mitochondrial targeting sequence under the control of *Drosophila spaghetti squash* (*sqh*) (regulatory light chain of the non-muscle type 2 myosin) promotor (Lajeunesse et al., 2004), which is expressed ubiquitously. *PLCγPH::ChFP* flies ubiquitously express the Phospholipases Cγ (*PLCγ)* pleckstrin homology (PH) domain fused to ChFP, which targets the ChFP protein to the cell membrane (Herszterg et al., 2013). In controls, we observed both round (Fig. 14 A-Ai, arrowheads) and filamentous (Fig. 14 A-Ai, arrows) mitochondria. In *Drp1* mutants, we observed very long and interconnected mitochondria (Fig. 14 B-Bi, arrows), while in *Opa1* mutants the overall mitochondrial morphology was similar to controls (Fig. 14, compare A-Ai with C-Ci).

Several methods have been developed to quantify mitochondria morphology by using images obtained from cells in culture (Dagda et al., 2009; Lihavainen et al., 2012; McClatchey et al., 2016; Nikolaisen et al., 2014; Valente et al., 2017; Westrate et al., 2014). We found that our in vivo system was more challenging. We had to find the adequate imaging settings that allowed us to obtain the best possible resolution without bleaching the signal. To improve image resolution, we performed image deconvolution using the Huygens software (Scientific Volume Imaging, The Netherlands). After this processing step, we tested three different mitochondrial morphology quantification tools, namely Mytoe (Lihavainen et al., 2012), Mito Morphology (Dagda et al., 2009) and Mitochondrial Network Analysis (MiNA) (Valente et al., 2017) (Fig. 15). Although these methods have technical differences in the image processing workflow and in the output parameters, they are based on the same fundamental steps:

1) Creation of a binary image by thresholding, where a foreground pixel (the signal of interest, in this case mitochondria) is assigned the maximum value (255) and background pixels are assigned the minimum possible value (0) (Fig. 15 B and C);

2) Creation of a skeleton representing the features in the original image using a wireframe of lines (Fig. 15 D);

3) Skeleton analysis to measure mitochondrial morphology parameters (Fig. 15 Bi-Di, Bii-Dii).

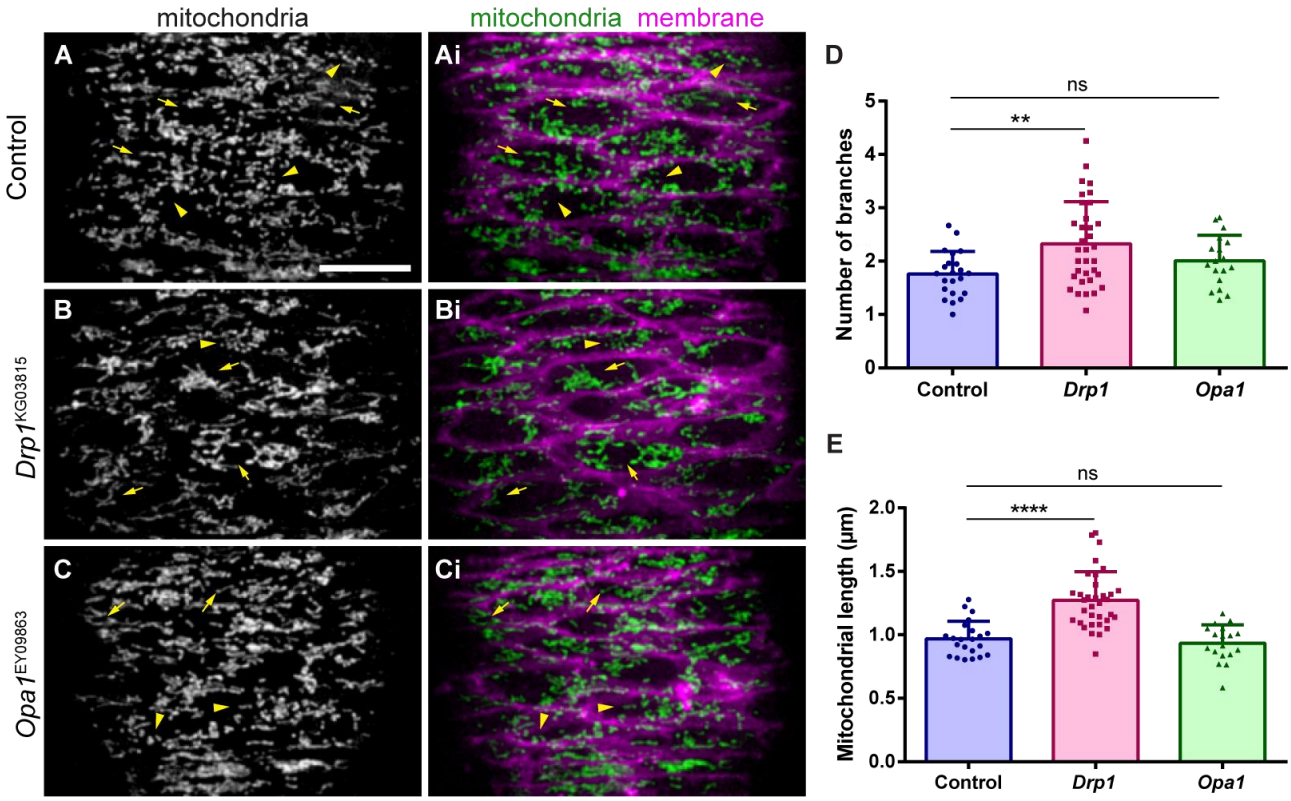

Figure 19. *Drp1* mutant embryos have altered mitochondrial morphology.
(A-Ai, B-Bi, C-Ci) Representative confocal images of the epidermis of control (A-Ai), *Drp1* (B-Bi) and *Opa1* (C-Ci) mutant embryos expressing mitochondrial (*EYFP::mito*, A-C, green in Ai-Ci) and membrane (*PLCγPH::ChFP*, magenta in Ai-Ci) markers. Genotypes are *PLCγPH::ChFP; EYFP::mito* for control, *Drp1*^{KG03815}, *PLCγPH::ChFP; EYFP::mito* for *Drp1* and *Opa1*^{EY09863}, *PLCγPH::ChFP; EYFP::mito* for *Opa1* mutant embryos. Images are maximum Z projections of 19 slices (5.3-µm-thick stack). Arrowheads point to punctate mitochondria. Arrows point to elongated mitochondria. The mitochondrial morphology of control (A-Ai) and *Opa1* mutant (C-Ci) embryos is similar, with both small round and filamentous mitochondria. In contrast, mitochondria in *Drp1* mutants (B-Bi) are more elongated and interconnected than in controls (A-Ai). Scale bar = 10 µm. (D) Graph of average number of branches in control, and *Drp1* and *Opa1* mutant embryos. (E) Graph shows the average mitochondrial length in control, and *Drp1* and *Opa1* mutant embryos. The mitochondrial network in *Drp1* mutants shows an increased number of branches and increased length, compared to controls. Mann-Whitney test was used to test for significant differences between groups. ns – not significant ($P > 0.05$), ** $P = 0.0059$, **** $P < 0.0001$. N(control) = 23 cells from 6 embryos, N(*Drp1*) = 34 cells from 6 embryos, N(*Opa1*) = 18 cells from 3 embryos. Error bars represent SD.

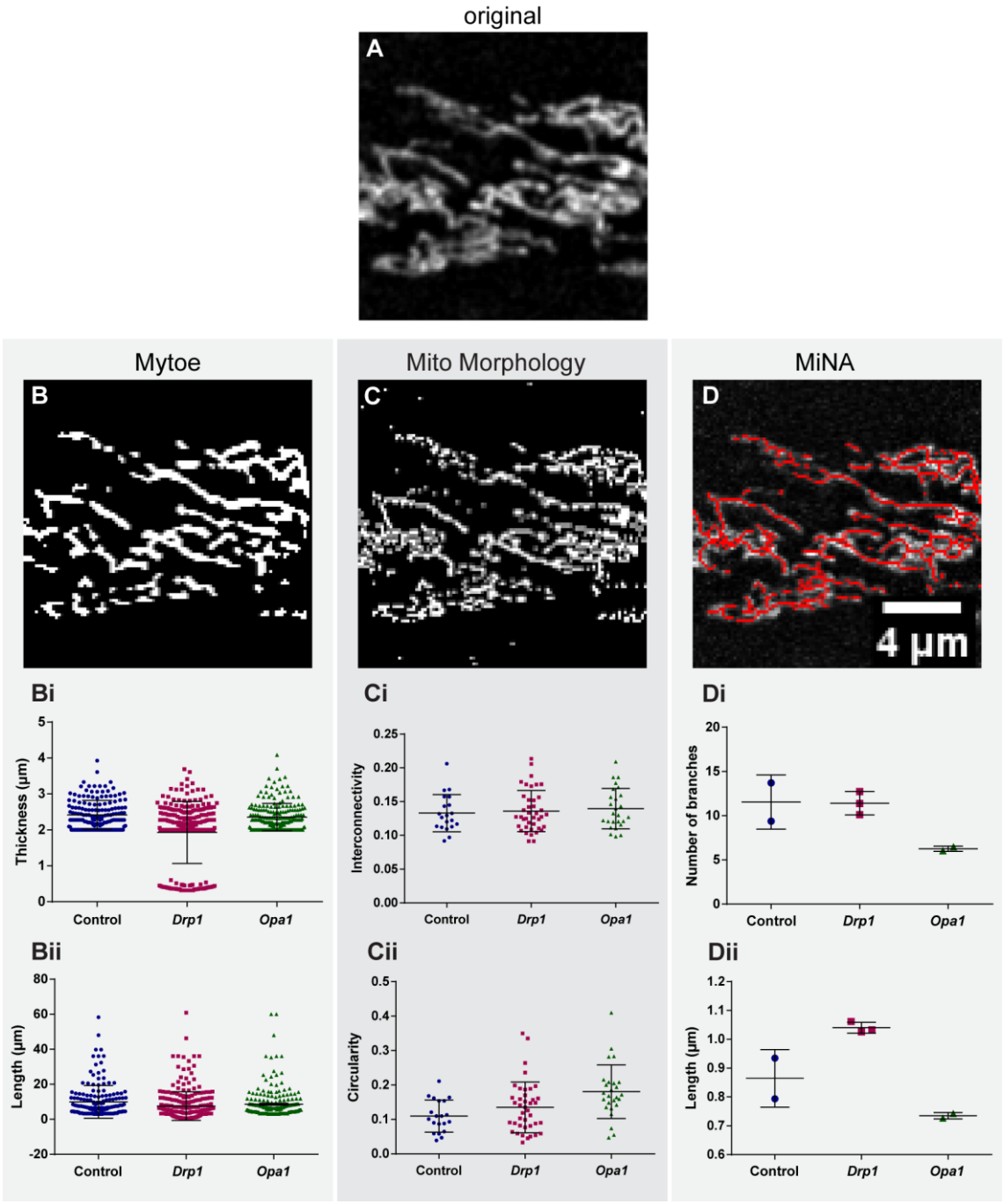

Figure 20. Different quantification methods applied to the analysis of mitochondrial morphology in the Drosophila embryonic epidermis.

(A) Representative deconvolved maximum Z projection of a Drp1 mutant epidermis labelled with a mitochondrial marker (EYFP::mito). (B-D) Resulting processed images using three different mitochondrial morphology quantification methods: Mytoe (B), Mito Morphology (C) and MiNA (D). (Bi-Di, Bii-Dii). Graphs showing the output parameters of the respective quantification methods, comparing control, and Drp1 and Opa1 mutant embryos. Error bars represent SD.

The Mytoe and Mito Morphology tools provide information for each identified individual mitochondrion while the MiNA plugin (Valente et al., 2017) produces the average value of the mitochondrial parameters. So, for the first two tools, each point in the graphs represents one mitochondrion (Fig. 15 Bi-Ci, Bii-Cii), while

for MiNA, each point is the average value of the corresponding embryo (Fig. 5 Di-Dii). We found that the quantification tool that better suited our sample was the MiNA toolset (Fig. 15 D-Diii). From the three tools, this one produced the best fitted skeleton (Fig. 15 D) and the output parameters were consistent with expected results (Fig. 15 Di-Dii). This preliminary analysis was used to choose the most suitable quantification tool and to validate our quantification pipeline, so the number of embryos was low and we did not perform statistical analysis at this time. Nevertheless, these first results suggested that the number of mitochondrial branches was lower in *Opa1* mutant embryos compared to controls (Fig. 15 Di), which was expected as the lack of Opa1 should prevent mitochondrial fusion. As anticipated, the length of mitochondria was reduced in *Opa1* mutants and increased in *Drp1* embryos, compared to controls. This indicates that, from the tool sets analysed, the MiNA is the more appropriate to measure differences in mitochondria morphology in the *Drosophila* embryonic epidermis. After choosing the most suitable quantification method, we increased the number of embryos per condition and quantified mitochondrial morphology in control, and in *Drp1* and *Opa1* mutant embryos (Fig. 14 D, E). We found that the number of mitochondrial branches (Fig. 14 D) and the length of mitochondria (Fig. 14 E) were increased in *Drp1* mutants compared to controls. No significant differences were found between control and *Opa1* mutant embryos (Fig. 14, D, E).

We have established the MiNa as a valid tool for the quantification of mitochondrial morphology in the *Drosophila* epidermis. Our results show that *Drp1*, but not *Opa1*, mutant embryos have altered mitochondrial morphology compared to controls. These data suggest that mitochondrial fission is critical for the maintenance of mitochondrial morphology in the embryonic epidermis.

4.3. Epithelial wounding leads to changes in mitochondrial morphology

Knowing that mitochondrial dynamics proteins are required for proper wound repair, we asked whether there is any change in mitochondrial morphology during wound healing. As mitochondrial function and morphology are intimately connected (Ferree and Shirihai, 2012), defects in mitochondrial morphology by Drp1 and Opa1 loss of function could affect mitochondrial function during wound healing.

We used spinning-disk confocal microscopy to image live embryos before and during wound closure. We used control, *Drp1* and *Opa1* mutant embryos expressing a UAS-dependent mitochondrial marker (*UAS-GFP::mito*) and an F-actin marker (*UAS-mCherry::Moesin*) under the control of the *e22c-Gal4* driver (Fig. 16). This driver leads to gene expression in ectodermal tissues (Lawrence et al., 1995), such as the embryonic epidermis. The *UAS-GFP::mito* construct encodes a peptide corresponding to the 31 amino acid mitochondrial import sequence from human cytochrome C oxidase subunit VIII fused to the N-terminus of

the S65T spectral variant of GFP (Rizzuto et al., 1995). The *UAS-mCherry::Moesin* construct encodes mCherry fused to the actin-binding domain of the *Drosophila* Moesin (C-terminal 137 residues) (Millard and Martin, 2008).

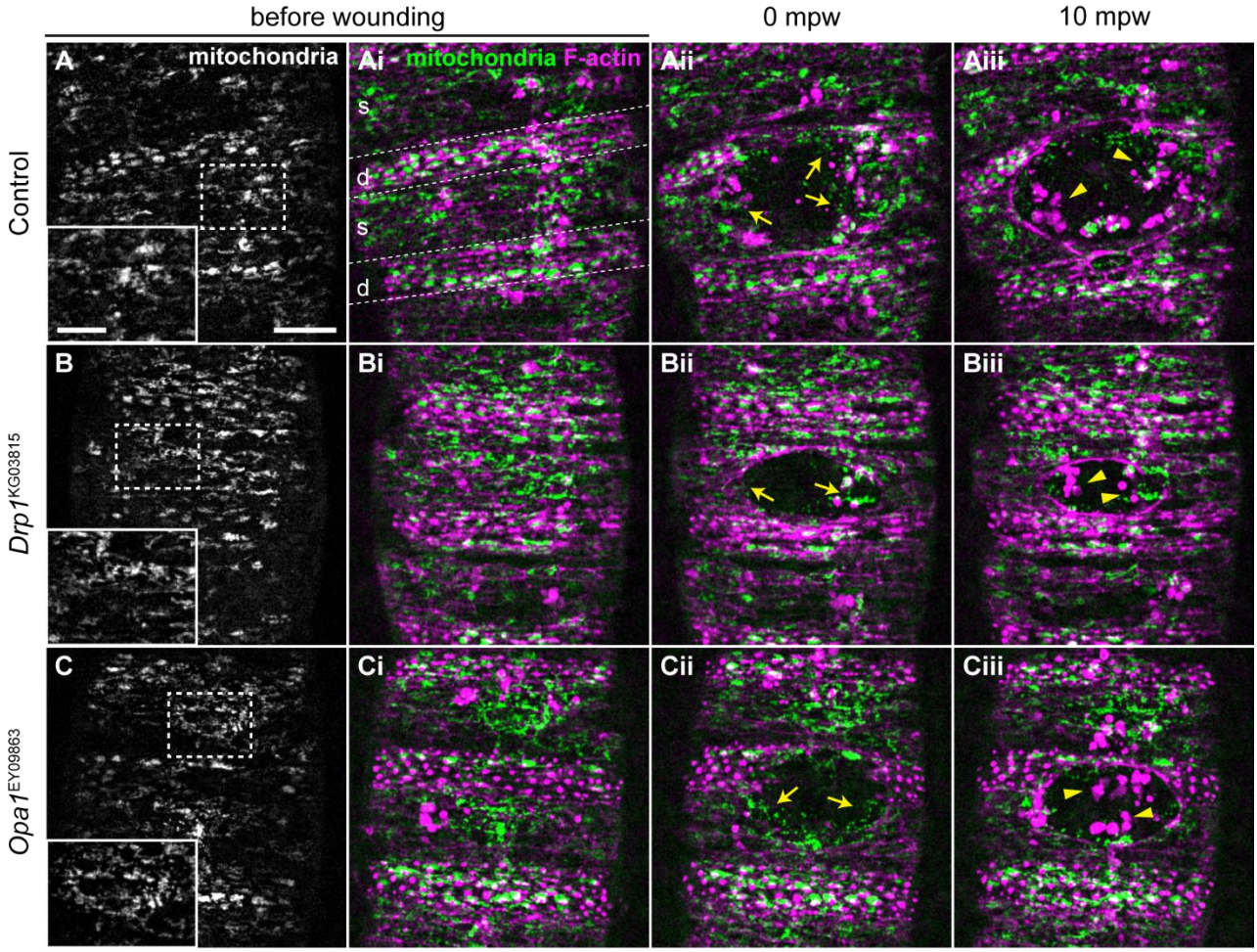

Figure 21. Mitochondrial morphology before and during wound healing.

(A-Ciii) Confocal images of control (A-Aiii), *Drp1*^{KG03815}(B-Biii) and *Opa1*^{EY09863} (C-Ciii) embryos expressing *UAS-mCherry::Moesin* (magenta in Ai-Aiii, Bi-Biii and Ci-Ciii) to mark F-actin and *UAS-GFP::mito* (A-C, green in Ai-Aiii, Bi-Biii and Ci-Ciii) to label mitochondria in the epidermis under the control of the *e22c-Gal4* driver, before (A,Ai,B,Bi,C,Ci) and during wound closure (Aii,Aiii,Bii,Biii,Cii,Ciii). Genotypes are *e22c-Gal4, UAS-mCherry::Moesin / UAS-GFP::mito* for control, *Drp1*^{KG03815}, *e22c-Gal4, UAS-mCherry::Moesin / Drp1*^{KG03815}, *UAS-GFP::mito* for *Drp1* and *Opa1*^{EY09863}, *e22c-Gal4, UAS-mCherry::Moesin / Opa1*^{EY09863}, *UAS-GFP::mito* for *Opa1* embryos. Insets are zoomed images of the dashed region in A, B, C. Control (A) embryos show a complex mitochondrial network, some mitochondria are long while others are smaller and round. *Drp1* mutants (B) seem to have more elongated mitochondria than controls while *Opa1* embryos (C) seem to have smaller mitochondria, compared to control embryos (A). In all cases, we observed different mitochondrial morphologies in smooth (s) and denticle (d) cells, depicted in Ai (but this applies to all genotypes). In denticle cells, we are not able to distinguish individual mitochondria, as mitochondria are very clustered together. We can only assess individual mitochondrial morphology by looking at smooth cells. Upon wounding, we observed fragmentation of mitochondria in the wound region (arrows in Aii to Cii). Most of these small mitochondria seem to be phagocytosed by hemocytes (arrowheads in Aiii-Ciii). Images are maximum Z projections of approximately 55 slices (15.4-µm-thick stack). Scale bar = 20 µm. Inset scale bar = 5 µm. s – smooth cells. d – denticle cells. Arrows – fragmented mitochondria. Arrowheads – hemocytes. mpw – minutes post wounding.

The ventral epidermis of late stage embryos is composed of two distinct cell types: cells decorated with actin-based cellular protrusions at the apical cell surface, called denticles; and cells apically naked or smooth, named after the absence of denticles (Dickinson and Thatcher, 1997; Hillman and Lesnik, 1970). These two cell types alternate, forming different segments (Fig. 16, Ai, s and d). Regardless of the genotype, we observed different mitochondrial morphologies in smooth (Fig. 16, s in Ai) and denticle cells (Fig. 16, d in Ai). In denticle cells, we were not able to distinguish individual mitochondria, as mitochondria are very clustered together. We could only observe individual mitochondrial morphology in smooth cells.

Corroborating our observations with other markers (Fig. 14), in control embryos, the epidermis presents a complex network of mitochondria: some mitochondria have a tubular and elongated morphology, while others are smaller and rounder (Fig. 16, A). Although the image resolution is not optimal to clearly evaluate mitochondrial morphology, *Drp1* mutants seem to have more elongated mitochondria (Fig. 16, B) than controls (Fig. 16, A). In contrast, *Opa1* mutants look more similar to controls, with the presence of small and round mitochondria (Fig. 16, C). Upon wounding, we observed fragmentation of mitochondria in the wound region, both in controls and mutant embryos (arrows in Aii to Cii), suggesting that wounding might trigger mitochondrial fission. However, we could not clearly discern whether these fragments were inside the wound-edge cells or part of cell debris, since most of these small mitochondria seem to be phagocytosed by hemocytes, the *Drosophila* macrophages (arrowheads in Aiii-Ciii). To understand if mitochondrial fission is induced in the wound leading-edge cells and to exclude that these are not just wound debris, we imaged the epidermis of control embryos with higher magnification and a shorter time interval to observe the mitochondrial morphology changes in the cells close to the wound before and after injury (Fig. 17).

We observed that mitochondria are more fragmented than before wounding in some cells close to the wound region, suggesting that mitochondrial fission is induced upon epithelia wounding (Fig. 17, compare mitochondria left to the asterisks in A-D). To confirm this hypothesis, we sought to quantify mitochondrial morphology after wounding. However, imaging of mitochondria in the wound closure context presented several challenges, which prevented us from performing these quantifications:

1) The embryonic epidermis is not completely flat, as the embryo has a fusiform shape. For live imaging, embryos are usually mounted on a glass-bottom petri dish. To flatten the epidermis, we tried to image them on a slide with a coverslip on top. It has been previously shown that this mounting method is not ideal for wound healing imaging (Abreu-Blanco et al., 2012b) but we thought we might be able to use it as long as the imaging duration was short. However, we have found that this mounting method was not suitable, as cells started to die shortly after the beginning of the imaging (data not shown).

2) The wound causes recoil of the tissue that compresses the cells closer to the wound, making it difficult to clearly discriminate mitochondrial shape.

3) As the wound closes, the epidermal tissue moves and sinks slightly. For long term imaging, in which we do not need a short time interval, we can image a considerable number of z slices and the sinking phenomenon is not limiting. However, to capture fast changes in mitochondrial morphology, we need a higher time-resolution, which limits the number of z stacks that can be acquired at each time point. Hence, any tissue movement easily leads to the image getting out of focus and, thus, a reduced fluorescence signal over time. This fact strongly limits an accurate mitochondrial morphology quantification throughout wound closure.

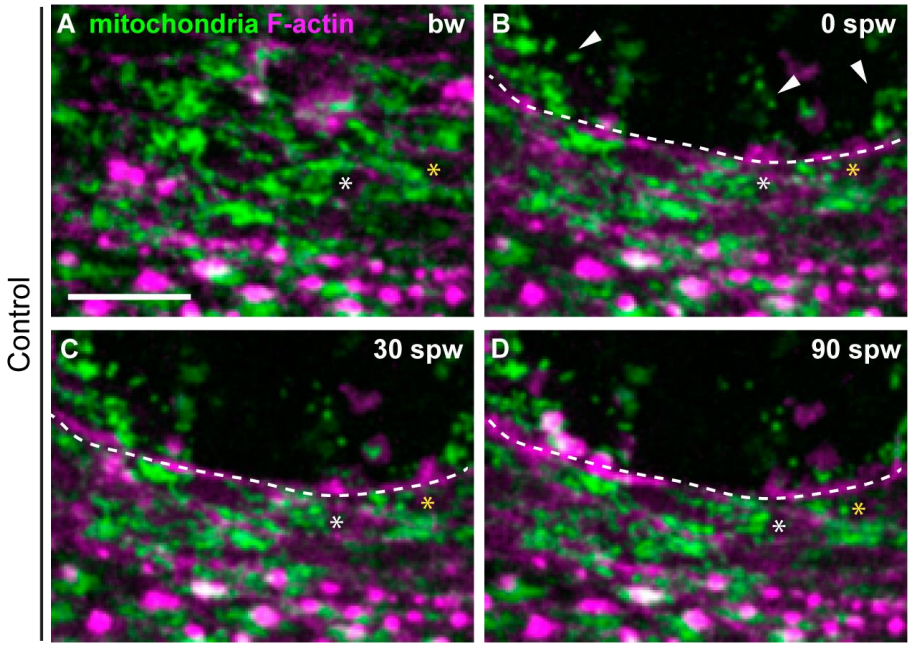

Figure 22. (A-D) Mitochondrial morphology changes upon wounding.
Embryo expressing a mitochondrial marker (*UAS-GFP::mito*, green) and an F-actin marker (*UAS-mCherry::Moesin*, magenta) in the epidermis (*e22c-Gal4*). Mitochondria become fragmented upon wounding, not only in the debris area (white arrowheads) but also in some cells around the wound (left of the asterisks), suggesting that the wound induces mitochondrial fission. Dashed line - wound margin. bw - before wounding. spw - seconds post wounding. Images are maximum Z projections of 22 slices (6.2-µm-thick stack). Scale bar = 10 µm.

In this work, we have characterized, for the first time, the mitochondrial morphology of the ventral epidermis of stage 15 *Drosophila* embryos, before and after wounding. Although we cannot conclude whether Drp1 and Opa1 influence mitochondrial morphology during wound closure, our observations indicate that wounding induces mitochondrial fission in the cells adjacent to the wound.

4.4. Mitochondrial localization is unaffected during wound closure

In our wounding assay screen (Fig. 11), we observed that *milt*^{EY01559} embryos had a mild increase in the percentage of open wounds compared to controls, suggesting that mitochondrial trafficking could be required for wound healing. From the maximum Z projections of the embryonic epidermis, we did not detect a change in mitochondrial localization upon wounding (Fig. 17). To further investigate mitochondrial localization after injury, we looked at YZ sections of the epidermis (Fig. 18). We observed that mitochondria were localized apically, bellow the F-actin cortical belt at the level of the Adherens Junctions (AJs), both before and after wounding (Fig. 18 B).

These results show that mitochondria do not seem to change their localization during wound healing, suggesting that their function during epithelial repair does not require a polarized distribution. It would be interesting to assess whether the *milt*^{EY01559} mutant mitochondria have a different localization compared to wild-type embryos, to further clarify the role of mitochondrial trafficking in wound healing.

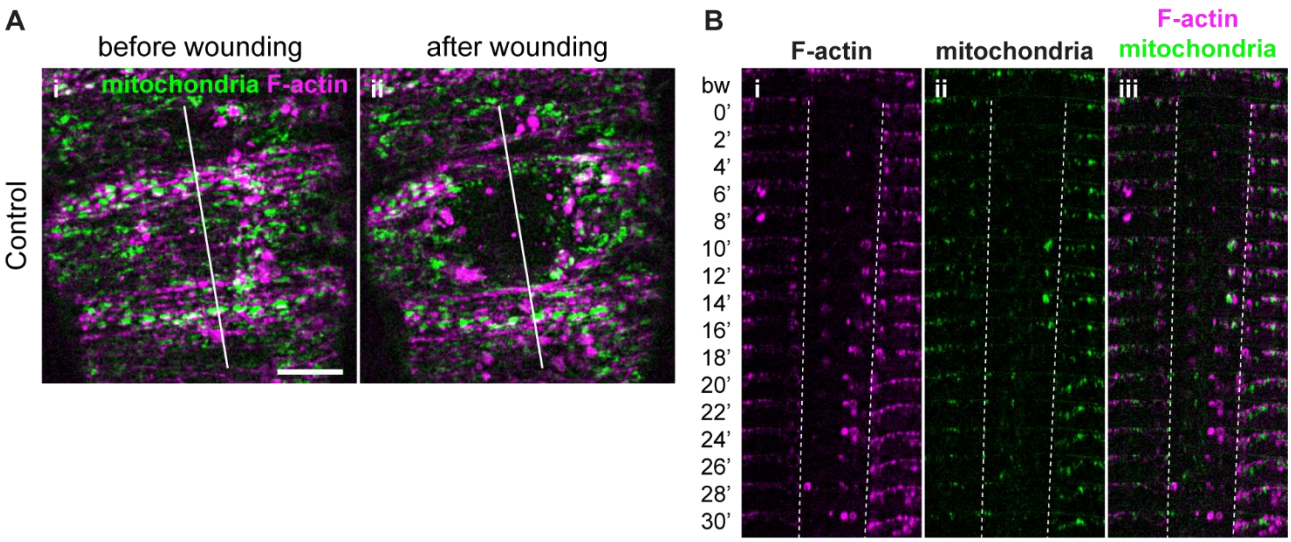

Figure 23. Mitochondrial localization upon wounding.
(A) Representative confocal images of a *Drosophila* embryo expressing a mitochondrial marker (*UAS-GFP::mito*, green) and an F-actin marker (*UAS-mCherry::Moesin*, magenta) in the epidermis (*e22c-Gal4*), before (Ai) and after wounding (Aii).. (B) Kymographs showing YZ sections of A (white line) before and in the first 30 minutes after wounding. White dashed lines outline the wound margins. We did not observe any striking change in mitochondrial localization upon wounding. Scale bar = 20 µm. bw – before wounding- ' – minutes.

5. Measurement of the mitochondrial membrane potential in the embryonic epidermis

The mitochondrial membrane potential (ΔΨm) is the driving force for ATP synthesis during oxidative phosphorylation. The measurement of ΔΨm is often used as a readout of mitochondrial function. For instance, depolarization of mitochondria (loss of ΔΨm) is an indicator of impaired mitochondrial function (Zorova et al., 2018). Interestingly, ΔΨm and mitochondrial dynamics are interconnected. Sustained dissipation of ΔΨm triggers Opa1 cleavage and degradation, inhibiting fusion and targeting mitochondria to degradation by mitophagy (Chan and Chan, 2011; Song et al., 2007). Conversely, knockdown of *Opa1* can lead to a decrease in ΔΨm (Trevisan et al., 2018).

We thus wondered whether wounding induces changes in mitochondrial function in the cells closer to the injury site. Moreover, knowing that there is an interplay between mitochondrial dynamics and ΔΨm, we aimed to understand whether the ΔΨm of *Drp1* and *Opa1* mutants was altered and could contribute to the observed wound healing defects. To measure ΔΨm, we used two different dyes: Mitotracker and TMRM (tetramethylrhodamine methyl ester). These cationic red-fluorescent dyes passively diffuse across the membrane and accumulate in active mitochondria. This accumulation correlates with ΔΨm (Poot et al., 1996).

Drosophila embryos present a challenge to the use of dyes because they are enveloped in a quite impermeable eggshell, composed by the vitelline membrane and the waxy layer (Margaritis et al., 1980). To allow penetration of the dyes, we tested three previously described permeabilization methods:

1) Razzell and colleagues have used a protocol in which embryos were incubated in heptane, a non-polar organic solvent (Razzell et al., 2013). In our hands, this treatment was too harsh and the embryos died by extreme desiccation.
2) Rand and colleagues have used D-limonene-based reagents to permeabilize embryos (Rand et al., 2010). We incubated embryos in solutions containing either D-limonene or Citrasolv, a commercially available cleaning agent (composed by D-limonene, an unknown mixture of surfactants and essential oils), followed by an incubation with 300 nM Mitotracker (Fig. 19). This concentration of Mitotracker has been used for staining of *Drosophila* larvae (Frei et al., 2005). Neither of these permeabilization reagents led to consistent results. We obtained variable Mitotracker staining: no staining (Fig. 19 A), partial staining (Fig. 9 B) and positive staining (Fig. 19 C).
3) Schulman and colleagues developed a more suitable permeabilization protocol for late stage embryos, using a 1:1 combination of D-limonene and heptane, called LH (Schulman et al., 2013).

However, in our hands this protocol induced high embryo lethality by desiccation, similar to the Protocol 1.

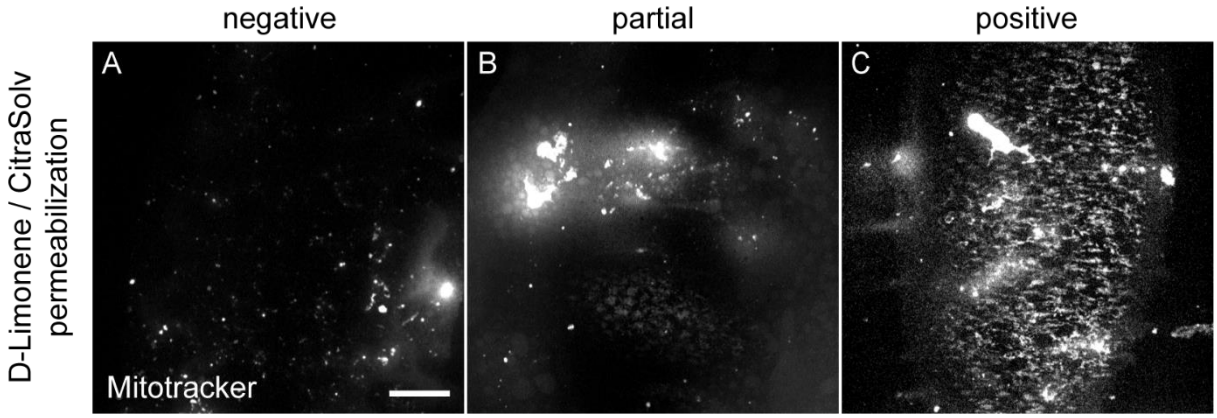

Figure 24. Mitochondrial membrane potential assessment with Mitotracker after embryo permeabilization.
(A-C) Representative confocal images of embryos submitted to the D-limonene/CitraSolv permeabilization protocol, followed by incubation with 300nM Mitotracker. Permeabilization protocol led to variable results: negative (A), partial (B) and positive (C) labelling of mitochondria with Mitotracker. Scale bar = 20 µm.

To summarize, none of the three different permeabilization protocols was suitable to assess ΔΨm. Therefore, we tested a different approach to deliver dyes into the embryo, by using a microinjection technique.

We started by validating the microinjection technique by injecting embryos with fluorescein (Fig. 20 A). After injection, we observed an increase in GFP fluorescence compared to uninjected controls (Fig. 20 A, compare i with ii), consistent with successful injection. To evaluate the changes in ΔΨm using the microinjection protocol, we decided to use the TMRM dye instead of Mitotracker. TMRM is more suitable to assess rapid changes in ΔΨm due to its ability to quickly enter or exit mitochondria depending on the ΔΨm. To confirm the accuracy of the microinjection, we co-injected the embryos with fluorescein (data not shown). We tried injecting in three different sites: into the perivitelline space (PVS), the space between the embryo proper and the vitelline envelope (Fig. 20 Bii,Cii); into the embryo, at the anterior or posterior pole (Fig. 10 Biii,Ciii); or into the embryo, at the lateral side (Fig. 20 Biv,Civ). Injection into the PVS usually resulted in TMRM staining only around the site of injection, indicating that the injection was not successful. Since the PVS is a very confined region, to specifically deliver TMRM into this space, we have to pierce the embryo with the needle and retract it a bit to release the dye only in the PVS. We believe that, instead of limiting TMRM delivery to the PVS, we damaged the anterior tip of the embryo, allowing some TMRM penetration in that region (Fig. 20 Cii). The lateral injection improved the homogeneity of TMRM staining throughout the embryo (Fig. 20 Ciii, Civ). Nevertheless, TMRM staining was variable, ranging from negative staining in the epidermis to positive staining, with a gradient of fluorescence intensity (Fig. 20 D). As we found no report using TMRM

in the *Drosophila* embryo we tried to optimize the staining protocol, by testing different TMRM concentrations, ranging from 125 µM to 25 mM (Fig. 20 E). The highest concentration was very toxic, as most mitochondria looked swollen (Fig. 20 Ei, inset), an indicator of mitochondrial dysfunction that precedes cell death (Bernardi et al., 1999). With concentrations in the µM range, the toxicity was reduced but we still observed swollen mitochondria (Fig. 20 Eii-iv, insets, yellow arrowheads). Lower concentrations (125 µM) resulted in absence of TMRM staining in the epidermis, even though fluorescein was able to diffuse. Occasionally, hemocytes were labeled (Fig. 20, E v).

In conclusion, the inconsistent results regarding Mitotracker and TMRM staining do not allow us to conclude about the ΔΨm in the *Drosophila* epidermis.

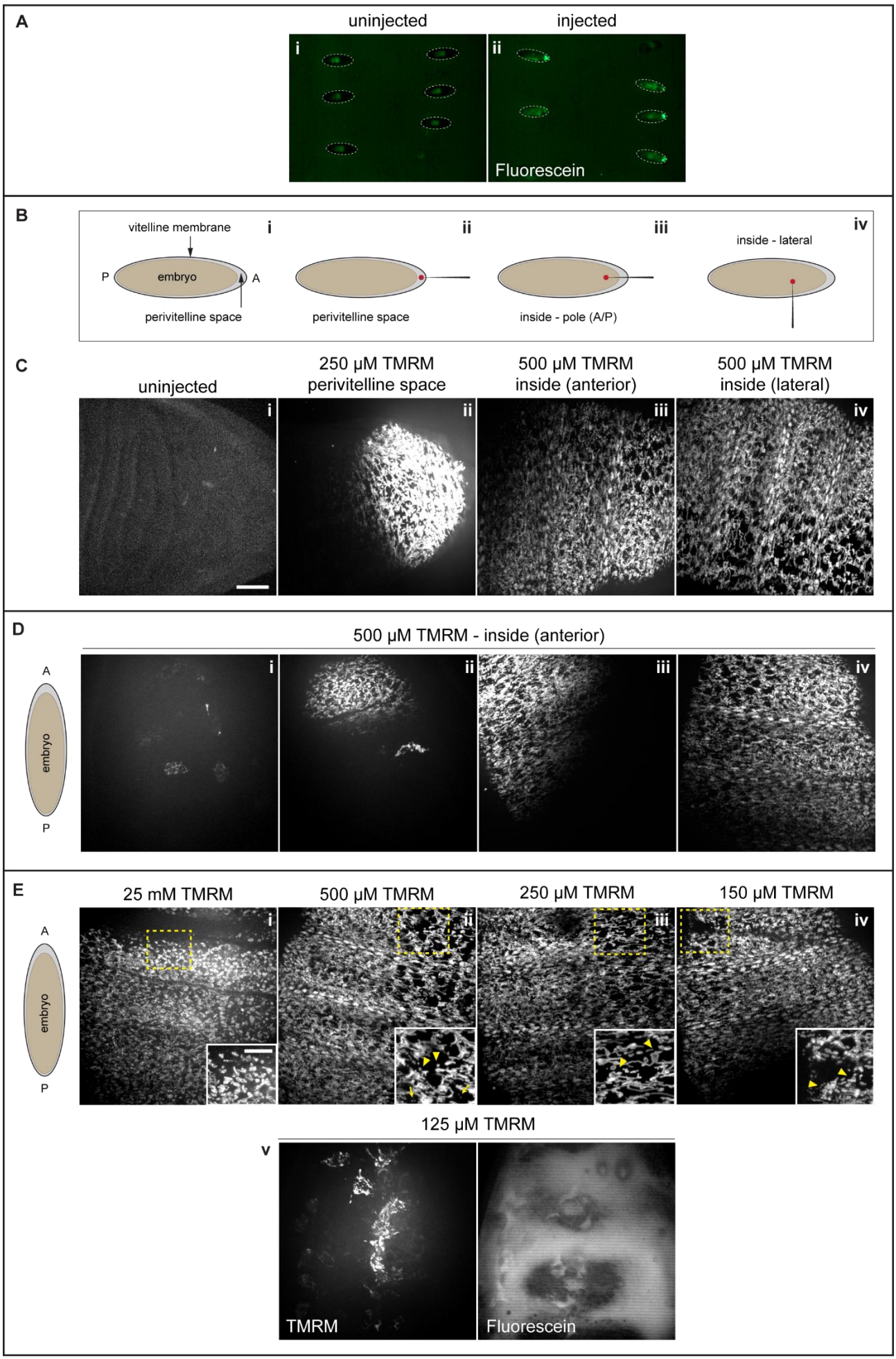
A
uninjected
injected
i
ii
Fluorescein
B
vitelline membrane
i
ii
iii
iv
inside - lateral
P
embryo
A
perivitelline space
perivitelline space
inside - pole (A/P)
C
uninjected
250 µM TMRM
perivitelline space
500 µM TMRM
inside (anterior)
500 µM TMRM
inside (lateral)
i
ii
iii
iv
D
500 µM TMRM - inside (anterior)
A
embryo
P
i
ii
iii
iv
E
25 mM TMRM
500 µM TMRM
250 µM TMRM
150 µM TMRM
A
embryo
P
i
ii
iii
iv
125 µM TMRM
v
TMRM
Fluorescein

Figure 25. Mitochondrial membrane potential assessment by microinjection of TMRM.
(A) Images depict *Drosophila* embryos without (i) and after fluorescein microinjection (ii). (B) Schematic representation of the embryo anatomy representing the vitelline membrane and perivitelline space (i) and the different sites of injection: into the perivitelline space (ii), into the embryo, at the anterior or posterior pole (iii) or into the embryo, at the lateral side (iv). (C) Confocal images showing TMRM staining in uninjected embryos (i) or embryos injected in the different sites described in B. (D) Confocal images of embryos injected laterally with 500µM TMRM, depicting the variability of the microinjection protocol. (E) Confocal images of embryos injected with different concentrations of TMRM. Insets are zoomed images of the region outlined by the yellow dashed line. Arrowheads point to swollen mitochondria. A – anterior. P – posterior. Scale bar = 20 µm. Inset scale bar = 10 µm. Embryos in C, D and E are oriented accordingly to the corresponding embryo scheme.

6. Assessment of mitophagy during wound healing

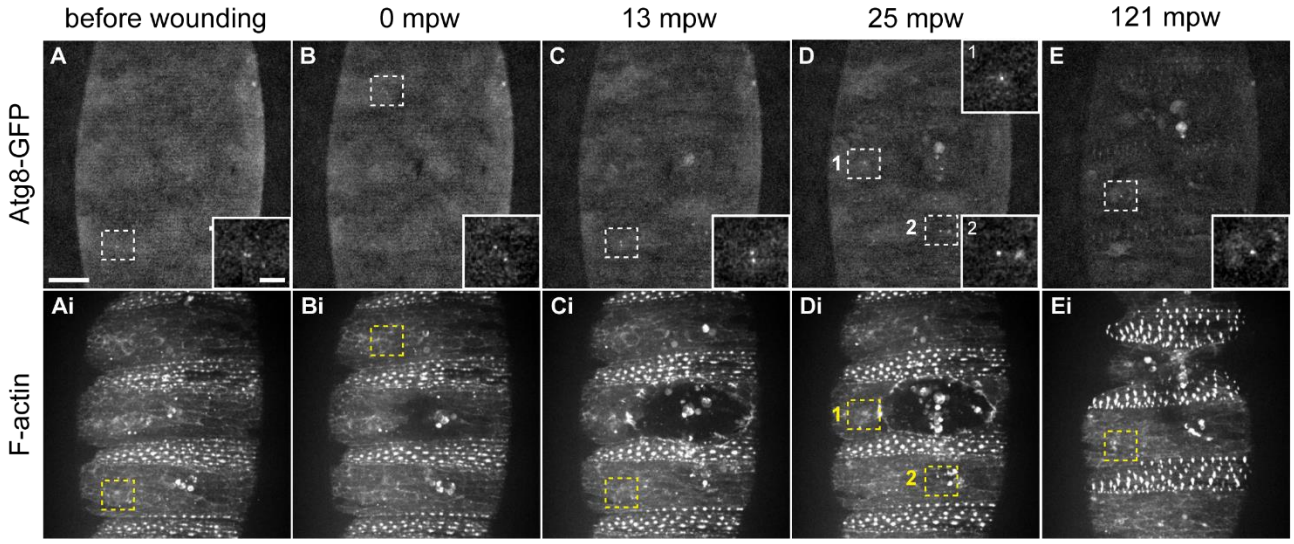

Figure 26. Wounding does not seem to induce autophagy.
(A-E, Ai-Ei) Representative confocal images of an embryo expressing *UAS-Atg8::GFP* (A-E) to label autophagosomes and *mCherry::Moesin* (Ai-Ei) to mark F-actin. Insets show zoomed images of the regions delimited by dashed squares in A-E. Yellow dashed squares show the same region in the F-actin marker channels, just for reference. Autophagy does not seem to be triggered by injury because most of the visualized Atg8::GFP spots appear away from the wound site. Images are maximum Z projections of 50 slices (5.3-µm-thick stack). mpw – minutes post wounding. Scale bar = 20 µm. Inset scale bar = 5 µm.

Macroautophagy of damaged mitochondria, referred as mitophagy, is a way of regulating mitochondrial quality within the cell (Moyzis et al., 2015). Our results indicate that wounding promotes an increase in mitochondrial fragmentation. We asked whether this fragmentation is due to the stress caused by wounding, that could impair mitochondrial function and target mitochondria to degradation by the mitophagy machinery. Mitophagy involves the formation of an autophagosome (double-membrane vesicle) that engulfs selected mitochondria and fuses with the lysosomes for degradation. Target mitochondria are recognized by

Microtubule-associated protein 1A/1B-light chain 3 (LC3) adapters (Yoo and Jung, 2018). LC3-conjugates are present in the autophagosome membrane and are often used as autophagy activity indicators (Nagy et al., 2015).

To determine whether wounding triggers mitophagy, we assessed whether wounding leads to the formation of LC3-positive autophagic structures. We used transgenic flies expressing *UAS-Atg8::GFP* (the *Drosophila* LC3 homolog) and an F-actin marker in the epidermis (*e22c-Gal4* driver) and used spinning-disk microscopy to image the wound closure process (Fig. 21). Although we observed transient spots of *Atg8::GFP* in the epidermis, there was no correlation between the sites of *Atg8::GFP* accumulation and the wound.

Our results suggest that mitophagy is not induced upon injury and is likely not relevant for the wound healing process. In the future, it might be worthwhile testing other autophagy reporters or antibodies to validate these results.

7. Characterization of the wound healing phenotype of *Drp1* and *Opa1* mutants

7.1. *Drp1* mutants show delayed wound healing

After analyzing several aspects related to mitochondrial dynamics and function during wound healing, mitochondrial fusion and fission seem to be the most relevant processes for the epithelial repair process. Therefore, we decided to evaluate in more detail the role of Drp1 and Opa1 in wound healing. We used spinning-disk microscopy to image control, and *Drp1* and *Opa1* mutant embryos expressing an F-actin marker, and followed the dynamics of wound closure. For technical reasons, we used two slightly different, but previously characterized F-actin markers for each of the mutants and their respective controls: for *Drp1* mutants we used *GFP::Moesin* (Kiehart et al., 2000) and for *Opa1* mutants we used *UAS-mCherry::Moesin* (Millard and Martin, 2008). In both constructs the actin-binding domain of Moesin is fused with a fluorescent protein. *mCherry::Moesin* expression is UAS dependent, while *GFP::Moesin* expressing is driven ubiquitously through the *sqh* promoter.

Control embryos accumulate F-actin at the wound edge (Fig. 22 A), forming the so-called actin cable, and the wound area progressively decreases until the hole is closed (Fig. 22 A-Aiii, F). Although the initial area was similar in both conditions (Fig. 22 D), *Drp1* mutant wounds took on average 128±34 min to close, significantly longer than controls (56±17 min) (Fig. 22 E).

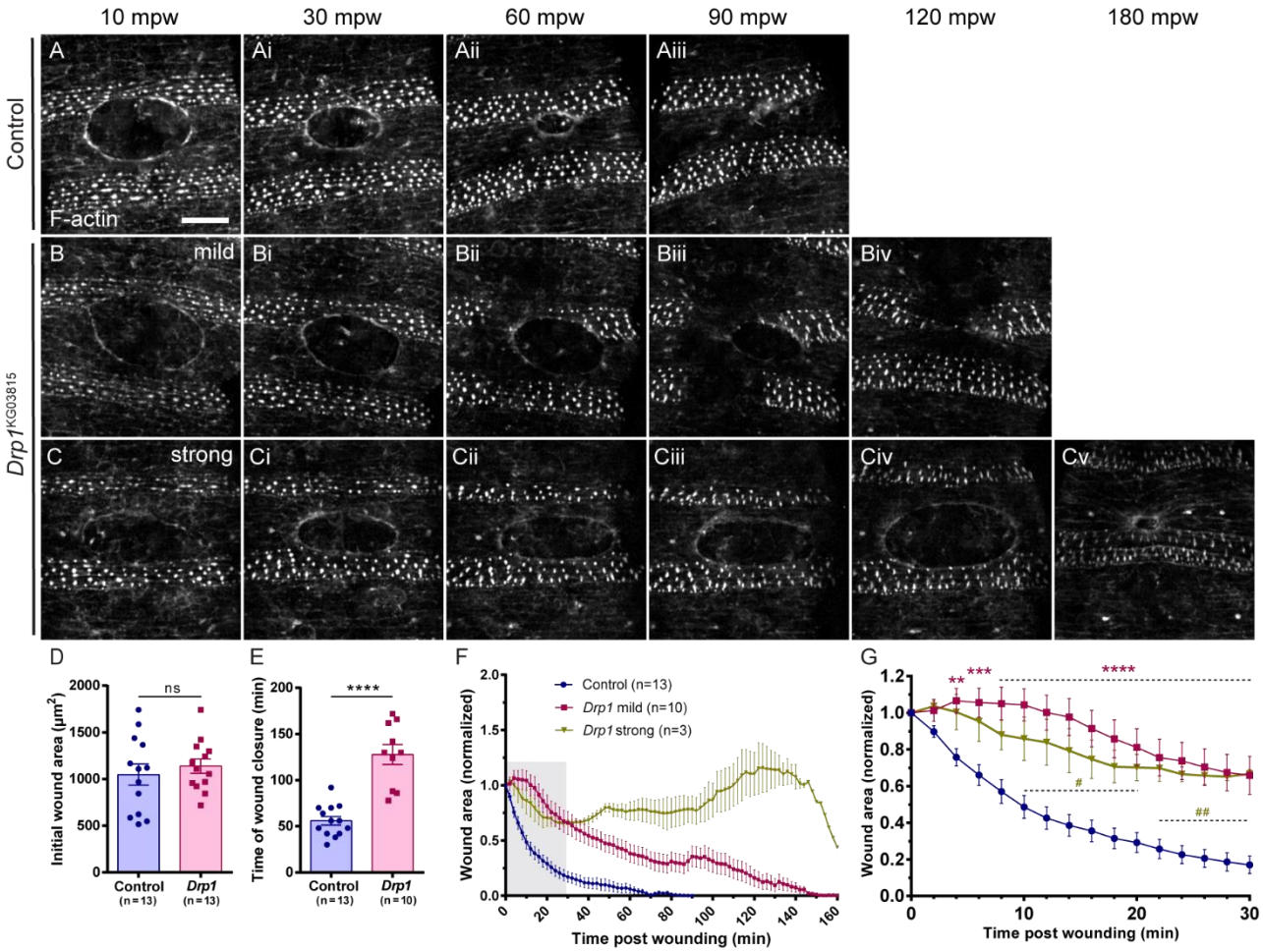

Figure 27. Drp1 mutant embryos show impaired wound closure dynamics.

(A-Aiii, B-Biv, C-Cv) Representative confocal images of the epidermis of control (A-Aiii), Drp1 mild (B-Biv) and Drp1 strong (C-Cv) mutant embryos expressing an F-actin marker (GFP::Moesin) during wound closure. Images are maximum Z projections of 60 slices (16.8-µm-thick stack). In Drp1 mild mutants (B-Biv) wounds close slower than in controls (compare B-Biv with A-Aiii). In Drp1 strong mutants (C-Cv), although the wound contracts in the first 40mpw (compare C with Ci), it then starts to expand (Cii-Civ). Later on, the wound contracts again and by 180 mpw it is almost closed (Cv). Scale bar = 20 µm. (D) Graph showing the average initial wound area in control and Drp1 mutant embryos (strong and mild). (E) Graph displaying the wound closure time in control and Drp1 mutant embryos. Although the initial wound area of control and Drp1 mutants was similar (D), Drp1 mutants took longer to close their wounds than controls (E). Unpaired t test with Welch's correction was performed to test for significant differences between groups in D and E. ns – not significant ($P > 0.05$), **** $P \leq 0.0001$. (F) Graph showing the average wound area in control, Drp1 mild and Drp1 strong mutants over time. Drp1 mild mutant wounds close slower than controls. Drp1 strong mutant wounds initially contract but start to expand after 40 mpw. At 120-130 mpw wounds start to contract again. (G) Graph indicates the average wound area in control, Drp1 mild and Drp1 strong mutants in the first 30 mpw, corresponding to the grey region in F. Significant differences between control and mutants start at 4 mpw in Drp1 mild mutants and at 10 mpw in Drp1 strong mutants. A two-way ANOVA with a Tukey correction for multiple comparisons was used to test for significant differences between groups in G. Asterisks (*) refer to control and Drp1 mild comparisons. Number signs (#) refer to control and Drp1 strong comparisons. Dashed lines depict an interval of points in which the comparison between groups gives the same degree of statistical significance, given by the symbols above. # - $P \leq 0.05$, ** or ## - $P \leq 0.01$, *** $P \leq 0.001$, **** $P \leq 0.0001$. Error bars represent SEM. Number of embryos per condition is shown in each graph. mpw – minutes post wounding.

We observed two phenotype strengths in *Drp1* mutants. In milder cases, wounds closed at a slower rate than controls (Fig. 22 B-Biv, F); in other cases (3 out of 13 *Drp1* mutant embryos), the phenotype was stronger: although the wound contracted for about 40 min post-wounding (mpw), after that its area began to increase again until 120-130 mpw (Fig. 22 C-Civ, F). After this expansion phase, wounds contracted again, and in one case it was almost closed by the end of imaging (Fig. 22 Cv, F). We quantified the wound area of control and *Drp1* mutants in the first 30 mpw and found significant differences in the first minutes after wounding (4 mpw and 10 mpw for mild and strong conditions, respectively) (Fig. 22 G). Our results show that Drp1 loss of function severely impairs wound closure dynamics, suggesting that mitochondrial fission is necessary for wound healing regulation.

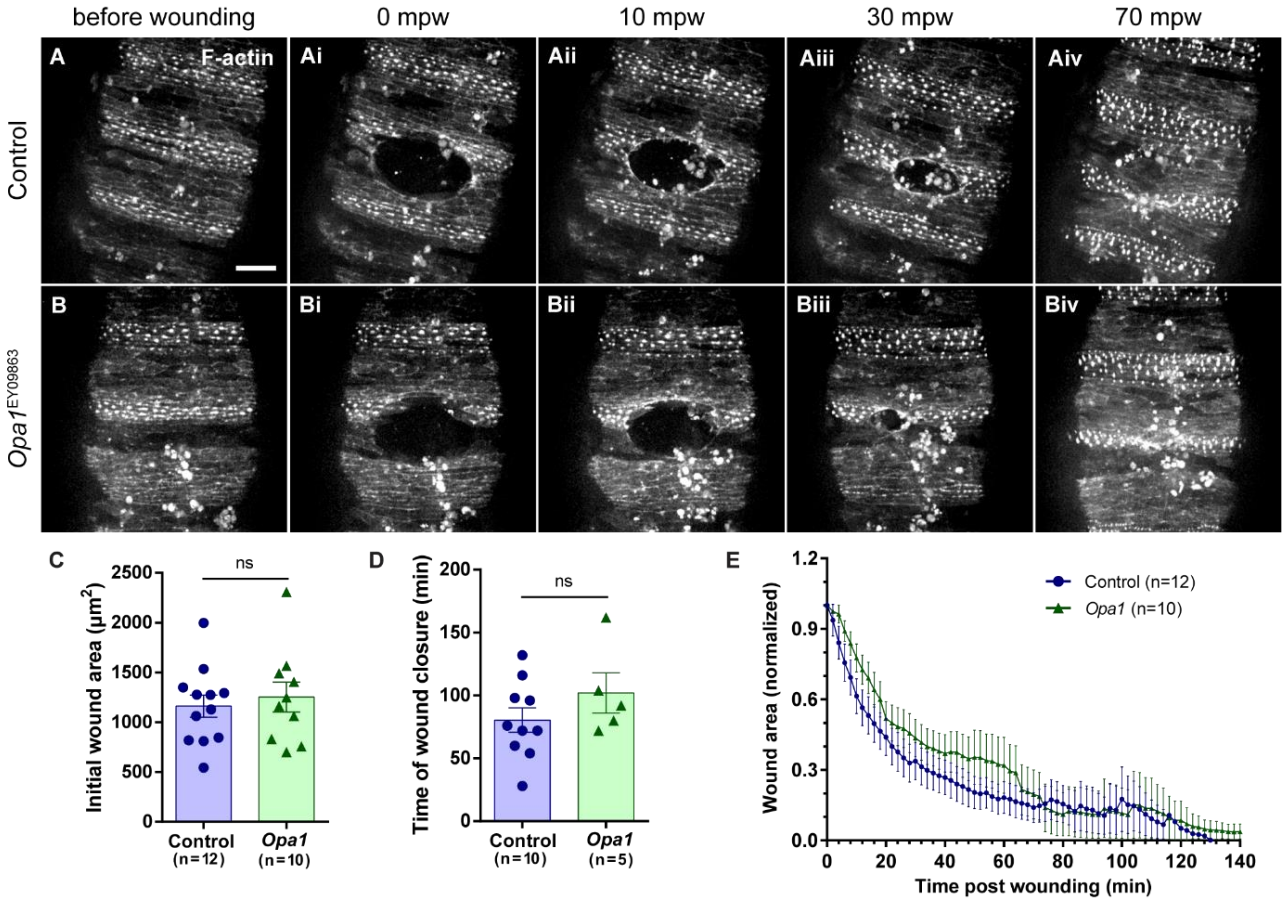

Figure 28. *Opa1* mutant embryos show no wound closure dynamics defects.
(A-Aiv, B-Biv) Representative confocal images of the epidermis of control (A-Aiv) and *Opa1* (B-Biv) mutant embryos expressing an F-actin marker (*UAS-mCherry::Moesin* under the control of the *e22c-Gal4* driver) during wound closure. Images are maximum Z projections of 40-50 slices (11.2 to 14-µm-thick stack). (C) Graph indicates the average initial wound area in control and *Opa1* mutant embryos (D) Graph showing quantification of wound closure time in control and *Opa1* mutant embryos. Unpaired t test with Welch's correction was performed to test for significant differences between groups in C and D. ns – not significant ($P > 0.05$). (E) Graph displaying the average wound area in control and *Opa1* mutants over time. A two-way ANOVA with a Tukey correction for multiple comparisons was used to test for significant differences between groups in E. No significant differences in either the time of wound closure or the wound area over time were found between control and *Opa1* mutant embryos. Error bars represent SEM. Number of embryos per condition is shown in each graph. mpw – minutes post wounding.

Regarding *Opa1* mutants, although they presented a phenotype in the wounding assay screen (Fig. 11), we did not observe significant differences in either the time of wound closure (Fig. 23, A-Aiv, B-Biv, D) or the wound area changes over time between mutants and controls (Fig. 23 A-Aiv, B-Biv, E). The discrepancy in the results of the two experiments could be related to the size of the wound. In the wounding assay screen, we used maximum laser power to inflict large wounds. In contrast, in order to follow the wound closure process by live imaging, we inflicted smaller wounds. Thus, our results suggest that mitochondrial fusion is required for the repair of larger wounds but not for the repair of small wounds.

7.2. *Drp1* and *Opa1* mutants have F-actin defects during wound closure

The assembly of the actomyosin cable is a hallmark of the epithelial wound repair process (Cordeiro and Jacinto, 2013; Martin and Lewis, 1992). Although cells can compensate for the loss of the actomyosin cable (Ducuing and Vincent, 2016), this structure is one of the main driving forces for wound healing (Zulueta-Coarasa and Fernandez-Gonzalez, 2017). So we quantified the fluorescence intensity of the F-actin marker in *Drp1* mutant embryos expressing *GFP::Moesin* (Kiehart et al., 2000) and *Opa1* mutant embryos expressing *UAS-mCherry::Moesin* (Millard and Martin, 2008) and respective control embryos. To quantify Myosin intensity, we used control, and *Drp1* and *Opa1* mutant embryos expressing a protein trap for Myosin II heavy chain (Zipper, Zip), *Zip $^{CPTI-100036}$::GFP* (Lye et al., 2014).

Although *Drp1* mutant embryos accumulated F-actin (Fig. 24 B-Biii) at the wound edge, they do so in significant lower levels than controls, from the early stages of wound closure (Fig. 24 C). Surprisingly, despite not having major wound closure defects (Fig. 23), we detected a significant decrease in F-actin levels in *Opa1* mutants, but only at 30 mpw, when compared to controls (Fig. 25, compare Aiii and Biii, C). Regarding myosin, we found no significant differences in Zip-GFP levels between control, and *Drp1* and *Opa1* mutant embryos (Fig. 26).

These results show that both Drp1 and Opa1 regulate F-actin but not myosin accumulation at the wound edge. This suggests that, in *Drp1* mutants, the F-actin defects detected shortly after wounding might underlie the observed wound healing phenotype. In contrast, in *Opa1* mutants, the observed defects in F-actin might be milder or compensated by other mechanisms, hence not leading to major wound healing impairment.

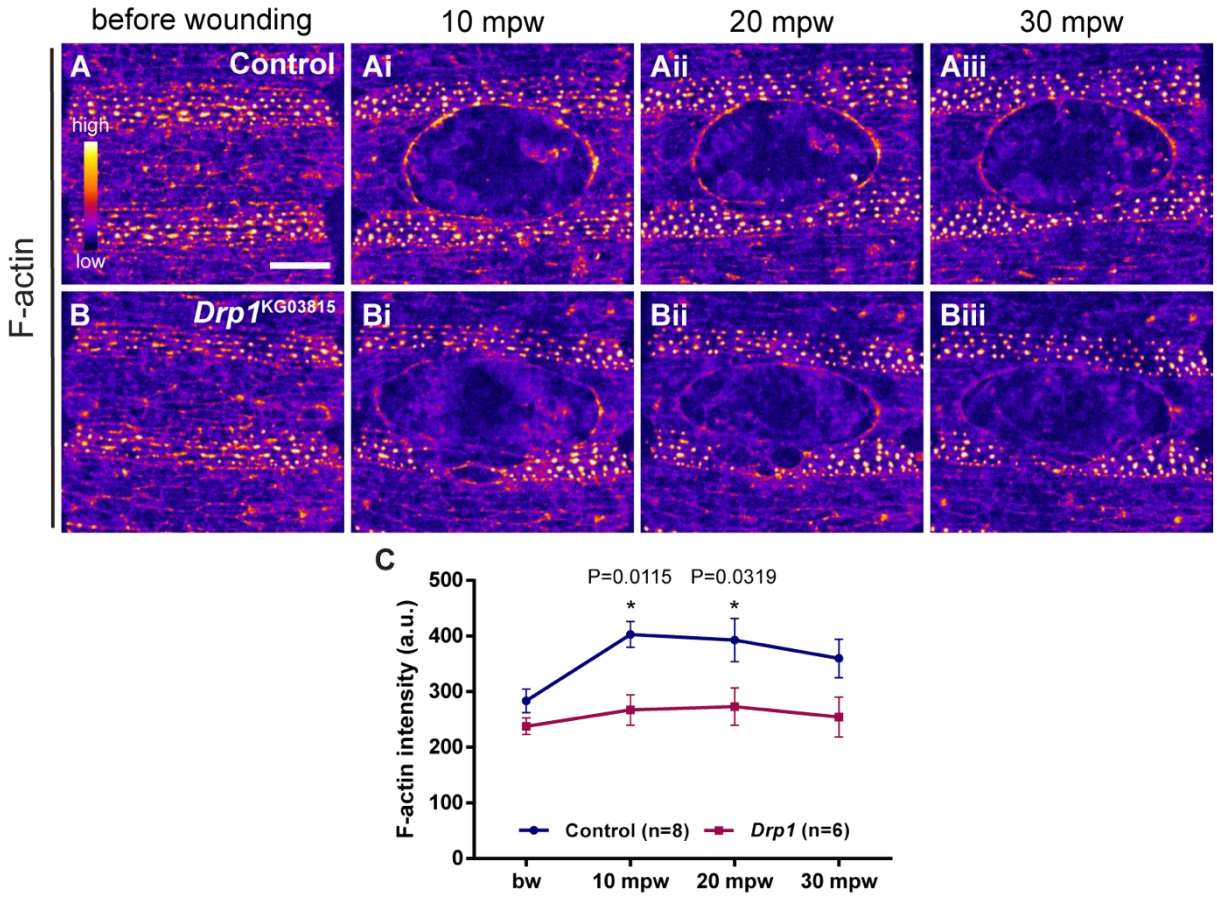

Figure 29. *Drp1* mutants show F-actin defects during wound closure.
(A-Aiii, B-Biii) Representative confocal images of control (A-Aiii) and *Drp1* (B-Biii) mutant embryos expressing an F-actin (*GFP::Moesin*) marker before (A,B) and after wounding (Ai-Aiii, Bi-Biii). Images are maximum Z projections of 60 slices (16.8-µm-thick stack). Images are pseudo-colored with a gradient of fluorescence intensity, ranging from blue (low) to yellow (high). Although no differences are evident before wounding (A, B), *Drp1* mutant embryos accumulate less F-actin at the wound edge than controls (compare Bi-Biii with Ai-Aiii). Scale bar = 20 µm. (C) Graph showing the average F-actin intensity at the cell cortex before wounding and at the wound edge. F-actin levels are significantly reduced in *Drp1* mutants at 10 and 20 mpw. A two-way ANOVA with a Sidak correction for multiple comparisons was used to test for significant differences between groups. Only significant differences ($P \leq 0.05$) are represented. Error bars represent SEM. Number of embryos per condition and P values are shown in C. a.u. - arbitrary units. mpw – minutes post wounding.

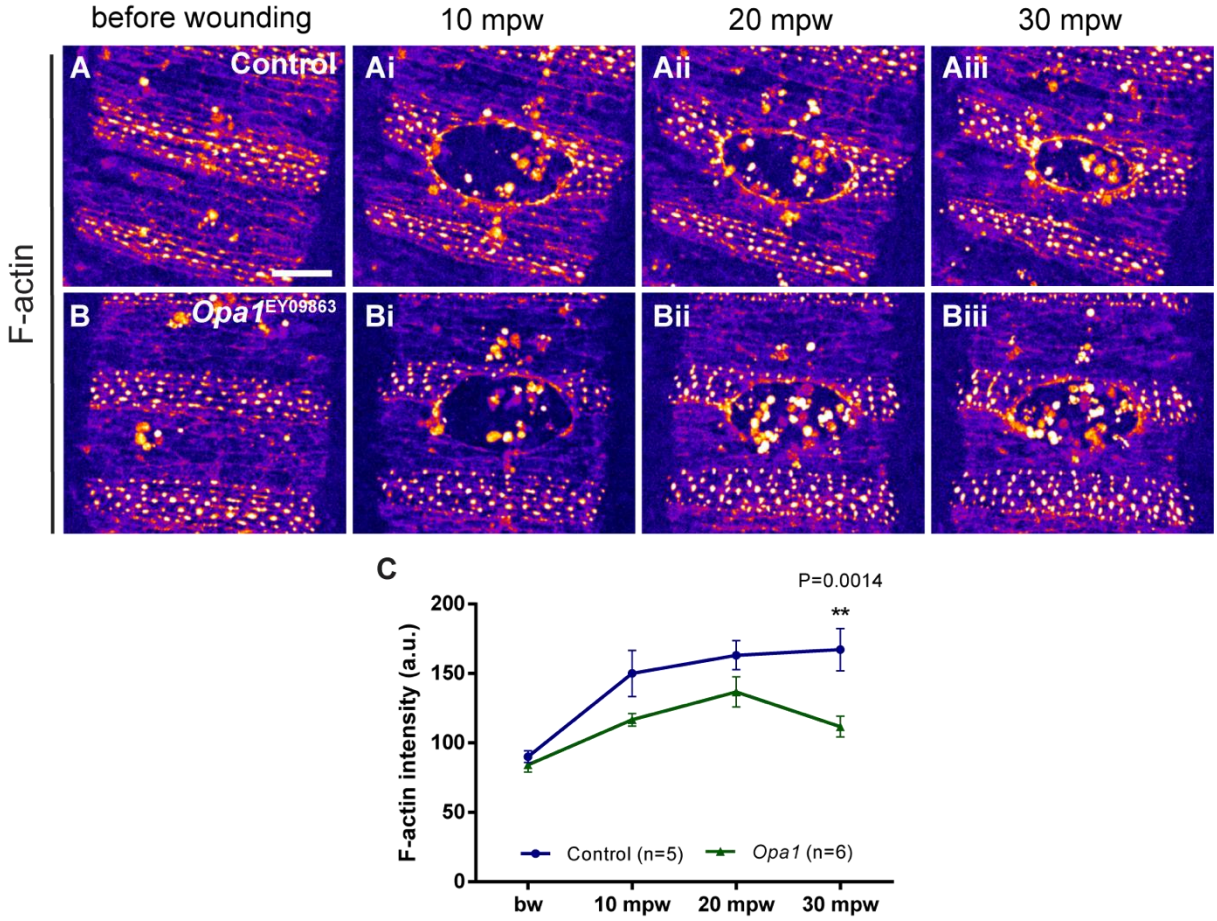

Figure 30 *Opa1* mutants show F-actin defects during wound closure.

(A-Aiii, B-Biii) Representative confocal images of the epidermis of control (A-Aiii) and *Opa1* (B-Biii) mutant embryos expressing an F-actin marker (*UAS-mCherry::Moesin* under the control of the *e22c-Gal4* driver) during wound closure. Images are maximum Z projections of 40-50 slices (11.2 to 14-µm-thick stack). Images are pseudo-colored with a gradient of fluorescence intensity, ranging from blue (low) to yellow (high). F-actin accumulation at the wound edge is reduced in *Opa1* mutant embryos compared to controls. Scale bar = 20 µm. (C) Graph of average F-actin intensity at the cell cortex before wounding and at the wound edge. F-actin levels are significantly reduced in *Opa1* mutants at 30 mpw when compared to controls. A two-way ANOVA with a Sidak correction for multiple comparisons was used to test for significant differences between groups. Only significant differences ($P \leq 0.05$) are represented. Error bars represent SEM. Number of embryos per condition and P value are shown in C. a.u. - arbitrary units. mpw – minutes post wounding.

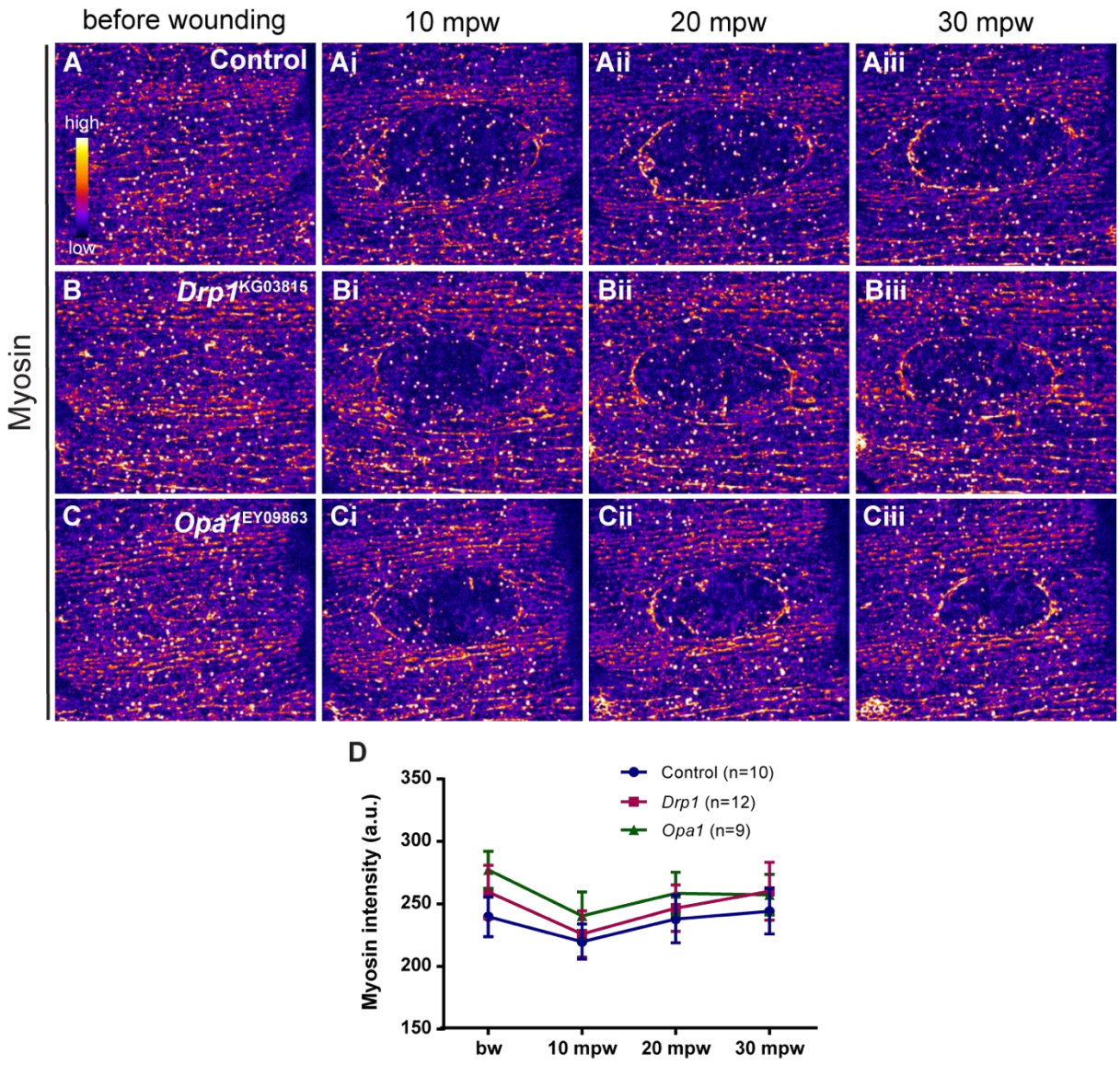

Figure 31. Myosin accumulation at the wound edge is unaffected in *Drp1* and *Opa1* mutants.
(A-Aiii, B-Biii, C-Ciii) Representative confocal images of the epidermis of control (A-Aiii), *Drp1* (B-Biii) and *Opa1* (C-Ciii) mutant embryos expressing a Myosin II heavy chain (Zip::GFP) (C-Ciii, D-Diii) marker before (A-C) and after wounding (Ai-Aiii, Bi-Biii, Ci-Ciii). Images are pseudo-colored with a gradient of fluorescence intensity, ranging from blue (low) to yellow (high). Myosin accumulation at the wound edge seems similar between control, and *Drp1* and *Opa1* mutants. Scale bar = 20 µm. (D) Graph of average Myosin intensity at the cell cortex before wounding and at the wound edge. No significant differences were found between control, and *Drp1* and *Opa1* mutant embryos ($P > 0.05$). A two-way ANOVA with a Sidak correction for multiple comparisons was used to test for significant differences between groups. Error bars represent SEM. Number of embryos per condition is shown in each graph. a.u. - arbitrary units. mpw – minutes post wounding.

7.3. Rok localization at the wound edge is affected in *Opa1* mutants

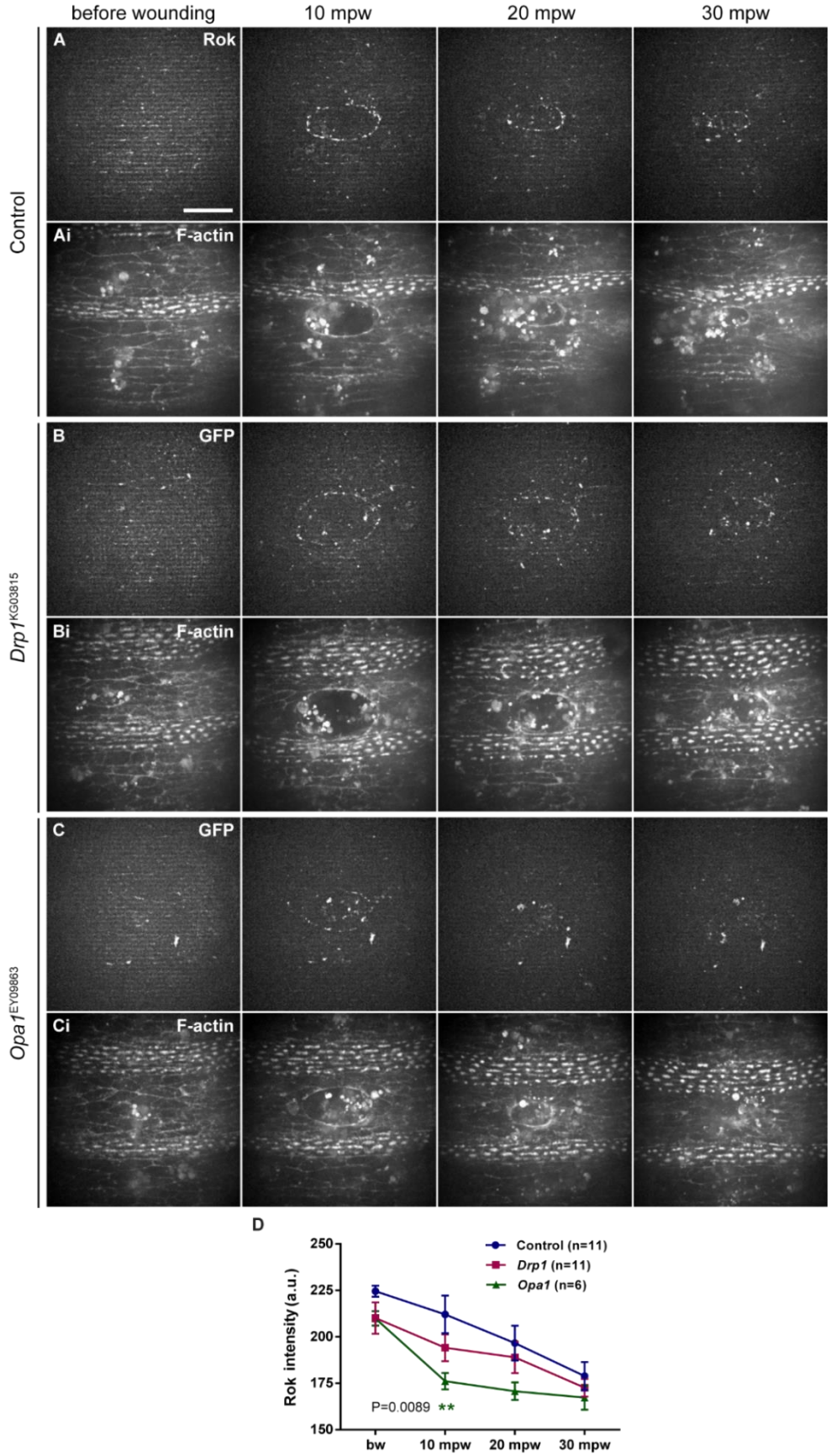

Figure 32. Rok localization in control, *Drp1* and *Opa1* mutants during the wound healing response.
(A–C) Representative confocal images of the epidermis during wound closure in control (A-Ai), *Drp1* (B-Bi) and *Opa1* (C-Ci) mutant embryos expressing *GFP::Rok* (A-C) and *mCherry::Moesin* labeling F-actin (Ai-Ci) before and upon laser wounding. Images are maximum Z projections of 33 slices (9.24-µm-thick stack). Upon wounding, Rok accumulates at the wound edge in controls, *Drp1* and *Opa1* mutants. Scale bar = 20 µm. (D) Graph displaying the average GFP::Rok fluorescence intensity at the cell cortex before wounding and at the wound edge. No significant differences were found between control and *Drp1* embryos, but *Opa1* mutants showed reduced Rok levels at the wound edge at 10 mpw, compared to controls. A two-way ANOVA with a Sidak correction for multiple comparisons was used to test for significant differences between groups. Error bars represent SEM. Number of embryos per condition and P value is shown D. a.u. - arbitrary units. mpw – minutes post wounding.

The cytoskeletal changes that occur during wound closure are regulated by proteins of the Rho-GTPase family (Verboon and Parkhurst, 2015). The GTP-dependent activation of these proteins leads to conformational changes that allow them to interact with downstream target proteins (Bishop and Hall, 2000; Bustelo et al., 2007). The Rho1 protein has been shown to regulate the actomyosin cable assembly and contraction during wound healing (Verboon and Parkhurst, 2015; Wood et al., 2002). One of the described functions of Rho1 is to activate Rho kinase (Rok) that phosphorylates myosin regulatory light chain (MRLC) (Kosako et al., 2000), therefore promoting actomyosin contractility (Antunes et al., 2013; Tamada et al., 2007; Vasquez et al., 2014).

Upon wounding, Rok accumulates at the cellular membranes facing the wound, and has been used as a read-out of Rho1 activity (Tamada et al., 2007; Verboon and Parkhurst, 2015). Therefore, to understand whether Drp1 and Opa1 regulate actomyosin cable function through Rho-GTPase activity, we analyzed Rok localization at the wound edge as a proxy for Rho1 activity. We used control, and *Drp1* and *Opa1* mutants expressing *GFP::Rok* (Abreu-Blanco et al., 2014) and the F-actin marker *mCherry::Moesin* (Millard and Martin, 2008) (Fig. 27). In the *GFP::Rok* construct, *sqh* promoter sequences drive ubiquitous expression of the *Rok* open reading frame which is tagged with GFP (Abreu-Blanco et al., 2014). We used the F-actin marker to accurately determine the wound boundary (Fig.27, Ai-Ci), and measured the *GFP::Rok* intensity at the wound edge and compared it to levels at the cortical region of cells before wounding (Fig.27, A-C).

Upon wounding, Rok accumulation was clear at 10 mpw and then decreased during wound closure (Fig. 27 A-C). Quantification of the *GFP::Rok* fluorescent intensity showed a decrease in Rok levels at the wound edge in *Opa1* mutants at 10 mpw but not at later time points, compared to controls, suggesting that Opa1 might influence the recruitment of this kinase (Fig. 27 D). It remains unclear why this defect in Rok localization does not lead to altered myosin levels in Opa1 loss of function.

In contrast, no significant difference in Rok intensity was found between control and *Drp1* mutant embryos (Fig. 27 D). These results suggest that Drp1 does not regulate Rok recruitment and are in line with

the lack of phenotype in myosin levels upon Drp1 loss of function. On the other hand, they suggest that the F-actin defects observed during wound closure in *Drp1* mutants are not related to impaired Rok activity. Instead, it is possible that other Rho1 targets, such as Protein kinase N (Pkn) and Diaphanous (Dia) (Abreu-Blanco et al., 2014; Matsubayashi et al., 2015), are involved. This aspect should thus be addressed in future studies.

7.4. E-cadherin remodelling during wound repair is unaffected in *Drp1* and *Opa1* mutants

The formation of the actomyosin cable depends on remodeling of the AJs (Abreu-Blanco et al., 2012b; Carvalho et al., 2014; Hunter et al., 2015; Matsubayashi et al., 2015). After wounding, the AJ protein E-cadherin is downregulated at the cell boundaries facing the wound, remaining only at the lateral junctions of leading-edge cells.

To test whether the F-actin phenotypes observed in *Drp1* and *Opa1* mutants were associated with E-cadherin remodeling defects, we imaged control, *Drp1* and Opa1 mutant embryos expressing *ubi-E-cadherin::GFP* (Oda and Tsukita, 1999) and *mCherry::Moesin* (Millard and Martin, 2008) before and upon wounding. We observed no significant differences between E-cadherin levels of control, and *Drp1* and *Opa1* mutant embryos, either before or after wounding (Fig. 28). These results suggest that Drp1 and Opa1 regulate F-actin dynamics during wound closure, independently of AJs remodeling, through an alternative mechanism.

7.5. *Drp1* and *Opa1* mutants have altered cytosolic calcium dynamics upon wounding

The first signal to be detected upon wounding is an intracellular calcium burst across several cell rows surrounding the wound (Antunes et al., 2013; Razzell et al., 2013; Sammak et al., 1997; Xu and Chisholm, 2011). This calcium increase regulates many wound healing steps, including actomyosin cable formation (Antunes et al., 2013; Xu and Chisholm, 2011). Mitochondria are known regulators of calcium homeostasis (Finkel et al., 2015; Giorgi et al., 2008; Rizzuto et al., 2012), so we asked whether the F-actin defects observed in *Drp1* and *Opa1* mutants could be due to impaired calcium dynamics.

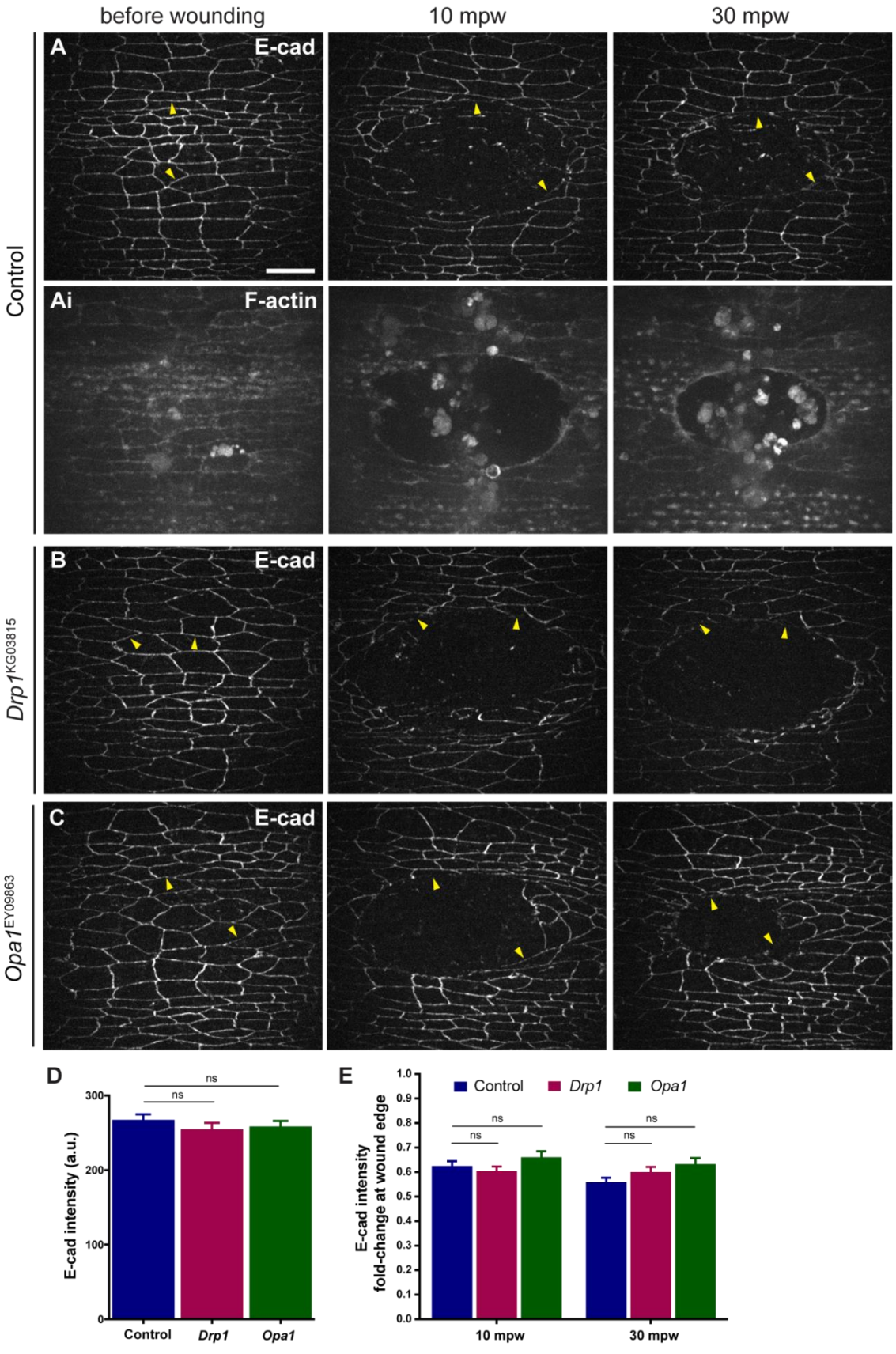
before wounding
10 mpw
30 mpw
Control
A
E-cad
Ai
F-actin
Drp1KG03815
B
E-cad
Opa1EY09863
C
E-cad
D
E-cad intensity (a.u.)
300
200
100
0
ns
ns
Control
Drp1
Opa1
E
Control
Drp1
Opa1
E-cad intensity fold-change at wound edge
1.0
0.9
0.8
0.7
0.6
0.5
0.4
0.3
0.2
0.1
0.0
ns
ns
ns
ns
10 mpw
30 mpw

Figure 33. E-cadherin localization in control, *Drp1* and *Opa1* mutants after wounding.
(A–C) Representative confocal images of the epidermis during wound closure in control (A-Ai), *Drp1* (B) and *Opa1* (C) mutant embryos expressing *ubi–E-cad::GFP* (A, B, C) and *mCherry::Moesin* labeling F-actin (Ai) before and upon laser wounding. Images are maximum Z projections of 35 slices (12.6-µm-thick stack). Upon wounding, E-cadherin intensity decreases at cell boundaries facing the wound edge in controls, *Drp1* and *Opa1* mutants (arrowheads mark the same junctions before and after wounding in each embryo). Scale bar = 10 µm. (D) Graph indicates the average E-cadherin fluorescence intensity in cells before wounding in controls, *Drp1* and *Opa1* mutants. (E) Graph showing the fold change decrease in E-cadherin fluorescence intensity in cell boundaries at the wound edge at 10 and 30 mpw (normalized to E-cadherin levels before wounding) in control, *Drp1* and *Opa1* mutant embryos. N(control)=52 junctions from six embryos; N(*Drp1*)=64 junctions from five embryos. N(*Opa1*)=66 junctions from six embryos. An unpaired t test (D) and a two-way ANOVA with a Tukey multiple comparisons test (E) were performed to test for significant differences between groups. Differences between groups are not significant (ns, $P > 0.05$). Error bars represent SEM. a.u. – arbitrary units. mpw – minutes post wounding. E-cad – E-cadherin

Thus, we imaged control, and *Drp1* and *Opa1* mutant embryos expressing the *GCaMP6f* calcium sensor (Chen et al., 2013) and the F-actin marker *mCherry::Moesin* (Millard and Martin, 2008), and measured calcium levels before and upon wounding. The *GCaMP6f* construct consists of a circularly permuted GFP (cpGFP), the calcium-binding protein calmodulin (CaM) and CaM-interacting M13 peptide. Calcium-dependent conformational changes in CaM–M13, cause increased brightness of the chromophore upon calcium binding (Chen et al., 2013). The F-actin marker was used to monitor the wound boundary over time.

As previously described (Razzell et al., 2013), wounding induces a dramatic and transient increase in cytosolic calcium levels in cells around the wound (Fig. 29 Ai-Aiii). In *Drp1* mutant embryos, the cytosolic calcium burst was less pronounced than in controls (Fig. 29, B-Biii, D). Moreover, the area around the wound where this calcium increase is detected was significantly reduced in *Drp1* mutants compared to controls (Fig. 29 E). These results suggest that impairing Drp1 function affects not only the calcium levels but also the intercellular calcium propagation. In *Opa1* mutants, cytosolic calcium levels were also reduced upon wounding (Fig. 29, C-Ciii, D), whereas the area of calcium increase seemed to be unaffected (Fig. 29 E), when compared to controls.

Knowing that impaired cytosolic calcium dynamics upon wounding compromises the actomyosin cable (Antunes et al., 2013; Xu and Chisholm, 2011), our results suggest that the F-actin defects during wound closure in *Drp1* and *Opa1* mutants may be a consequence of altered cytosolic calcium. It would be interesting to confirm this hypothesis by rescuing cytosolic calcium levels in *Drp1* and *Opa1* mutants, and then assess whether the F-actin levels are recovered.

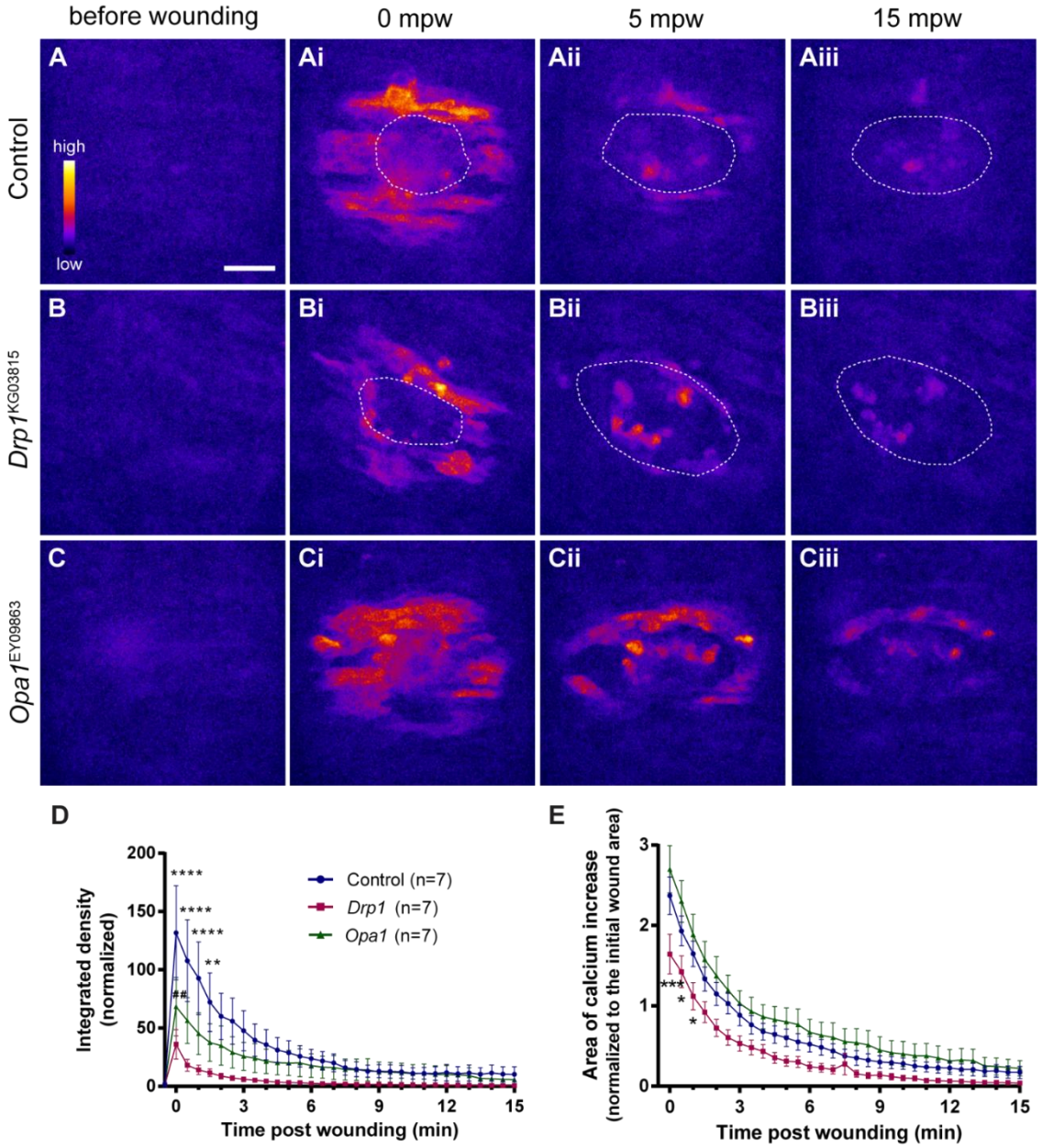

Figure 34. *Drp1* and *Opa1* mutant embryos show altered cytosolic calcium dynamics.
(A-Aiii, B-Biii) Confocal images of the epidermis of control (A-Aiii), *Drp1* (B-Biii) and *Opa1* (C-Ciii) mutant embryos expressing a cytosolic calcium sensor (*GCaMP6f*) before and after wounding. Images are pseudo-colored with a gradient of fluorescence intensity, ranging from blue (low) to yellow (high). Dashed lines show the wound boundaries. Scale bar = 20 µm. mpw – minutes post wounding. Control, *Drp1* and *Opa1* mutant cells around the wound dramatically increase cytosolic calcium levels immediately upon wounding (Ai- Ci). Intensity returns to pre wound levels after approximately 15 min (Aiii-Ciii). calcium levels and area of cells that respond to the wound are lower in *Drp1* (Bi) mutants compared to controls (Ai). In *Opa1* mutants (Ci), only the calcium levels are slightly reduced compared to controls (Ai). (D) Graph of cytosolic calcium intensity in control, *Drp1* and *Opa1* mutants shows that cytosolic calcium is lower in *Drp1* and *Opa1* mutants (in the first 2.5 mpw and immediately upon wounding, respectively) compared to controls. (E) Graph of average area of elevated cytosolic calcium in control, *Drp1* and *Opa1* mutants shows that the calcium burst area is lower in *Drp1* mutants compared to controls from 0 to 1 mpw. A two-way ANOVA with a Sidak correction for multiple comparisons was used to test for significant differences between groups in D and E. Asterisks (*) refer to control and *Drp1* mutant comparisons. Number signs (#) refer to control and *Opa1* mutant comparisons. Only significant differences are represented: ## P=0.0038, * P ≤ 0.05, ** P ≤ 0.01, *** P ≤ 0.001, **** P ≤ 0.0001. Error bars represent SEM. Number of embryos per condition is shown in graph D.

7.6. *Drp1* mutants have altered mitochondrial calcium dynamics upon wounding

Mitochondria are known for their calcium buffering ability. When cytosolic calcium increases, either by influx from the extracellular environment or release from internal stores such as the endoplasmic reticulum (ER), the mitochondria in the vicinity of calcium channels uptake calcium from the cytosol. This local cytosolic calcium modulation regulates the activity of calcium channels, controlling cytosolic calcium oscillations (Rizzuto et al., 2012; Szabadkai and Duchen, 2008). For example, in *X. laevis* oocytes, mitochondrial calcium uptake leads to cytosolic calcium transients by stimulating calcium release from ER channels (Jouaville et al., 1995). Interestingly, mitochondrial morphology has been shown to influence mitochondrial calcium levels, both by changing the close contacts between mitochondria and with ER or plasma membrane channels, and by affecting the ΔΨm (Bianchi et al., 2006; Brand, 1975; Gerencser and Adam-Vizi, 2005; Szabadkai et al., 2004). Furthermore, a mitochondrial calcium burst has been observed during wound repair in the *C. elegans* epidermis (Xu and Chisholm, 2014). So, we asked whether this is a conserved response during epithelial repair. In particular, our hypothesis is that mitochondrial dynamics influences the calcium buffering capacity of mitochondria and, consequently, the cytosolic calcium burst already shown to be essential for proper wound closure. To address this, we investigated whether mitochondrial calcium oscillations also occur in our system, the *Drosophila* embryonic epidermis*,* and, if so, whether Drp1 loss of function affects this process. We chose to focus on the role of Drp1, as *Drp1* mutants showed consistent and clear phenotypes in terms of cytosolic calcium, mitochondrial morphology and wound closure, in contrast to *Opa1* mutants.

We examined control and *Drp1* mutant embryos expressing the mitochondria-targeted *GCaMP3* calcium sensor [*mito::GCaMP3* (Lutas et al., 2012)] and the F-actin marker *mCherry::Moesin* (Millard and Martin, 2008), before and upon wounding. The F-actin marker was used to follow the wound edge over time.

Concomitantly with the cytosolic response, we observed a sharp increase in mitochondrial calcium around the wound in both control (Fig. 30 A-Aiii) and *Drp1* mutants (Fig. 20, B-Biii), similar to what has been previously observed in *C. elegans* (Xu and Chisholm, 2014). Notably, quantification of mitochondrial calcium intensity showed a significantly reduced response upon wounding in *Drp1* mutant embryos compared to controls (Fig. 30 C, 0 mpw). No differences were found in the area of increased mitochondrial calcium (Fig. 30 D), suggesting that in contrast to what was observed for cytosolic calcium, mitochondrial calcium propagation is not affected.

In conclusion, our results strongly suggest that *Drp1* mutant mitochondria have reduced mitochondrial calcium buffering capacity, which can impact on cytosolic calcium and cause the observed cytosolic calcium burst defects. To validate this hypothesis, it will be important in future studies to assess whether

experimentally manipulating mitochondrial calcium entry or exit phenocopies the *Drp1* wound healing defects.

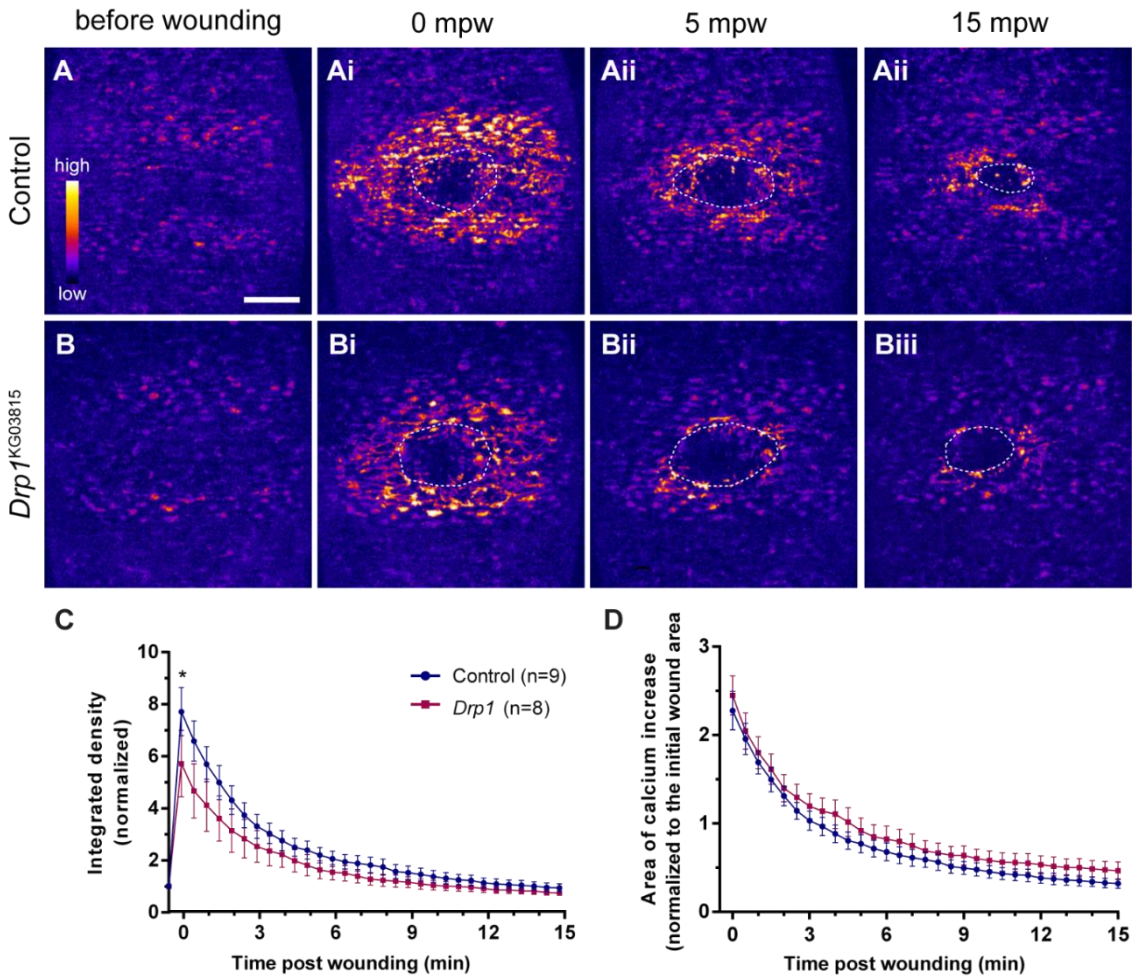

Figure 35. *Drp1* mutants show altered mitochondrial calcium dynamics.
(A-Aiii, B-Biii) Confocal images of the epidermis of control (A-Aiii) and *Drp1* (B-Biii) mutants expressing a mitochondrial calcium sensor (*mito::GCaMP3*) before and after wounding. Wounding triggers an increase in mitochondrial calcium levels in both control and *Drp1* mutant cells around the wound (Ai, Bi). (C) Graph of mitochondrial calcium intensity in control and *Drp1* mutants. *Drp1* mutants have a significantly reduced mitochondrial calcium burst at 0 mpw, compared to controls. (D) Graph of average area of elevated mitochondrial calcium in controls and *Drp1* embryos. No significant differences were found between control and *Drp1* mutants. Images are pseudo-colored with a gradient of fluorescence intensity, ranging from blue (low) to yellow (high). Dashed lines show the wound boundaries. Scale bar = 20 µm. mpw – minutes post wounding. A two-way ANOVA with a Sidak correction for multiple comparisons was used to test for significant differences between groups in C and D. Only significant differences are represented: * $P \leq 0.05$. Error bars represent SEM. Number of embryos per condition is shown in C.

7.7. Measurement of Reactive Oxygen Species in the embryonic epidermis

ROS constitute a double-edge sword in tissue repair in mammalian models: whereas low ROS levels are beneficial, sustained oxidative stress leads to impaired wound healing (Dunnill et al., 2017; Schäfer and Werner, 2008). Interestingly, Xu and Chisholm found that ROS production is downstream of the observed mitochondrial calcium burst and regulates actin cytoskeleton dynamics in *C. elegans* epidermis wound healing (Xu and Chisholm, 2014).

It is well known that ROS can be produced by mitochondria (Murphy, 2009) and that this mitochondrial function can be regulated by mitochondrial dynamics. Fragmentation of the mitochondrial network is associated with increased ROS production and inhibition of mitochondrial fission can reduce oxidative stress (Galloway et al., 2012). As we have shown that Drp1 regulates calcium^{+} and F-actin dynamics during wound closure, we hypothesized that ROS production might provide a link between calcium activity and F-actin dynamics. Therefore, we investigated whether *Drp1* mutants have altered ROS production.

To measure ROS production, we took advantage of transgenic flies expressing genetically encoded ROS sensors based on the roGFP probe. RoGFP contains cysteines engineered in a way that their redox equilibrium is associated with measurable ratiometric fluorescent changes (Hanson et al., 2004). Albrecht and colleagues developed transgenic flies bearing roGFP coupled to oxidant receptor peroxidase 1 (Orp1) that make the GFP fluorophore responsive to changes in hydrogen peroxide (H_2O_2), respectively(Albrecht et al., 2011).

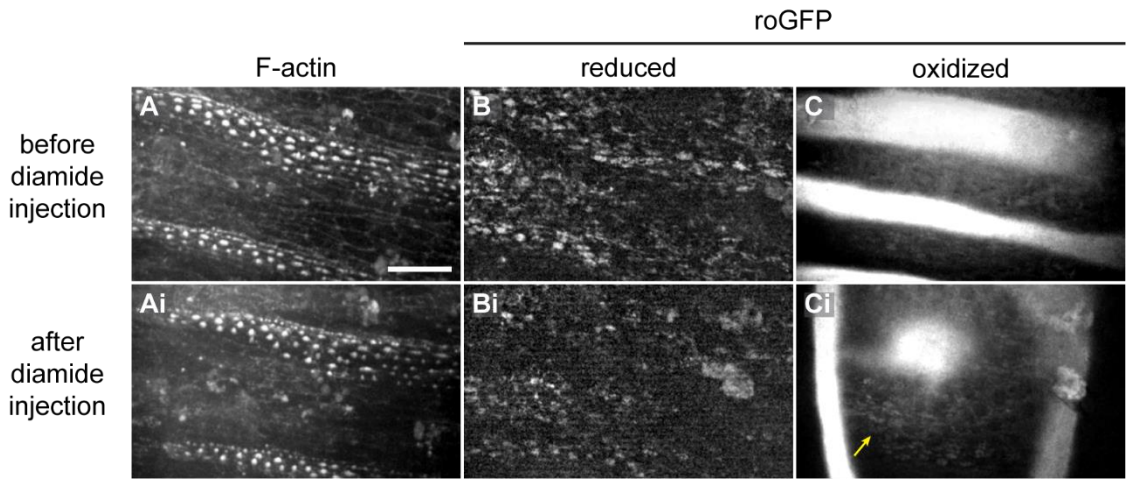

Figure 36. Changes in roGFP emission spectrum upon oxidation after injection of Diamide.
(A-Ci) Representative confocal images of embryos expressing *UAS-mito::roGFP2-Orp1* and the F-actin marker *mCherry::Moesin* in the epidermis (*e22c-Gal4* driver) before (A-C) and after (Ai-Ci) injection of diamide, an oxidant agent. A-B, Ai-Bi are maximum Z projections. C, Cii are individual slices. Upon diamide injection, a small increase in the roGFP oxidized intensity is detected (Ci, arrow). Scale bar = 20 µm.

To test the sensitivity of the ROS sensors to oxidation in our experimental system, we performed a positive control, using an oxidant agent – diamide. We imaged embryos expressing the mitochondrial H_2O_2 sensor (*UAS-mito::roGFP2-Orp1*) (Albrecht et al., 2011) and an F-actin marker (*mCherry::Moesin*) (Millard and Martin, 2008) in the epidermis, before and after diamide injection (Fig. 31). We observed a slight increase in the oxidized roGFP signal (Fig. 31 Ci, arrow), confirming that it is sensitive to oxidative stress. To quantify the changes in redox potential, we should calculate the ratio between the oxidized and the reduced roGFP intensities. However, we were unable to perform these quantifications because the oxidized roGFP signal was not bright enough. The vitelline membrane autofluorescence masks the signal of the oxidized roGFP, posing a challenge for ROS quantification in the embryo using this sensor.

Due to time constraints, we were not able to explore other alternatives to ROS measurement but previous studies have reported several fluorescent dyes that successfully labelled ROS production upon wounding in the *Drosophila* embryonic epidermis (Hunter et al., 2018a; Razzell et al., 2013)

CHAPTER 4. DISCUSSION

“Nothing in life is to be feared, it is only to be understood. Now is the time to understand more, so that we may fear less.”

— Marie Curie

Epithelial tissues line our body inside and out and are thus essential to protect us against the external environment (Lowe and Anderson, 2015). Therefore, any injury must be solved quickly to restore the epithelial barrier. Studies in simple epithelia, such as the ones performed in embryonic stages, have proven to be useful to understand the molecular mechanisms that control epithelial repair (Cordeiro and Jacinto, 2013; Garcia-Fernandez et al., 2009; Rothenberg and Fernandez-Gonzalez, 2019). Embryonic wound healing is characterized by the accumulation of F-actin and Non-muscle Myosin II (Myosin) in the wound leading-edge cells, forming an actomyosin cable that contracts and brings cells together, thereby closing the wound (Bement et al., 1999; Danjo and Gipson, 1998; Kiehart et al., 2000; Xu and Chisholm, 2011). Additionally, wound repair involves cell crawling mediated by actin protrusions (Abreu-Blanco et al., 2012b; Verboon and Parkhurst, 2015) and cellular rearrangements (Carvalho et al., 2018; Razzell et al., 2014).

With this work we aimed to broaden the knowledge about the role of mitochondria in the wound healing response. Besides the evidence from both simple and complex epithelia models about the involvement of reactive oxygen species (ROS) and in the regulation of the wound healing process (Hunter et al., 2018b; Sanchez et al., 2018; Xu and Chisholm, 2014), little was known about other mitochondrial functions required for this process. Mitochondrial function is influenced by mitochondrial dynamics, a term that describes the dynamic changes in mitochondrial number, shape and localization in the cell. Although the impact of mitochondrial dynamics in mitochondrial function has been studied in different contexts, and some evidence shows that it can regulate cell migration, the contribution to embryonic wound repair has never been addressed, which highlights the novelty of this work and its potential implication to the tissue repair field.

To summarize our most relevant results, we have identified mitochondrial dynamics proteins as novel embryonic wound healing regulators. The analysis of mitochondrial morphology suggested that wounding triggers mitochondrial fission. To understand how mitochondrial fission contributes to epithelial repair, we characterized the phenotype of *Dynamin-related protein 1* (*Drp1*) mutants. Drp1 loss of function led to defects in the cytosolic and mitochondrial calcium bursts upon wounding and deficient F-actin accumulation at the wound edge, culminating in wound healing impairment.

1. Mitochondrial dynamics proteins as novel embryonic wound healing regulators

We started by performing a small screen to uncover whether the mitochondrial dynamics machinery is required for wound healing. This wounding assay screen has been useful in the identification of multiple wound healing regulators (Campos et al., 2010; Carvalho et al., 2018). In this context, the opposed action of

mitochondrial fission and fusion control mitochondria morphology and number. These processes are mediated by large GTPases, namely Dynamin-related protein 1 (Drp1), which mediates mitochondrial fission; and Optic atrophy 1 (Opa1) and Mitofusins (Mfns) [Mitochondrial assembly regulatory factor (Marf) in *Drosophila*] that control the fusion of the mitochondrial membranes. Regarding mitochondrial fusion proteins, out of the four tested *Marf* alelles, only *Marf* ^{J} mutants showed an increased number of open wounds compared to controls. It is unclear why only one *Marf* mutant allele (*Marf* ^{J}) showed wound closure defects. The four *Marf* alleles carry different point mutations that can differently impact on mitochondrial function. The effects of *Marf* ^{I} and *Marf* ^{J} mutants have never been characterized before. Previous work using the *Marf* ^{B} allele indicates that it is a severe loss of function or null allele, and that the underlying mutation is in the GTPase domain (Sandoval et al., 2014). However, *Marf* ^{B} did not lead to wound healing impairment. A genetic and biochemical analysis of the effects of the *Marf* ^{J} mutation on protein function, together with further characterization of the wound healing phenotype is needed to validate the requirement of Marf for epithelial repair. In addition to *Marf* ^{J}, both *Opa1* mutant alleles showed a significant wound healing phenotype, indicating that mitochondrial fusion is necessary for proper embryonic wound healing. In addition, all the tested mitochondrial fission genes are required for wound healing. *Drp1* mutants, as well as mutants for *Mitochondrial fission protein 1* (*Fis1*) and *Ganglioside-induced differentiation-associated protein 1* (*Gdap1*), genes encoding proteins that recruit Drp1 to mitochondria, showed an increased percentage of open wound compared to control embryos. We also observed a significant wound healing phenotype in *milt*^{EY01559} mutants. Milton (Milt) usually interacts with mitochondria-bound Mitochondrial Rho (Miro) to mediate mitochondrial trafficking. However, no significant wound healing phenotype was observed in *Miro*^{B682} mutant embryos. In both *milt*^{EY01559} and *Miro*^{B682}, there was a higher frequency of open and intermediate wounds than in controls. Since we do not understand the significance of the intermediate phenotype and had to exclude these wounds from the statistical analysis, this may imply that the wounding assay is less sensitive to mutations that induce milder phenotypes. Overall, the wounding screen led to the identification of mitochondrial fusion, fission and trafficking proteins as novel regulators of embryonic wound healing.

To understand the role of mitochondrial dynamics in wound healing we decided to characterize in more detail the phenotype of *Drp1*^{KG03815} and *Opa1*^{EY09863} mutant embryos. We have excluded the hypothesis that the wound healing impairment in these mutants is caused by pre-existing embryonic defects in cell viability, as our preliminary results show no striking difference in the number of apoptotic cells between mutants and controls. However, based on published data, we were expecting to observe a reduction in the number of apoptotic cells in *Drp1* mutants and increased apoptosis in *Opa1* mutants. In *Drosophila*, similar to what is observed in mammals, different apoptotic stimuli lead to mitochondrial fragmentation and membrane disruption (Abdelwahid et al., 2007; Goyal et al., 2007). Inhibition of Drp1-mediated mitochondrial fission

protects cells from apoptosis (Abdelwahid et al., 2007; Clavier et al., 2015; Goyal et al., 2007). Opa1 is also important in the regulation of apoptosis. In mammals, the function of Opa1 in stabilizing the IMM cristae prevents cytochrome c release and consequent apoptosis (Frezza et al., 2006; Griparic et al., 2004). Cellular stress can induce excessive cleavage of the full length Opa1 (L-Opa1) into short Opa1 form (S-Opa1). S-Opa1 lacks the transmembrane domain required for anchoring to the IMM. An increase in S-Opa1 form impairs IMM fusion and facilitates mitochondrial fission and the induction of apoptosis (MacVicar and Langer, 2016). In *Drosophila*, although the role of Opa1 in apoptosis has not been so extensively studied, the excessive cleavage of Opa1 has also been implicated in apoptosis (Rahman and Kylsten, 2011). In summary, lack of Opa1 and excessive Opa1 cleavage facilitates apoptosis by disruption of the cristae structure or by an imbalance in the fusion/fission equilibrium, respectively. Although our preliminary data on apoptosis lack the quantification of the number of dying cells, they suggest that apoptosis is unaffected in *Drp1* and *Opa1* mutants. A thorough analysis of apoptosis in different embryonic tissues, using other apoptotic markers (e.g. activated caspase-3, acridine orange staining), would be helpful to validate our results. As we only assessed apoptosis in an uninjured situation, a further analysis of the number of apoptotic cells after wounding is necessary to understand if Drp1 and Opa1 differentially regulate apoptosis upon wounding. Although induction of apoptosis has not been observed in embryonic wound healing (Abreu-Blanco et al., 2012b) in a wild-type condition, we cannot exclude the possibility that it happens when the mitochondrial dynamics machinery is affected.

2. Epithelial wounding induces changes in mitochondrial morphology

Knowing that both Drp1 and Opa1 loss of function lead to wound healing impairment and that these proteins regulate mitochondrial shape, we characterized the mitochondrial morphology in the *Drosophila* embryonic epidermis in homeostasis and upon wounding. In homeostasis, we observed a different mitochondrial morphology in the smooth and denticle epidermis cells. Denticle cells, which are much smaller than smooth cells, showed a very condensed mitochondrial distribution and we were only able to distinguish individual mitochondria in smooth cells.

In homeostasis, we observed that late-stage embryos (Stage 15) have smaller and rounder mitochondria, compared to younger (stage 13) embryos (Macchi et al., 2013). *Drosophila* embryos undergo a metabolic switch to aerobic glycolysis, that begins midway through embryogenesis, to prepare for the transition from differentiated to proliferative cells in larval stages (Tennessen et al., 2011; Tennessen et al., 2014). Interestingly, highly proliferative cells such as cancer or stem cells, which favour aerobic glycolysis for energy production, also present a more fragmented mitochondrial network (Chen and Chan, 2017; Deng et

al., 2018; Seo et al., 2018; Yadav and Srikrishna, 2019). Hence, our observations support the hypothesis that mitochondrial shape correlates with the metabolic state in the cell. What is the cause and what is the consequence remains unclear.

We showed that, whereas Drp1 loss of function strongly affects the shape of mitochondria, Opa1 mutation has no effect. Given that the mitochondrial morphology of control embryos is already very fragmented at late stages, the result observed in the context of *Opa1* mutation is not surprising. On the other hand, Drp1 seems to be required at late embryogenesis stages to regulate mitochondrial fission. This is consistent with what has been observed in younger embryos (Macchi et al., 2013) and in other *Drosophila* tissues (Sandoval et al., 2014; Verstreken et al., 2005).

Upon wounding, we observed mitochondrial fragmentation, not only restricted to the damaged cell debris, but also in cells at the wound edge, suggesting that wounding triggers mitochondrial fission. This is consistent with the defective wound closure observed *Drp1* mutants. Unfortunately, we were not able to accurately follow and quantify the mitochondrial morphology, due to tissue movements and cell shape changes inherent to wound closure. On the other hand, although we show that Opa1 is also required for wound healing, we did not detect obvious mitochondrial fusion events upon wounding. Still, it is possible that mitochondrial fusion occurs at later stages of wound closure or that our current imaging method does have enough resolution to detect these changes. Imaging of mitochondrial morphology with higher resolution, for example by using super-resolution microscopy, would help to understand the requirement of mitochondrial fusion and fission during the wound healing process.

Regarding mitochondrial localization, we did not observe any striking change during wound closure. In migrating cells, mitochondria localize close the leading edge to provide energy for cell migration (Schuler et al., 2017). Since both the polymerization of F-actin and myosin contractility are energy-consuming processes (Lymn and Taylor, 1971), we hypothesized that mitochondria would localize close to the actomyosin cable, but we did not observe any preferential localization towards the leading-edge. We also did not observe any change in apico-basal movement of mitochondria. These were puzzling results, as *milt*^{EY01559} mutants showed wound healing impairment. It would be interesting to compare the mitochondrial localization in wild-type and *milt*^{EY01559} mutant embryos to clarify its role of in wound healing.

Overall, our results suggest that wound closure does not require polarization of mitochondria and that wounding induces mitochondrial fission, further implicating this process in the regulation of wound healing. Mitochondrial fission facilitates the removal of dysfunctional mitochondrial by mitophagy (Burman et al., 2017; Ikeda et al., 2015), so we hypothesized that the wound could be a stress factor for the epithelial tissue and induce mitochondrial fission followed by mitophagy. However, we did not detect any autophagic events

close to the wound site. To confirm the role of mitophagy in wound healing we should test other mitophagy markers and test whether blocking mitophagy leads to wound closure defects. So far, our preliminary results suggest that mitophagy does not play a key role in embryonic wound healing. It would also be interesting to investigate whether mitochondrial biogenesis, which promotes the increase of mitochondrial mass to restore cellular function upon damage, is involved. This pathway has been observed as a response to brain or heart injuries, in which hypoxia causes oxidative damage to the cells, and constitutes a therapeutic target for these conditions (Marquez et al., 2016; Scholpa and Schnellmann, 2017; Yin et al., 2008). Interestingly, a recent study about keloid fibroblasts, which are cells present in aberrant scars that form in response to cutaneous wound healing, has reported an increase in mitochondrial biogenesis (Li et al., 2019). It would be interesting to understand if mitochondrial biogenesis also happens in epithelial cells and if this pathway is conserved in the repair of simple epithelia. As mitochondrial biogenesis involves a transcriptional response that leads to increased expression of mitochondrial and nuclear encoded proteins (Ventura-Clapier et al., 2008), it may not be relevant in the first stages of embryonic repair (which take place in the first minutes after wounding), but may be important later on to fully restore the epithelial integrity.

3. Mitochondrial fusion and fission proteins regulate wound healing events

To understand the role of mitochondrial dynamics during embryonic wound healing, we characterized the phenotype of Drp1 and Opa1 loss of function by live imaging of specific features of the wound closure process. Embryonic wound healing is mediated by the formation of an actomyosin cable at the wound edge, that contracts and coordinates the collective tissue movement to close the wound (Bement et al., 1999; Danjo and Gipson, 1998; Kiehart et al., 2000; Xu and Chisholm, 2011). The formation of the actomyosin cable has been shown to depend on an intracellular calcium increase upon wounding (Antunes et al., 2013; Razzell et al., 2013; Xu and Chisholm, 2011), that in turn is regulates the remodelling of the Adherens Junctions (AJs) (Abreu-Blanco et al., 2012b; Carvalho et al., 2014; Hunter et al., 2015) and the activation of the Rho family of GTPases and its targets, all required for proper actomyosin dynamics and contractility (Brock, 1996; Verboon and Parkhurst, 2015; Wood et al., 2002). Therefore, we investigated whether these processes were impaired in the absence of Drp1 and Opa1.

3.1. The mitochondrial fusion protein Opa1 is required for calcium and F-actin dynamics during wound closure

Regarding mitochondrial fusion, we found no significant difference in how the wound area changes over time in *Opa1* mutants compared to controls. In both cases the actomyosin cable forms at the wound edge and progressively contracts until the wound is closed, with similar wound closure speeds. These results came as a surprise given that, in the initial wounding assay screen, *Opa1* mutants showed a significant increase in the percentage of open wounds compared to controls.

Nevertheless, we found defects in F-actin accumulation and Rho GTPase activation at the wound edge in these mutants. Myosin, on the other hand, seems to be unaffected. Contractile actomyosin structures are regulated by Rho GTases. Rho 1 and its downstream effectors have been shown to regulate wound healing in the *Drosophila* embryonic epidermis (Matsubayashi et al., 2015; Verboon and Parkhurst, 2015). The Rho1 effector Rho kinase (Rok) accumulates at the wound edge (Verboon and Parkhurst, 2015) and has been shown to regulate for the actomyosin cable formation during wound healing (Antunes et al., 2013; Verboon and Parkhurst, 2015). Rok regulates myosin by phosphorylation the myosin regulatory light chain (MRLC), or inhibition of the MRLC phosphatase, thus activating myosin contractility (Amano et al., 2010; Dawes-Hoang et al., 2005; Kimura et al., 1996; Royou et al., 2002). Thus, it was surprising to find that there were no significant differences in myosin levels at the wound edge between *Opa1* mutants and controls, while Rok levels were decreased. Thus, it would be useful to look at alternative reporters of myosin activity, for example by measuring phosphorylated MRLC, to clarify whether myosin contractility is in fact affected when mitochondrial fission is impaired. We can propose two hypotheses to explain these seemingly contradictory results. On one hand, Rok is also known to regulate F-actin dynamics through LIM kinase (Julian and Olson, 2014), so the activity of Rok during wound healing might be more associated with F-actin instead of myosin. On the other hand, it is possible that other kinases compensate for the reduced Rok levels, leading to unaffected myosin levels. Indeed, in single cell wound repair, Rok has been shown to cooperate with MRLC kinase in the phosphorylation of MRLC (Russo et al., 2005).

The actomyosin contractility is regulated by an intracellular calcium increase in the cells closer to the wound. This calcium burst is the first signal to be detected upon wounding and impairment of calcium flux leads to actomyosin cable defects. Evidence suggests that calcium regulates the actomyosin cable by activating actin regulatory proteins and the remodelling of AJs (Antunes et al., 2013; Hunter et al., 2018a; Xu and Chisholm, 2011). *Opa1* mutants show a reduced calcium burst compared to control embryos. This reduction could also explain the observed reduced F-actin levels at the wound edge.

Even though *Opa1* mutants show calcium and F-actin defects, the wounds still managed to close at a similar rate than controls. Either the calcium and F-actin defects are not sufficient to delay wound healing or there are other compensatory mechanisms involved. Another possibility is that the requirement of Opa1 depends on the extension of the wound. In the wounding assay screen, we used maximum laser power to inflict large wounds. In contrast, in order to follow the wound closure process by live imaging, we inflicted smaller wounds. Thus, our results suggest that mitochondrial fusion is required for the repair of larger wounds. To better understand the role of mitochondrial fusion in wound healing, it will be helpful to analyse the phenotype of other *Opa1* null mutant alleles and to explore the contribution of other fission-related proteins.

In conclusion, although we do not fully understand the contribution of Opa1 to wound closure, we have found that it regulates F-actin and calcium during wound healing.

3.2. The mitochondrial fission protein Drp1 is essential for wound healing

3.2.1. Drp1 regulates F-actin accumulation at the wound edge

The analysis of the wound closure dynamics revealed that *Drp1* mutants have a significant wound healing impairment, taking more than two times longer to close the wounds that control embryos. Moreover, we could identify two degrees of wound closure phenotypes: a mild phenotype, in which the wound progressively contracted but at a slower rate than in controls; and a strong phenotype, in which the wound area expanded. *Drp1* mutants showed strong defects in F-actin accumulation at the wound edge, while myosin levels were unaffected. However, in contrast to *Opa1* mutants, the lack of Drp1 does not affect Rok localization at the wound edge. This suggests that mitochondrial fission does not regulate Rok and its targets that control myosin contractility, but instead is required for F-actin dynamics. As mentioned above (section 3.1), testing other myosin and Rok markers would be helpful to validate these results. Several actin regulators, such as Diaphanous (Formin), which are also activated by Rho GTPases, have been shown to regulate F-actin dynamics in simple epithelia wound healing (Antunes et al., 2013; Matsubayashi et al., 2015). Future studies should thus address whether Drp1 controls the activity of Rho GTPases and their different effectors. In addition to the actomyosin cable, wound healing involves cell crawling mediated by actin protrusions (Abreu-Blanco et al., 2012b; Verboon and Parkhurst, 2015) and cellular rearrangements (Carvalho et al., 2018; Razzell et al., 2014). It would be interesting to understand how these processes are affected in *Drp1* mutants and if their compensatory action in the absence of a proper actomyosin cable can explain the milder *Drp1* wound healing phenotype.

3.2.2. Drp1 regulates cytosolic and mitochondrial calcium dynamics upon wounding

Our results suggest that the wound healing impairment in *Drp1* mutants could be due to F-actin defects. The analysis of E-cadherin localization shows that the F-actin defects are independent of AJs remodelling, so alternative molecular mechanisms must be involved in the regulation of F-actin assembly at the wound margin in *Drp1* mutants. Quantification of the cytosolic calcium burst induced by wounding revealed that it is strikingly reduced in *Drp1* mutants compared to controls. Previous studies have shown that injury triggers calcium influx from the extracellular environment (Antunes et al., 2013; Razzell et al., 2013; Xu and Chisholm, 2011). The elevated cytosolic calcium levels induce calcium release from the endoplasmic reticulum (ER) mediated by the inositol-3-phosphate (IP3) receptor (IP3R), followed by propagation of calcium and IP3 to neighbouring cells through Gap Junctions (Narciso et al., 2015; Razzell et al., 2013; Restrepo and Basler, 2016), in a wave-like manner. After this initial spreading of calcium to regions more distal to the wound site, calcium levels decrease from the periphery to the edge of the wound. Our results show that, not only the calcium levels are lower in *Drp1* mutants, but also that the area of calcium increase is reduced, compared to the controls. These results strongly suggest that Drp1 regulates the propagation of intercellular calcium across the epidermis.

Mitochondria can uptake calcium from the cytosol, thereby modulating cytosolic calcium levels (Szabadkai and Duchen, 2008). Moreover, mitochondrial morphology can influence mitochondrial calcium levels (Bianchi et al., 2006; Gerencser and Adam-Vizi, 2005; Szabadkai et al., 2004). Consistent with a previous report on wound healing in the epidermis of *C. elegans* (Xu and Chisholm, 2014), we have also observed an increase in mitochondrial calcium around the wound, similar to what is observed with cytosolic calcium (Antunes et al., 2013; Razzell et al., 2011; Xu and Chisholm, 2011). Xu and colleagues have mentioned that the mitochondrial calcium wave starts after and travels slower than the cytosolic calcium wave, supporting the idea that mitochondria uptake calcium as a consequence of the dramatic increase in cytosolic calcium. Observations from our laboratory in the wound healing of the pupal epidermis are consistent with this finding (Cristo I, unpublished data). This suggests that, similarly to the cytosolic calcium burst, the rise in mitochondrial calcium levels is a conserved response to tissue injury. We found the mitochondrial calcium levels upon wounding are reduced in *Drp1* mutants compared to controls. In contrast to cytosolic calcium, the area of tissue that responds to the wound by increasing calcium levels is not affected in *Drp1* mutants. The reduction in calcium levels is not as dramatic as seen for cytosolic calcium. This might be due to the higher sensitivity of the cytosolic calcium sensor compared to the mitochondrial version. The mitochondrial calcium sensor is based on GCaMP3 while the cytosolic calcium was measured with GCaMP6, an improved version of the GCaMP calcium sensors that leads to increased fluorescence upon calcium binding (Chen et

al., 2013). In summary, our results show that Drp1 regulates mitochondrial and cytosolic calcium dynamics upon wounding.

But how can the mitochondria control cytosolic calcium levels and how can we interpret these results? First of all, mitochondrial calcium uptake depends on an increase in cytosolic calcium levels (Lawrie et al., 1996; Rizzuto et al., 1992; Rutter et al., 1993). So, one hypothesis is that *Drp1* mutants have a reduced cytosolic calcium burst and consequently less calcium goes into the mitochondria. Given that Drp1 is a protein that influences mitochondrial morphology and function, we hypothesize that the cytosolic calcium increase leads to mitochondrial calcium uptake, which in turn modulates the cytosolic calcium concentration. Mitochondria localize close to the ER, forming calcium signalling microdomains. Calcium uptake by mitochondria reduces the cytosolic calcium levels close to the open ER channels (local cytosolic calcium), preventing their calcium-dependent inactivation. By controlling ER calcium channels activity, mitochondrial calcium uptake affects global cytosolic calcium (Billups and Forsythe, 2002; Rizzuto et al., 2012). Our results lead us to speculate that, upon wounding, mitochondria remove calcium from the ER-mitochondria microdomain, preventing IP3R inactivation and favouring calcium release from the ER. When the calcium buffering capacity of mitochondria is compromised, as it seems to be in *Drp1* mutants, the high local cytosolic calcium levels could inhibit IP3R opening and reduce calcium release, resulting in lower global cytosolic calcium levels. This would then affect the cytosolic calcium wave propagation, as less calcium and/or IP3 would cross Gap Junctions.

To support our hypothesis, further work is necessary to understand the molecular mechanisms by which Drp1 regulates the calcium buffering capacity of mitochondria. Mitochondrial calcium levels are determined by: (1) calcium uptake into mitochondria; (2) calcium efflux; (3) calcium buffering activity in the mitochondrial matrix, through the formation of calcium phosphate complexes (Nicholls and Chalmers, 2004). Prudent and colleagues have shown that the Mitochondrial Calcium Uniporter (MCU), the main mitochondrial calcium influx channel, is required for cell migration. Knockdown of MCU in human cell lines leads to increased actin stiffness, loss of cell polarization and impaired migratory capacity, due to reduced activity of the Rho GTPases RhoA and Rac1 (Prudent et al., 2016). The MCU is conserved in *Drosophila* and mediates ER-to-mitochondrial calcium transfer via IP3R (Choi et al., 2017). The calcium efflux channels are also conserved in *Drosophila* (Haug-Collet et al., 1999; McQuibban et al., 2010) but their role in wound healing has not been investigated. How mitochondrial dynamics impacts on mitochondrial calcium buffering capacity is nor clearly understood. A recent study in muscle myofibers showed that DRP1-deficient mice present lower cytosolic calcium levels and increased mitochondrial levels, due to the increased expression of MCU (Favaro et al., 2019). Here, we observed the opposite effect, suggesting that the role of Drp1 on mitochondrial calcium regulation may be context dependent. Further work is needed to understand how Drp1 regulates mitochondrial calcium uptake

in the *Drosophila* epidermis. Another factor that could regulate mitochondrial calcium is the proximity of mitochondria to ER or plasma membrane calcium channels, which in turn are affected by the mitochondrial shape and localization in the cell. A recent study suggested that mitochondrial elongation increases the number of ER-mitochondrial contacts in human cell lines (Cieri et al., 2018). It would be interesting to investigate whether this is true for the epidermis of the *Drosophila* embryos. Additionally, calcium influx into mitochondria is dependent on the mitochondrial membrane potential (ΔΨmt). Unfortunately, we were not able to measure the ΔΨmt in the embryonic epidermis to understand if it was a limiting factor in mitochondrial function and calcium uptake.

It has also been shown that mitochondrial calcium triggers mitochondrial ROS production, that in turn regulates the F-actin cytoskeleton through RHO-1 (Xu and Chisholm, 2014). A recent work by Hunter and colleagues has shown that calcium-dependent mitochondrial ROS production regulates the actomyosin cytoskeleton and wound healing in the *Drosophila* and the zebrafish (*Danio rerio*) embryos (Hunter et al., 2018a). The analysis of ROS levels in *Drp1* mutants would be useful to establish the place of Drp1 in the known mechanism of calcium-dependent regulation of wound closure.

Hence, our hypothesis is that Drp1 controls F-actin accumulation at the wound edge, and consequently wound healing, by controlling mitochondrial and cytosolic calcium levels. To confirm this, we would need to test whether increasing mitochondrial calcium uptake or the retention of calcium inside mitochondria in *Drp1* mutants rescues the cytosolic calcium and the F-actin dynamics during wound closure. Nevertheless, we cannot exclude the possibility that Drp1 regulates F-actin in a calcium-independent manner. Drp1 can directly bind F-actin (DuBoff et al., 2012; Ji et al., 2015), but the interaction between these molecules has been mainly studied in the context of the mitochondrial fission process (De Vos et al., 2005; Ji et al., 2015). However, how Drp1 loss-of-function can impact on F-actin dynamics is still not well understood. Drp1 has been shown to regulate F-actin dynamics in glioma cells, in which Drp1 knockdown reduced the formation of actin protrusions and invasiveness of these cells (Yin et al., 2016). Moreover, Yin and colleagues showed that Drp1 can bind to RHOA and activate the RHOA/ROCK pathway (Yin et al., 2016), known to regulate cytoskeleton dynamics (Amano et al., 2010). Future studies should investigate the activity of F-actin regulatory proteins involved in wound healing in *Drp1* mutants to understand how Drp1 can impact on the actomyosin cable.

The wound expansion phenotype of *Drp1* strong mutants is similar to what has been described in mutants for a component of the invertebrate Occluding Junctions (OJs). In the absence of OJs, the epidermis presents defects in the actomyosin cable, cellular shapes and rearrangements as well as in tissue mechanical properties (Carvalho et al., 2018). Notably, Gangwar and colleagues have found that mitochondrial dysfunction caused by calcium-mediated oxidative stress leads to the disruption of OJs in human cell line

(Gangwar et al., 2017). It would be interesting to explore in future studies the link between mitochondria and OJs in the context of *Drosophila* wound healing.

To strengthen the claim that mitochondrial fission is required for wound healing it would be helpful to investigate the wound healing phenotype of other molecular players involved in mitochondrial fission, such as Fis1 and Gdap1. The mitochondrial fission machinery also mediates peroxisome division, so we cannot exclude the possibility that *Drp1* mutants also have peroxisomal defects (Honsho et al., 2016). It would be interesting to explore whether any potential peroxisomal defects contribute to the wound healing phenotype.

In conclusion, our work has identified important novel regulators of wound healing – the mitochondrial dynamics machinery. In particular, we have shown that mitochondrial fission is induced upon wounding and that this is key for proper embryonic wound repair. Finally, we propose that mitochondrial fission is required for the regulation of F-actin dynamics and calcium signalling.

4. Conclusions and future perspectives

Our work has revealed that mitochondrial dynamics proteins are novel regulators of embryonic wound healing. We show for the first time that mitochondrial fusion, fission and trafficking proteins are required for proper wound healing of the *Drosophila* embryonic epidermis.

Mitochondrial fission seems to be particularly important for the wound healing process. The injury induces mitochondrial fission in cells adjacent to the wound. The factors that trigger mitochondrial fission upon wounding remain to be investigated, but we hypothesize that calcium might be one of these factors. Several reports have shown that an increase in intracellular calcium triggers mitochondrial fission. In cultured neurons, calcium influx activates the calcium/calmodulin-dependent protein kinase Iα (CaMKIα), that in turn phosphorylates Drp1, leading to its activation and, consequently, mitochondrial fission (Han et al., 2008). Using a liver cell line, Hom and colleagues have shown that the calcium-mediated mitochondrial fission could be prevented by inhibiting ER-calcium release and that calcium influx into mitochondria was necessary to induce mitochondrial fission (Hom et al., 2007). In the embryonic epidermis, there is an increase in intracellular calcium immediately upon wounding that involves ER-calcium release (Razzell et al., 2013). Moreover, we showed that, in agreement with other wound healing models (Zhao et al., 2011b), wounding leads to mitochondrial calcium increase and mitochondrial calcium uptake. Hence, calcium seems like a strong candidate to be regulating mitochondrial fission upon wounding.

We have also shown that both Drp1 and Opa1 loss of function promote F-actin and calcium defects during wound closure. Embryonic wound healing relies on the formation and the contraction of the actomyosin cable, as well as actin-based cell crawling (Rothenberg and Fernandez-Gonzalez, 2019). The F-actin defects might explain the severe wound healing impairment in the *Drp1* mutants. Recent studies have shown the ability of Drp1 to regulate F-actin mediated protrusions. Drp1 knockdown reduced the formation of actin protrusions and invasiveness of glioma cells (Yin et al., 2016). Inhibition of Drp1 in a breast cancer cell line impaired the migratory capacity of these cells (Peiris-Pagès et al., 2018), as well as in thyroid cancer cells (Ferreira-da-Silva et al., 2015). The mechanisms through which Drp1 regulates F-actin are not well understood. In the glioma cells, Yin and colleagues showed that Drp1 can bind to RHOA and activate the RHOA/ROCK pathway (Yin et al., 2016), known to regulate cytoskeleton dynamics (Amano et al., 2010). This pathway also regulates embryonic wound repair (Abreu-Blanco et al., 2012b; Brock, 1996; Verboon and Parkhurst, 2015; Wood et al., 2002). Rok localization was unaffected in Drp1 mutants, so the role of other Rho effectors and other Rho GTPases should be explored in future studies. Another way to regulate F-actin is through calcium. Impairing the intracellular calcium burst upon wounding leads to actomyosin cable defects and wound healing impairment (Antunes et al., 2013; Xu and Chisholm, 2011). Calcium can activate calcium-dependent actin-binding proteins, such as gelsolin, that regulate F-actin polymerization at the wound edge (Antunes et al., 2013). Calcium can also indirectly activate Rho GTPases by the production of ROS. Rho GTPases contain oxidation sensitive motifs that promote their activation upon ROS production (Xu and Chisholm, 2014). *Drp1* mutants displayed a striking reduction in cytosolic calcium levels upon wounding, suggesting that this could be the upstream event responsible for the F-actin defects and failure of wound closure. The role of calcium in wound healing is not restricted to simple or embryonic epithelia. It is involved in complex epithelia repair at the level of the clot formation during the hemostasis phase (Palta et al., 2014), and it has been implicated in the regulation of keratinocyte and fibroblast differentiation, proliferation and migration (Dulbecco and Elkington, 1975; Magee et al., 1987; Navarro-Requena et al., 2018), as well as ECM deposition (Rokosova and Peter Bentley, 1986). Calcium regulation is thus a universal player in different aspects of wound healing. In addition to cytosolic calcium defects, *Drp1* mutants showed a reduced mitochondrial calcium burst upon wounding. The role of mitochondria in calcium uptake and consequent regulation of the cytosolic calcium levels is not understood in the context of wound healing. Recent studies point to a role of mitochondrial calcium in cell migration (Prudent et al., 2013; Prudent et al., 2016; Tang et al., 2015; Tosatto et al., 2016) and wound healing, but how the mitochondrial and cytosolic calcium dynamics are connected remains unclear.

In conclusion, we have found that Drp1 regulates conserved and key events required for wound healing in different epithelia. We have shown that the *Drosophila* embryonic wound healing model is highly suitable

to address the role of mitochondria in *in* vivo wound repair and hopefully this knowledge can contribute to the better understanding of the wound healing process as a hole.

In the future it would be interesting to investigate how mitochondrial fission is triggered upon wounding, how it impacts on the mitochondrial and cytosolic calcium dynamics and which are the downstream targets of calcium responsible for the regulation of the wound healing events. Additionally, many other mitochondrial functions can have an impact on wound healing and have not been addressed so far. As an example, a previous screen from our lab has identified two genes required for embryonic wound healing that are related to mitochondrial metabolism: *aralar1* and *Mitochondrial trifunctional protein α subunit* (*Mtpα*) (Campos et al., 2010). Aralar 1 is a calcium-dependent aspartate-glutamate carrier (Palmieri et al., 2001), whereas Mtpα is an enzyme subunit involved in the fatty acid β-oxidation (Xia et al., 2019). Actin accumulation at the wound edge is an energy-dependent process (Yumura et al., 2014), so the contribution of mitochondrial metabolism should be further examined. Moreover, mitochondrial morphology changes are coupled to metabolism (Wai and Langer, 2016), so the relationship between these processes in the context of wound healing is worth investigating.

CHAPTER 5. BIBLIOGRAPHY

"If I have seen further it is by standing on the shoulders of Giants."

— Isaac Newton."

Abdelwahid, E., Yokokura, T., Krieser, R. J., Balasundaram, S., Fowle, W. H. and White, K. (2007). Mitochondrial disruption in Drosophila apoptosis. *Dev. Cell* **12**, 793–806.

Abreu-Blanco, M. T., Verboon, J. M. and Parkhurst, S. M. (2011). Cell wound repair in Drosophila occurs through three distinct phases of membrane and cytoskeletal remodeling. *J. Cell Biol.* **193**, 455–64.

Abreu-Blanco, M. T., Watts, J. J., Verboon, J. M. and Parkhurst, S. M. (2012a). Cytoskeleton responses in wound repair. *Cell. Mol. Life Sci.* **69**, 2469–2483.

Abreu-Blanco, M. T., Verboon, J. M., Liu, R., Watts, J. J. and Parkhurst, S. M. (2012b). Drosophila embryos close epithelial wounds using a combination of cellular protrusions and an actomyosin purse string. *J. Cell Sci.* **125**, 5984–5997.

Abreu-Blanco, M. T., Verboon, J. M. and Parkhurst, S. M. (2014). Coordination of Rho family GTPase activities to orchestrate cytoskeleton responses during cell wound repair. *Curr. Biol.* **24**, 144–155.

Ahmad, T., Mukherjee, S., Pattnaik, B., Kumar, M., Singh, S., Rehman, R., Tiwari, B. K., Jha, K. A., Barhanpurkar, A. P., Wani, M. R., et al. (2014). Miro1 regulates intercellular mitochondrial transport & enhances mesenchymal stem cell rescue efficacy. *EMBO J.* **33**, 994–1010.

Albrecht, S. C., Barata, A. G., Großhans, J., Teleman, A. A., Dick, T. P., Grosshans, J., Teleman, A. A., Dick, T. P., Großhans, J., Teleman, A. A., et al. (2011). In vivo mapping of hydrogen peroxide and oxidized glutathione reveals chemical and regional specificity of redox homeostasis. *Cell Metab.* **14**, 819–829.

Aldridge, A. C., Benson, L. P., Siegenthaler, M. M., Whigham, B. T., Stowers, R. S. and Hales, K. G. (2007). Roles for Drp1, a dynamin-related protein, and milton, a kinesin-associated protein, in mitochondrial segregation, unfurling and elongation during Drosophila spermatogenesis. *Fly (Austin).* **1**, 38–46.

Alexander, C., Votruba, M., Pesch, U. E. A., Thiselton, D. L., Mayer, S., Moore, A., Rodriguez, M., Kellner, U., Leo-Kottler, B., Auburger, G., et al. (2000). OPA1, encoding a dynamin-related GTPase, is mutated in autosomal dominant optic atrophy linked to chromosome 3q28. *Nat. Genet.* **26**, 211–215.

Allen, J. F. (1996). Separate Sexes and the Mitochondrial Theory of Ageing. *J. Theor. Biol.* **180**, 135–140.

Allio, R., Donega, S., Galtier, N. and Nabholz, B. (2017). Large variation in the ratio of mitochondrial to nuclear mutation rate across animals: Implications for genetic diversity and the use of mitochondrial DNA as a molecular marker. *Mol. Biol. Evol.* **34**, 2762–2772.

Altan, Z. M. and Fenteany, G. (2004). C-Jun N-terminal kinase regulates lamellipodial protrusion and cell sheet migration during epithelial wound closure by a gene expression-independent mechanism. *Biochem. Biophys. Res. Commun.* **322**, 56–67.

Altschafl, B. A., Beutner, G., Sharma, V. K., Sheu, S. S. and Valdivia, H. H. (2007). The mitochondrial ryanodine receptor in rat heart: A pharmaco-kinetic profile. *Biochim. Biophys. Acta - Biomembr.* **1768**, 1784–1795.

Amano, M., Ito, M., Kimura, K., Fukata, Y., Chihara, K., Nakano, T., Matsuura, Y. and Kaibuchi, K. (1996). Phosphorylation and activation of myosin by Rho-associated kinase (Rho- kinase). *J. Biol. Chem.* **271**,

20246–20249.

Amano, M., Nakayama, M. and Kaibuchi, K. (2010). Rho-kinase/ROCK: A key regulator of the cytoskeleton and cell polarity. *Cytoskeleton* **67**, 545–554.

Anand, R., Wai, T., Baker, M. J., Kladt, N., Schauss, A. C., Rugarli, E. and Langer, T. (2013). The i-AAA protease YME1L and OMA1 cleave OPA1 to balance mitochondrial fusion and fission. *J. Cell Biol.* **204**, 919–929.

Anderson, G. R., Wardell, S. E., Cakir, M., Yip, C., Ahn, Y. R., Ali, M., Yllanes, A. P., Chao, C. A., McDonnell, D. P. and Wood, K. C. (2018). Dysregulation of mitochondrial dynamics proteins are a targetable feature of human tumors. *Nat. Commun.* **9**, 1677.

Anesti, V. and Scorrano, L. (2006). The relationship between mitochondrial shape and function and the cytoskeleton. *Biochim. Biophys. Acta - Bioenerg.* **1757**, 692–699.

Antunes, M., Pereira, T., Cordeiro, J. V., Almeida, L. and Jacinto, A. (2013). Coordinated waves of actomyosin flow and apical cell constriction immediately after wounding. *J. Cell Biol.* **202**, 365–379.

Arama, E. and Steller, H. (2006). Detection of apoptosis by terminal deoxynucleotidyl transferase-mediated dUTP nick-end labeling and acridine orange in Drosophila embryos and adult male gonads. *Nat. Protoc.* **1**, 1725–1731.

Austefjord, M. W., Gerdes, H. and Wang, X. (2014). Tunneling nanotubes. *Commun. Integr. Biol.* **7**, e27934.

Baar, K., Wende, A. R., Jones, T. E., Marison, M., Nolte, L. A., Chen, M., Kelly, D. P. and Holloszy, J. O. (2002). Adaptations of skeletal muscle to exercise: Rapid increase in the transcriptional coactivator PGC-1. *FASEB J.* **16**, 1879–1886.

Babcock, D. T., Brock, A. R., Fish, G. S., Wang, Y., Perrin, L., Krasnow, M. A. and Galko, M. J. (2008). Circulating blood cells function as a surveillance system for damaged tissue in Drosophila larvae. *Proc. Natl. Acad. Sci. U. S. A.* **105**, 10017–10022.

Backes, S. and Herrmann, J. M. (2017). Protein translocation into the intermembrane space and matrix of mitochondria: Mechanisms and driving forces. *Front. Mol. Biosci.* **4**, 1–11.

Bardet, P. L., Kolahgar, G., Mynett, A., Miguel-Aliaga, I., Briscoe, J., Meier, P. and Vincent, J. P. (2008). A fluorescent reporter of caspase activity for live imaging. *Proc. Natl. Acad. Sci. U. S. A.* **105**, 13901–13905.

Barlan, K. and Gelfand, V. I. (2017). Microtubule-based transport and the distribution, tethering, and organization of organelles. *Cold Spring Harb. Perspect. Biol.* **9**, 1–12.

Baughman, J. M., Perocchi, F., Girgis, H. S., Plovanich, M., Belcher-Timme, C. A., Sancak, Y., Bao, X. R., Strittmatter, L., Goldberger, O., Bogorad, R. L., et al. (2011). Integrative genomics identifies MCU as an essential component of the mitochondrial calcium uniporter. *Nature* **476**, 341–345.

Begnaud, S., Chen, T., Delacour, D., Mège, R. and Ladoux, B. (2016). Mechanics of epithelial tissues during gap closure. *Curr. Opin. Cell Biol.* **42**, 52–62.

Bellen, H. J., Levis, R. W., Liao, G., He, Y., Carlson, J. W., Tsang, G., Evans-Holm, M., Hiesinger, P. R., Schulze, K. L., Rubin, G. M., et al. (2004). The BDGP gene disruption project: single transposon insertions associated with 40% of Drosophila genes. *Genetics* **167**, 761–81.

Belosludtsev, K. N., Dubinin, M. V., Belosludtseva, N. V. and Mironova, G. D. (2019). Mitochondrial Ca2+ Transport: Mechanisms, Molecular Structures, and Role in Cells. *Biochem.* **84**, 593–607.

Bement, W. M., Forscher, P. and Mooseker, M. S. (1993). A novel cytoskeletal structure involved in purse string wound closure and cell polarity maintenance. *J. Cell Biol.* **121**, 565–78.

Bement, W. M., Mandato, C. A. and Kirsch, M. N. (1999). Wound-induced assembly and closure of an actomyosin purse string in Xenopus oocytes. *Curr. Biol.* **9**, 579–587.

Bender, D. A. (2003). TRICARBOXYLIC ACID CYCLE. In *Encyclopedia of Food Sciences and Nutrition*, pp. 5851–5856. Elsevier.

Benink, H. A. and Bement, W. M. (2005). Concentric zones of active RhoA and Cdc42 around single cell wounds. *J. Cell Biol.* **168**, 429–439.

Bereiter-Hahn, J. (1990). Behavior of Mitochondria in the Living Cell. *Int. Rev. Cytol.* **122**, 1–63.

Bereiter-Hahn, J. and Vöth, M. (1994). Dynamics of mitochondria in living cells: shape changes, dislocations, fusion, and fission of mitochondria. *Microsc. Res. Tech.* **27**, 198–219.

Bernardi, P., Scorrano, L., Colonna, R., Petronilli, V. and Di Lisa, F. (1999). Mitochondria and cell death. Mechanistic aspects and methodological issues. *Eur. J. Biochem.* **264**, 687–701.

Betapudi, V. (2014). Life without double-headed non-muscle myosin II motor proteins. *Front. Chem.* **2**, 1–13.

Bhatti, J. S., Bhatti, G. K. and Reddy, P. H. (2017). Mitochondrial dysfunction and oxidative stress in metabolic disorders - A step towards mitochondria based therapeutic strategies. *Biochim. Biophys. Acta* **1863**, 1066–1077.

Bi, G. Q., Alderton, J. M. and Steinhardt, R. A. (1995). Calcium-regulated exocytosis is required for cell membrane resealing. *J. Cell Biol.* **131**, 1747–1758.

Bianchi, K., Vandecasteele, G., Carli, C., Romagnoli, A., Szabadkai, G. and Rizzuto, R. (2006). Regulation of Ca2+ signalling and Ca2+-mediated cell death by the transcriptional coactivator PGC-1alpha. *Cell Death Differ.* **13**, 586–596.

Billups, B. and Forsythe, I. D. (2002). Presynaptic Mitochondrial Calcium Sequestration Influences Transmission at Mammalian Central Synapses. *J. Neurosci.* **22**, 5840–5847.

Bishop, A. L. and Hall, A. (2000). Rho GTPases and their effector proteins. *Biochem. J.* **348**, 241–255.

Bleazard, W., McCaffery, J. M., King, E. J., Bale, S., Mozdy, A., Tieu, Q., Nunnari, J. and Shaw, J. M. (1999). The dynamin-related GTPase Dnm1 regulates mitochondrial fission in yeast. *Nat. Cell Biol.* **1**, 298–304.

Bliek, A. M. Van Der (1999). Functional diversity in the dynamin family. *Trends Cell Biol.* **8924**, 96–102.

Brand, M. D. (1975). Stoichiometry Accumulation of H+ Ejection during Respiration-dependent of Ca2+ by Rat Liver Mitochondria*.

Brand, M. D. (2000). Uncoupling to survive? The role of mitochondrial inefficiency in ageing. *Exp. Gerontol.* **35**, 811–820.

Bravo-Sagua, R., Parra, V., López-Crisosto, C., Díaz, P., Quest, A. F. G. and Lavandero, S. (2017). Calcium Transport and Signaling in Mitochondria. In *Comprehensive Physiology*, pp. 623–634. Hoboken, NJ, USA: John Wiley & Sons, Inc.

Brdiczka, D. (1991). Contact sites between mitochondrial envelope membranes. Structure and function in energy- and protein-transfer. *BBA - Rev. Biomembr.* **1071**, 291–312.

Brock, J. (1996). Healing of incisional wounds in the embryonic chick wing bud: characterization of the actin purse-string and demonstration of a requirement for Rho activation. *J. Cell Biol.* **135**, 1097–1107.

Buhlman, L., Damiano, M., Bertolin, G., Ferrando-Miguel, R., Lombès, A., Brice, A. and Corti, O. (2014). Functional interplay between Parkin and Drp1 in mitochondrial fission and clearance. *Biochim. Biophys. Acta* **1843**, 2012–26.

Burman, J. L., Pickles, S., Wang, C., Sekine, S., Vargas, J. N. S., Zhang, Z., Youle, A. M., Nezich, C. L., Wu, X., Hammer, J. A., et al. (2017). Mitochondrial fission facilitates the selective mitophagy of protein aggregates. *J. Cell Biol.* **216**, 3231–3247.

Busiello, R. A., Savarese, S. and Lombardi, A. (2015). Mitochondrial uncoupling proteins and energy metabolism. *Front. Physiol.* **6**, 36.

Bustelo, X. R., Sauzeau, V. and Berenjeno, I. M. (2007). GTP-binding proteins of the Rho/Rac family: Regulation, effectors and functions in vivo. *BioEssays* **29**, 356–370.

Cabezas-Opazo, F. A., Vergara-Pulgar, K., Pérez, M. J., Jara, C., Osorio-Fuentealba, C. and Quintanilla, R. A. (2015). Mitochondrial Dysfunction Contributes to the Pathogenesis of Alzheimer's Disease. *Oxid. Med. Cell. Longev.* **2015**, 1–12.

Cai, C., Masumiya, H., Weisleder, N., Matsuda, N., Nishi, M., Hwang, M., Ko, J. K., Lin, P., Thornton, A., Zhao, X., et al. (2009). MG53 nucleates assembly of cell membrane repair machinery. *Nat. Cell Biol.* **11**, 56–64.

Campos-Ortega, J. A. and Hartenstein, V. (1997). Stages of Drosophila Embryogenesis. In *The Embryonic Development of Drosophila melanogaster*, pp. 9–102. Berlin, Heidelberg: Springer Berlin Heidelberg.

Campos, I., Geiger, J. A., Santos, A. C., Carlos, V. and Jacinto, A. (2010). Genetic screen in Drosophila melanogaster uncovers a novel set of genes required for embryonic epithelial repair. *Genetics* **184**, 129–40.

Carafoli, E., Tiozzo, R., Lugli, G., Crovetti, F. and Kratzing, C. (1974). The release of calcium from heart mitochondria by sodium. *J. Mol. Cell. Cardiol.* **6**, 361–71.

Carvalho, L., Jacinto, A. and Matova, N. (2014). The Toll/NF-kappaB signaling pathway is required for epidermal wound repair in Drosophila. *Proc Natl Acad Sci U S A* **111**, E5373-82.

Carvalho, L., Patricio, P., Ponte, S., Heisenberg, C. P., Almeida, L., Nunes, A. S., Araújo, N. A. M. and Jacinto, A. (2018). Occluding junctions as novel regulators of tissue mechanics during wound repair. *J. Cell Biol.* **217**, 4267–4283.

Cerveny, K. L., Studer, S. L., Jensen, R. E. and Sesaki, H. (2007). Yeast Mitochondrial Division and Distribution Require the Cortical Num1 Protein. *Dev. Cell* **12**, 363–375.

Chai, J., Du, C., Wu, J.-W., Kyin, S., Wang, X. and Shi, Y. (2000). Structural and biochemical basis of apoptotic activation by Smac/DIABLO. *Nature* **406**, 855–862.

Chan, N. C. and Chan, D. C. (2011). Parkin uses the UPS to ship off dysfunctional mitochondria. *Autophagy* **7**, 771–772.

Chang, C. R. and Blackstone, C. (2007). Cyclic AMP-dependent protein kinase phosphorylation of Drp1 regulates its GTPase activity and mitochondrial morphology. *J. Biol. Chem.* **282**, 21583–21587.

Chang, C.-R. and Blackstone, C. (2010). Dynamic regulation of mitochondrial fission through modification of the dynamin-related protein Drp1. *Ann. N. Y. Acad. Sci.* **1201**, 34–9.

Chaturvedi, R. K. and Flint Beal, M. (2013). Mitochondrial diseases of the brain. *Free Radic. Biol. Med.* **63**, 1–29.

Chaturvedi, R. K., Adhihetty, P., Shukla, S., Hennessy, T., Calingasan, N., Yang, L., Starkov, A., Kiaei, M., Cannella, M., Sassone, J., et al. (2009). Impaired PGC-1α function in muscle in Huntington's disease. *Hum. Mol. Genet.* **18**, 3048–3065.

Chen, H. and Chan, D. C. (2009). Mitochondrial dynamics--fusion, fission, movement, and mitophagy--in neurodegenerative diseases. *Hum. Mol. Genet.* **18**, R169-76.

Chen, H. and Chan, D. C. (2017). Mitochondrial Dynamics in Regulating the Unique Phenotypes of Cancer and Stem Cells. *Cell Metab.* **26**, 39–48.

Chen, Y. and Dorn, G. W. (2013). PINK1- Phosphorylated Mitofusin 2 is a Parkin Receptor for Culling Damaged Mitochondria. *Science (80-.).* **340**, 471–475.

Chen, H., Detmer, S. A., Ewald, A. J., Griffin, E. E., Fraser, S. E. and Chan, D. C. (2003). Mitofusins Mfn1 and Mfn2 coordinately regulate mitochondrial fusion and are essential for embryonic development. *J. Cell Biol.* **160**, 189–200.

Chen, H., Chomyn, A. and Chan, D. C. (2005). Disruption of fusion results in mitochondrial heterogeneity and dysfunction. *J. Biol. Chem.* **280**, 26185–26192.

Chen, T.-W., Wardill, T. J., Sun, Y., Pulver, S. R., Renninger, S. L., Baohan, A., Schreiter, E. R., Kerr, R. A., Orger, M. B., Jayaraman, V., et al. (2013). Ultrasensitive fluorescent proteins for imaging neuronal activity. *Nature* **499**, 295–300.

Choi, S., Quan, X., Bang, S., Yoo, H., Kim, J., Park, J., Park, K. S. and Chung, J. (2017). Mitochondrial calcium uniporter in Drosophila transfers calcium between the endoplasmic reticulum and mitochondria in oxidative stress-induced cell death. *J. Biol. Chem.* **292**, 14473–14485.

Cieri, D., Vicario, M., Giacomello, M., Vallese, F., Filadi, R., Wagner, T., Pozzan, T., Pizzo, P., Scorrano, L., Brini, M., et al. (2018). SPLICS: A split green fluorescent protein-based contact site sensor for narrow and wide heterotypic organelle juxtaposition. *Cell Death Differ.* **25**, 1131–1145.

Clary, D. O. and Wolstenholme, D. R. (1985). The mitochondrial DNA molecule of Drosophila yakuba: Nucleotide sequence, gene organization, and genetic code. *J. Mol. Evol.* **22**, 252–271.

Clavier, A., Ruby, V., Rincheval-Arnold, A., Mignotte, B. and Guénal, I. (2015). The Drosophila retinoblastoma protein, Rbf1, induces a Debcl- and Drp1-dependent mitochondrial apoptosis. *J. Cell Sci.* **128**, 3239–3249.

Collins, T. J., Berridge, M. J., Lipp, P. and Bootman, M. D. (2002). Mitochondria are morphologically and functionally heterogeneous within cells. *EMBO J.* **21**, 1616–1627.

Colombini, M. (1980). Structure and Mode of Action of a Voltage Dependent Anion-Selective Channel (Vdac) Located in the Outer Mitochondrial Membrane Dependent Anion-Selective Channel (Vdac). *Ann. N. Y. Acad. Sci.* **341**, 552–563.

Colombini, M. (2012). VDAC structure, selectivity, and dynamics. *Biochim. Biophys. Acta - Biomembr.* **1818**, 1457–1465.

Consolato, F., Maltecca, F., Tulli, S., Sambri, I. and Casari, G. (2018). m-AAA and i-AAA complexes coordinate to regulate OMA1, the stress-activated supervisor of mitochondrial dynamics. *J. Cell Sci.* **131**,.

Cooper, S. T. and McNeil, P. L. (2015). Membrane repair: Mechanisms and pathophysiology. *Physiol. Rev.* **95**, 1205–1240.

Cordeiro, J. V and Jacinto, A. (2013). The role of transcription-independent damage signals in the initiation of epithelial wound healing. *Nat. Rev. Mol. Cell Biol.* **14**, 249–62.

Corrotte, M., Almeida, P. E., Tam, C., Castro-Gomes, T., Fernandes, M. C., Millis, B. A., Cortez, M., Miller, H., Song, W., Maugel, T. K., et al. (2013). Caveolae internalization repairs wounded cells and muscle fibers. *Elife* **2013**, 1–30.

Cox, C. J., Foster, P. G., Hirt, R. P., Harris, S. R. and Embley, T. M. (2008). The archaebacterial origin of eukaryotes. *Proc. Natl. Acad. Sci. U. S. A.* **105**, 20356–20361.

Cribbs, J. T. and Strack, S. (2007). Reversible phosphorylation of Drp1 by cyclic AMP-dependent protein kinase and calcineurin regulates mitochondrial fission and cell death. *EMBO Rep.* **8**, 939–44.

Csordás, G., Golenár, T., Seifert, E. L., Kamer, K. J., Sancak, Y., Perocchi, F., Moffat, C., Weaver, D., Perez, S. de la F., Bogorad, R., et al. (2013). MICU1 Controls Both the Threshold and Cooperative Activation of the Mitochondrial Ca2+ Uniporter. *Cell Metab.* **17**, 976–987.

Daems, W. T. and Wisse, E. (1966). Shape and attachment of the cristae mitochondriales in mouse hepatic cell mitochondria. *J. Ultrastruct. Res.* **16**, 123–140.

Dagda, R. K., Cherra, S. J., Kulich, S. M., Tandon, A., Park, D. and Chu, C. T. (2009). Loss of PINK1 function promotes mitophagy through effects on oxidative stress and mitochondrial fission. *J. Biol. Chem.* **284**, 13843–13855.

Danial, N. N. and Korsmeyer, S. J. (2004). Cell Death: Critical Control Points. *Cell* **116**, 205–219.

Danjo, Y. and Gipson, I. K. (1998). Actin "purse string" filaments are anchored by E-cadherin-mediated adherens junctions at the leading edge of the epithelial wound, providing coordinated cell movement. *J. Cell Sci.* **111 (Pt 2**, 3323–32.

Davenport, N. R. and Bement, W. M. (2016). Cell repair: Revisiting the patch hypothesis. *Commun. Integr. Biol.* **9**, e1253643.

Dawes-Hoang, R. E., Parmar, K. M., Christiansen, A. E., Phelps, C. B., Brand, A. H. and Wieschaus, E. F. (2005). Folded gastrulation, cell shape change and the control of myosin localization. *Development* **132**, 4165–4178.

De Brito, O. M. and Scorrano, L. (2008). Mitofusin 2 tethers endoplasmic reticulum to mitochondria. *Nature* **456**, 605–610.

De Stefani, D., Raffaello, A., Teardo, E., Szabò, I. and Rizzuto, R. (2011). A 40 kDa protein of the inner membrane is the mitochondrial calcium uniporter. *Nature* **476**, 336–340.

De Stefani, D., Rizzuto, R. and Pozzan, T. (2016). Enjoy the Trip: Calcium in Mitochondria Back and Forth. *Annu. Rev. Biochem.* **85**, 161–192.

De Vos, K. J., Allan, V. J., Grierson, A. J. and Sheetz, M. P. (2005). Mitochondrial function and actin regulate dynamin-related protein 1-dependent mitochondrial fission. *Curr. Biol.* **15**, 678–83.

Dekker, P. J. T., Martin, F., Maarse, A. C., Bömer, U., Müller, H., Guiard, B., Meijer, M., Rassow, J. and Pfanner, N. (1997). The Tim core complex defines the number of mitochondrial translocation contact sites and can hold arrested preproteins in the absence of matrix Hsp70-Tim44. *EMBO J.* **16**, 5408–5419.

Delettre, C., Lenaers, G., Griffoin, J., Gigarel, N., Lorenzo, C., Belenguer, P., Pelloquin, L., Grosgeorge, J., Turc-carel, C., Perret, E., et al. (2000). Nuclear gene OPA1, encoding a mitochondrial dynamin-related protein, is mutated in dominant optic atrophy. *Nat. Genet.* **26**, 207–210.

DeLuca, H. F. and Engstrom, G. W. (1961). Calcium uptake by rat kidney mitochondria. *Proc. Natl. Acad. Sci.* **47**, 1744–1750.

Demyanenko, I. A., Popova, E. N., Zakharova, V. V., Ilyinskaya, O. P., Vasilieva, T. V., Romashchenko, V. P., Fedorov, A. V., Manskikh, V. N., Skulachev, M. V., Zinovkin, R. A., et al. (2015). Mitochondria-targeted antioxidant SkQ1 improves impaired dermal wound healing in old mice. *Aging (Albany. NY).* **7**, 475–485.

Demyanenko, I. A., Zakharova, V. V., Ilyinskaya, O. P., Vasilieva, T. V., Fedorov, A. V., Manskikh, V. N.,

Zinovkin, R. A., Pletjushkina, O. Y., Chernyak, B. V., Skulachev, V. P., et al. (2017). Mitochondria-Targeted Antioxidant SkQ1 Improves Dermal Wound Healing in Genetically Diabetic Mice. *Oxid. Med. Cell. Longev.* **2017**, 6408278.

Deng, H., Takashima, S., Paul, M., Guo, M. and Hartenstein, V. (2018). Mitochondrial dynamics regulates Drosophila intestinal stem cell differentiation. *Cell Death Discov.* **4**, 17.

Detmer, S. a and Chan, D. C. (2007). Complementation between mouse Mfn1 and Mfn2 protects mitochondrial fusion defects caused by CMT2A disease mutations. *J. Cell Biol.* **176**, 405–414.

Dickinson, B. C. and Chang, C. J. (2011). Chemistry and biology of reactive oxygen species in signaling or stress responses. *Nat. Chem. Biol.* **7**, 504–511.

Dickinson, W. J. and Thatcher, J. W. (1997). Morphogenesis of denticles and hairs in Drosophila embryos: Involvement of actin-associated proteins that also affect adult structures. *Cell Motil. Cytoskeleton* **38**, 9–21.

Dorn, G. W. (2018). Evolving Concepts of Mitochondrial Dynamics. *Annu. Rev. Physiol.* **81**, 1–17.

Dorn, G. W., Vega, R. B. and Kelly, D. P. (2015). Mitochondrial biogenesis and dynamics in the developing and diseased heart. *Genes Dev.* **29**, 1981–1991.

DuBoff, B., Götz, J. and Feany, M. B. (2012). Tau promotes neurodegeneration via DRP1 mislocalization in vivo. *Neuron* **75**, 618–32.

Ducuing, A. and Vincent, S. (2016). The actin cable is dispensable in directing dorsal closure dynamics but neutralizes mechanical stress to prevent scarring in the Drosophila embryo. *Nat. Cell Biol.* **18**, 1149–1160.

Dulbecco, R. and Elkington, J. (1975). Induction of growth in resting fibroblastic cell cultures by Ca++. *Proc. Natl. Acad. Sci.* **72**, 1584–1588.

Dunn, C. D. (2017). Some Liked It Hot: A Hypothesis Regarding Establishment of the Proto-Mitochondrial Endosymbiont During Eukaryogenesis. *J. Mol. Evol.* **85**, 99–106.

Dunnill, C., Patton, T., Brennan, J., Barrett, J., Dryden, M., Cooke, J., Leaper, D. and Georgopoulos, N. T. (2017). Reactive oxygen species (ROS) and wound healing: the functional role of ROS and emerging ROS-modulating technologies for augmentation of the healing process. *Int. Wound J.* **14**, 89–96.

Durr, M., Escobar-henriques, M., Merz, S., Geimer, S., Langer, T. and Westermann, B. (2006). Nonredundant Roles of Mitochondria-associated F-Box Proteins Mfb1 and Mdm30 in Maintenance of Mitochondrial Morphology in Yeast □. *Mol. Biol. Cell* **17**, 3745–3755.

Ehses, S., Raschke, I., Mancuso, G., Bernacchia, A., Geimer, S., Tondera, D., Martinou, J. C., Westermann, B., Rugarli, E. I. and Langer, T. (2009). Regulation of OPA1 processing and mitochondrial fusion by m-AAA protease isoenzymes and OMA1. *J. Cell Biol.* **187**, 1023–1036.

Eisner, V., Picard, M. and Hajnóczky, G. (2018). Mitochondrial dynamics in adaptive and maladaptive cellular

stress responses. *Nat. Cell Biol.* 1.

El-Hattab, A. W., Craigen, W. J. and Scaglia, F. (2017). Mitochondrial DNA maintenance defects. *Biochim. Biophys. Acta - Mol. Basis Dis.* **1863**, 1539–1555.

Elachouri, G., Vidoni, S., Zanna, C., Pattyn, A., Boukhaddaoui, H., Gaget, K., Yu-wai-man, P., Gasparre, G., Loiseau, D., Sarzi, E., et al. (2011). OPA1 links human mitochondrial genome maintenance to mtDNA replication and distribution. *Genome Res.* **21**, 12–20.

Elmore, S. (2007). Apoptosis: A Review of Programmed Cell Death. *Toxicol. Pathol.* **35**, 495–516.

Favaro, G., Romanello, V., Varanita, T., Andrea Desbats, M., Morbidoni, V., Tezze, C., Albiero, M., Canato, M., Gherardi, G., De Stefani, D., et al. (2019). DRP1-mediated mitochondrial shape controls calcium homeostasis and muscle mass. *Nat. Commun.* **10**, 2576.

Fawcett, D. W. (1975). The mammalian spermatozoon. *Dev. Biol.* **44**, 394–436.

Feng, S., Li, H., Tai, Y., Huang, J., Su, Y., Abramowitz, J., Zhu, M. X., Birnbaumer, L. and Wang, Y. (2013). Canonical transient receptor potential 3 channels regulate mitochondrial calcium uptake. *Proc. Natl. Acad. Sci. U. S. A.* **110**, 11011–11016.

Fenteany, G., Janmey, P. A. and Stossel, T. P. (2000). Signaling pathways and cell mechanics involved in wound closure by epithelial cell sheets. *Curr. Biol.* **10**, 831–838.

Fernie, A. R., Carrari, F. and Sweetlove, L. J. (2004). Respiratory metabolism: Glycolysis, the TCA cycle and mitochondrial electron transport. *Curr. Opin. Plant Biol.* **7**, 254–261.

Ferree, A. and Shirihai, O. (2012). Mitochondrial Dynamics: The Intersection of Form and Function. *Adv. Exp. Med. Biol.* **748**, 13–40.

Ferreira-da-Silva, A., Valacca, C., Rios, E., Pópulo, H., Soares, P., Sobrinho-Simões, M., Scorrano, L., Máximo, V. and Campello, S. (2015). Mitochondrial dynamics protein Drp1 is overexpressed in oncocytic thyroid tumors and regulates cancer cell migration. *PLoS One* **10**, 1–17.

Filadi, R., Greotti, E., Turacchio, G., Luini, A., Pozzan, T. and Pizzo, P. (2015). Mitofusin 2 ablation increases endoplasmic reticulum-mitochondria coupling. *Proc. Natl. Acad. Sci. U. S. A.* **112**, E2174–E2181.

Finkel, T., Menazza, S., Holmström, K. M., Parks, R. J., Liu, J., Sun, J., Liu, J., Pan, X. and Murphy, E. (2015). The ins and outs of mitochondrial calcium. *Circ. Res.* **116**, 1810–9.

Foe, V. E. and Alberts, B. M. (1983). Studies of nuclear and cytoplasmic behavior during the five mitotic cycles that precede gastrulation in Drosophila embryogenesis. *J. Cell Sci.* **Vol. 61**, 31–70.

Forini, F., Nicolini, G. and Iervasi, G. (2015). Mitochondria as key targets of cardioprotection in cardiac ischemic disease: Role of thyroid hormone triiodothyronine. *Int. J. Mol. Sci.* **16**, 6312–6336.

Forster, B., Van De Ville, D., Berent, J., Sage, D. and Unser, M. (2004). Complex wavelets for extended depth-of-field: A new method for the fusion of multichannel microscopy images. *Microsc. Res. Tech.* **65**, 33–

42.

Franco, R. and Cidlowski, J. A. (2009). Apoptosis and glutathione: Beyond an antioxidant. *Cell Death Differ.* **16**, 1303–1314.

Frank, S., Gaume, B., Bergmann-Leitner, E. S., Leitner, W. W., Robert, E. G., Catez, F., Smith, C. L. and Youle, R. J. (2001). The Role of Dynamin-Related Protein 1, a Mediator of Mitochondrial Fission, in Apoptosis. *Dev. Cell* **1**, 515–525.

Frei, C., Galloni, M., Hafen, E. and Edgar, B. A. (2005). The Drosophila mitochondrial ribosomal protein mRpL12 is required for Cyclin D/Cdk4-driven growth. *EMBO J.* **24**, 623–634.

Frezza, C., Cipolat, S., Martins de Brito, O., Micaroni, M., Beznoussenko, G. V, Rudka, T., Bartoli, D., Polishuck, R. S., Danial, N. N., De Strooper, B., et al. (2006). OPA1 Controls Apoptotic Cristae Remodeling Independently from Mitochondrial Fusion. *Cell* **126**, 177–189.

Friedman, J. R. and Nunnari, J. (2014). Mitochondrial form and function. *Nature* **505**, 335–343.

Friedman, J. R., Lackner, L. L., West, M., DiBenedetto, J. R., Nunnari, J. and Voeltz, G. K. (2011). ER Tubules Mark Sites of Mitochondrial Division. *Science (80-.).* **334**, 358–362.

Frykberg, R. G. and Banks, J. (2015). Challenges in the Treatment of Chronic Wounds. *Adv. wound care* **4**, 560–582.

Fujimoto, M. and Hayashi, T. (2011). *New Insights into the Role of Mitochondria-Associated Endoplasmic Reticulum Membrane*. 1st ed. Elsevier Inc.

Fukumitsu, K., Hatsukano, T., Yoshimura, A., Heuser, J., Fujishima, K. and Kengaku, M. (2016). Mitochondrial fission protein Drp1 regulates mitochondrial transport and dendritic arborization in cerebellar Purkinje cells. *Mol. Cell. Neurosci.* **71**, 56–65.

Galloway, C. A., Lee, H., Nejjar, S., Jhun, B. S., Yu, T., Hsu, W. and Yoon, Y. (2012). Transgenic control of mitochondrial fission induces mitochondrial uncoupling and relieves diabetic oxidative stress. *Diabetes* **61**, 2093–2104.

Galluzzi, L., Vitale, I., Abrams, J. M., Alnemri, E. S., Baehrecke, E. H., Blagosklonny, M. V., Dawson, T. M., Dawson, V. L., El-Deiry, W. S., Fulda, S., et al. (2012). Molecular definitions of cell death subroutines: Recommendations of the Nomenclature Committee on Cell Death 2012. *Cell Death Differ.* **19**, 107–120.

Gandre-Babbe, S. and van der Bliek, A. M. (2008). The novel tail-anchored membrane protein Mff controls mitochondrial and peroxisomal fission in mammalian cells. *Mol. Biol. Cell* **19**, 2402–12.

Garcia-Fernandez, B., Campos, I., Geiger, J., Santos, A. C. and Jacinto, A. (2009). Epithelial resealing. *Int J Dev Biol* **53**, 1549–56.

Gerencser, A. A. and Adam-Vizi, V. (2005). Mitochondrial Ca2+ Dynamics Reveals Limited Intramitochondrial Ca2+ Diffusion. *Biophys. J.* **88**, 698–714.

Gincel, D., Zaid, H. and Shoshan-Barmatz, V. (2001). Calcium binding and translocation by the voltage-dependent anion channel: a possible regulatory mechanism in mitochondrial function. *Biochem. J.* **358**, 147.

Giorgi, C., Romagnoli, A., Pinton, P. and Rizzuto, R. (2008). Ca2+ signaling, mitochondria and cell death. *Curr. Mol. Med.* **8**, 119–30.

Goyal, G., Fell, B., Sarin, A., Youle, R. J. and Sriram, V. (2007). Role of mitochondrial remodeling in programmed cell death in Drosophila melanogaster. *Dev. Cell* **12**, 807–16.

Gray, M. W. (2012). Mitochondrial Evolution. *Cold Spring Harb. Perspect. Biol.* **4**, a011403–a011403.

Gray, M. W. (2017). Lynn Margulis and the endosymbiont hypothesis: 50 years later. *Mol. Biol. Cell* **28**, 1285–1287.

Griffin, E. E., Graumann, J. and Chan, D. C. (2005). The WD40 protein Caf4p is a component of the mitochondrial fission machinery and recruits Dnm1p to mitochondria. *J. Cell Biol.* **170**, 237–248.

Griparic, L., Van Der Wel, N. N., Orozco, I. J., Peters, P. J. and Van Der Bliek, A. M. (2004). Loss of the Intermembrane Space Protein Mgm1/OPA1 Induces Swelling and Localized Constrictions along the Lengths of Mitochondria. *J. Biol. Chem.* **279**, 18792–18798.

Guo, X., Macleod, G. T., Wellington, A., Hu, F., Panchumarthi, S., Schoenfield, M., Marin, L., Charlton, M. P., Atwood, H. L. and Zinsmaier, K. E. (2005). The GTPase dMiro Is Required for Axonal Transport of Mitochondria to Drosophila Synapses. *Neuron* **47**, 379–393.

Guo, Q., Koirala, S., Perkins, E. M., McCaffery, J. M. and Shaw, J. M. (2012). The Mitochondrial Fission Adaptors Caf4 and Mdv1 Are Not Functionally Equivalent. *PLoS One* **7**,.

Guo, R., Davis, D. and Fang, Y. (2018). Intercellular transfer of mitochondria rescues virus-induced cell death but facilitates cell-to-cell spreading of porcine reproductive and respiratory syndrome virus. *Virology* **517**, 122–134.

Gurtner, G. C., Werner, S., Barrandon, Y. and Longaker, M. T. (2008). Wound repair and regeneration. *Nature* **453**, 314–21.

Hackenbrock, C. R. (1966). Ultrastructural bases for metabolically linked mechanical activity in mitochondria. I. Reversible ultrastructural changes with change in metabolic steady state in isolated liver mitochondria. *J. Cell Biol.* **30**, 269–297.

Haelterman, N. A., Jiang, L., Li, Y., Bayat, V., Sandoval, H., Ugur, B., Tan, K. L., Zhang, K., Bei, D., Xiong, B., et al. (2014). Large-scale identification of chemically induced mutations in Drosophila melanogaster. *Genome Res.* **24**, 1707–1718.

Hales, K. G. and Fuller, M. T. (1997). Developmentally regulated mitochondrial fusion mediated by a conserved, novel, predicted GTPase. *Cell* **90**, 121–9.

Halfon, M. S., Gisselbrecht, S., Lu, J., Estrada, B., Keshishian, H. and Michelson, A. M. (2002). New

fluorescent protein reporters for use with the Drosophila Gal4 expression system and for vital detection of balancer chromosomes. *Genesis* **34**, 135–8.

Hall, A. (1994). Small GTP-binding proteins and the regulation of the actin cytoskeleton. *Annu. Rev. Cell Biol.* **10**, 31–54.

Hammermeister, M., Schödel, K. and Westermann, B. (2010). Mdm36 is a mitochondrial fission-promoting protein in Saccharomyces cerevisiae. *Mol. Biol. Cell* **21**, 2443–52.

Han, X.-J., Lu, Y.-F., Li, S.-A., Kaitsuka, T., Sato, Y., Tomizawa, K., Nairn, A. C., Takei, K., Matsui, H. and Matsushita, M. (2008). CaM kinase I alpha-induced phosphorylation of Drp1 regulates mitochondrial morphology. *J. Cell Biol.* **182**, 573–85.

Hanna, R. A., Quinsay, M. N., Orogo, A. M., Giang, K., Rikka, S. and Gustafsson, Å. B. (2012). Microtubule-associated protein 1 light chain 3 (LC3) interacts with Bnip3 protein to selectively remove endoplasmic reticulum and mitochondria via autophagy. *J. Biol. Chem.* **287**, 19094–19104.

Hanson, G. T., Aggeler, R., Oglesbee, D., Cannon, M., Capaldi, R. A., Tsien, R. Y. and Remington, S. J. (2004). Investigating Mitochondrial Redox Potential with Redox-sensitive Green Fluorescent Protein Indicators. *J. Biol. Chem.* **279**, 13044–13053.

Hardie, D. G. (2007). AMP-activated/SNF1 protein kinases: Conserved guardians of cellular energy. *Nat. Rev. Mol. Cell Biol.* **8**, 774–785.

Harman, D. (1956). Aging: A Theory Based on Free Radical and Radiation Chemistry. *J. Gerontol.* **11**, 298–300.

Hartsock, A. and Nelson, W. J. (2008). Adherens and tight junctions: Structure, function and connections to the actin cytoskeleton. *Biochim. Biophys. Acta - Biomembr.* **1778**, 660–669.

Hatch, A. L., Gurel, P. S. and Higgs, H. N. (2014). Novel roles for actin in mitochondrial fission. *J. Cell Sci.* **127**, 4549–60.

Haug-Collet, K., Pearson, B., Webel, R., Szerencsei, R. T., Winkfein, R. J., Schnetkamp, P. P. M. and Colley, N. J. (1999). Cloning and characterization of a potassium-dependent sodium/calcium exchanger in Drosophila. *J. Cell Biol.* **147**, 659–669.

Havran, W. L. and Jameson, J. M. (2010). Epidermal T Cells and Wound Healing. *J. Immunol.* **184**, 5423–5428.

Haworth, R. A. and Hunter, D. R. (1979). The Ca2+-induced membrane transition in mitochondria. II. Nature of the Ca2+ trigger site. *Arch. Biochem. Biophys.* **195**, 460–467.

Heasman, S. J. and Ridley, A. J. (2008). Mammalian Rho GTPases: new insights into their functions from in vivo studies. *Nat. Rev. Mol. Cell Biol.* **9**, 690–701.

Heilbrunn, L. V. (1930). The action of various salts on the first stage of the surface precipitation reaction in Arbacia egg protoplasm. *Protoplasma* **11**, 558–573.

Henson, J. H., Nazarian, R., Schulberg, K. L., Trabosh, V. A., Kolnik, S. E., Burns, A. R. and McPartland, K. J.

(2002). Wound closure in the lamellipodia of single cells: mediation by actin polymerization in the absence of an actomyosin purse string. *Mol. Biol. Cell* **13**, 1001–14.

Herlan, M., Vogel, F., Bornhövd, C., Neupert, W. and Reichert, A. S. (2003). Processing of Mgm1 by the rhomboid-type protease Pcp1 is required for maintenance of mitochondrial morphology and of mitochondrial DNA. *J. Biol. Chem.* **278**, 27781–27788.

Herszterg, S., Leibfried, A., Bosveld, F., Martin, C. and Bellaiche, Y. (2013). Interplay between the Dividing Cell and Its Neighbors Regulates Adherens Junction Formation during Cytokinesis in Epithelial Tissue. *Dev. Cell* **24**, 256–270.

Hillman, R. and Lesnik, L. H. (1970). Cuticle formation in the embryo of Drosophila melanogaster. *J. Morphol.* **131**, 383–395.

Hinman, E. L., Beilman, G. J., Groehler, K. E. and Sammak, P. J. (1997). Wound-induced calcium waves in alveolar type II cells. *Am. J. Physiol. - Lung Cell. Mol. Physiol.* **273**, 1242–1248.

Hom, J. R., Gewandter, J. S., Michael, L., Sheu, S.-S. and Yoon, Y. (2007). Thapsigargin induces biphasic fragmentation of mitochondria through calcium-mediated mitochondrial fission and apoptosis. *J. Cell. Physiol.* **212**, 498–508.

Honsho, M., Yamashita, S. and Fujiki, Y. (2016). Peroxisome homeostasis: Mechanisms of division and selective degradation of peroxisomes in mammals. *Biochim. Biophys. Acta - Mol. Cell Res.* **1863**, 984–991.

Hoppins, S., Collins, S. R., Cassidy-Stone, A., Hummel, E., DeVay, R. M., Lackner, L. L., Westermann, B., Schuldiner, M., Weissman, J. S. and Nunnari, J. (2011). A mitochondrial-focused genetic interaction map reveals a scaffold-like complex required for inner membrane organization in mitochondria. *J. Cell Biol.* **195**, 323–340.

Horvath, S. E. and Daum, G. (2013). Lipids of mitochondria. *Prog. Lipid Res.* **52**, 590–614.

Houten, S. M. and Wanders, R. J. A. (2010). A general introduction to the biochemistry of mitochondrial fatty acid β-oxidation. *J. Inherit. Metab. Dis.* **33**, 469–477.

Huber, N., Guimaraes, S., Schrader, M., Suter, U. and Niemann, A. (2013). Charcot-Marie-Tooth disease-associated mutants of GDAP1 dissociate its roles in peroxisomal and mitochondrial fission. *EMBO Rep.* **14**, 545–552.

Hunter, M. V., Lee, D. M., Harris, T. J. C. and Fernandez-Gonzalez, R. (2015). Polarized E-cadherin endocytosis directs actomyosin remodeling during embryonic wound repair. *J. Cell Biol.* **210**, 801–816.

Hunter, M. V., Willoughby, P. M., Bruce, A. E. E. and Fernandez-Gonzalez, R. (2018a). Oxidative Stress Orchestrates Cell Polarity to Promote Embryonic Wound Healing. *Dev. Cell* **47**, 377-387.e4.

Hunter, M. V, Willoughby, P. M., Bruce, A. E. E., Fernandez-gonzalez, R., Hunter, M. V, Willoughby, P. M., Bruce, A. E. E. and Fernandez-gonzalez, R. (2018b). Short Article Oxidative Stress Orchestrates Cell Polarity to Short Article Oxidative Stress Orchestrates Cell Polarity to Promote Embryonic Wound

Healing. *Dev. Cell* **47**, 377-387.e4.

Hwa, J. J., Hiller, M. A., Fuller, M. T. and Santel, A. (2002). Differential expression of the Drosophila mitofusin genes fuzzy onions (fzo) and dmfn. *Mech. Dev.* **116**, 213–6.

Idone, V., Tam, C., Goss, J. W., Toomre, D., Pypaert, M. and Andrews, N. W. (2008). Repair of injured plasma membrane by rapid Ca2+ dependent endocytosis. *J. Cell Biol.* **180**, 905–914.

Ikeda, Y., Shirakabe, A., Maejima, Y., Zhai, P., Sciarretta, S., Toli, J., Nomura, M., Mihara, K., Egashira, K., Ohishi, M., et al. (2015). Endogenous Drp1 mediates mitochondrial autophagy and protects the heart against energy stress. *Circ. Res.* **116**, 264–278.

Ingerman, E., Perkins, E. M., Marino, M., Mears, J. A., McCaffery, J. M., Hinshaw, J. E. and Nunnari, J. (2005). Dnm1 forms spirals that are structurally tailored to fit mitochondria. *J. Cell Biol.* **170**, 1021–1027.

Ishihara, N., Fujita, Y., Oka, T. and Mihara, K. (2006). Regulation of mitochondrial morphology through proteolytic cleavage of OPA1. *EMBO J.* **25**, 2966–77.

Ishihara, N., Nomura, M., Jofuku, A., Kato, H., Suzuki, S. O., Masuda, K., Otera, H., Nakanishi, Y., Nonaka, I., Goto, Y.-I., et al. (2009). Mitochondrial fission factor Drp1 is essential for embryonic development and synapse formation in mice. *Nat. Cell Biol.* **11**, 958–66.

Jacinto, A., Wood, W., Woolner, S., Hiley, C., Turner, L., Wilson, C., Martinez-Arias, A. and Martin, P. (2002). Dynamic Analysis of Actin Cable Function during Drosophila Dorsal Closure. *Curr. Biol.* **12**, 1245–1250.

Jajoo, R., Jung, Y., Huh, D., Viana, M. P., Rafelski, S. M., Springer, M. and Paulsson, J. (2016). Accurate concentration control of mitochondria and nucleoids. *Science (80-.).* **351**, 169–172.

James, D. I., Parone, P. A., Mattenberger, Y. and Martinou, J. C. (2003). hFis1, a novel component of the mammalian mitochondrial fission machinery. *J. Biol. Chem.* **278**, 36373–36379.

Janda, J., Nfonsam, V., Calienes, F., Sligh, J. E. and Jandova, J. (2016). Modulation of ROS levels in fibroblasts by altering mitochondria regulates the process of wound healing. *Arch. Dermatol. Res.* **308**, 239–48.

Jansen, R. P. S. (2000). Origin and persistence of the mitochondrial genome. *Hum. Reprod.* **15**, 1–10.

Ji, W., Hatch, A. L., Merrill, R. A., Strack, S. and Higgs, H. N. (2015). Actin filaments target the oligomeric maturation of the dynamin GTPase Drp1 to mitochondrial fission sites. *Elife* **4**, e11553.

Jiang, D., Zhao, L. and Clapham, D. E. (2009). Genome-wide RNAi screen identifies Letm1 as a mitochondrial Ca 2+ /H + antiporter. *Science (80-.).* **326**, 144–147.

Johri, A. and Beal, M. F. (2012). Mitochondrial Dysfunction in Neurodegenerative Diseases. *J. Pharmacol. Exp. Ther.* **342**, 619–630.

Jones, B. A. and Fangman, W. L. (1992). Mitochondrial DNA maintenance in yeast requires a protein containing a region related to the GTP-binding domain of dynamin. *Genes Dev.* **6**, 380–389.

Jonusaite, S., Donini, A. and Kelly, S. P. (2016). Occluding junctions of invertebrate epithelia. *J. Comp. Physiol.*

B Biochem. Syst. Environ. Physiol. **186**, 17–43.

Jornayvaz, F. R. and Shulman, G. I. (2010). Regulation of mitochondrial biogenesis. *Essays Biochem.* **47**, 69–84.

Jouaville, L. S., Ichas, F., Holmuhamedov, E. L., Camacho, P. and Lechleiter, J. D. (1995). Synchronization of calcium waves by mitochondrial substrates in Xenopus laevis oocytes. *Nature* **377**, 438–441.

Julian, L. and Olson, M. F. (2014). Rho-associated coiled-coil containing kinases (ROCK). *Small GTPases* **5**, e29846.

Kanazawa, T., Zappaterra, M. D., Hasegawa, A., Wright, A. P. and Erin, D. (2008). The C . elegans Opa1 Homologue EAT-3 Is Essential for Resistance to Free Radicals. *PLoS Genet.* **4**, 1–12.

Karbowski, M., Jeong, S. Y. and Youle, R. J. (2004). Endophilin B1 is required for the maintenance of mitochondrial morphology. *J. Cell Biol.* **166**, 1027–1039.

Karnkowska, A., Vacek, V., Zubáčová, Z., Treitli, S. C., Petrželková, R., Eme, L., Novák, L., Žárský, V., Barlow, L. D., Herman, E. K., et al. (2016). A eukaryote without a mitochondrial organelle. *Curr. Biol.* **26**, 1274–1284.

Kashatus, D. F., Lim, K.-H., Brady, D. C., Pershing, N. L. K., Cox, A. D. and Counter, C. M. (2011). RALA and RALBP1 regulate mitochondrial fission at mitosis. *Nat. Cell Biol.* **13**, 1108–1115.

Kasza, K. E. and Zallen, J. A. (2011). Dynamics and regulation of contractile actin–myosin networks in morphogenesis. *Curr. Opin. Cell Biol.* **23**, 30–38.

Kiehart, D. P., Galbraith, C. G., Edwards, K. A., Rickoll, W. L. and Montague, R. A. (2000). Multiple forces contribute to cell sheet morphogenesis for dorsal closure in Drosophila. *J. Cell Biol.* **149**, 471–490.

Kijima, K., Numakura, C., Izumino, H., Umetsu, K., Nezu, A., Shiiki, T., Ogawa, M., Ishizaki, Y., Kitamura, T., Shozawa, Y., et al. (2005). Mitochondrial GTPase mitofusin 2 mutation in Charcot-Marie-Tooth neuropathy type 2A. *Hum. Genet.* **116**, 23–27.

Kim, Y., Sung, J. Y., Ceglia, I., Lee, K. W., Ahn, J. H., Halford, J. M., Kim, A. M., Kwak, S. P., Park, J. B., Ho Ryu, S., et al. (2006). Phosphorylation of WAVE1 regulates actin polymerization and dendritic spine morphology. *Nature* **442**, 814–817.

Kim, J.-S., Huang, T. Y. and Bokoch, G. M. (2009). Reactive Oxygen Species Regulate a Slingshot-Cofilin Activation Pathway. *Mol. Biol. Cell* **20**, 2650–2660.

Kimura, K., Ito, M., Amano, M., Chihara, K., Fukata, Y., Nakafuku, M., Yamamori, B., Feng, J., Nakano, T., Okawa, K., et al. (1996). Regulation of Myosin Phosphatase by Rho and Rho-Associated Kinase (Rho-Kinase). *Science (80-.).* **273**, 245–248.

Ko, S. H., Choi, G. E., Oh, J. Y., Lee, H. J., Kim, J. S., Chae, C. W., Choi, D. and Han, H. J. (2017). Succinate promotes stem cell migration through the GPR91-dependent regulation of DRP1-mediated mitochondrial fission. *Sci. Rep.* **7**, 1–14.

Korobova, F., Ramabhadran, V. and Higgs, H. N. (2013). An actin-dependent step in mitochondrial fission mediated by the ER-associated formin INF2. *Science* **339**, 464–7.

Korobova, F., Gauvin, T. J. and Higgs, H. N. (2014). A role for myosin II in mammalian mitochondrial fission. *Curr. Biol.* **24**, 409–14.

Kosako, H., Yoshida, T., Matsumura, F., Ishizaki, T., Narumiya, S. and Inagaki, M. (2000). Rho-kinase/ROCK is involved in cytokinesis through the phosphorylation of myosin light chain and not ezrin/radixin/moesin proteins at the cleavage furrow. *Oncogene* **19**, 6059–6064.

Koshiba, T., Detmer, S. A., Kaiser, J. T., Chen, H., McCaffery, J. M. and Chan, D. C. (2004). Structural basis of mitochondrial tethering by mitofusin complexes. *Science (80-.).* **305**, 858–862.

Kroemer, G., Galluzzi, L. and Brenner, C. (2007). Mitochondrial membrane permeabilization in cell death. *Physiol. Rev.* **87**, 99–163.

Kumari, A. (2018). Citric Acid Cycle. In *Sweet Biochemistry*, pp. 7–11. Elsevier.

Kuo, I. Y. and Ehrlich, B. E. (2015). Signaling in muscle contraction. *Cold Spring Harb. Perspect. Biol.* **7**, 1–14.

Kuznetsov, A. V., Hermann, M., Saks, V., Hengster, P. and Margreiter, R. (2009). The cell-type specificity of mitochondrial dynamics. *Int. J. Biochem. Cell Biol.* **41**, 1928–1939.

Labrousse, A. M., Zappaterra, M. D., Rube, D. A. and Van der Bliek, A. M. (1999). C. elegans dynamin-related protein DRP-1 controls severing of the mitochondrial outer membrane. *Mol. Cell* **4**, 815–826.

Lajeunesse, D. R., Buckner, S. M., Lake, J., Na, C., Pirt, A. and Fromson, K. (2004). Three new Drosophila markers of intracellular membranes. *Biotechniques* **36**, 784–790.

Lamark, T., Kirkin, V., Dikic, I. and Johansen, T. (2009). NBR1 and p62 as cargo receptors for selective autophagy of ubiquitinated targets. *Cell Cycle* **8**, 1986–1990.

Lane, N. and Martin, W. (2010). The energetics of genome complexity. *Nature* **467**, 929–934.

Lawrence, P. A., Bodmer, R. and Vincent, J. P. (1995). Segmental patterning of heart precursors in Drosophila. *Development* **121**, 4303–4308.

Lawrie, A. M., Rizzuto, R., Pozzan, T. and Simpson, A. W. M. (1996). A Role for Calcium Influx in the Regulation of Mitochondrial Calcium in Endothelial Cells. *J. Biol. Chem.* **271**, 10753–10759.

Leal, N. S., Schreiner, B., Pinho, C. M., Filadi, R., Wiehager, B., Karlström, H., Pizzo, P. and Ankarcrona, M. (2016). Mitofusin-2 knockdown increases ER – mitochondria contact and decreases amyloid b -peptide production. *J Cell Mol Med* **20**, 1686–1695.

Lee, S. and Min, K. T. (2018). The interface between ER and mitochondria: Molecular compositions and functions. *Mol. Cells* **41**, 1000–1007.

Lee, H. and Yoon, Y. (2016). Mitochondrial Fission and Fusion. *Biochem. Soc. Trans.* **44**, 1725–1735.

Lee, Y., Lee, H. Y., Hanna, R. A. and Gustafsson, A. B. (2011). Mitochondrial autophagy by bnip3 involves drp1-mediated mitochondrial fission and recruitment of parkin in cardiac myocytes. *Am. J. Physiol. - Hear. Circ. Physiol.* **301**, 1924–1931.

Lee, J. E., Westrate, L. M., Wu, H., Page, C. and Voeltz, G. K. (2016). Multiple dynamin family members collaborate to drive mitochondrial division. *Nature* **540**, 139–143.

Legesse-Miller, A., Massol, R. H. and Kirchhausen, T. (2003). Constriction and Dnm1p Recruitment Are Distinct Processes in Mitochondrial Fission. *Mol. Biol. Cell* **14**, 1953–1963.

Leiper, L. J., Walczysko, P., Kucerova, R., Ou, J., Shanley, L. J., Lawson, D., Forrester, J. V., McCaig, C. D., Zhao, M. and Collinson, J. M. (2006). The roles of calcium signaling and ERK1/2 phosphorylation in a Pax6+/- mouse model of epithelial wound-healing delay. *BMC Biol.* **4**, 1–14.

Lewis, M. R. and Lewis, W. H. (1914). Mitochondria (and other cytoplasmic structures) in tissue cultures. *Science (80-.).* **39**, 330–333.

Li, J., Chen, J. and Kirsner, R. (2007). Pathophysiology of acute wound healing. *Clin. Dermatol.* **25**, 9–18.

Li, H., Ruan, Y., Zhang, K., Jian, F., Hu, C., Miao, L., Gong, L., Sun, L., Zhang, X., Chen, S., et al. (2016). Mic60/Mitofilin determines MICOS assembly essential for mitochondrial dynamics and mtDNA nucleoid organization. *Cell Death Differ.* **23**, 380–392.

Li, Q., Qin, Z., Chen, B., An, Y., Nie, F., Yang, X., Pan, B. and Bi, H. (2019). Mitochondrial Dysfunction and Morphological Abnormality in Keloid Fibroblasts. *Adv. Wound Care* **00**, 1–14.

Lihavainen, E., Mäkelä, J., Spelbrink, J. N. and Ribeiro, A. S. (2012). Mytoe: automatic analysis of mitochondrial dynamics. *Bioinformatics* **28**, 1050–1.

Lin, Q. T. and Stathopulos, P. B. (2019). Molecular mechanisms of leucine zipper EF-hand containing transmembrane protein-1 function in health and disease. *Int. J. Mol. Sci.* **20**, 1–17.

Littleton, J. T. and Bellen, H. J. (1994). Genetic and phenotypic analysis of thirteen essential genes in cytological interval 22F1-2; 23B1-2 reveals novel genes required for neural development in Drosophila. *Genetics* **138**, 111–123.

Liu, L., Feng, D., Chen, G., Chen, M., Zheng, Q., Song, P., Ma, Q., Zhu, C., Wang, R., Qi, W., et al. (2012). Mitochondrial outer-membrane protein FUNDC1 mediates hypoxia-induced mitophagy in mammalian cells. *Nat. Cell Biol.* **14**, 177–185.

Lodish, H., Berk, A., Zipursky, S. L., Matsudaira, P., Baltimore, D. and Darnell, J. (2000). Section 18.1, The Actin Cytoskeleton. In *Molecular Cell Biology*, p. New York: W. H. Freeman.

Logan, D. C. (2006). The mitochondrial compartment. *J. Exp. Bot.* **57**, 1225–1243.

López-Doménech, G., Covill-Cooke, C., Ivankovic, D., Halff, E. F., Sheehan, D. F., Norkett, R., Birsa, N. and Kittler, J. T. (2018). Miro proteins coordinate microtubule- and actin-dependent mitochondrial transport and distribution. *EMBO J.* **37**, 321–336.

López del Amo, V., Palomino-Schätzlein, M., Seco-Cervera, M., García-Giménez, J. L., Pallardó, F. V., Pineda-Lucena, A. and Galindo, M. I. (2017). A Drosophila model of GDAP1 function reveals the involvement of insulin signalling in the mitochondria-dependent neuromuscular degeneration. *Biochim. Biophys. Acta - Mol. Basis Dis.* **1863**, 801–809.

Losón, O. C., Song, Z., Chen, H. and Chan, D. C. (2013). Fis1, Mff, MiD49, and MiD51 mediate Drp1 recruitment in mitochondrial fission. *Mol. Biol. Cell* **24**, 659–667.

Lovas, J. R. and Wang, X. (2013). The meaning of mitochondrial movement to a neuron's life. *Biochim. Biophys. Acta - Mol. Cell Res.* **1833**, 184–194.

Lowe, J. S. and Anderson, P. G. (2015). Epithelial Cells. In *Stevens Lowes Human Histology*, pp. 37–54. Elsevier.

Lu, Y. and Settleman, J. (1999). The Drosophila Pkn protein kinase is a Rho/Rac effector target required for dorsal closure during embryogenesis. *Genes Dev.* **13**, 1168–1180.

Lutas, A., Wahlmark, C. J., Acharjee, S. and Kawasaki, F. (2012). Genetic analysis in Drosophila reveals a role for the mitochondrial protein p32 in synaptic transmission. *G3 (Bethesda).* **2**, 59–69.

Luxardi, G., Reid, B., Maillard, P. and Zhao, M. (2014). Single cell wound generates electric current circuit and cell membrane potential variations that requires calcium influx. *Integr. Biol. (United Kingdom)* **6**, 662–672.

Lye, C. M., Naylor, H. W. and Sanson, B. (2014). Subcellular localisations of the CPTI collection of YFP-tagged proteins in Drosophila embryos. *Development* **141**, 4006–4017.

Lymn, R. W. and Taylor, E. W. (1971). Mechanism of Adenosine Triphosphate Hydrolysis by Actomyosin. *Biochemistry* **10**, 4617–4624.

Macchi, M., El Fissi, N., Tufi, R., Bentobji, M., Liévens, J.-C., Martins, L. M., Royet, J. and Rival, T. (2013). The Drosophila inner-membrane protein PMI controls crista biogenesis and mitochondrial diameter. *J. Cell Sci.* **126**, 814–24.

MacVicar, T. and Langer, T. (2016). OPA1 processing in cell death and disease - the long and short of it. *J. Cell Sci.* **129**, 2297–2306.

Magee, A. I., Lytton, N. A. and Watt, F. M. (1987). Calcium-induced changes in cytoskeleton and motility of cultured human keratinocytes. *Exp. Cell Res.* **172**, 43–53.

Magie, C. R., Meyer, M. R., Gorsuch, M. S. and Parkhurst, S. M. (1999). Mutations in the Rho1 small GTPase disrupt morphogenesis and segmentation during early Drosophila development. *Development* **126**, 5353–64.

Mandato, C. a and Bement, W. M. (2001). Contraction and polymerization cooperate to assemble and close actomyosin rings around Xenopus oocyte wounds. *J. Cell Biol.* **154**, 785–97.

Mannella, C. A., Marko, M., Penczek, P., Barnard, D. and Frank, J. (1994). The internal compartmentation of

rat-liver mitochondria: Tomographic study using the high-voltage transmission electron microscope. *Microsc. Res. Tech.* **27**, 278–283.

Manor, U., Bartholomew, S., Golani, G., Christenson, E., Kozlov, M., Higgs, H., Spudich, J. and Lippincott-Schwartz, J. (2015). A mitochondria-anchored isoform of the actin-nucleating spire protein regulates mitochondrial division. *Elife* **4**, 1–27.

Mao, K., Wang, K., Liu, X. and Klionsky, D. J. (2013). The scaffold protein Atg11 recruits fission machinery to drive selective mitochondria degradation by autophagy. *Dev. Cell* **26**, 9–18.

Marchi, S. and Pinton, P. (2014). The mitochondrial calcium uniporter complex: Molecular components, structure and physiopathological implications. *J. Physiol.* **592**, 829–839.

Margaritis, L. H., Kafatos, F. C. and Petri, W. H. (1980). The eggshell of Drosophila melanogaster. I. Fine structure of the layers and regions of the wild-type eggshell. *J. Cell Sci.* **43**, 1–35.

Marín-García, J. (2013). *Mitochondria and Their Role in Cardiovascular Disease*. Boston, MA: Springer US.

Marín-García, J. and Akhmedov, A. T. (2016). Mitochondrial dynamics and cell death in heart failure. *Heart Fail. Rev.* **21**, 123–136.

Marinelli, F., Almagor, L., Hiller, R., Giladi, M., Khananshvili, D. and Faraldo-Gómez, J. D. (2014). Sodium recognition by the Na^+/Ca^{2+} exchanger in the outward-facing conformation. *Proc. Natl. Acad. Sci. U. S. A.* **111**, E5354–E5362.

Marquez, J., Lee, S. R., Kim, N. and Han, J. (2016). Rescue of heart failure by mitochondrial recovery. *Int. Neurourol. J.* **20**, 5–12.

Martin, P. and Lewis, J. (1992). Actin cables and epidermal movement in embryonic wound healing. *Nature* **360**, 179–183.

Marzo, L., Gousset, K. and Zurzolo, C. (2012). Multifaceted roles of tunneling nanotubes in intercellular communication. *Front. Physiol.* **3 APR**, 1–14.

Matsubayashi, Y., Coulson-Gilmer, C. and Millard, T. H. (2015). Endocytosis-dependent coordination of multiple actin regulators is required for wound healing. *J. Cell Biol.* **210**, 419–33.

McClatchey, P. M., Keller, A. C., Bouchard, R., Knaub, L. A. and Reusch, J. E. B. (2016). Fully automated software for quantitative measurements of mitochondrial morphology. *Mitochondrion* **26**, 58–71.

McCluskey, J. and Martin, P. (1995). Analysis of the Tissue Movements of Embryonic Wound Healing-DiI Studies in the Limb Bud Stage Mouse Embryo. *Dev. Biol.* **170**, 102–114.

McNeil, P. L., Vogel, S. S., Miyake, K. and Terasaki, M. (2000). Patching plasma membrane disruptions with cytoplasmic membrane. *J. Cell Sci.* **113**, 1891–1902.

McQuibban, G. A., Lee, J. R., Zheng, L., Juusola, M. and Freeman, M. (2006). Normal Mitochondrial Dynamics Requires Rhomboid-7 and Affects Drosophila Lifespan and Neuronal Function. *Curr. Biol.* **16**, 982–989.

McQuibban, A. G., Joza, N., Megighian, A., Scorzeto, M., Zanini, D., Reipert, S., Richter, C., Schweyen, R. J. and Nowikovsky, K. (2010). A Drosophila mutant of LETM1, a candidate gene for seizures in Wolf-Hirschhorn syndrome. *Hum. Mol. Genet.* **19**, 987–1000.

Mears, J. A., Lackner, L. L., Fang, S., Ingerman, E., Nunnari, J. and Hinshaw, J. E. (2011). Conformational changes in Dnm1 support a contractile mechanism for mitochondrial fission. *Nat. Struct. Mol. Biol.* **18**, 20–27.

Meeusen, S., Mccaffery, J. M. and Nunnari, J. (2004). Mitochondrial Fusion Intermediates Revealed in Vitro. *Science (80-.).* **305**, 1747–1752.

Meeusen, S., DeVay, R., Block, J., Cassidy-Stone, A., Wayson, S., McCaffery, J. M. and Nunnari, J. (2006). Mitochondrial Inner-Membrane Fusion and Crista Maintenance Requires the Dynamin-Related GTPase Mgm1. *Cell* **127**, 383–395.

Meng, W. and Takeichi, M. (2009). Adherens junction: molecular architecture and regulation. *Cold Spring Harb. Perspect. Biol.* **1**, 1–13.

Messina, A., Reina, S., Guarino, F. and De Pinto, V. (2012). VDAC isoforms in mammals. *Biochim. Biophys. Acta - Biomembr.* **1818**, 1466–1476.

Metallo, C. M. and Vander Heiden, M. G. (2013). Understanding Metabolic Regulation and Its Influence on Cell Physiology. *Mol. Cell* **49**, 388–398.

Metaxakis, A., Oehler, S., Klinakis, A. and Savakis, C. (2005). Minos as a genetic and genomic tool in Drosophila melanogaster. *Genetics* **171**, 571–81.

Miki, H. and Takenawa, T. (2003). Regulation of Actin Dynamics by WASP Family Proteins. *J. Biochem.* **134**, 309–313.

Millard, T. H. and Martin, P. (2008). Dynamic analysis of filopodial interactions during the zippering phase of Drosophila dorsal closure. *Development* **135**, 621–6.

Misaka, T., Miyashita, T. and Kubo, Y. (2002). Primary Structure of a Dynamin-related Mouse Mitochondrial GTPase and Its Distribution in Brain , Subcellular Localization , and Effect on Mitochondrial Morphology *. *J. Biol. Chem.* **277**, 15834–15842.

Misko, A., Jiang, S., Wegorzewska, I., Milbrandt, J. and Baloh, R. H. (2010). Mitofusin 2 is necessary for transport of axonal mitochondria and interacts with the Miro/Milton complex. *J. Neurosci.* **30**, 4232–4240.

Mitchell, P. (1966). Chemiosmotic coupling in oxidative and photosynthetic phosphorylation. *Biol. Rev. Camb. Philos. Soc.* **41**, 445–502.

Miyake, K. and McNeil, P. L. (1995). Vesicle accumulation and exocytosis at sites of plasma membrane disruption. *J. Cell Biol.* **131**, 1737–1745.

Miyake, K., McNeil, P. L., Suzuki, K., Tsunoda, R. and Sugai, N. (2001). An actin barrier to resealing. *J. Cell*

Sci. **114**, 3487–94.

Moreira, S., Stramer, B., Evans, I., Wood, W. and Martin, P. (2010). Prioritization of Competing Damage and Developmental Signals by Migrating Macrophages in the Drosophila Embryo. *Curr. Biol.* **20**, 464–470.

Morris, R. L. and Hollenbeck, P. J. (1995). Axonal transport of mitochondria along microtubules and F-actin in living vertebrate neurons. *J. Cell Biol.* **131**, 1315–1326.

Moyzis, A. G., Sadoshima, J. and Gustafsson, Å. B. (2015). Mending a broken heart: The role of mitophagy in cardioprotection. *Am. J. Physiol. - Hear. Circ. Physiol.* **308**, H183–H192.

Mozdy, A. D., McCaffery, J. M. and Shaw, J. M. (2000). Dnm1p GTPase-mediated mitochondrial fission is a multi-step process requiring the novel integral membrane component Fis1p. *J. Cell Biol.* **151**, 367–379.

Muliyil, S. and Narasimha, M. (2014). Mitochondrial ROS regulates cytoskeletal and mitochondrial remodeling to tune cell and tissue dynamics in a model for wound healing. *Dev. Cell* **28**, 239–52.

Munro, D. and Treberg, J. R. (2017). A radical shift in perspective: Mitochondria as regulators of reactive oxygen species. *J. Exp. Biol.* **220**, 1170–1180.

Muro, I., Berry, D. L., Huh, J. R., Chen, C. H., Huang, H., Yoo, S. J., Guo, M., Baehrecke, E. H. and Hay, B. A. (2006). The Drosphila caspase Ice is important for many apoptotic cell deaths and for spermatid individualization, a nonapoptotic process. *Development* **133**, 3305–3315.

Murphy, M. P. (1989). Slip and leak in mitochondrial oxidative phosphorylation. *BBA - Bioenerg.* **977**, 123–141.

Murphy, M. P. (2009). How mitochondria produce reactive oxygen species. *Biochem. J.* **417**, 1–13.

Nagata, N., Saito, C., Sakai, A., Kuroiwa, H. and Kuroiwa, T. (1999). Decrease in mitochondrial DNA and concurrent increase in plastid DNA in generative cells of Pharbitis nil during pollen development. *Eur. J. Cell Biol.* **78**, 241–248.

Nagy, P., Varga, Á., Kovács, A. L., Takáts, S. and Juhász, G. (2015). How and why to study autophagy in Drosophila: it's more than just a garbage chute. *Methods* **75**, 151–61.

Nakada, K., Sato, A. and Hayashi, J. I. (2009). Mitochondrial functional complementation in mitochondrial DNA-based diseases. *Int. J. Biochem. Cell Biol.* **41**, 1907–1913.

Nakamura, M., Verboon, J. M. and Parkhurst, S. M. (2017). Prepatterning by RhoGEFs governs Rho GTPase spatiotemporal dynamics during wound repair. *J. Cell Biol.* **216**, 3959–3969.

Nakamura, M., Dominguez, A. N. M., Decker, J. R., Hull, A. J., Verboon, J. M. and Parkhurst, S. M. (2018). Into the breach: How cells cope with wounds. *Open Biol.* **8**,.

Narciso, C., Wu, Q., Brodskiy, P., Garston, G., Baker, R., Fletcher, A. and Zartman, J. (2015). Patterning of wound-induced intercellular Ca2+ flashes in a developing epithelium. *Phys. Biol.* **12**, 56005.

Narumiya, S., Ishizaki, T. and Watanabe, N. (1997). Rho effecters and reorganization of actin cytoskeleton.

FEBS Lett. **410**, 68–72.

Navarro-Requena, C., Pérez-Amodio, S., Castano, O. and Engel, E. (2018). Wound healing-promoting effects stimulated by extracellular calcium and calcium-releasing nanoparticles on dermal fibroblasts. *Nanotechnology* **29**,.

Naylor, K., Ingerman, E., Okreglak, V., Marino, M., Hinshaw, J. E. and Nunnari, J. (2006). Mdv1 interacts with assembled Dnm1 to promote mitochondrial division. *J. Biol. Chem.* **281**, 2177–2183.

Nicholls, D. G. and Chalmers, S. (2004). The integration of mitochondrial calcium transport and storage. *J. Bioenerg. Biomembr.* **36**, 277–281.

Niemann, A., Ruegg, M., La Padula, V., Schenone, A. and Suter, U. (2005). Ganglioside-induced differentiation associated protein 1 is a regulator of the mitochondrial network: New implications for Charcot-Marie-Tooth disease. *J. Cell Biol.* **170**, 1067–1078.

Niethammer, P., Grabher, C., Look, A. T. and Mitchison, T. J. (2009a). A tissue-scale gradient of hydrogen peroxide mediates rapid wound detection in zebrafish. *Nature* **459**, 996–999.

Niethammer, P., Grabher, C., Look, A. T. and Mitchison, T. J. (2009b). A tissue-scale gradient of hydrogen peroxide mediates rapid wound detection in zebrafish. *Nature* **459**, 996–999.

Nikolaisen, J., Nilsson, L. I. H., Pettersen, I. K. N., Willems, P. H. G. M., Lorens, J. B., Koopman, W. J. H. and Tronstad, K. J. (2014). Automated quantification and integrative analysis of 2D and 3D mitochondrial shape and network properties. *PLoS One* **9**, e101365.

Ninov, N., Chiarelli, D. A. and Martín-Blanco, E. (2007). Extrinsic and intrinsic mechanisms directing epithelial cell sheet replacement during Drosophila metamorphosis. *Development* **134**, 367–379.

Nisoli, E., Clementi, E., Paolucci, C., Cozzi, V., Tonello, C., Sciorati, C., Bracale, R., Valerio, A., Francolini, M., Moncada, S., et al. (2003). Mitochondrial biogenesis in mammals: The role of endogenous nitric oxide. *Science (80-.).* **299**, 896–899.

Novak, I., Kirkin, V., McEwan, D. G., Zhang, J., Wild, P., Rozenknop, A., Rogov, V., Löhr, F., Popovic, D., Occhipinti, A., et al. (2010). Nix is a selective autophagy receptor for mitochondrial clearance. *EMBO Rep.* **11**, 45–51.

Oda, H. and Tsukita, S. (1999). Nonchordate classic cadherins have a structurally and functionally unique domain that is absent from chordate classic cadherins. *Dev. Biol.* **216**, 406–422.

Oeding, S. J., Majstrowicz, K., Hu, X. P., Schwarz, V., Freitag, A., Honnert, U., Nikolaus, P. and Bähler, M. (2018). Identification of Miro1 and Miro2 as mitochondrial receptors for myosin XIX. *J. Cell Sci.* **131**,.

Olichon, A., Baricault, L., Gas, N., Guillou, E., Valette, A., Belenguer, P. and Lenaers, G. (2003). Loss of OPA1 perturbates the mitochondrial inner membrane structure and integrity, leading to cytochrome c release and apoptosis. *J. Biol. Chem.* **278**, 7743–7746.

Otera, H., Wang, C., Cleland, M. M., Setoguchi, K., Yokota, S., Youle, R. J. and Mihara, K. (2010). Mff is an

essential factor for mitochondrial recruitment of Drp1 during mitochondrial fission in mammalian cells. *J. Cell Biol.* **191**, 1141–1158.

Otsu, N. (1979). A Threshold Selection Method from Gray-Level Histograms. *IEEE Trans. Syst. Man. Cybern.* **9**, 62–66.

Otsuga, D., Keegan, B. R., Brisch, E., Thatcher, J. W., Hermann, G. J., Bleazard, W. and Shaw, J. M. (1998). The dynamin-related GTPase, Dnm1p, controls mitochondrial morphology in yeast. *J. Cell Biol.* **143**, 333–49.

Paillard, M., Csordás, G., Szanda, G., Golenár, T., Debattisti, V., Bartok, A., Wang, N., Moffat, C., Seifert, E. L., Spät, A., et al. (2017). Tissue-Specific Mitochondrial Decoding of Cytoplasmic Ca 2+ Signals Is Controlled by the Stoichiometry of MICU1/2 and MCU. *Cell Rep.* **18**, 2291–2300.

Pakyari, M., Farrokhi, A., Maharlooei, M. K. and Ghahary, A. (2013). Critical Role of Transforming Growth Factor Beta in Different Phases of Wound Healing. *Adv. Wound Care* **2**, 215–224.

Palade, G. E. (1952). The fine structure of mitochondria. *Anat. Rec.* **114**, 427–451.

Palmer, C. S., Osellame, L. D., Laine, D., Koutsopoulos, O. S., Frazier, A. E. and Ryan, M. T. (2011). MiD49 and MiD51, new components of the mitochondrial fission machinery. *EMBO Rep.* **12**, 565–73.

Palmer, C. S., Elgass, K. D., Parton, R. G., Osellame, L. D., Stojanovski, D. and Ryan, M. T. (2013). Adaptor proteins MiD49 and MiD51 can act independently of Mff and Fis1 in Drp1 recruitment and are specific for mitochondrial fission. *J. Biol. Chem.* **288**, 27584–27593.

Palmieri, L., Pardo, B., Lasorsa, F. M., del Arco, A., Kobayashi, K., Iijima, M., Runswick, M. J., Walker, J. E., Saheki, T., Satrústegui, J., et al. (2001). Citrin and aralar1 are Ca2+-stimulated aspartate/glutamate transporters in mitochondria. *EMBO J.* **20**, 5060–5069.

Palta, S., Saroa, R. and Palta, A. (2014). Overview of the coagulation system. *Indian J. Anaesth.* **58**, 515–523.

Palty, R., Silverman, W. F., Hershfinkel, M., Caporale, T., Sensi, S. L., Parnis, J., Nolte, C., Fishman, D., Shoshan-Barmatz, V., Herrmann, S., et al. (2010). NCLX is an essential component of mitochondrial Na+/Ca 2+ exchange. *Proc. Natl. Acad. Sci. U. S. A.* **107**, 436–441.

Park, J. E. and Barbul, A. (2004). Understanding the role of immune regulation in wound healing. *Am. J. Surg.* **187**, S11–S16.

Pastar, I., Stojadinovic, O., Yin, N. C., Ramirez, H., Nusbaum, A. G., Sawaya, A., Patel, S. B., Khalid, L., Isseroff, R. R. and Tomic-Canic, M. (2014). Epithelialization in Wound Healing: A Comprehensive Review. *Adv. Wound Care* **3**, 445–464.

Pedrola, L., Espert, A., Wu, X., Claramunt, R., Shy, M. E. and Palau, F. (2005). GDAP1, the protein causing Charcot-Marie-Tooth disease type 4A, is expressed in neurons and is associated with mitochondria. *Hum. Mol. Genet.* **14**, 1087–1094.

Peiris-Pagès, M., Bonuccelli, G., Sotgia, F. and Lisanti, M. P. (2018). Mitochondrial fission as a driver of

stemness in tumor cells: mDIVI1 inhibits mitochondrial function, cell migration and cancer stem cell (CSC) signalling. *Oncotarget* **9**, 13254–13275.

Perkins, G. A., Song, J. Y., Tarsa, L., Deerinck, T. J., Ellisman, M. H. and Frey, T. G. (1998). Electron tomography of mitochondria from brown adipocytes reveals crista junctions. *J. Bioenerg. Biomembr.* **30**, 431–442.

Perocchi, F., Gohil, V. M., Girgis, H. S., Bao, X. R., McCombs, J. E., Palmer, A. E. and Mootha, V. K. (2010). MICU1 encodes a mitochondrial EF hand protein required for Ca2+ uptake. *Nature* **467**, 291–296.

Pfanner, N., Wiedemann, N., Meisinger, C. and Lithgow, T. (2004). Assembling the mitochondrial outer membrane. *Nat. Struct. Mol. Biol.* **11**, 1044–1048.

Pierce, G. F., Mustoe, T. A., Altrock, B. W., Deuel, T. F. and Thomason, A. (1991). Role of platelet-derived growth factor in wound healing. *J. Cell. Biochem.* **45**, 319–326.

Pinto, M. C. X., Kihara, A. H., Goulart, V. A. M., Tonelli, F. M. P., Gomes, K. N., Ulrich, H. and Resende, R. R. (2015). Calcium signaling and cell proliferation. *Cell. Signal.* **27**, 2139–2149.

Plotnikov, E. Y., Babenko, V. A., Silachev, D. N., Zorova, L. D., Khryapenkova, T. G., Savchenko, E. S., Pevzner, I. B. and Zorov, D. B. (2015). Intercellular transfer of mitochondria. *Biochem.* **80**, 542–548.

Plovanich, M., Bogorad, R. L., Sancak, Y., Kamer, K. J., Strittmatter, L., Li, A. A., Girgis, H. S., Kuchimanchi, S., De Groot, J., Speciner, L., et al. (2013). MICU2, a Paralog of MICU1, Resides within the Mitochondrial Uniporter Complex to Regulate Calcium Handling. *PLoS One* **8**,.

Pokutta, S., Herrenknecht, K., Kemler, R. and Engel, J. (1994). Conformational changes of the recombinant extracellular domain of E-cadherin upon calcium binding. *Eur. J. Biochem.* **223**, 1019–1026.

Pollard, T. D. (2010). Mechanics of cytokinesis in eukaryotes. *Curr. Opin. Cell Biol.* **22**, 50–56.

Poot, M., Zhang, Y. Z., Krämer, J. A., Wells, K. S., Jones, L. J., Hanzel, D. K., Lugade, A. G., Singer, V. L. and Haugland, R. P. (1996). Analysis of mitochondrial morphology and function with novel fixable fluorescent stains. *J. Histochem. Cytochem.* **44**, 1363–1372.

Pozzan, T., Bragadin, M. and Azzone, G. F. (1977). Disequilibrium between Steady-State ca2+ Accumulation Ratio and Membrane Potential in Mitochondria. Pathway and Role of ca2+ Efflux. *Biochemistry* **16**, 5618–5625.

Prudent, J. and McBride, H. M. (2016). Mitochondrial Dynamics: ER Actin Tightens the Drp1 Noose. *Curr. Biol.* **26**, R207-9.

Prudent, J., Popgeorgiev, N., Bonneau, B., Thibaut, J., Gadet, R., Lopez, J., Gonzalo, P., Rimokh, R., Manon, S., Houart, C., et al. (2013). Bcl-wav and the mitochondrial calcium uniporter drive gastrula morphogenesis in zebrafish. *Nat. Commun.* **4**,.

Prudent, J., Popgeorgiev, N., Gadet, R., Deygas, M., Rimokh, R. and Gillet, G. (2016). Mitochondrial Ca2+ uptake controls actin cytoskeleton dynamics during cell migration. *Sci. Rep.* **6**, 36570.

Puigserver, P., Wu, Z., Park, C. W., Graves, R., Wright, M. and Spiegelman, B. M. (1998). A Cold-Inducible Coactivator of Nuclear Receptors Linked to Adaptive Thermogenesis. *Cell* **92**, 829–839.

Pyle, A., Hudson, G., Wilson, I. J., Coxhead, J., Smertenko, T., Herbert, M., Santibanez-Koref, M. and Chinnery, P. F. (2015). Extreme-Depth Re-sequencing of Mitochondrial DNA Finds No Evidence of Paternal Transmission in Humans. *PLoS Genet.* **11**, 1–12.

Quintero, O. A., DiVito, M. M., Adikes, R. C., Kortan, M. B., Case, L. B., Lier, A. J., Panaretos, N. S., Slater, S. Q., Rengarajan, M., Feliu, M., et al. (2009). Human Myo19 Is a Novel Myosin that Associates with Mitochondria. *Curr. Biol.* **19**, 2008–2013.

Rabello, F. B., Souza, C. D. and Farina, J. A. (2014). Update on hypertrophic scar treatment. *Clinics* **69**, 565–573.

Raffaello, A., De Stefani, D., Sabbadin, D., Teardo, E., Merli, G., Picard, A., Checchetto, V., Moro, S., Szabò, I. and Rizzuto, R. (2013). The mitochondrial calcium uniporter is a multimer that can include a dominant-negative pore-forming subunit. *EMBO J.* **32**, 2362–2376.

Rahman, M. and Kylsten, P. (2011). Rhomboid-7 over-expression results in Opa1-like processing and malfunctioning mitochondria. *Biochem. Biophys. Res. Commun.* **414**, 315–320.

Rämet, M., Lanot, R., Zachary, D. and Manfruelli, P. (2002). JNK Signaling Pathway Is Required for Efficient Wound Healing in Drosophila. *Dev. Biol.* **241**, 145–156.

Rand, M. D., Kearney, A. L., Dao, J. and Clason, T. (2010). Permeabilization of Drosophila embryos for introduction of small molecules. *Insect Biochem. Mol. Biol.* **40**, 792–804.

Rapaport, D. (2002). Biogenesis of the mitochondrial TOM complex. *Trends Biochem. Sci.* **27**, 191–197.

Rastogi, A., Joshi, P., Contreras, E. and Gama, V. (2019). Remodeling of mitochondrial morphology and function: an emerging hallmark of cellular reprogramming. *Cell Stress* **3**, 181–194.

Ray, P. D., Huang, B. W. and Tsuji, Y. (2012). Reactive oxygen species (ROS) homeostasis and redox regulation in cellular signaling. *Cell. Signal.* **24**, 981–990.

Razzell, W., Wood, W. and Martin, P. (2011). Swatting flies: Modelling wound healing and inflammation in Drosophila. *DMM Dis. Model. Mech.* **4**, 569–574.

Razzell, W., Evans, I. R. R., Martin, P. and Wood, W. (2013). Calcium Flashes Orchestrate the Wound Inflammatory Response through DUOX Activation and Hydrogen Peroxide Release. *Curr. Biol.* **23**, 424–429.

Razzell, W., Wood, W. and Martin, P. (2014). Recapitulation of morphogenetic cell shape changes enables wound re-epithelialisation. *Development* **141**, 1814–20.

Reddy, P. H. (2014). Increased mitochondrial fission and neuronal dysfunction in Huntington's disease: implications for molecular inhibitors of excessive mitochondrial fission. *Drug Discov. Today* **19**, 951–955.

Reddy, P. H., Reddy, T. P., Manczak, M., Calkins, M. J., Shirendeb, U. and Mao, P. (2011). Dynamin-related protein 1 and mitochondrial fragmentation in neurodegenerative diseases. *Brain Res. Rev.* **67**, 103–118.

Restrepo, S. and Basler, K. (2016). Drosophila wing imaginal discs respond to mechanical injury via slow InsP3R-mediated intercellular calcium waves. *Nat. Commun.* **7**, 12450.

Rhee, S. G., Yang, K.-S., Kang, S. W., Woo, H. A. and Chang, T.-S. (2005). Controlled Elimination of Intracellular H2 O2: Regulation of Peroxiredoxin, Catalase, and Glutathione Peroxidase via Post-translational Modification. *Antioxid. Redox Signal.* **7**, 619–626.

Rizzuto, R., Simpson, A. W. M., Brini, M. and Pozzan, T. (1992). Rapid changes of mitochondrial Ca2+ revealed by specifically targeted recombinant aequorin. *Nature* **358**, 325–327.

Rizzuto, R., Brini, M., Murgia, M. and Pozzan, T. (1993). Microdomains with high Ca2+ close to IP3-sensitive channels that are sensed by neighboring mitochondria. *Science (80-.).* **262**, 744–747.

Rizzuto, R., Brini, M., Pizzo, P., Murgia, M. and Pozzan, T. (1995). Chimeric green fluorescent protein as a tool for visualizing subcellular organelles in living cells. *Curr. Biol.* **5**, 635–42.

Rizzuto, R., Pinton, P., Carrington, W., Fay, F. S., Fogarty, K. E., Lifshitz, L. M., Tuft, R. A. and Pozzan, T. (1998). Close contacts with the endoplasmic reticulum as determinants of mitochondrial Ca2+ responses. *Science (80-.).* **280**, 1763–1766.

Rizzuto, R., De Stefani, D., Raffaello, A. and Mammucari, C. (2012). Mitochondria as sensors and regulators of calcium signalling. *Nat. Rev. Mol. Cell Biol.* **13**, 566–578.

Rohn, J. L., Patel, J. V., Neumann, B., Bulkescher, J., Mchedlishvili, N., McMullan, R. C., Quintero, O. A., Ellenberg, J. and Baum, B. (2014). Myo19 ensures symmetric partitioning of mitochondria and coupling of mitochondrial segregation to cell division. *Curr. Biol.* **24**, 2598–605.

Rojo, M., Legros, F., Chateau, D. and Lombès, A. (2002). Membrane topology and mitochondrial targeting of mitofusins, ubiquitous mammalian homologs of the transmembrane GTPase Fzo. *J. Cell Sci.* **115**, 1663–74.

Rokosova, B. and Peter Bentley, J. (1986). Effect of calcium on cell proliferation and extracellular matrix synthesis in arterial smooth muscle cells and dermal fibroblasts. *Exp. Mol. Pathol.* **44**, 307–317.

Roote, J. and Prokop, A. (2013). How to design a genetic mating scheme: a basic training package for Drosophila genetics. *G3 (Bethesda).* 353–358.

Rosenblatt, J., Raff, M. C. and Cramer, L. P. (2001). An epithelial cell destined for apoptosis signals its neighbors to extrude it by an actin- and myosin-dependent mechanism. *Curr. Biol.* **11**, 1847–1857.

Rosenkilde, M. M. and Schwartz, T. W. (2004). The chemokine system - A major regulator of angiogenesis in health and disease. *Apmis* **112**, 481–495.

Rothenberg, K. E. and Fernandez-Gonzalez, R. (2019). Forceful closure: cytoskeletal networks in embryonic wound repair. *Mol. Biol. Cell* **30**, 1353–1358.

Rovira-Llopis, S., Bañuls, C., Diaz-Morales, N., Hernandez-Mijares, A., Rocha, M. and Victor, V. M. (2017). Mitochondrial dynamics in type 2 diabetes: Pathophysiological implications. *Redox Biol.* **11**, 637–645.

Roy, M., Reddy, P. H., Iijima, M. and Sesaki, H. (2015). Mitochondrial division and fusion in metabolism. *Curr. Opin. Cell Biol.* **33**, 111–8.

Royou, A., Sullivan, W. and Karess, R. (2002). Cortical recruitment of nonmuscle myosin II in early syncytial Drosophila embryos: Its role in nuclear axial expansion and its regulation by Cdc2 activity. *J. Cell Biol.* **158**, 127–137.

Russo, J. M., Florian, P., Shen, L., Graham, W. V., Tretiakova, M. S., Gitter, A. H., Mrsny, R. J. and Turner, J. R. (2005). Distinct temporal-spatial roles for rho kinase and myosin light chain kinase in epithelial purse-string wound closure. *Gastroenterology* **128**, 987–1001.

Russo, G. J., Louie, K., Wellington, A., Macleod, G. T., Hu, F., Panchumarthi, S. and Zinsmaier, K. E. (2009). Drosophila Miro is required for both anterograde and retrograde axonal mitochondrial transport. *J. Neurosci.* **29**, 5443–5455.

Rutter, G. A., Theler, J. M., Murgia, M., Wollheim, C. B., Pozzan, T. and Rizzuto, R. (1993). Stimulated Ca2+ influx raises mitochondrial free Ca2+ to supramicromolar levels in a pancreatic ??-cell line: Possible role in glucose and agonist-induced insulin secretion. *J. Biol. Chem.* **268**, 22385–22390.

Ryu, S.-Y., Beutner, G., Dirksen, R. T., Kinnally, K. W. and Sheu, S.-S. (2010). Mitochondrial ryanodine receptors and other mitochondrial Ca 2+ permeable channels. *FEBS Lett.* **584**, 1948–1955.

Sagan, L. (1967). On the origin of mitosing cells. *J. Theor. Biol.* **14**, 225-IN6.

Salazar-Roa, M. and Malumbres, M. (2017). Fueling the Cell Division Cycle. *Trends Cell Biol.* **27**, 69–81.

Sammak, P. J., Hinman, L. E., Tran, P. O., Sjaastad, M. D. and Machen, T. E. (1997). How do injured cells communicate with the surviving cell monolayer? *J. Cell Sci.* **110 (Pt 4**, 465–75.

Sancak, Y., Markhard, A. L., Kitami, T., Kovacs-Bogdan, E., Kamer, K. J., Udeshi, N. D., Carr, S. A., Chaudhuri, D., Clapham, D. E., Li, A. A., et al. (2013). EMRE Is an Essential Component of the Mitochondrial Calcium Uniporter Complex. *Science (80-.).* **342**, 1379–1382.

Sanchez, M. C., Lancel, S., Boulanger, E., Neviere, R., Cano Sanchez, M., Lancel, S., Boulanger, E. and Neviere, R. (2018). Targeting Oxidative Stress and Mitochondrial Dysfunction in the Treatment of Impaired Wound Healing: A Systematic Review. *Antioxidants* **7**, 98.

Sandoval, H., Yao, C.-K., Chen, K., Jaiswal, M., Donti, T., Lin, Y. Q., Bayat, V., Xiong, B., Zhang, K., David, G., et al. (2014). Mitochondrial fusion but not fission regulates larval growth and synaptic development through steroid hormone production. *Elife* **3**, 1–23.

Saotome, M., Safiulina, D., Szabadkai, G., Das, S., Fransson, A., Aspenstrom, P., Rizzuto, R. and Hajnóczky, G. (2008). Bidirectional Ca2+-dependent control of mitochondrial dynamics by the Miro GTPase. *Proc. Natl. Acad. Sci. U. S. A.* **105**, 20728–33.

Schäfer, M. and Werner, S. (2008). Oxidative stress in normal and impaired wound repair. *Pharmacol. Res.* **58**, 165–171.

Scharwey, M., Tatsuta, T. and Langer, T. (2013). Mitochondrial lipid transport at a glance. *J. Cell Sci.* **126**, 5317–5323.

Schenkel, L. C. and Bakovic, M. (2014). Formation and regulation of mitochondrial membranes. *Int. J. Cell Biol.* **2014**,.

Schindelin, J., Arganda-Carreras, I., Frise, E., Kaynig, V., Longair, M., Pietzsch, T., Preibisch, S., Rueden, C., Saalfeld, S., Schmid, B., et al. (2012). Fiji: an open-source platform for biological-image analysis. *Nat. Methods* **9**, 676–82.

Scholpa, N. E. and Schnellmann, R. G. (2017). Mitochondrial-based therapeutics for the treatment of spinal cord injury: Mitochondrial biogenesis as a potential pharmacological target. *J. Pharmacol. Exp. Ther.* **363**, 303–313.

Schuler, M. H., Lewandowska, A., Di Caprio, G., Skillern, W., Upadhyayula, S., Kirchhausen, T., Shaw, J. M. and Cunniff, B. (2017). Miro1-mediated mitochondrial positioning shapes intracellular energy gradients required for cell migration. *Mol. Biol. Cell* **28**, 2159–2169.

Schulman, V. K., Folker, E. S. and Baylies, M. K. (2013). A method for reversible drug delivery to internal tissues of Drosophila embryos. *Fly (Austin).* **7**, 193–203.

Schultz, G., Clark, W. and Rotatori, D. S. (1991). EGF and TGF-α in wound healing and repair. *J. Cell. Biochem.* **45**, 346–352.

Schwarz, T. L. (2013). Mitochondrial trafficking in neurons. *Cold Spring Harb. Perspect. Med.* **3**, 1–16.

Scorrano, L., Ashiya, M., Buttle, K., Weiler, S., Oakes, S. A., Mannella, C. A. and Korsmeyer, S. J. (2002). <Dev Cell 2002 Scorrano-1.pdf>. **2**, 55–67.

Scott, I. and Youle, R. J. (2010). Mitochondrial fission and fusion. *Essays Biochem.* **47**, 85–98.

Sebastián, D., Palacín, M. and Zorzano, A. (2017). Mitochondrial Dynamics: Coupling Mitochondrial Fitness with Healthy Aging. *Trends Mol. Med.* **23**, 201–215.

Senior, A. E., Nadanaciva, S. and Weber, J. (2002). The molecular mechanism of ATP synthesis by F_1F_0-ATP synthase. *Biochim. Biophys. Acta - Bioenerg.* **1553**, 188–211.

Seo, B. J., Yoon, S. H. and Do, J. T. (2018). Mitochondrial dynamics in stem cells and differentiation. *Int. J. Mol. Sci.* **19**,.

Shabir, S. and Southgate, J. (2008). Calcium signalling in wound-responsive normal human urothelial cell monolayers. *Cell Calcium* **44**, 453–464.

Shannon, E. K., Stevens, A., Edrington, W., Zhao, Y., Jayasinghe, A. K., Page-McCaw, A. and Hutson, M. S. (2017). Multiple Mechanisms Drive Calcium Signal Dynamics around Laser-Induced Epithelial Wounds.

Biophys. J. **113**, 1623–1635.

Shen, L. (2012). Tight junctions on the move: Molecular mechanisms for epithelial barrier regulation. *Ann. N. Y. Acad. Sci.* **1258**, 9–18.

Shneyer, B. I., Ušaj, M. and Henn, A. (2016). Myo19 is an outer mitochondrial membrane motor and effector of starvation-induced filopodia. *J. Cell Sci.* **129**, 543–556.

Shoshan-Barmatz, V., De Pinto, V., Zweckstetter, M., Raviv, Z., Keinan, N. and Arbel, N. (2010). VDAC, a multi-functional mitochondrial protein regulating cell life and death. *Mol. Aspects Med.* **31**, 227–285.

Simula, L., Pacella, I., Colamatteo, A., Matarese, G., Piconese, S., Simula, L., Pacella, I., Colamatteo, A., Procaccini, C., Cancila, V., et al. (2018). Drp1 Controls Effective T Cell Immune-Surveillance by Regulating T Cell Migration , Proliferation , and cMyc-Dependent Metabolic Reprogramming Article Drp1 Controls Effective T Cell Immune-Surveillance by Regulating T Cell Migration , Proliferation , and . *CellReports* **25**, 3059-3073.e10.

Sit, S.-T. and Manser, E. (2011). Rho GTPases and their role in organizing the actin cytoskeleton. *J. Cell Sci.* **124**, 679–83.

Sjöstrand, F. S. (1956). The Ultrastructure of Cells as Revealed by the Electron Microscope. In *International Review of cytology*, pp. 455–533.

Smedley, B. M. J. and Stanisstreet, M. (1984). Scanning electron microscopy of wound healing in rat embryos. *J. Embryol. exp. Morph.* **117**, 109–117.

Smirnova, E., Shurland, D. L., Ryazantsev, S. N. and Van Der Bliek, A. M. (1998). A human dynamin-related protein controls the distribution of mitochondria. *J. Cell Biol.* **143**, 351–358.

Smirnova, E., Griparic, L., Shurland, D.-L. and van der Bliek, A. M. (2001). Dynamin-related Protein Drp1 Is Required for Mitochondrial Division in Mammalian Cells. *Mol. Biol. Cell* **12**, 2245–2256.

Sodmergen, Zhang, Q., Zhang, Y., Sakamoto, W. and Kuroiwa, T. (2002). Reduction in amounts of mitochondrial DNA in the sperm cells as a mechanism for maternal inheritance in Hordeum vulgare. *Planta* **216**, 235–244.

Song, Z., Chen, H., Fiket, M., Alexander, C. and Chan, D. C. (2007). OPA1 processing controls mitochondrial fusion and is regulated by mRNA splicing, membrane potential, and Yme1L. *J. Cell Biol.* **178**, 749–755.

Sonnemann, K. J. and Bement, W. M. (2011). Wound repair: toward understanding and integration of single-cell and multicellular wound responses. *Annu. Rev. Cell Dev. Biol.* **27**, 237–63.

Sousa, J. S., D'Imprima, E. and Vonck, J. (2018). Mitochondrial Respiratory Chain Complexes. In *Subcellular Biochemistry*, pp. 167–227.

Spees, J. L., Olson, S. D., Whitney, M. J. and Prockop, D. J. (2006). Mitochondrial transfer between cells can rescue aerobic respiration. *Proc. Natl. Acad. Sci. U. S. A.* **103**, 1283–1288.

Spelbrink, J. N. (2010). Functional organization of mammalian mitochondrial DNA in nucleoids: History, recent developments, and future challenges. *IUBMB Life* **62**, 19–32.

Spinelli, J. B. and Haigis, M. C. (2018). The multifaceted contributions of mitochondria to cellular metabolism. *Nat. Cell Biol.* **20**, 745–754.

Spradling, A. C., Stern, D., Beaton, A., Rhem, E. J., Laverty, T., Mozden, N., Misra, S. and Rubin, G. M. (1999). The Berkeley Drosophila Genome Project gene disruption project: Single P-element insertions mutating 25% of vital Drosophila genes. *Genetics* **153**, 135–177.

Srinivasula, S. M., Gupta, S., Datta, P., Zhang, Z. J., Hegde, R., Cheong, N. E., Fernandes-Alnemri, T. and Alnemri, E. S. (2003). Inhibitor of apoptosis proteins are substrates for the mitochondrial serine protease Omi/HtrA2. *J. Biol. Chem.* **278**, 31469–31472.

Stanisstreet, M., Wakely, J. and England, M. A. (1980). Scanning electron microscopy of wound healing in Xenopus and chicken embryos. *J. Embryol. Exp. Morphol.* **59**, 341–53.

Steinhardt, R., Bi, G. and Alderton, J. (1994). Cell membrane resealing by a vesicular mechanism similar to neurotransmitter release. *Science (80-.).* **263**, 390–393.

Stojanovski, D., Koutsopoulos, O. S., Okamoto, K. and Ryan, M. T. (2004). Levels of human Fis1 at the mitochondrial outer membrane regulate mitochondrial morphology. *J. Cell Sci.* **117**, 1201–1210.

Stramer, B., Wood, W., Galko, M. J., Redd, M. J., Jacinto, A., Parkhurst, S. M. and Martin, P. (2005). Live imaging of wound inflammation in Drosophila embryos reveals key roles for small GTPases during in vivo cell migration. *J. Cell Biol.* **168**, 567–573.

Südhof, T. C. (2012). Calcium control of neurotransmitter release. *Cold Spring Harb. Perspect. Biol.* **4**,.

Sun, H. Q., Yamamoto, M., Mejillano, M. and Yin, H. L. (1999). Gelsolin, a Multifunctional Actin Regulatory Protein. *J. Biol. Chem.* **274**, 33179–33182.

Sung, Y. J., Sung, Z., Ho, C. L., Lin, M. Te, Wang, J. S., Yang, S. C., Chen, Y. J. and Lin, C. H. (2003). Intercellular calcium waves mediate preferential cell growth toward the wound edge in polarized hepatic cells. *Exp. Cell Res.* **287**, 209–218.

Sung, J. Y., Engmann, O., Teylan, M. A., Nairn, A. C., Greengard, P. and Kim, Y. (2008). WAVE1 controls neuronal activity-induced mitochondrial distribution in dendritic spines. *Proc. Natl. Acad. Sci. U. S. A.* **105**, 3112–3116.

Sutovsky, P., Navara, C. S. and Schatten, G. (1996). Fate of the Sperm Mitochondria, and the Incorporation, Conversion, and Disassembly of the Sperm Tail Structures during Bovine Fertilization1. *Biol. Reprod.* **55**, 1195–1205.

Sutovsky, P., Moreno, R. D., Ramalho-Santos, J., Dominko, T., Simerly, C. and Schatten, G. (1999). Ubiquitin tag for sperm mitochondria. *Nature* **402**, 371–372.

Suzuki, K., Kirisako, T., Kamada, Y., Mizushima, N., Noda, T. and Ohsumi, Y. (2001). The pre-autophagosomal

structure organized by concerted functions of APG genes is essential for autophagosome formation. *EMBO J.* **20**, 5971–5981.

Szabadkai, G. and Duchen, M. R. (2008). Mitochondria: the hub of cellular Ca2+ signaling. *Physiology (Bethesda).* **23**, 84–94.

Szabadkai, G., Simoni, A. M., Chami, M., Wieckowski, M. R., Youle, R. J. and Rizzuto, R. (2004). Drp-1-dependent division of the mitochondrial network blocks intraorganellar Ca2+ waves and protects against Ca 2+-mediated apoptosis. *Mol. Cell* **16**, 59–68.

Taguchi, N., Ishihara, N., Jofuku, A., Oka, T. and Mihara, K. (2007). Mitotic phosphorylation of dynamin-related GTPase Drp1 participates in mitochondrial fission. *J. Biol. Chem.* **282**, 11521–11529.

Takeichi, M. (1988). The cadherins: cell-cell adhesion molecules controlling animal morphogenesis. *Development* **102**, 639–55.

Tam, C., Idone, V., Devlin, C., Fernandes, M. C., Flannery, A., He, X., Schuchman, E., Tabas, I. and Andrews, N. W. (2010). Exocytosis of acid sphingomyelinase by wounded cells promotes endocytosis and plasma membrane repair. *J. Cell Biol.* **189**, 1027–1038.

Tamada, M., Perez, T. D., Nelson, W. J. and Sheetz, M. P. (2007). Two distinct modes of myosin assembly and dynamics during epithelial wound closure. *J. Cell Biol.* **176**, 27–33.

Tan, W. and Colombini, M. (2007). VDAC closure increases calcium ion flux. *Biochim. Biophys. Acta - Biomembr.* **1768**, 2510–2515.

Tanaka, A., Cleland, M. M., Xu, S., Narendra, D. P., Suen, D., Karbowski, M. and Youle, R. J. (2010). Proteasome and p97 mediate mitophagy and degradation of mitofusins induced by Parkin. *J. Cell Biol.* **191**, 1367–1380.

Tang, S., Wang, X., Shen, Q., Yang, X., Yu, C., Cai, C., Cai, G., Meng, X. and Zou, F. (2015). Mitochondrial Ca 2+ uniporter is critical for store-operated Ca 2+ entry-dependent breast cancer cell migration. *Biochem. Biophys. Res. Commun.* **458**, 186–193.

Tennessen, J. M., Baker, K. D., Lam, G., Evans, J. and Thummel, C. S. (2011). The Drosophila estrogen-related receptor directs a metabolic switch that supports developmental growth. *Cell Metab.* **13**, 139–48.

Tennessen, J. M., Bertagnolli, N. M., Evans, J., Sieber, M. H., Cox, J. and Thummel, C. S. (2014). Coordinated metabolic transitions during Drosophila embryogenesis and the onset of aerobic glycolysis. *G3 (Bethesda).* **4**, 839–50.

Terasaki, M., Miyake, K. and McNeil, P. L. (1997). Large plasma membrane disruptions are rapidly resealed by Ca2+- dependent vesicle-vesicle fusion events. *J. Cell Biol.* **139**, 63–74.

Thiruvoth, F., Mohapatra, D., Sivakumar, D., Chittoria, R. and Nandhagopal, V. (2015). Current concepts in the physiology of adult wound healing. *Plast. Aesthetic Res.* **2**, 250.

Thompson, W. E., Ramalho-Santos, J. and Sutovsky, P. (2003). Ubiquitination of Prohibitin in Mammalian

Sperm Mitochondria: Possible Roles in the Regulation of Mitochondrial Inheritance and Sperm Quality Control1. *Biol. Reprod.* **69**, 254–260.

Thurmond, J., Goodman, J. L., Strelets, V. B., Attrill, H., Gramates, L. S. S., Marygold, S. J., Matthews, B. B., Millburn, G., Antonazzo, G., Trovisco, V., et al. (2019). FlyBase 2.0: the next generation. *Nucleic Acids Res.* **47**, D759–D765.

Tieu, Q. and Nunnari, J. (2000). Mdv1p is a WD repeat protein that interacts with the dynamin-related GTPase, Dnm1p, to trigger mitochondrial division. *J. Cell Biol.* **151**, 353–365.

Togo, T., Alderton, J. M., Bi, G. Q. and Steinhardt, R. A. (1999). The mechanism of facilitated cell membrane resealing. *J. Cell Sci.* **112**, 719–731.

Togo, T., Krasieva, T. B. and Steinhardt, R. A. (2000). A Decrease in Membrane Tension Precedes Successful Cell-Membrane Repair. *Mol. Biol. Cell* **11**, 4339–4346.

Tondera, D., Czauderna, F., Paulick, K., Schwarzer, R., Kaufmann, J. and Santel, A. (2005). The mitochondrial protein MTP18 contributes to mitochondrial fission in mammalian cells. *J. Cell Sci.* **118**, 3049–3059.

Tonelli, F. M. P., Santos, A. K., Gomes, D. A., da Silva, S. L., Gomes, K. N., Ladeira, L. O. and Resende, R. R. (2012). Stem Cells and Calcium Signaling. In *Advances in Experimental Medicine and Biology* (ed. Islam, M. S.), pp. 891–916. Dordrecht: Springer Netherlands.

Tosatto, A., Sommaggio, R., Kummerow, C., Bentham, R. B., Blacker, T. S., Berecz, T., Duchen, M. R., Rosato, A., Bogeski, I., Szabadkai, G., et al. (2016). The mitochondrial calcium uniporter regulates breast cancer progression via HIF -1α . *EMBO Mol. Med.* **8**, 569–585.

Trenker, M., Malli, R., Fertschai, I., Levak-Frank, S. and Graier, W. F. (2007). Uncoupling proteins 2 and 3 are fundamental for mitochondrial Ca2+ uniport. *Nat. Cell Biol.* **9**, 445–452.

Trevisan, T., Pendin, D., Montagna, A., Bova, S., Ghelli, A. M. and Daga, A. (2018). Manipulation of Mitochondria Dynamics Reveals Separate Roles for Form and Function in Mitochondria Distribution. *Cell Rep.* **23**, 1742–1753.

Trotta, A. P. and Chipuk, J. E. (2017). Mitochondrial dynamics as regulators of cancer biology. *Cell. Mol. Life Sci.* **74**, 1999–2017.

Tsai, M. F., Jiang, D., Zhao, L., Clapham, D. and Miller, C. (2014). Functional reconstitution of the mitochondrial Ca 2+ /H + antiporter letm1. *J. Gen. Physiol.* **143**, 67–73.

Tsai, F. C., Kuo, G. H., Chang, S. W. and Tsai, P. J. (2015). Ca^{2+} signaling in cytoskeletal reorganization, cell migration, and cancer metastasis. *Biomed Res. Int.* **2015**,.

Tsuyama, T., Tsubouchi, A., Usui, T., Imamura, H. and Uemura, T. (2017). Mitochondrial dysfunction induces dendritic loss via eIF2α phosphorylation. *J. Cell Biol.* **216**, 815–834.

Twig, G., Elorza, A., Molina, A. J. A., Mohamed, H., Wikstrom, J. D., Walzer, G., Stiles, L., Haigh, S. E., Katz, S., Las, G., et al. (2008). Fission and selective fusion govern mitochondrial segregation and elimination

by autophagy. *EMBO J.* **27**, 433–446.

Ueda, K., Murata-Hori, M., Tatsuka, M. and Hosoya, H. (2002). Rho-kinase contributes to diphosphorylation of myosin ii regulatory light chain in nonmuscle cells. *Oncogene* **21**, 5852–5860.

Vais, H., Mallilankaraman, K., Mak, D. O. D., Hoff, H., Payne, R., Tanis, J. E. and Foskett, J. K. (2016). EMRE Is a Matrix Ca2+ Sensor that Governs Gatekeeping of the Mitochondrial Ca2+ Uniporter. *Cell Rep.* **14**, 403–410.

Vakifahmetoglu-Norberg, H., Ouchida, A. T. and Norberg, E. (2017). The role of mitochondria in metabolism and cell death. *Biochem. Biophys. Res. Commun.* **482**, 426–431.

Valente, A. J., Maddalena, L. A., Robb, E. L., Moradi, F. and Stuart, J. A. (2017). A simple ImageJ macro tool for analyzing mitochondrial network morphology in mammalian cell culture. *Acta Histochem.* **119**, 315–326.

van der Bliek, A. M., Shen, Q. and Kawajiri, S. (2013). Mechanisms of mitochondrial fission and fusion. *Cold Spring Harb. Perspect. Biol.* **5**, 1–16.

Van Der Giezen, M. (2009). Hydrogenosomes and mitosomes: Conservation and evolution of functions1. *J. Eukaryot. Microbiol.* **56**, 221–231.

Van Laar, V. S. and Berman, S. B. (2009). Mitochondrial dynamics in Parkinson's disease. *Exp. Neurol.* **218**, 247–256.

Vasington, F. D. and Murphy, J. V. (1962). Ca ion uptake by rat kidney mitochondria and its dependence on respiration and phosphorylation. *J. Biol. Chem.* **237**, 2670–7.

Vasquez, C. G., Tworoger, M. and Martin, A. C. (2014). Dynamic myosin phosphorylation regulates contractile pulses and tissue integrity during epithelial morphogenesis. *J. Cell Biol.* **206**, 435–450.

Venken, K. J. T., Schulze, K. L., Haelterman, N. A., Pan, H., He, Y., Evans-Holm, M., Carlson, J. W., Levis, R. W., Spradling, A. C., Hoskins, R. A., et al. (2011). MiMIC: A highly versatile transposon insertion resource for engineering Drosophila melanogaster genes. *Nat. Methods* **8**, 737–747.

Ventura-Clapier, R., Garnier, A. and Veksler, V. (2008). Transcriptional control of mitochondrial biogenesis: The central role of PGC-1α. *Cardiovasc. Res.* **79**, 208–217.

Verboon, J. M. and Parkhurst, S. M. (2015). Rho family GTPase functions in Drosophila epithelial wound repair. *Small GTPases* **6**, 28–35.

Verstreken, P., Ly, C. V., Venken, K. J. T., Koh, T.-W., Zhou, Y. and Bellen, H. J. (2005). Synaptic mitochondria are critical for mobilization of reserve pool vesicles at Drosophila neuromuscular junctions. *Neuron* **47**, 365–78.

Virbasius, J. V. and Scarpulla, R. C. (1994). Activation of the human mitochondrial transcription factor A gene by nuclear respiratory factors: A potential regulatory link between nuclear and mitochondrial gene expression in organelle biogenesis. *Proc. Natl. Acad. Sci. U. S. A.* **91**, 1309–1313.

von der Malsburg, K., Müller, J. M., Bohnert, M., Oeljeklaus, S., Kwiatkowska, P., Becker, T., Loniewska-Lwowska, A., Wiese, S., Rao, S., Milenkovic, D., et al. (2011). Dual Role of Mitofilin in Mitochondrial Membrane Organization and Protein Biogenesis. *Dev. Cell* **21**, 694–707.

Wai, T. and Langer, T. (2016). Mitochondrial Dynamics and Metabolic Regulation. *Trends Endocrinol. Metab.* **27**, 105–117.

Wallace, D. C. (2012). Mitochondria and cancer. *Nat. Rev. Cancer* **12**, 685–98.

Wallace, D. C., Ye, J., Neckelmann, S. N., Singh, G., Webster, K. A. and Greenberg, B. D. (1987). Sequence analysis of cDNAs for the human and bovine ATP synthase β subunit: mitochondrial DNA genes sustain seventeen times more mutations. *Curr. Genet.* **12**, 81–90.

Wang, P. T. C., Garcin, P. O., Fu, M., Masoudi, M., St-Pierre, P., Panté, N. and Nabi, I. R. (2015). Distinct mechanisms controlling rough and smooth endoplasmic reticulum contacts with mitochondria. *J. Cell Sci.* **128**, 2759–2765.

Waterham, H. R., Koster, J., van Roermund, C. W. T., Mooyer, P. A. W., Wanders, R. J. A. and Leonard, J. V. (2007). A Lethal Defect of Mitochondrial and Peroxisomal Fission. *N. Engl. J. Med.* **356**, 1736–1741.

Westermann, B. (2010). Mitochondrial dynamics in model organisms: What yeasts, worms and flies have taught us about fusion and fission of mitochondria. *Semin. Cell Dev. Biol.* **21**, 542–549.

Westermann, B. (2012). Bioenergetic role of mitochondrial fusion and fission. *Biochim. Biophys. Acta - Bioenerg.* **1817**, 1833–1838.

Westrate, L. M., Drocco, J. A., Martin, K. R., Hlavacek, W. S. and MacKeigan, J. P. (2014). Mitochondrial morphological features are associated with fission and fusion events. *PLoS One* **9**, e95265.

Wilgus, T. A., Roy, S. and McDaniel, J. C. (2013). Neutrophils and Wound Repair: Positive Actions and Negative Reactions. *Adv. Wound Care* **2**, 379–388.

Wingrove, D. E. and Gunter, T. E. (1986). Kinetics of mitochondrial calcium transport. II. A kinetic description of the sodium-dependent calcium efflux mechanism of liver mitochondria and inhibition by ruthenium red and by tetraphenylphosphonium. *J. Biol. Chem.* **261**, 15166–15171.

Wong, E. D., Wagner, J. A., Gorsich, S. W., Mccaffery, J. M., Shaw, J. M. and Nunnari, J. (2000). The Dynamin-related GTPase , Mgm1p , Is an Intermembrane Space Protein Required for Maintenance of Fusion Competent Mitochondria. *J. Cell Biol.* **151**, 341–352.

Wood, W., Jacinto, A., Grose, R., Woolner, S., Gale, J., Wilson, C. and Martin, P. (2002). Wound healing recapitulates morphogenesis in Drosophila embryos. *Nat. Cell Biol.* **4**, 907–912.

Wood, W., Faria, C. and Jacinto, A. (2006). Distinct mechanisms regulate hemocyte chemotaxis during development and wound healing in Drosophila melanogaster. *J. Cell Biol.* **173**, 405–416.

Wu, Z., Puigserver, P., Andersson, U., Zhang, C., Adelmant, G., Mootha, V., Troy, A., Cinti, S., Lowell, B., Scarpulla, R. C., et al. (1999). Mechanisms controlling mitochondrial biogenesis and respiration through

the thermogenic coactivator PGC-1. *Cell* **98**, 115–124.

Wu, H., Kanatous, S. B., Thurmond, F. A., Gallardo, T., Isotani, E., Bassel-Duby, R. and Williams, R. S. (2002). Regulation of mitochondrial biogenesis in skeletal muscle by caMK. *Science (80-.).* **296**, 349–352.

Wu, Z., Huang, X., Feng, Y., Handschin, C., Feng, Y., Gullicksen, P. S., Bare, O., Labow, M., Spiegelman, B. and Stevenson, S. C. (2006). Transducer of regulated CREB-binding proteins (TORCs) induce PGC-1α transcription and mitochondrial biogenesis in muscle cells. *Proc. Natl. Acad. Sci. U. S. A.* **103**, 14379–14384.

Xia, C., Fu, Z., Battaile, K. P. and Kim, J. J. P. (2019). Crystal structure of human mitochondrial trifunctional protein, a fatty acid β-oxidation metabolon. *Proc. Natl. Acad. Sci. U. S. A.* **116**, 6069–6074.

Xie, X. Y. and Barrett, J. N. (1991). Membrane resealing in cultured rat septal neurons after neurite transection: evidence for enhancement by Ca(2+)-triggered protease activity and cytoskeletal disassembly. *J. Neurosci.* **11**, 3257–67.

Xiong, Y., Uys, J. D., Tew, K. D. and Townsend, D. M. (2011). S-Glutathionylation: From molecular mechanisms to health outcomes. *Antioxidants Redox Signal.* **15**, 233–270.

Xu, S. and Chisholm, A. D. (2011). A Gαq-Ca^{2+} signaling pathway promotes actin-mediated epidermal wound closure in C. elegans. *Curr. Biol.* **21**, 1960–7.

Xu, S. and Chisholm, A. D. (2014). C. elegans epidermal wounding induces a mitochondrial ROS burst that promotes wound repair. *Dev. Cell* **31**, 48–60.

Yadav, A. K. and Srikrishna, S. (2019). scribble (scrib) knockdown induces tumorigenesis by modulating Drp1-Parkin mediated mitochondrial dynamics in the wing imaginal tissues of Drosophila. *Mitochondrion* **44**, 103–110.

Yang, P. L. (2016). Metabolomics and Lipidomics: Yet More Ways Your Health is Influenced by Fat. In *Viral Pathogenesis: From Basics to Systems Biology: Third Edition*, pp. 181–198. Elsevier.

Yang, Q. H., Church-Hajduk, R., Ren, J., Newton, M. L. and Du, C. (2003). Omi/HtrA2 catalytic cleavage of inhibitor of apoptosis (IAP) irreversibly inactivates IAPs and facilitates caspase activity in apoptosis. *Genes Dev.* **17**, 1487–1496.

Yang, Y., Ouyang, Y., Yang, L., Beal, M. F., McQuibban, A., Vogel, H. and Lu, B. (2008). Pink1 regulates mitochondrial dynamics through interaction with the fission/fusion machinery. *Proc. Natl. Acad. Sci. U. S. A.* **105**, 7070–5.

Yao, C.-H., Wang, R., Wang, Y., Kung, C.-P., Weber, J. D. and Patti, G. J. (2019). Mitochondrial fusion supports increased oxidative phosphorylation during cell proliferation. *Elife* **8**, 1–19.

Yarosh, W., Monserrate, J., Tong, J. J., Tse, S., Le, P. K., Nguyen, K., Brachmann, C. B., Wallace, D. C. and Huang, T. (2008). The molecular mechanisms of OPA1-mediated optic atrophy in Drosophila model and prospects for antioxidant treatment. *PLoS Genet.* **4**, 0062–0071.

Yin, W., Signore, A. P., Iwai, M., Cao, G., Gao, Y. and Chen, J. (2008). Rapidly increased neuronal mitochondrial biogenesis after hypoxic-ischemic brain injury. *Stroke* **39**, 3057–3063.

Yin, M., Lu, Q., Liu, X., Wang, T., Liu, Y. and Chen, L. (2016). Silencing Drp1 inhibits glioma cells proliferation and invasion by RHOA/ ROCK1 pathway. *Biochem. Biophys. Res. Commun.* **478**, 663–8.

Yoo, S.-M. and Jung, Y. (2018). A Molecular Approach to Mitophagy and Mitochondrial Dynamics. *Mol. Cells* **41**, 18–26.

Yoon, Y., Pitts, K. R. and McNiven, M. A. (2001). Mammalian dynamin-like protein DLP1 tubulates membranes. *Mol. Biol. Cell* **12**, 2894–905.

Yoon, Y., Krueger, E. W., Oswald, B. J. and McNiven, M. A. (2003). The mitochondrial protein hFis1 regulates mitochondrial fission in mammalian cells through an interaction with the dynamin-like protein DLP1. *Mol. Cell. Biol.* **23**, 5409–20.

Youle, R. J. and Narendra, D. P. (2011). Mechanisms of mitophagy. *Nat. Rev. Mol. Cell Biol.* **12**, 9–14.

Young, P. E., Richman, A. M., Ketchum, A. S. and Kiehart, D. P. (1993). Morphogenesis in Drosophila requires nonmuscle myosin heavy chain function. *Genes Dev.* **7**, 29–41.

Yumura, S., Hashima, S. and Muranaka, S. (2014). Myosin II does not contribute to wound repair in dictyostelium cells. *Biol. Open* **3**, 966–973.

Zaja-Milatovic, S. and Richmond, A. (2008). CXC chemokines and their receptors: a case for a significant biological role in cutaneous wound healing. *Histol. Histopathol.* **23**, 1399–407.

Zhang, J. H. and Xu, M. (2000). DNA fragmentation in apoptosis. *Cell Res.* **10**, 205–211.

Zhao, J., Liu, T., Jin, S., Wang, X., Qu, M., Uhlén, P., Tomilin, N., Shupliakov, O., Lendahl, U. and Nistér, M. (2011a). Human MIEF1 recruits Drp1 to mitochondrial outer membranes and promotes mitochondrial fusion rather than fission. *EMBO J.* **30**, 2762–2778.

Zhao, Y., Jin, J., Hu, Q., Zhou, H.-M., Yi, J., Yu, Z., Xu, L., Wang, X., Yang, Y. and Loscalzo, J. (2011b). Genetically encoded fluorescent sensors for intracellular NADH detection. *Cell Metab.* **14**, 555–66.

Zhao, J., Zhang, J., Yu, M., Xie, Y., Huang, Y., Wolff, D. W., Abel, P. W. and Tu, Y. (2013). Mitochondrial dynamics regulates migration and invasion of breast cancer cells. *Oncogene* **32**, 4814–24.

Zhivotovsky, B. and Orrenius, S. (2011). Calcium and cell death mechanisms: A perspective from the cell death community. *Cell Calcium* **50**, 211–221.

Zhou, X., Li, M., Xiao, M., Ruan, Q., Chu, Z., Ye, Z., Zhong, L., Zhang, H., Huang, X., Xie, W., et al. (2019). ERβ Accelerates Diabetic Wound Healing by Ameliorating Hyperglycemia-Induced Persistent Oxidative Stress. *Front. Endocrinol. (Lausanne).* **10**, 1–11.

Zhu, X., Perry, G., Smith, M. A. and Wang, X. (2012). Abnormal Mitochondrial Dynamics in the Pathogenesis of Alzheimer's Disease. *J. Alzheimer's Dis.* **33**, S253–S262.

Zinovkina, L. A. (2019). DNA Replication in Human Mitochondria. *Biochem.* **84**, 884–895.

Zong, H., Ren, J. M., Young, L. H., Pypaert, M., Mu, J., Birnbaum, M. J. and Shulman, G. I. (2002). AMP kinase is required for mitochondrial biogenesis in skeletal muscle in response to chronic energy deprivation. *Proc. Natl. Acad. Sci. U. S. A.* **99**, 15983–15987.

Zorov, D. B., Juhaszova, M. and Sollott, S. J. (2014). Mitochondrial reactive oxygen species (ROS) and ROS-induced ROS release. *Physiol. Rev.* **94**, 909–950.

Zorova, L. D., Popkov, V. A., Plotnikov, E. Y., Silachev, D. N., Pevzner, I. B., Jankauskas, S. S., Babenko, V. A., Zorov, S. D., Balakireva, A. V, Juhaszova, M., et al. (2018). Mitochondrial membrane potential. *Anal. Biochem.* **552**, 50–59.

Zorzano, A. and Claret, M. (2015). Implications of mitochondrial dynamics on neurodegeneration and on hypothalamic dysfunction. *Front. Aging Neurosci.* **7**, 101.

Züchner, S., Mersiyanova, I. V., Muglia, M., Bissar-Tadmouri, N., Rochelle, J., Dadali, E. L., Zappia, M., Nelis, E., Patitucci, A., Senderek, J., et al. (2004). Mutations in the mitochondrial GTPase mitofusin 2 cause Charcot-Marie-Tooth neuropathy type 2A. *Nat. Genet.* **36**, 449–451.

Zulian, A., Schiavone, M., Giorgio, V. and Bernardi, P. (2016). Forty years later: Mitochondria as therapeutic targets in muscle diseases. *Pharmacol. Res.* **113**, 563–573.

Zulueta-Coarasa, T. and Fernandez-Gonzalez, R. (2017). Tension (re)builds: Biophysical mechanisms of embryonic wound repair. *Mech. Dev.* **144**, 43–52.

Zulueta-Coarasa, T., Tamada, M., Lee, E. J. and Fernandez-Gonzalez, R. (2014). Automated multidimensional image analysis reveals a role for Abl in embryonic wound repair. *Dev.* **141**, 2901–2911.